AD-A072 438 JOHNS HOPKINS UNIV LAUREL MD APPLIED PHYSICS LAB F/G 22/2
INSTRUMENTATION DEVELOPED BY THE JOHNS HOPKINS UNIVERSITY APPLI--ETC(U)
NOV 78 N00024-78-C-5384
UNCLASSIFIED APL/JHU/SDO-4100 NL

1 OF 3
AD
A072438

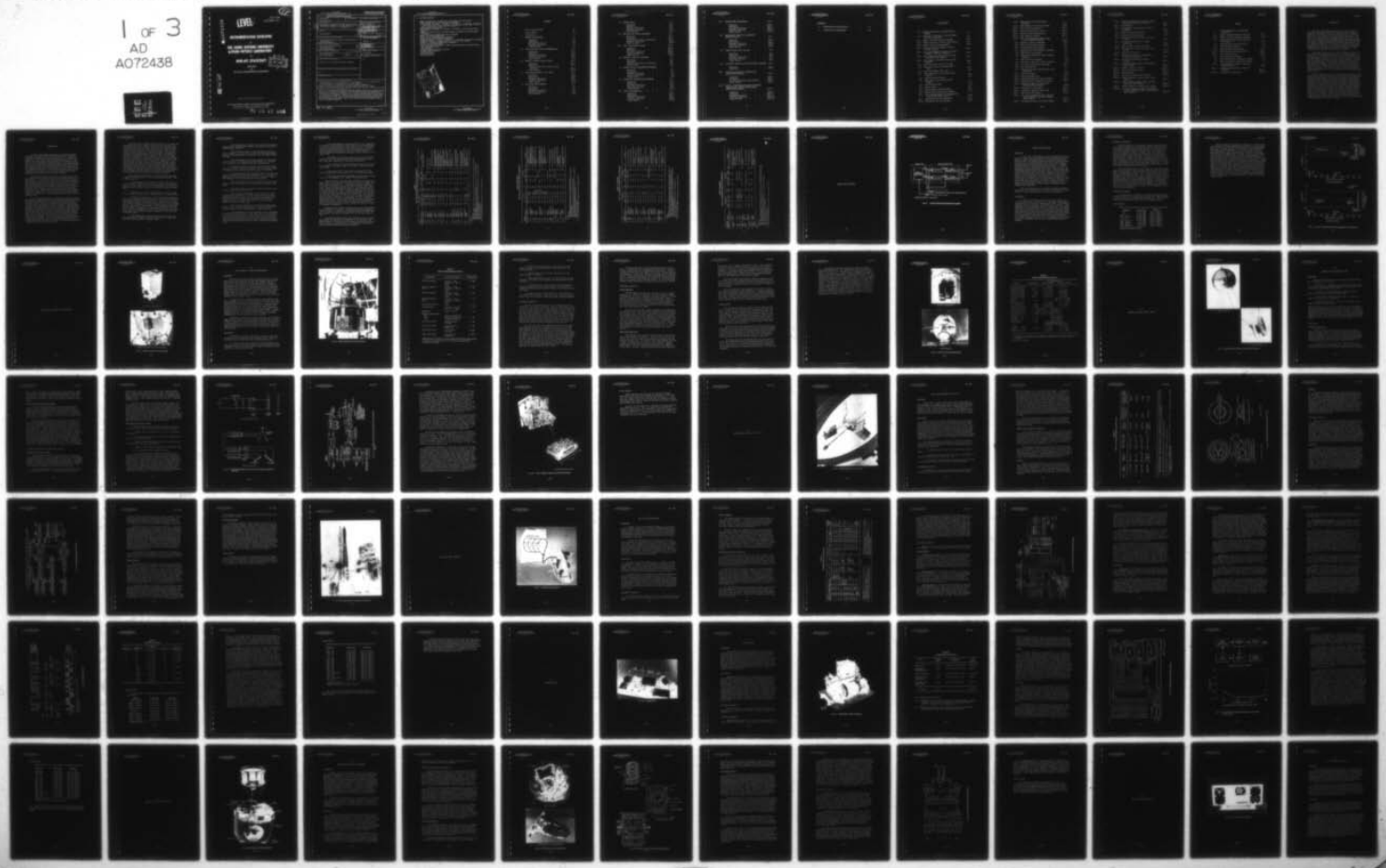

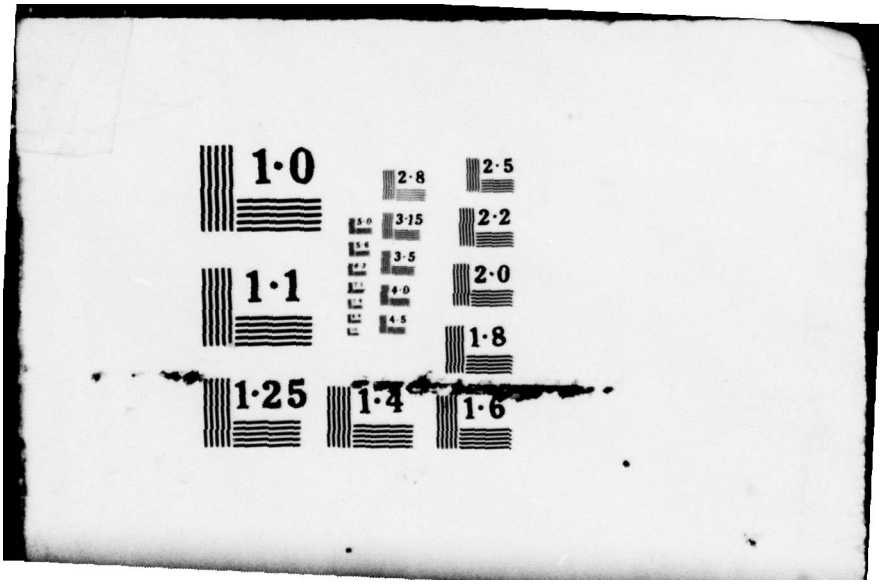
1·0
1·1
1·25
1·4
1·6
1·8
2·0
2·2
2·5
2·8
3·15
3·5
4·0
4·5

LEVEL II

SDO-4100
DECEMBER 1977

INSTRUMENTATION DEVELOPED

by

THE JOHNS HOPKINS UNIVERSITY APPLIED PHYSICS LABORATORY

for

NON-APL SPACECRAFT

PREPARED
by
THE SPACE DEVELOPMENT DEPARTMENT

THE JOHNS HOPKINS UNIVERSITY ■ APPLIED PHYSICS LABORATORY
Johns Hopkins Road ○ Laurel, Maryland ○ 20810
Operating under Contract N00017-72-C4401 with the Department of the Navy

Unclassified

SECURITY CLASSIFICATION OF THIS PAGE

PLEASE FOLD BACK IF NOT NEEDED FOR BIBLIOGRAPHIC PURPOSES

REPORT DOCUMENTATION PAGE

1. REPORT NUMBER: APL/JHU SDO-4100

2. GOVT ACCESSION NO.

3. RECIPIENT'S CATALOG NUMBER

4. TITLE (*and Subtitle*): Instrumentation Developed by The Johns Hopkins University Applied Physics Laboratory for Non-APL Spacecraft

5. TYPE OF REPORT & PERIOD COVERED: Status Report, 1960 to date

6. PERFORMING ORG. REPORT NUMBER: APL/JHU SDO-4100

7. AUTHOR(s): Space Department

8. CONTRACT OR GRANT NUMBER(s): N00024-78-C-5384; N00017-72-C-4401

9. PERFORMING ORGANIZATION NAME & ADDRESS: The Johns Hopkins University Applied Physics Laboratory, Johns Hopkins Road, Laurel, Maryland 20810

10. PROGRAM ELEMENT, PROJECT, TASK AREA & WORK UNIT NUMBERS: Task Y22

11. CONTROLLING OFFICE NAME & ADDRESS: Naval Plant Representative Office, Johns Hopkins Road, Laurel, Maryland 20810

12. REPORT DATE: November 1978

13. NUMBER OF PAGES: 216

14. MONITORING AGENCY NAME & ADDRESS: Naval Plant Representative Office, Johns Hopkins Road, Laurel, Maryland 20810

15. SECURITY CLASS. (*of this report*): Unclassified

15a. DECLASSIFICATION/DOWNGRADING SCHEDULE: N/A

16. DISTRIBUTION STATEMENT (*of this Report*)

Approved for public release; distribution unlimited.

17. DISTRIBUTION STATEMENT (*of the abstract entered in Block 20, if different from Report*)

N/A

18. SUPPLEMENTARY NOTES

19. KEY WORDS (*Continue on reverse side if necessary and identify by block number*)

Transit-on-Discover-9, -10, -11 (1960 Delta 1), -14 (1960 Kappa 1), -16, -17 (1960 Omicron 1), -18 (1960 Sigma 1), -20 (1961 Epsilon 1), -23 (1961 Lambda 1);
INJUN-1 (1961 02) and -3 (1962 Beta Tau 2) Satellite Proton Instrumentation;
Explorer 32 (1966 44A) and Explorer 38 (1968 55A) Magnetic Attitude Control System;

20. ABSTRACT (*Continue on reverse side if necessary and identify by block number*)

Scientific and engineering instrumentation and support equipment developed by the Applied Physics Laboratory of The Johns Hopkins University for non-APL spacecraft since 1960 are described. The descriptions are arranged in chronological order according to experiment and include illustrations and system block diagrams. References and a listing of APL contributions to space research and technology are included. This report is updated from time to time with the issuance of new and revised material, and is one of a series that includes APL/JHU SDO-1600 "Artificial Earth Satellites Designed and Fabricated by JHU/APL" and APL/JHU SDO-3100 "Navy Navigation Satellite System User Equipment Handbook."

Instrumentation described includes: → (cont. on p. iv)

DD FORM 1 JAN 73 1473

Unclassified

SECURITY CLASSIFICATION OF THIS PAGE

031650

19. KEY WORDS (continued)

Explorer -34 (1967 51A), -41 (1969 53A), -43 (1971 19A) Solar Proton Monitor;
ITOS-1 (1970 08A), -E, -H (1976 77A) Solar Proton Monitor;
Doppler Beacon-1 (1970 16A), -2 (1970 40A), -3 (1970 98A), -4, -5 (1971 22A), -6 (1971 76A), -7 (1973 14A), -8 (1973 46A), -9 (1973 88A), -10 (1974 20A), -11 (1974 85A), -12 (1975 51A), -13 (1975 114A), -15 (1976 65A), -17 (1977 112);
Orbiting Frog Otolith (1970 94A);
NOAA-1 (ITOS-A), -2 (ITOS-B), -2 (1972 82A), -3 (1973 86A), -5 (1976 77A) Solar Proton Monitor;
Explorer -47 (1972 73A) and -50 (1973 86A) Energetic and Charged Particles Measurement Experiments;
Apollo-17 (1972 96A) Ultraviolet Spectrometer Experiment;
Skylab-1 (1973 27A) Experiment M131;
Explorer 51 (1973 101A) Photoelectron Spectrometer;
Apollo-Soyuz Ultraviolet Absorption Experiment;
Atmospheric Explorer-C (1973 101A), -D (1975 96A), -E (1975 107A) Photoelectron Spectrometer;
Navigational Package -1, -2/Doppler Beacon -16, -17 on 1977 56A, 1978 29A;
Voyager -1, -2 Low Energy Charged Particle Experiments;
IUE (1978 12A) Proton Flux Monitor;
SEASAT-A (1978 64A) Radar Altimeter, Synthetic Aperture Radar Data Link, Doppler Beacon, Laser Retroreflector Array;
Geiger Telescope;
Low Energy Magnetospheric Particle Analyzer;
Low Energy Particle Telescope;
Oculogyral Illusion;
Polar Cap Absorption;
Rotating Litter Chair

CONTENTS

APPENDIXES

ILLUSTRATIONS

TABLES

INTRODUCTION

The Space Development Department of the Applied Physics Laboratory was formed to direct the program of the US Navy to establish a navigation capability through the use of artificial satellites. This program, conceived and developed by APL, was begun in 1959 and was put into operational use in 1964. In support of the Navy Navigation Satellite System, the Department has carried out a number of investigations which range from fundamental research through exploratory and advanced development to actual hardware evaluation. The problems in research and analysis associated with the system, and the opportunities presented for additional space studies, have allowed the Department to make contributions in many areas of the space sciences.

The broad and varied space research programs conducted by the Applied Physics Laboratory began in late 1960 when Drs. G. F. Pieper and C. O. Bostrom joined the staff of the Space Development Department to measure and study the radiation environment of the Navy Navigation Satellites (then known as Transit). In June 1961, the University of Iowa research satellite called INJUN 1 was launched pickaback on APL Transit Satellite 4-A with instrumentation that included a set of solid state proton detectors furnished by APL. These detectors made the first direct measurements of low energy solar protons in the polar regions and contributed significantly to our understanding of the inner Van Allen radiation belt.

Early satellites that also included APL scientific instrumentation were TRAAC (Transit Research and Attitude Control) which was launched in November 1961 and included particle and neutron detectors, INJUN 3 which was launched in December 1962 and included a proton spectrometer, and the 5E-series of Navy research satellites that carried various APL instruments. Satellite 5E-1, launched in September 1963 with several onboard electron and proton detectors, has become one of the longest lived and most productive satellites ever launched as data were acquired continuously for six years and the satellite has functioned for a full solar cycle (11 years). Research on the short and long term changes in the radiation belts, solar particles and their effects on the polar ionosphere, and the discovery and study of field aligned currents in the auroral regions have been reported in some 43 papers based on Satellite 5E-1 data.

INTRODUCTION

The Space Development Department of the Applied Physics Laboratory was formed to direct the program of the US Navy to establish a navigation capability through the use of artificial satellites. This program, conceived and developed by APL, was begun in 1959 and was put into operational use in 1964. In support of the Navy Navigation Satellite System, the Department has carried out a number of investigations which range from fundamental research through exploratory and advanced development to actual hardware evaluation. The problems in research and analysis associated with the system, and the opportunities presented for additional space studies, have allowed the Department to make contributions in many areas of the space sciences.

The broad and varied space research programs conducted by the Applied Physics Laboratory began in late 1960 when Drs. G. F. Pieper and C. O. Bostrom joined the staff of the Space Development Department to measure and study the radiation environment of the Navy Navigation Satellites (then known as Transit). In June 1961, the University of Iowa research satellite called INJUN 1 was launched pickaback on APL Transit Satellite 4-A with instrumentation that included a set of solid state proton detectors furnished by APL. These detectors made the first direct measurements of low energy solar protons in the polar regions and contributed significantly to our understanding of the inner Van Allen radiation belt.

Early satellites that also included APL scientific instrumentation were TRAAC (Transit Research and Attitude Control) which was launched in November 1961 and included particle and neutron detectors, INJUN 3 which was launched in December 1962 and included a proton spectrometer, and the 5E-series of Navy research satellites that carried various APL instruments. Satellite 5E-1, launched in September 1963 with several onboard electron and proton detectors, has become one of the longest lived and most productive satellites ever launched as data were acquired continuously for six years and the satellite has functioned for a full solar cycle (11 years). Research on the short and long term changes in the radiation belts, solar particles and their effects on the polar ionosphere, and the discovery and study of field aligned currents in the auroral regions have been reported in some 43 papers based on Satellite 5E-1 data.

When the Transit system became operational in the 1960s and Navy support for basic research in space science decreased, the Laboratory turned to the flight opportunities provided by NASA. Six Solar Proton Monitors (SPMs) were built for a series of NASA sounding rockets launched from Fort Churchill, Canada, during several solar particle events beginning in 1966. The satellite versions of this monitor were included on IMP F (Interplanetary Monitoring Platform) launched in May 1967, IMP G in June 1969, and IMP I in March 1971. Data from the three satellite monitors provided a continuous time history of solar protons from May 1967 until December 1974 when IMP I reentered the atmosphere. Other NASA directed satellite projects that carried APL built instruments included the IMP-H and IMP-J satellites (Charged Particle Measurements Experiments), the ITOS (Improved TIROS Operational Satellite) series of weather satellites (Solar Proton Monitors), the Atmospheric Explorer satellites (Photoelectron Spectrometers), Skylab (Experiment M131), Apollo 17 (Ultraviolet Spectrometer), and the Apollo-Soyuz (Ultraviolet Absorption Experiment).

APL scientific instrumentation and observations have made a number of contributions to space research and technology. Some of these include:

- First observation of low-energy (1 MeV) solar protons in the polar region, first use of solid state particle detectors in space, and first study of inner zone trapped proton belt stability during a period of major solar activity (INJUN 1 launched in June 1961).

- Discovery of a "second" radiation belt due to the Starfish high altitude nuclear burst (TRAAC launched in November 1961).

- Discovery and mapping of currents flowing along magnetic field lines connected to the auroral oval, first quantitative model magnetosphere derived from observations of asymmetry in the outer zone trapped electrons, first long-term (>5 years) study of trapped particle time variations and decay of Starfish electron belt, first detailed correlation of solar protons, VLF propagation, and HF absorption (PCA), development of an ion chemistry model of the ionosphere, and first quantitative connection of solar cosmic ray ionization effects to ground-based radio transmissions (5E-1 launched in September 1963).

- First observation and determination of high order resonant geopotentional harmonic effects in the motion of near-earth satellites (5BN-2 launched in December 1963).

- First simultaneous observations of solar protons inside and outside the magnetosphere (INJUN 4 and Mariner IV launched in November 1964, and 5E-1).

- First satellite survey of celestial sources of ultraviloet radiation, and first high accuracy (Rb-vapor magnetometer) magnetic field measurements by satellite (5E-5 launched in December 1964).

- First measurement of the radial gradient of low-energy (<1 MeV) protons in interplanetary space (Explorer 33 and Mariner V launched in July 1966 and June 1967, respectively).

- First operational solar proton monitoring system (IMPs F through I, ITOS-1, and NOAA 1 through 4 in a continuing program that started with the first satellite launched in May 1967).

- First theoretically derived global ionospheric model for effects on satellite ranging and confirmation of its validity from experimental data (Syncom 3 and ATS-1 and -3 launched in August 1964, December 1966, and November 1967, respectively).

- First measurement of short period (3-240 seconds) hydromagnetic waves near synchronous altitude (DODGE launched in July 1967).

- First observation of low-energy (sub-MeV) medium nuclei in solar flare events (Explorer 35).

- First detailed measurements of the solar flare proton spectrum at low energies ($E \sim 0.3$ MeV) and derivation of strict quantitative limits on solar particle storage hypothesis, first detailed mapping of trapped alpha particles, and discovery of heavy ions (C, N, O) trapped in the Earth's radiation belts (INJUN-5 launched in August 1968).

- First detailed analysis of field-aligned currents with visible aurora, and first observations of these currents in the southern auroral region (TRIAD launched in September 1972).

- First measurements of time variations in the composition of energetic nuclei emitted in solar flares and in the variations of iron nuclei emitted during a solar particle event, first association of helium-enriched solar particle emission with coronal holes and high speed streamers, and the first observation of shock-accelerated interplanetary electrons (IMP H launched in September 1972).

- First measurements of time variations in the composition of energetic nuclei emitted in solar flares and in the variations of iron nuclei emitted during a solar particle event, first association of helium-enriched solar particle emission with coronal holes and high speed streamers, and the first observation of shock-accelerated interplanetary electrons (IMP H launched in September 1972).

- Development of prediction technique for solar wind disturbances using interplanetary scintillation measurements (IMP H and 34 MHz radio telescope at Clark Lake, California).

- First precisely controlled rotating litter chair to measure changes in vestibular organs of astronauts (Skylab launched in May 1973).

- First association of low-energy solar particles with structure observed in X-ray images of the sun (IMP H and Skylab).

- First high resolution measurements of photoelectron spectrum in the thermosphere (AE-C launched in December 1973).

Many of the previously mentioned satellites (the Navy Navigation Satellites, TRAAC, the 5E series of satellites, DODGE, and TRIAD) were developed by APL. Descriptions of these satellites are included in APL/JHU document SDO 1600, Artificial Earth Satellites Designed and Fabricated by APL/JHU. This publication discusses support and experimental systems developed by APL and flown on non-APL satellites. Table 1 presents a chronological listing of these satellites and associated instrumentation. Also included are satellite launch and orbital data, and the prime contracting agency or Project Director. In some cases the specific satellite instrumentation may have been developed by APL for a different agency; this will be noted in the individual equipment description. Abbreviations used in this publication are listed in Appendix A; reference and bibliographic material arranged according to section is presented in Appendix B.

Navigation and geodetic equipments that have been developed by the Laboratory for users of the APL-developed Navy Navigation Satellite System are described in APL/JHU document SDO 3100, which was originally published in November 1971 and has since been updated.

Like SDO 3100 and SDO 1600, this publication is ring bound and formatted to facilitate the addition of new material. The dissemination of revised and/or new equipment descriptions will be made according to a distribution list maintained at the Applied Physics Laboratory/Space Development Department.

Table 1
APL Instrumentation on Non-APL/JHU Spacecraft*

No.	APL Instrumentation[1a]	Satellite[1b]	Launch Data[1c] Date[2]	Site	Vehicle	Proj. Dir.	Orbit Data[3] Period	Perigee	Apogee	Incl.	Remarks
1	TOD-1	Discoverer 9	2/ 4/60	WTR	Thor-Agena A	USAF		(Failed to orbit)			Signals received during launch.
2	TOD-2	Discoverer 10	2/19/60	WTR	Thor-Agena A	USAF		(Failed to orbit)			— — —
3	TOD-3	Discoverer 11 (1960 Δ1)	4/15/60	WTR	Thor-Agena A	USAF	92.3	166	603	80.1	Good data received.
4	TOD-4	Discoverer 14 (1960 κ1)	8/18/60	WTR	Thor-Agena A	USAF	94.5	182	808	79.6	No signal received.
5	TOD-5	Discoverer 16	10/26/60	WTR	Thor-Agena B	USAF		(Failed to orbit)			Signals received during powered flight.
6	TOD-6	Discoverer 17 (1960 o1)	11/12/60	WTR	Thor-Agena B	UASF	96.4	182	988	81.9	Good data obtained during 72 satellite passes; orbital SAO data and TOD doppler data in excellent agreement.
7	TOD-7	Discoverer 18 (1960 Σ1)	12/ 7/60	WTR	Thor-Agena B	USAF	93.8	230	685	80.8	Good data obtained during 93 satellite passes; good orbits computed.
8	TOD-8	Discoverer 20 (1961 E1)	2/17/61	WTR	Thor-Agena B	USAF	95.4	285	782	80.4	Stations tracked TOD on a convenience basis; good data obtained.
9	TOD-9	Discoverer 23 (1961 Λ1)	4/ 8/61	WTR	Thor-Agena B	USAF	101.2	203	1 419	81.9	Stations tracked TOD on a convenience basis; good data obtained during 88 satellite passes.
10	PD	INJUN-1 (1961 02)	6/29/61	ETR	Thor-Able-Star	USAF	103.8	859	1 020	67	Data obtained for 13 months; terminated by payload failure due to Starfish nuclear event.
11	PS	INJUN-3 (1962 βr2)	12/12/62	WTR	Thor-Agena D	USN	116.3	246	2 782	70.3	Data obtained for 11 months, terminated by payload failure.
12	MACS	Explorer 32 (AE-B) (1966 44A)	5/25/66	ETR	Delta	NASA	116	278	2 622	64.7	Good data received until Dec.
13	SPM	Explorer 34 (IMP F) (1967 51A)	5/24/67	WTR	TAD	USAF/ USN	6 231	248	1 097	67.1	Continuous data obtained from launch through satellite reentry in May 1969.
14	MACS	Explorer 38 (RAE-1) (1968 55A)	7/4/68	WTR	TAID	NASA	224	5 852	5 860	120.8	Current, good data received.
15	SPM	Explorer 41 (IMP G) (1969 53A)	6/21/69	WTR	TAID	NASA	4 840	338	152 896	83.8	Good data obtained from launch to Nov. 1971, and Nov. 1971 through satellite reentry in Dec. 1972.
16	SPM	ITOS-1 (TIROS M) (1970 08A)	1/23/70	WTR	TAT-Delta M	NASA	115	1 435	1 482	102	Data recorded sporadically from 12 Feb. 1970 to Nov. 1970.
17	DB-1	1970 16A	3/ 4/70	WTR	Thorad-Agena D	USAF	89	180	284	88	Good data obtained until DB turned off 24 Mar. 1970.

*Footnotes

1. Abbreviations:
   a. TOD = Transit on Discoverer, PD, PS = Proton Detector, Spectrometer, SPM = Solar Proton Monitor, DB = Doppler Beacon, MACS = Magnetic Attitude Control System.
   b. IMP = Interplanetary Monitoring Platform, ITOS = Improved TIROS Operational Satellite, TIROS = Television Infrared Observation Satellite, AE = Atmospheric Explorer, RAE = Radio Astronomy Explorer.
   c. WTR = Western Test Range, ETR = Eastern Test Range, TAD = Thrust Augmented Delta, TAID = Thrust Augmented Improved Delta, TAT = Thrust Augmented Thor.
2. Launch Date = local time at launch site.
3. Period in minutes, Perigee and Apogee in kilometers (approx.), Inclination in degrees from equator.

Table 1 (Continued)
APL Instrumentation on Non-APL/JHU Spacecraft*

No.	APL Instrumentation[1a]	Satellite[1b]	Launch Data[1c] Date[2]	Site	Vehicle	Proj. Dir.	Orbit Data[3] Period	Perigee	Apogee	Incl.	Remarks
18	DB-2	1970 40A	5/20/70	WTR	Thor-Agena D	USAF	89	154	265	83	Good data obtained until DB turned off 16 June 1970.
19	OFOE	OFO-1 Radiation (1970 94A)	11/ 9/70	WI	Scout	NASA	92.64	302	515	37.4	Good data obtained for 6 days on the effects of weightlessness on frog inner ear.
20	DB-3	1970 98A	11/18/70	WTR	Thorad-Agena D	USAF	89	154	184	83	Good data obtained until DB turned off 10 Oct. 1970.
21	SPM	NOAA-1 (ITOS-A)	12/11/70	WTR	Long Tank TAT Delta	NASA	114.93	1 429	1 472	101.94	Good data obtained from launch through Aug. 1971.
22	DB-4	— — —	2/17/71	WTR	Thor-Agena	USAF	(Failed to orbit)				— — —
23	SPM	Explorer 43 (IMP I) (1971 19A)	3/13/71	ETR	Long Tank Thor-Delta	NASA	5 628	235	196 563	28.75	Good data obtained from launch through satellite reentry on 2 Oct. 1974.
24	DB-5	1971 22A	3/24/71	WTR	Long Tank Thorad	USAF	89	154	245	82	Good data obtained until DB turned off 10 April 1971.
25	DB-6	1971 76A	9/10/71	WTR	LTTAT-Agena D	USAF	89	156	243	75	Good data obtained until DB turned off 5 Oct. 1971.
26	SPM	NOAA-2 (ITOS-B)	10/21/71	WTR	Delta N	NASA	(Failed to orbit)				— — —
27	CPME EPE	Explorer 47 (IMP H) (1972 73A)	9/23/72	ETR	Delta	NASA	17 702	201 599	235 639	17.2	Current, good data being received.
28	SPM	NOAA-2 (ITOS-D) (1972 82A)	10/15/72	WTR	Delta	NASA	115	1 448	1 453	101.8	Current, good data being received.
29	USE S169	Apollo 17 (1972 96A)	12/ 7/72	KSC	Saturn V	NASA	(Manned lunar mission)				Good data obtained throughout mission.
30	DB-7	1973 14A	3/ 9/73	WTR	Titan 3D	USAF	88.8	152	270	95.7	Good data obtained until DB turned off 28 April 1973.
31	Exp. M131	Skylab 1 (1973 27A)	5/14/73	ETR	Saturn V	NASA	93.2	422	442	50.0	Good data obtained.
32	DB-8	1973 46A	6/13/73	WTR	Titan 3D	USAF	88.8	156	269	96.2	Good data obtained until DB turned off 29 Aug. 1973.

*Footnotes

1. Abbreviations:
   a. DB = Doppler Beacon, SPM = Solar Proton Monitor, EPE = Energetic Particle Experiment, OFOE = Orbiting Frog Otolith Experiment, USE = Ultraviolet Spectrometer Experiment, CPME = Charged Particle Measurement Experiment.
   b. OFO = Orbiting Frog Otolith, NOAA = National Oceanic and Atmospheric Administration.
   c. WTR = Western Test Range, ETR = Eastern Test Range, TAT = Thrust Augmented Thor, LTTAT = Long Tank Thrust Augmented Thor, KSC = Kennedy Space Center, WI = Wallops Island.
2. Launch Date = local time at launch site.
3. Period in minutes, Perigee and Apogee in kilometers (approx.), Inclination in degrees from equator.

Table 1 (Continued)
APL Instrumentation on Non-APL/JHU Spacecraft*

No.	APL Instrumentation[1a]	Satellite[1b]	Launch Data[1c] Date[2]	Site	Vehicle	Proj. Dir.	Orbit Data[3] Period	Perigee	Apogee	Incl.	Remarks
33	SPM	ITOS-E	7/16/73	WTR	Delta	NASA	*(Failed to orbit)*				
34	EPE CPME	Explorer 50 (IMP J) (1973 78A)	10/25/73	ETR	Delta	NASA	17 551.5	145 380	289 302	28.2	Current, good data being received.
35	SPM	NOAA-3 (ITOS-F) (1973 86A)	11/ 6/73	WTR	Delta	NASA	116.1	1 500	1 509	102.1	Current, good data being received.
36	DB-9	1973 88A	11/10/73	WTR	Titan 3D	USAF	88.8	159	271	96.9	Good data obtained until DB turned off 9 Jan. 1974.
37	PES	Explorer 51 (AE-C) (1973 101A)	12/13/73	WTR	Delta	NASA	132.4	155	4 297	68.1	Current, good data being received.
38	DB-10	1974 20A	4/10/74	WTR	Titan 3D	USAF	89	158	291	95	Good data obtained until DB turned off 14 June 1974.
39	DB-11	1974 85A	10/29/74	WTR	Titan 3D	USAF	89	165	282	96.7	Good data obtained until DB turned off 1 Jan. 1975.
40	SPM	NOAA-4 (ITOS-G) (1974 89A)	11/15/74	WTR	Thorad Delta	NOAA	114.9	2 681	2 707	101.7	Good data obtained.
41	DB-12	1975 51A	6/ 8/75	WTR	Titan 3D	USAF	89	165	289	96.4	Good data obtained until DB turned off 3 Aug. 1975.
42	UAE (MA-059)	Apollo-Soyuz Test Project	6/15/75	KSC	Saturn IB	NASA	Manned Space Mission ≈223 km Circular Earth Orbit				Good data obtained.
43	PES	Explorer (AE-D) (1975 96A)	10/ 6/75	WTR	Delta	NASA	117.6	135	3 004	90.1	Good data obtained until 28 Jan. 1976; satellite reentered 12 Mar. 1976.
44	PES	Explorer (AE-E) (1975 107A)	11/20/75	WTR	Delta	NASA	114.3	152	2 707	19.7	Current, good data being received.
45	DB-13	1975 114A	12/ 4/75	WTR	Titan 3D	USAF	88.3	168	260	96.2	Good data obtained until DB turned off 6 Feb. 1976.
46	DB-14 (P/O MSD 180 Program	1976 38D 1976 38C 1976 38J	4/30/76	ETR	Titan 3D	NRL	107.5	1 087	1 132	63.4	Current, good data received.
47	DB-15	1976 65A	7/ 8/76	WTR	Titan 3D	USAF	88.6	168	262	96.9	Good data obtained until DB turned off 10 Sept. 1976.

*Footnotes

1. Abbreviations:
   a. SPM = Solar Proton Monitor, DB = Doppler Beacon, EPE = Energetic Particle Experiment, CPME = Charged Particle Measurement Experiment, PES = Photoelectron Spectrometer, MSD = Multiple Satellite Dispenser.
   b. NOAA = National Oceanic and Atmospheric Administration, ITOS = Improved TIROS Operational Satellite, TIROS = Television Infrared Observation Satellite, IMP = Interplanetary Monitoring Platform, AE = Atmospheric Explorer, UAE = Ultraviolet Absorption Exp.
   c. WTR = Western Test Range, ETR = Eastern Test Range, KSC = Kennedy Space Center.
2. Launch Date = local time at launch site.
3. Period in minutes, Perigee and Apogee in kilometers (approx.), Inclination in degrees from equator.

Table 1 (Concluded)
APL Instrumentation on Non-APL/JHU Spacecraft*

No.	APL Instrumentation[1a]	Satellite[1b]	Launch Data[1c] Date[2]	Site	Vehicle	Proj. Dir.	Orbit Data[3] Period	Perigee	Apogee	Incl.	Remarks
48	SPM	NOAA-5 (ITOS-H) (1976-77A)	7/29/76	WTR	Delta	NASA	116.2	1 507	1 522	102.0	Current, good data being received.
49	NAVPAC-1 DB-16	1977-56A	6/27/77	WTR	Titan 3D	USAF	88.4	168	268	96.9	Good data obtained until DB and NAVPAC turned off 21 Oct. and 23 Dec. 1977, resp.
50	LECP Exp.	Voyager 2	8/20/77	ETR	Titan IIIE/ Centaur D-1T	NASA		Interplanetary probe			Current, good data being received.
51	LECP Exp.	Voyager 1	9/5/77	ETR	Titan IIIE/ Centaur D-1T	NASA		Interplanetary probe			Current, good data being received.
52	DB-17(P/O) MSD Program	1977-112A 1977-112B 1977-112E	12/8/77	ETR	Titan 3D	NRL	107.5	1 054	1 167	63.4	Good data obtained until DB turned off 14 Feb. 1978.
53	PFM	IUE (1978-12A)	1/26/78	ETR	Delta	NASA	Modified geosynchronous orbit				Current, good data being received.
54	NAVPAC-2 DB-18	1978-29A	3/16/78	WTR	Titan 3D	USAF	88.3	171	259	96.4	Current, good data being received.
55	RA, SAR Data Link, DB, LRA	SEASAT-A (1978-64A)	6/27/78	WTR	Atlas F	NASA	100.7	769	799	108	Good data obtained until spacecraft electrical system malfunctioned on 10 Oct. 1978.

*Footnotes

1. Abbreviations:
   a. SPM = Solar Proton Monitor, Navigational Package, DB = Doppler Beacon, LECP Exp. = Low Energy Charged Particle Experiment, MSD = Multiple Satellite Dispenser, PFM = Particle Flux Monitor, IUE = International Ultraviolet Explorer, RA = Radar Altimeter, SAR = Synthetic Aperture Radar, LRA = Laser Retroreflector Array.
   b. NOAA = National Oceanic and Atmospheric Administration, ITOS = Improved TIROS Operational Satellite.
   c. WTR = Western Test Range, ETR = Eastern Test Range.
2. Launch Data = local time at launch site.
3. Period in minutes, Perigee and Apogee in kilometers (approx.), Inclination in degrees from equator.

I

TRANSIT-ON-DISCOVERER

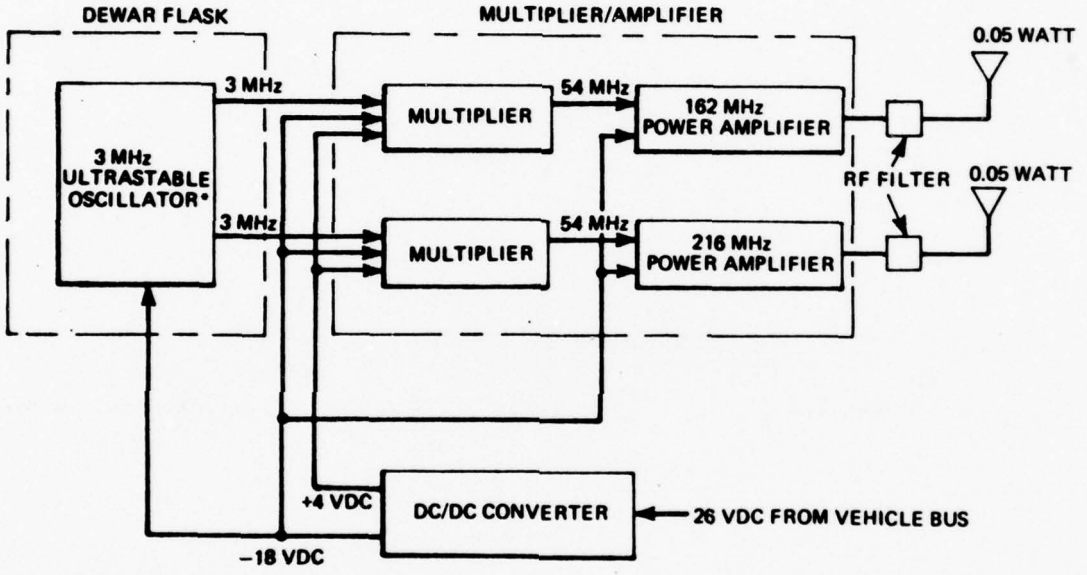

*FREQUENCY STABILITY: 1 PART IN 10^9

Fig. I-1 Transit-on-Discoverer Simplified Block Diagram

I

TRANSIT-ON-DISCOVERER

BACKGROUND

In July 1959, representatives of the Lockheed Missiles and Space Co. (LMSC) first discussed with APL the feasibility of employing a doppler tracking system on the Discoverer spacecraft launch vehicle. The doppler satellite navigation system had been conceived and was being developed by APL for the APL-proposed Transit satellites (now Navy Navigation Satellites). Tracking data obtained with the Transit-on-Discoverer (Fig. I-1) were to supplement optical tracking data that were being provided by the Smithsonian Astrophysical Observatory (SAO). Weather permitting, the SAO Baker-Nunn satellite tracking cameras were used to photograph an optical beacon system which consisted of four lamps mounted on the spacecraft vehicle and which were turned on by a vehicle orbital programmer. The photographs, together with the times taken, were used by SAO to prepare orbital parameters. The few precise fixes provided by the highly accurate SAO data were used to evaluate the APL doppler tracking technique and the VERLORT (Very Long Range Tracking) system of obtaining orbital elements and ephemerides.

TOD was a predecessor to the Doppler Beacons discussed in Section VI. The first beacons were flown in early 1970, and they are still being provided by APL to various user agencies.

APPLICATION

To track the Discoverer vehicles in their typically low altitude polar orbits, LMSC desired a lightweight, high-accuracy tracking system consisting of operationally simple, relatively inexpensive satellite equipment and ground support stations. Since preparations for a TOD flight were not unlike those for a Transit satellite, they afforded APL with the opportunity for exercising and perfecting Transit satellite ground station equipment, developing methods for coordinated station communications and station alerting, and preparing computing and analysis programs and facilities. Additionally, APL could verify the accuracy of doppler tracking by comparing TOD fixes with corresponding fixes provided by the SAO photographs and the radar tracking observations of VERLORT.

EQUIPMENT DESCRIPTION

The TOD consisted of an extremely stable transmitter which continuously transmitted two frequencies (162 MHz and 216 MHz) so as to ensure adequate correction for ionospheric refraction. To maintain the desired frequency stability, the 3 MHz crystal used in the oscillator was placed in a Dewar flask. The flask consisted of concentric cylinders of aluminum which were polished and gold plated for heat reflection. The unit was filled with dry nitrogen prior to flight, but vented to ambient pressure before orbit injection. The oscillator was located inside the first cylinder of the Dewar flask such that the heat generated by the oscillator transistors did not affect the crystal temperature. Provided with its own antenna system, the TOD operated independently of the payload and required only satellite power.

Discoverer consisted of a first stage Thor and second stage Agena-B launch vehicle. About one day after the Agena had achieved orbit, the payload was ejected from the vehicle in the vicinity of Hawaii for subsequent recovery. Thus, the Discoverer orbit was in two phases; the first 24 hours prior to payload ejection and the remaining several days prior to battery exhaustion and radio silence. Doppler tracking of the TOD 162/216 MHz signals was performed at five TRANET stations, including APL/JHU Station 111 in Maryland, and at a cooperating station in Lasham, England. The stations were controlled by the Satellite Control and Communications Center at APL, and all data were sent to the Center for processing to obtain accurate orbit ephemerides.

FUNCTIONAL OPERATION

The principles of operation for Transit-on-Discoverer were similar to those of the Doppler Beacon, except that TOD transmitted on 162/216 MHz and the beacons employ 162/324 MHz. Refer to Section VI for a functional description of the Doppler Beacon.

FLIGHT RESULTS

TODs were flown aboard the following Discoverer spacecraft:

Satellite	Launch Date	Reference
--*	4 Feb 1960	line 1, Table 1
--*	19 Feb 1960	line 2, Table 1
1960 Delta 1	15 Apr 1960	line 3, Table 1
1960 Kappa 1	18 Aug 1960	line 4, Table 1
--*	26 Oct 1960	line 5, Table 1
1960 Omicron 1	12 Nov 1960	line 6, Table 1
1960 Sigma 1	7 Dec 1960	line 7, Table 1
1961 Epsilon 1	17 Feb 1961	line 8, Table 1
1961 Lambda 1	8 Apr 1961	line 9, Table 1

*Failed to achieve orbit.

Right ascension and declination comparisons of APL computed values derived from TOD ephemerides were found to be in good agreement with SAO values derived from Baker-Nunn camera observations. Forty sets of usable SAO data, i.e., those for which APL had prepared ephemerides, were received from camera sites in Curacao, Dutch West Indies, Organ Pass, New Mexico, and Tokyo, Japan from the Discoverer 17 (1960 Omicron 1) flight. Right ascension differences are shown in Fig. I-2(a) and declination differences are shown in Fig. I-2(b). Each point is the mean value of six to nine differences which occur within an interval of one minute. The line drawn to either side of the point specifies the SAO standard deviation at the minimum range of the satellite for which the point is plotted. The dashed line indicates the mean value of the differences, and the solid lines represent the standard deviation of the differences from the mean value. Curacao and Organ Pass differences were found to yield a standard deviation of less than ±3 km ascension and of less than ±7 km in declination. The Tokyo data were not included in the analysis since they produced differences of about 200 km and, as later corroborated by radar data, were obviously invalid.

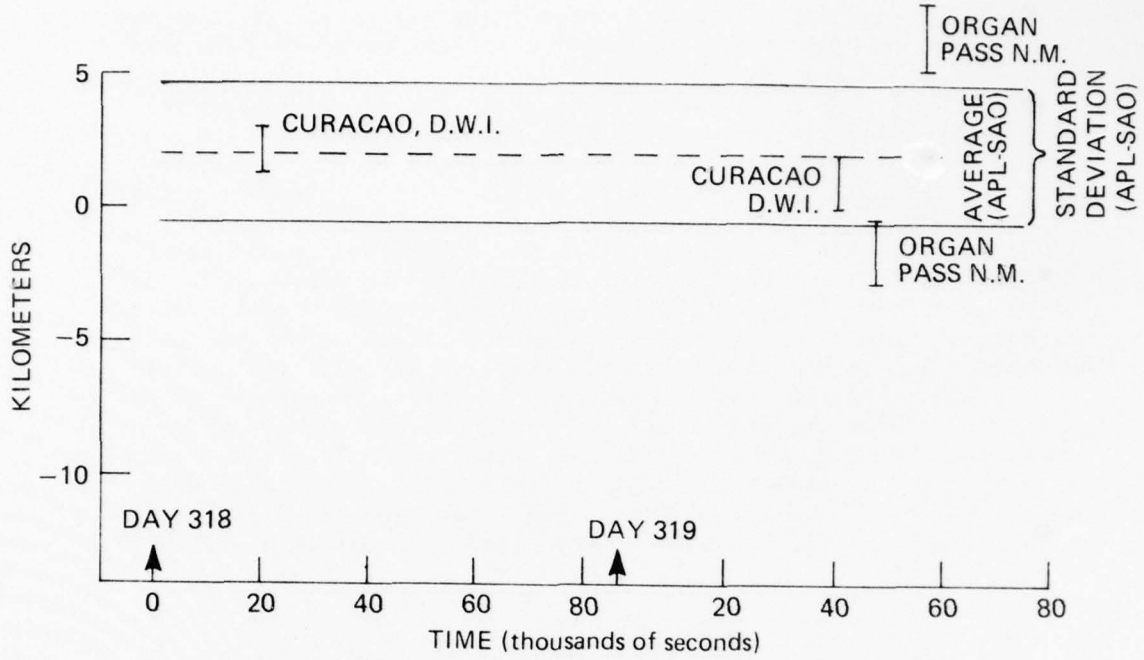

(a) RIGHT ASCENSION

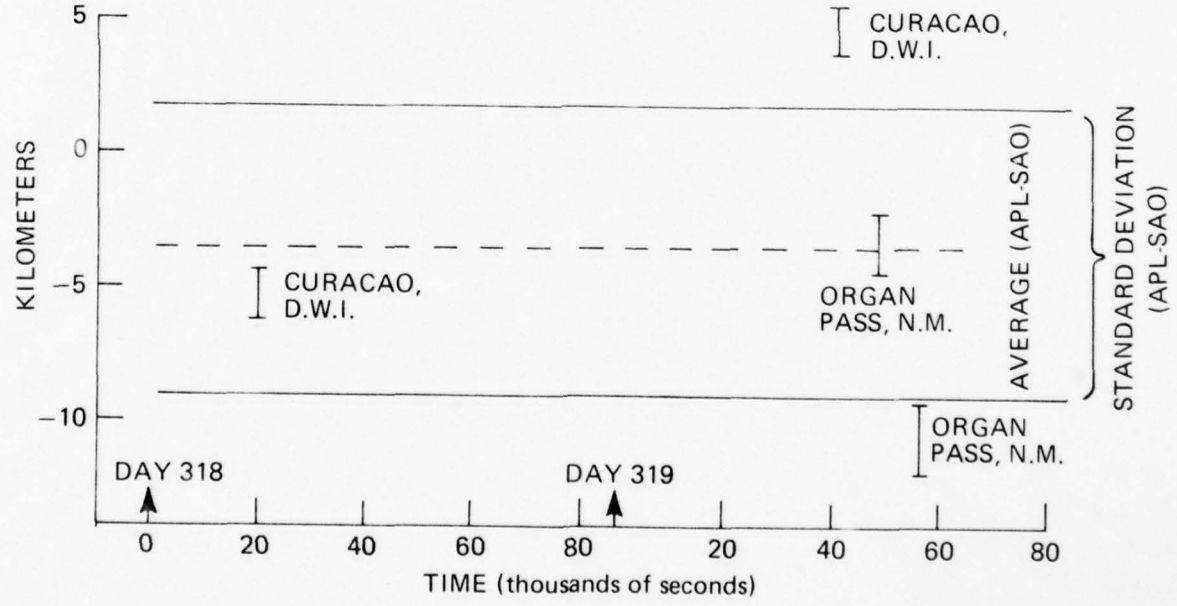

(b) DECLINATION

Fig. I-2 Discover 17 SAO Optical and TOD Doppler Data Fix Comparisons

II

INJUN SATELLITE PROTON INSTRUMENTATION

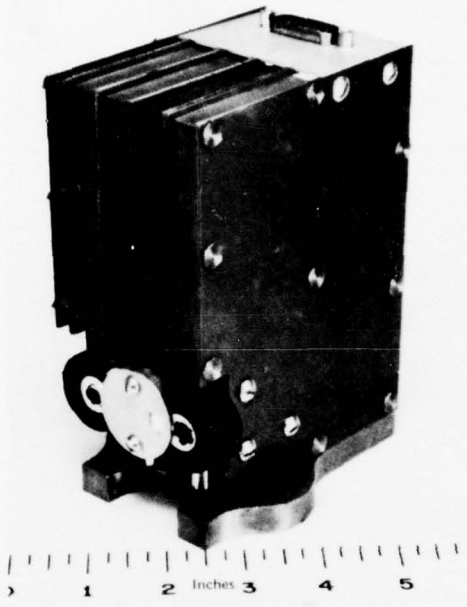

APL Proton detector package

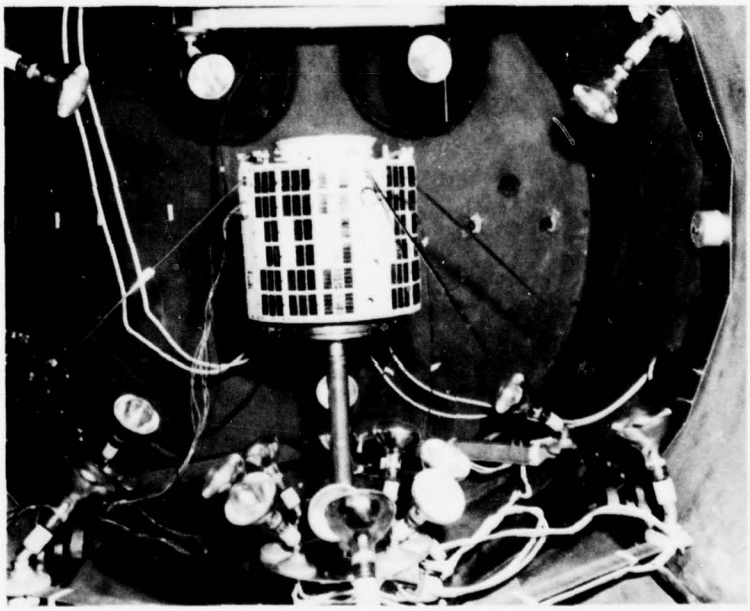

Satellite during thermal vacuum tests at APL

Fig. II-1 INJUN 1 and Proton Detector Package

II

INJUN SATELLITE PROTON INSTRUMENTATION

BACKGROUND

The first solid-state radiation detectors flown on a satellite were the low energy Proton Detectors developed and built by APL for the State University of Iowa (SUI) INJUN-1 satellite (Fig. II-1). This radiation research satellite was designed to provide further information on the energy spectra of the protons and electrons that make up the geomagnetically trapped radiation zones discovered by SUI Professor J. A. Van Allen, formerly Supervisor of Upper Air Exploration at APL/JHU. While much had been learned about the composition and extent of the Van Allen Belt, further data were required to account in detail for the origin and behavior of the radiation zones.

In addition to its scientific value to the geophysics community, however, a more accurate description of the Van Allen Belt than presently existed was of great importance to APL for the very practical reason that ionizing radiations have a damaging effect on the operation of solar cells, transistors, and various other satellite components. It was imperative that the operational environment of the Navy Navigation Satellite System (NNSS — formerly known as Transit), then in advanced development at APL, be well understood so that the satellites could be designed to operate satisfactorily for the required five-year lifetime.

The INJUN-1 satellite and the NRL (Naval Research Laboratory) GREB (Galactic Radiation Energy Balance) satellite, which was designed to measure solar Lyman-alpha and X-radiation, were included in the APL Transit 4-A satellite launching to fully utilize the payload capability of the Thor-Able Star launch vehicle (Fig. II-2). This launching marked the first attempt to orbit three satellites simultaneously.

APPLICATION

The INJUN-1 instrument complement is listed in Table II-1; as noted, the Proton Detectors were provided by APL. Scientific objectives of the INJUN satellites included the following:

1. Measure, with total energy and selective energy detectors, the particle fluxes moving parallel and perpendicular to the geomagnetic field over a wide range of magnetic latitudes, including both Van Allen radiation zones.

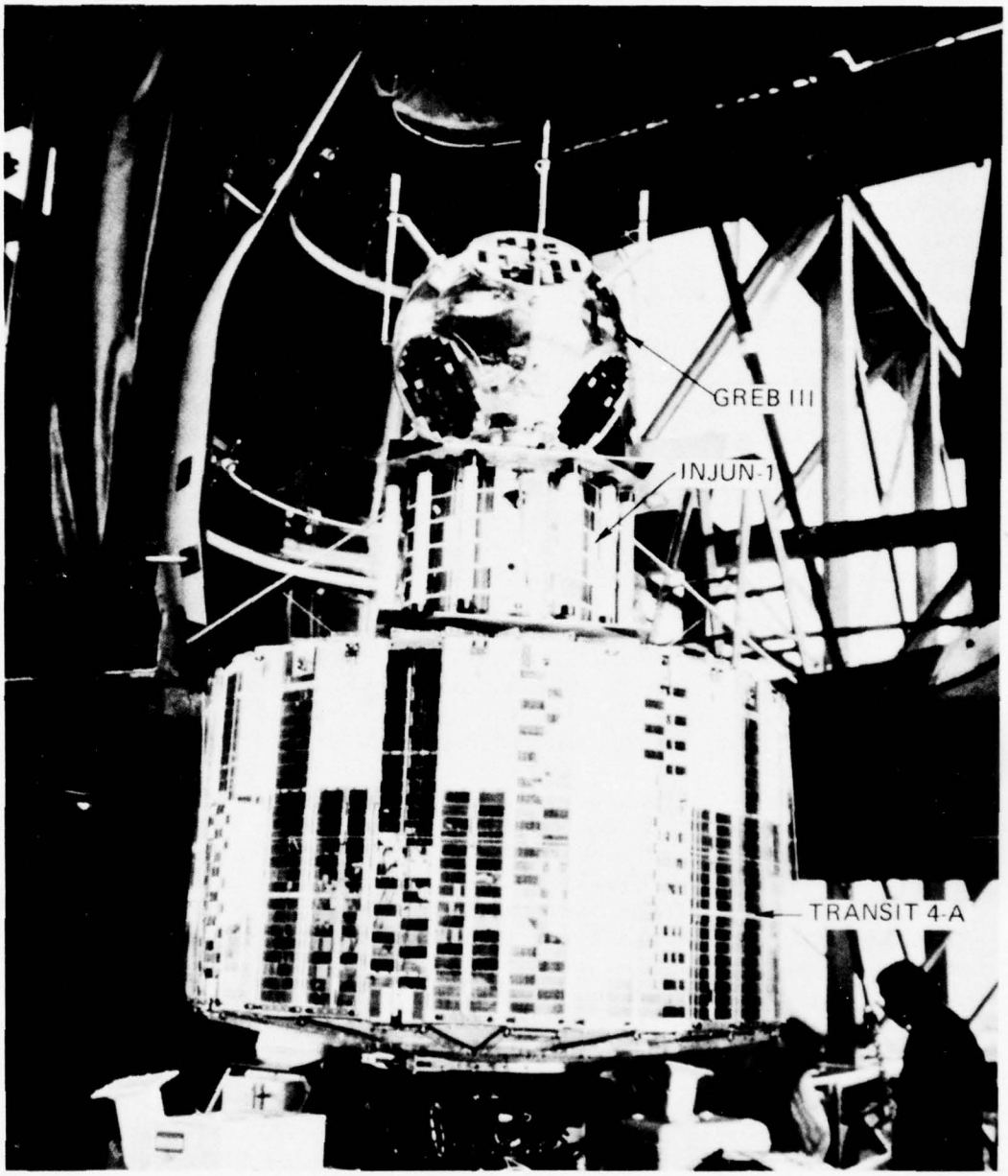

Fig. II-2 INJUN-1 Satellite in First Triple Payload

Table II-1

INJUN-1 Satellite Radiation Detectors

Instrument	Detection Feature	Orientation*
CdS Total Energy	Proton > 5 keV Electrons > 100 eV Light	$\theta = 180°$
CdS with Magnetic Broom	Protons > 5 keV Electrons > 250 keV Light	$\theta = 180°$
CdS Total Energy	Protons > 5 keV Electrons > 100 eV Light	$\theta = 90°$
CdS with Magnetic Broom	Protons > 5 keV Electrons > 250 keV Light	$\theta = 90°$
CdS Optical Monitor	Light	$\theta = 90°$
213 GM Counter	Electrons > 30 keV Protons > 0.5 MeV	$\theta = 90°$
Photometer	Light of 5577 Å	$\theta = 0°$
Magnetic Spectrometer		
GM a	Electrons 45-60 keV	
GM b	Electrons 80-100 keV	$\theta = 90°$
GM c	Background Monitor	
Proton Detector**	Trapped Protons 1-17 MeV	$\theta = 90°$
Proton Detector**	Trapped Protons, Background	$\theta = 90°$
Proton Detector**	Solar Protons 1-17 MeV	$\theta = 180°$
Proton Detector**	Solar Protons, Background	$\theta = 180°$

*Orientation is referred to the magnetic field line, with $\theta = 0°$ being the downward direction in the Northern Hemisphere.
**Provided by APL/JHU.

2. Measure the absolute particle flux trapped in both radiation zones, and provide data for a limited study of its energy dependence.

3. Monitor cosmic rays and solar protons over a wide range of magnetic latitudes.

4. Enable detailed plotting of the auroral zones by both photometric and particle flux methods with high spatial and time resolution.

5. Provide data for a study of the latitude variation of airglow and auroral emissions and subsequent correlation with phenomena measured at several ground stations in the United States and Canada.

Instruments similar to many of those on the INJUN satellites were carried on other, later satellites. This made comparisons of data thus obtained in different flights highly meaningful.

EQUIPMENT DESCRIPTION

The APL proton-detection units for the INJUN-1 satellite consisted of two pairs of detectors. One pair was mounted so that the two detectors looked out at right angles to the satellite axis and thus at right angles to the earth's magnetic field. This pair measured trapped protons in the inner Van Allen radiation zone. The other pair was mounted so that the detectors looked out parallel to the satellite axis and thus parallel to the magnetic field. These two detectors actually looked out through the bottom of the satellite (as viewed on the launch pad) and thus, because of the orientation of the satellite's permanent magnet, they looked upward at high northern latitudes to measure solar protons.

All four detectors were symmetrically mounted in an aluminum housing so that they were essentially identically shielded. Small permanent magnets were mounted over the detectors to prevent electrons of less than 250 keV from reaching the detectors. One detector of each pair had an opening of 0.18 steradian through the magnet; the other detector of the pair had an aluminum plug in its opening so as to serve as a background monitor for the active detector. Each detector was 4 by 4 mm in area and all were made from the same resistivity silicon and were similarly biased to ensure identical operation and thus facilitate intercomparisons. Since the detectors were light sensitive, the active member of each pair was covered with aluminized Mylar foil. The response range for the active detectors was 1-15 MeV.

The electronic circuit of each detector consisted of four parts: a charge sensitive preamplifier followed by two stages of voltage amplification and a discriminator pulse shaper. The discrimination level set at the output of the second voltage amplifier was adjusted to correspond to 900 keV energy deposition in the detector. Pulses large enough to pass the discrimination threshold fired a univibrator whose output was tailored to the input requirements of the satellite data handling system. The proton detector package weighed 1060 grams and required 250 milliwatts at +18 VDC.

FUNCTIONAL OPERATION

Proton Detectors

The APL charged particle detectors were of the p-n silicon junction type. When such a junction is reverse biased, a region is formed that is free of conducting electrons and holes. The passage of a charged particle through the depleted layer creates electron-hole pairs that are separated by the electric field, and the electrons and holes are collected at the junction surfaces. The collection of the charge can be observed and the passage of the incident particle thus noted exactly as is done with an ordinary gas filled ionization chamber.

Junction detectors have several advantages for measurements of protons in space. They are small and light, can be operated on low voltages (e.g., 10-50 volts), and consume essentially no power. The depletion layer is so thin, generally on the order of 100 microns, that the junctions are insensitive to X-rays and bremstrahlung; in addition, they can be made insensitive to electrons. The size of the output pulse of the detection unit is proportional to the energy deposited in the junction's depletion layer. By selecting an appropriate absorber to cover the entrance hole in a suitable shield and by adjusting the discrimination level, it is generally possible to select a desired energy range with a given detector.

Spacecraft Subsystems

The satellite data handling system consisted of 64 four-bit binary shift register accumulators. Each of the 14 radiation detectors was allotted a number of accumulators consistent with the expected counting rate. In addition, the digital message contained a Barker synchronizing word, the satellite clock data, various voltage and temperature measurements, and data from a magnetic aspect sensor. Data were read continuously from the accumulators at the rate of 256 bps. Thirteen of the detectors were read once

per second, or to a spatial resolution of 10 km. The last detector was, in effect, read four times per second, or to a spatial resolution of 2.5 km, in order to investigate localized auroral phenomena. A frequency-shift keying between 3072 and 4096 Hz was used to indicate binary information readout of the accumulators. Data were transmitted to ground stations using amplitude modulation on a 136.5 MHz carrier with 200 mW of power.

The data encoding and telemetry system was designed to permit a direct output from simple ground receiving equipment into a digital computer. The predicted S/N ratio at a 3000 km slant range was above 21 dB, at least 9 dB above the threshold for automatic data processing.

The total satellite power required was 2.0 watts. Since this was not sufficient for all components to operate continuously, the satellite subsystems remained normally in a standby condition with only a command receiver and part of the data system operating. The command receiver was interrogated from ground stations at Iowa City, Iowa, and Lima, Peru, and the satellite turned fully on for various periods subject to the available satellite power.

FLIGHT RESULTS

The simultaneous launch of INJUN 1 with the GREB and Transit 4-A satellites on 29 June 1961 was successful except for the failure of the separation mechanism between INJUN and GREB. The INJUN magnetic attitude control system could not orient the combined payloads, and the photometer was shielded by GREB and thus rendered useless; all other satellite components operated satisfactorily. The INJUN-1 high inclination orbit (line 10, Table 1) made it well suited to the taking of radiation measurements as it passed through the auroral zones, the lower reaches of the outer Van Allen Belt, and the inner belt.

The period 12-28 July 1961 was noted by the appearance of a large number of solar flares followed by such geophysical phenomena as magnetic storms and ionospheric disturbances. Protons emitted by the sun were observed in the terrestrial atmosphere by the satellite detectors, permitting for the first time a quantitative analysis of the proton flux and its variation in the geomagnetic field during both quiet and disturbed magnetic conditions.

The INJUN-1 satellite represented the first APL attempt to assess the environment in which the operational NNSS would function. The success of the experiments, particularly the operation of the Proton Detectors, led to an expanded research program at APL concerning particle measurements and their effects on satellite components.

The INJUN-3 satellite, essentially a 60.96-cm diameter sphere weighing about 47.6 Hg, included the APL Proton Spectrometers shown in Fig. II-3. Launched on 12 December 1962 (line 11, Table 1), the satellite's initial apogee and perigee altitudes of 2782 km and 246 km, respectively, differed significantly from the nominal orbit that was to be circular at 950 km. INJUN 3 carried 18 particle detectors, three photometers, and a VLF electromagnetic wave detector (Table II-2). While an operational satellite, the effects of the undesired orientation and apogee included the following: (1) several detectors that were installed to detect particles causing auroras, or in general dumped particles in the planned orbit, detected trapped particles instead, (2) because the orbit was changing due to atmospheric drag, it was difficult to measure accurately and command scheduling predictions were accurate, and (3) the planned study of diurnal variations of several phenomena was rendered almost impossible.

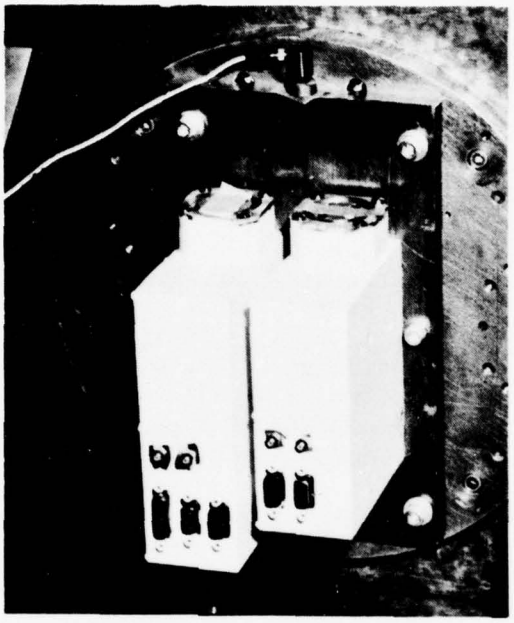

APL Proton spectrometers

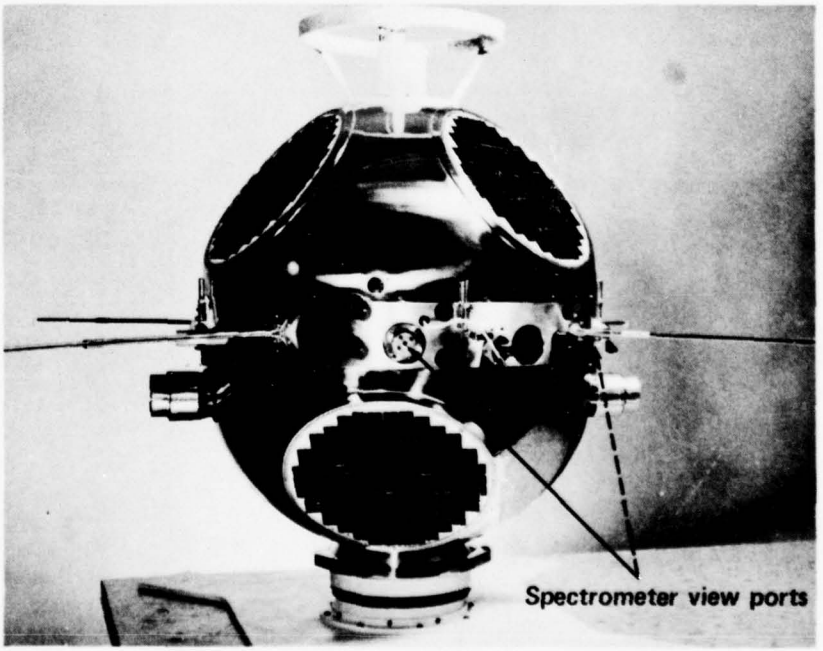

INJUN-3 Satellite

Fig. II-3 INJUN 3 and Proton Spectrometers

Table II-2
INJUN-3 Satellite Radiation Detectors

Detector	Orientation*	Detectable Radiation: Proton Energies	Detectable Radiation: Electron Energies
213 Geiger Counter	α - 90°	E $\gtrsim$ 0.5 MeV	E $\gtrsim$ 40 KeV
Pulse Scintillator	Omni.	E $\gtrsim$ 36 MeV	- -
213 Geiger Counter	α - 90°	E $\gtrsim$ 4 MeV	E $\gtrsim$ 250 KeV
213 Geiger Counter	α - 130°	E $\gtrsim$ 0.5 MeV	E $\gtrsim$ 40 KeV
213 Geiger Counter	α - 180°	E $\gtrsim$ 0.5 MeV	E $\gtrsim$ 40 KeV
302 Geiger Counter	Omni.	E $\gtrsim$ 20 MeV	E $\gtrsim$ 1.5 MeV
Magnetic (a)		- -	40 < E < 60 KeV
Electron (b)	α - 90°	- -	80 < E < 110 MeV
Spectrometer (c)		E > 40 MeV	E > 5 MeV
D.C. Scintillator	α - 130°	E $\gtrsim$ 100 KeV	E > 5 KeV
Electron Multiplier	α - 130°	E $\gtrsim$ 100 KeV	E > 5 KeV
P-N Junction (a)**	α - 90°	0.5 < E < 2 MeV (for each pair)	- -
P-N Junction (b)**	α - 90°	2 < E < 8 MeV (for each pair)	- -
P-N Junction (c)**	α - 180°	8 < E < 26 MeV (for each pair)	- -
P-N Junction (d)**	α - 180°	26 < E < 160 MeV (for each pair)	- -
Photometer (a)	α - 0°	Light of 5577 Å	
Photometer (b)	α - 0°	Light of 6300 Å	
Photometer (c)	α - 180°	Light of 5577 Å	
VLF Detector	-----	VLF 1 kHz to 20 kHz in 6 Frequency Bands and Carrier Modulation 1 to 5 kHz	
Integral (a)	α - 90°	E $\gtrsim$ 4 MeV	E $\gtrsim$ 500 KeV
Magnetic (b)	α - 90°	E $\gtrsim$ 4 MeV	E $\gtrsim$ 1 MeV
Spectrometer (c)	α - 90°	E $\gtrsim$ 40 MeV	E $\gtrsim$ 5 MeV

* Orientation is referred to the direction of the magnetic field line, such that α=0° corresponds to a detector looking downwards towards the earth in the northern hemisphere.

** Provided by APL/JHU.

III

MAGNETIC ATTITUDE CONTROL SYSTEM

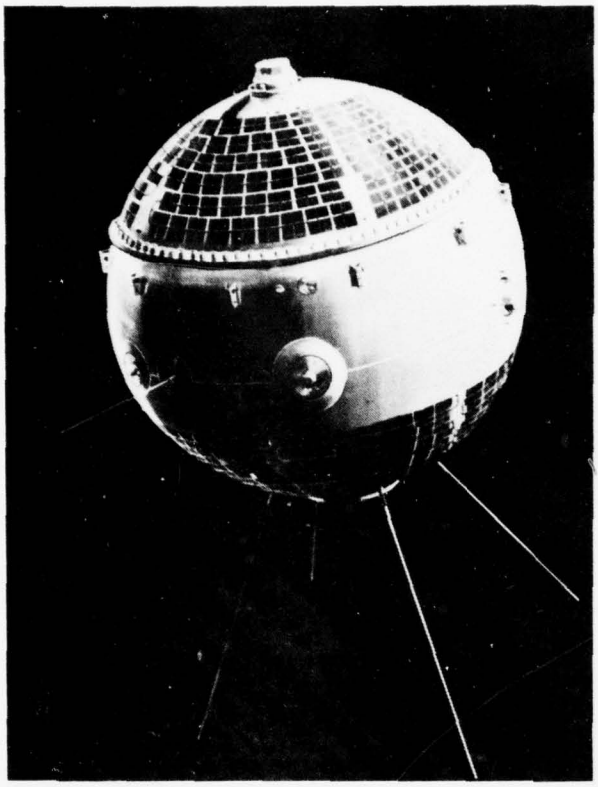

(a) AE-B (1966 44A)

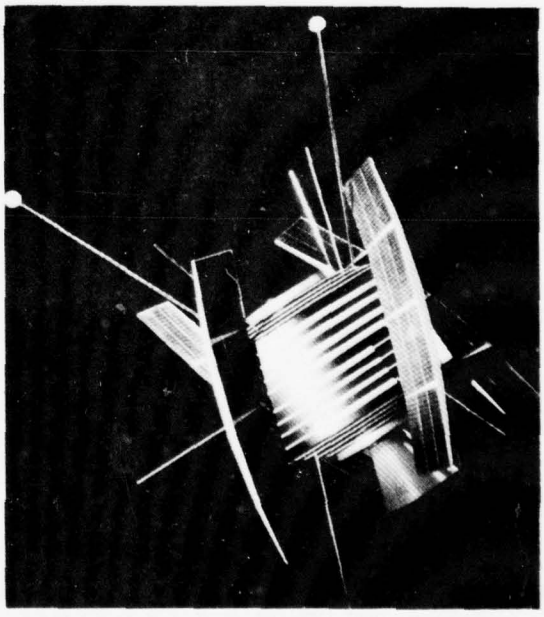

(b) RAE-1 (1968 55A)

Fig. III-1 Satellites With APL Magnetic Attitude Control Systems

III

MAGNETIC ATTITUDE CONTROL SYSTEM

BACKGROUND

Satellites with attitude control systems developed by APL have established such firsts as:

- The first use of magnetic techniques for attitude orientation, and of magnetic hysteresis rods for damping satellite motion (Transit 1B launched in April 1960).

- First use of electromagnets for temporary magnetic stabilization (TRAAC launched in November 1961).

- First gravity gradient stabilization of a satellite (Transit 5A-3 launched in June 1963).

- First design and use of a magnetic spin/despin system (DME-A launched in November 1965).

Several contributions to the art of satellite control and stabilization were also made with the launch in July 1967 of the DODGE (Department of Defense Gravity Experiment) satellite. These satellites were designed and fabricated at APL. In addition, satellites developed by other agencies have employed attitude control systems supplied by APL. These include the NASA/GSFC-developed AE-B (Atmospheric Explorer-B) and RAE-1 (Radio Astronomy Explorer-1) satellites.

APPLICATION

Scientific Objectives

The AE-B satellite (Fig. III-1a) mission was to obtain direct measurement data to help define the structure of the atmosphere on a global basis, to aid in the study of the physics of the upper atmosphere, and to extend the knowledge of solar-terrestrial relationships. AE-B consisted of a 76.2 cm stainless steel spherical shell which housed six aeronomy experiments and associated electronics for a total weight of about 218 kg.

The mission of the RAE-1 satellite (Fig. III-1b) was to monitor low frequency radio signals from cosmic sources, from our own solar system, and from the earth's magnetosphere and radiation

belts. Also, to monitor the sporadic radio bursts from the region of Jupiter for correlation with simultaneous high frequency observations made by the global Jupiter Monitoring Network. The satellite body was a cylindrical aluminum structure with four 150 cm long helical solar panels, and the total satellite weight was about 189 kg.

Attitude Control System Requirements

The spin stabilized (30 rpm) AE-B had mounted about its equator a number of sampling devices, and it was desired that these devices view both the forward and wake regions of the free stream during each revolution so that compensation for forward velocity could more easily be made. To achieve this at all points in the orbit, it was required that the spin axis be oriented normal to the plane of the orbit.

The RAE-1 launch sequence required that the satellite plus its fourth stage apogee kick motor be placed into a transition orbit of 550 km perigee by 6000 km apogee and be spin stabilized at 74 rpm. Attitude measurements were then made to determine spin axis orientation to ensure proper attitude prior to firing the apogee boost motor. After the satellite was boosted into circular orbit, the fourth stage was ejected and the yo-yo despin cables were deployed to reduce the spin rate to a nominal 5 rpm. The magnetic torquing control system then reduced the residual spin and tumble to zero, and stabilized the spacecraft so that its Z-axis tracked the earth's magnetic field. Two V experiment antennas were then formed by deploying four booms 250 m in length. The spacecraft was gravity stabilized such that one V antenna pointed toward earth and the other toward the galactic sphere. A third antenna consisted of a dipole deployed normal to the Z axis of the satellite.

EQUIPMENT DESCRIPTION AND FUNCTIONAL OPERATION

AE-B Satellite Control System

The forerunner of AE-B, the AE-A satellite, experienced large variations in spin axis orientation with time. This unwanted precession apparently originated from the interaction of the earth's magnetic field with the natural satellite dipole moment. The AE-B magnetic attitude control system (MACS) included magnetic actuators to control the precession such as observed on AE-A, and a second set of magnetic actuators to control satellite spin rate.

Spin-axis orientation was controlled by artificially creating a dipole moment of M or O. The AE-B variable magnet was a

permanent one, with a dipole monent M/2, and a variable magnet, with a dipole-moment range ±M/2 (Fig. III-2a). Upon ground command, a capacitor bank was discharged through the windings of the variable magnet, in one direction or the other, to produce dipole moments of M or 0. The variable magnet was built from a vanadium-permendur alloy.

The AE-B could be spun up or down by ground command. Two electromagnets, shown in Fig. III-2b, were aligned with the two satellite axes perpendicular to the spin axis. Torque about the spin axis was generated, after the fashion of a dc motor, by interaction between the earth's field and the electromagnetic fields. The vector magnetometers generated signals proportional to the earth's field. These were amplified to activate the electromagnets. To obtain dc motor action, the X-axis magnetometer drove the Y-axis electromagnet with a 180° phase change, and the Y-axis magnetometer drove the X-axis electromagnet. The change in the AE-B spin rate, using this approach, could be as high as 15 rpm/day.

RAE-1 Satellite Control System

To achieve magnetic stabilization of the RAE-1, an active control system was required which would perform the following:

1. Magnetic field measurements to be used for attitude determination,

2. Spin axis orientation prior to firing the apogee motor while in the transition orbit,

3. Damping of spacecraft spin and tumble following injection of the satellite into final orbit,

4. Magnetic stabilization and damping of oscillations, and

5. As a backup system for damping libration.

To meet the objectives, APL supplied the MACS shown in Fig. III-3. Most of the magnetic attitude control functions intended for RAE are provided for on APL low altitude satellites by magnetometers, an electromagnet, and a set of passive hysteresis rods. However, passive rods could not be used on RAE because the magnetic field is quite weak at 6000 km and long hysteresis rods could not be tolerated within the spacecraft. A scheme of "enhanced" magnetic damping was therefore developed by APL in which a hysteresis function generator was used in conjunction with a set of electromagnets. This system provided detumble and magnetic stabilization equivalent to passive rods at lower orbits.

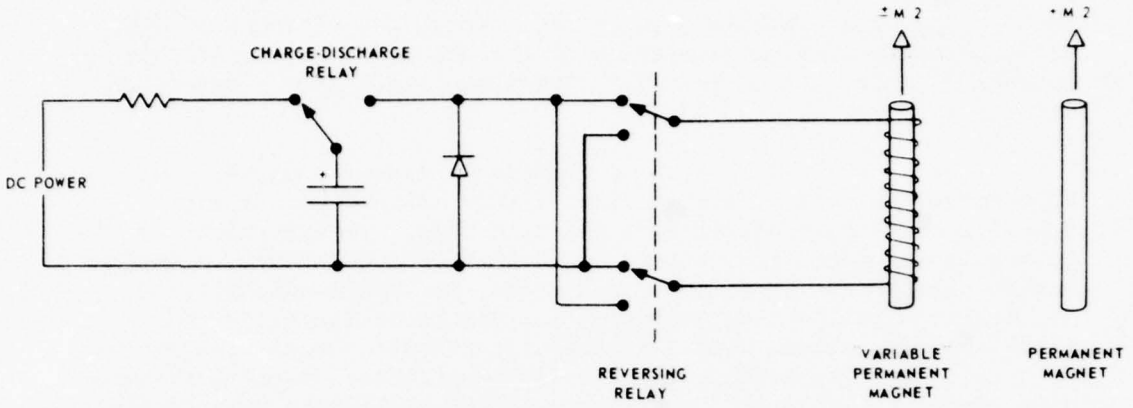

(a) PULSE MAGNETIZER SYSTEM

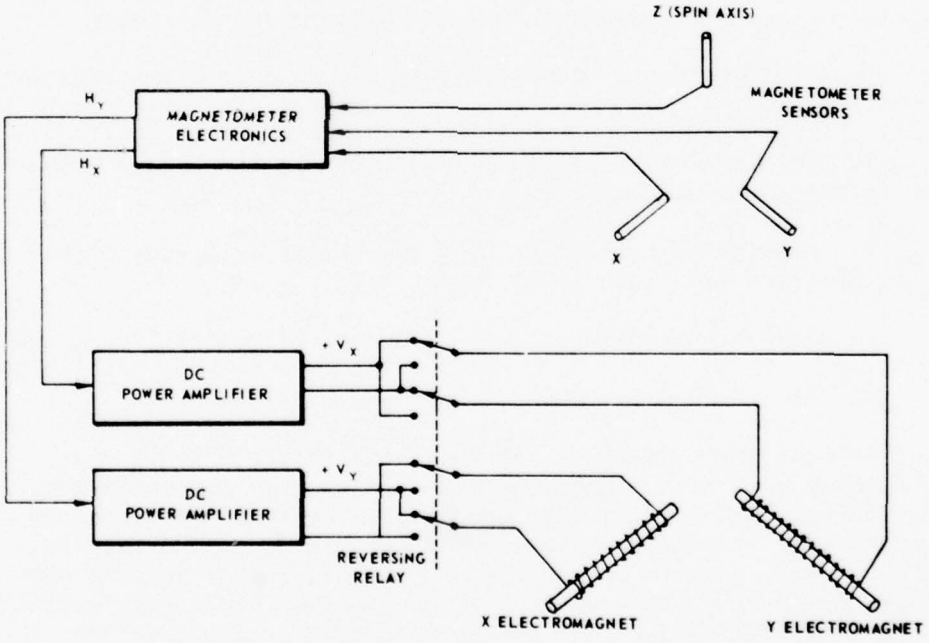

(b) SPIN TORQUE SYSTEM

Fig. III-2 AE-B Pulsed Magnetic Actuator and Torque Systems, Simplified Schematics

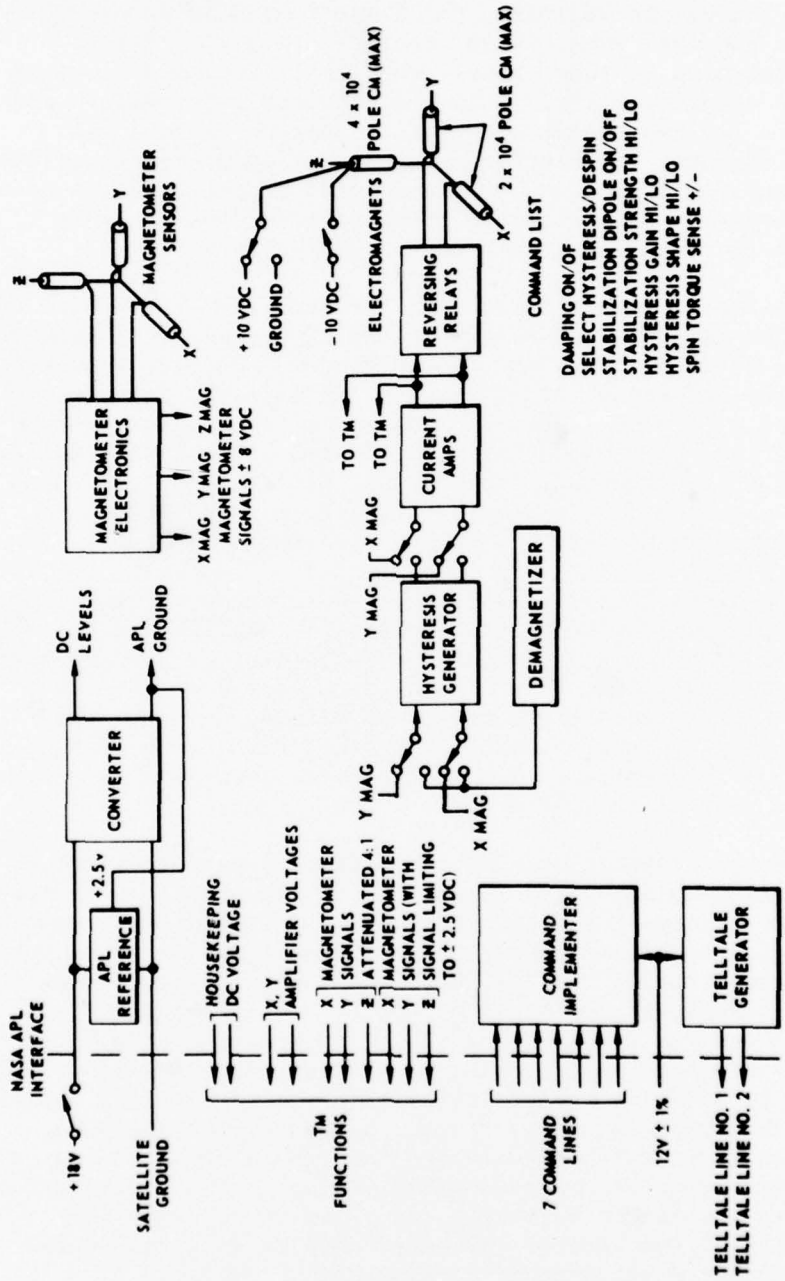

Fig. III-3 RAE-1 Magnetic Attitude Control System, Functional Block Diagram

A three-axis vector magnetometer measured the earth's magnetic field and produced three output signals proportional to the field components. The nominal linear range of the magnetometers was ±100 moe. These signals were telemetered to ground for attitude determination. In addition, the X and Y signals served as inputs to the damping system which consisted of a two-channel hysteresis generator, a two-channel power amplifier, and a set of X- and Y-axis electromagnets. Both the hysteresis generators and the amplifiers had two operational gain states which could be selected by command. The electromagnets provided magnetic torques for damping satellite spin and tumble as well as oscillations associated with magnetic stabilization. The maximum dipole moment strength of these electromagnets was 2×10^4 pole-cm.

A Z-axis electromagnet was used for spin axis precession and tracking of the earth's magnetic field during the magnetic stabilization phase. This electromagnet could be commanded to produce a constant dipole moment of 4×10^4 or 1×10^4 pole-cm, or it could be turned off. The MACS included a magnetometer compensation system, a passive feedback network, which removed the magnetic fields produced by the electomagnets from the magnetometer sensors. The demagnetizer was used in conjunction with the damping system to erase on command the history of the hysteresis generators.

The electronic hardware was packaged in three rectangular books (Fig. III-4). The total package was 12.7 by 17.8 cm by 10.8 cm deep and weighed 3.2 kg. The magnetometer sensors were mounted external to the book. The X and Y electromagnets were 40.6 cm long by 1.4 cm diameter Mumetal cores and weighed 0.09 kg each. The Z electromagnet consisted of four Mumetal rods, each 30.5 cm long by 1.17 cm in diameter. The four rods weighed 1.54 kg. Total weight of the system was 6.58 kg.

Operational capabilities of the MACS were verified through analog simulation by APL prior to spacecraft integration. In these simulations, prototype and flight unit control systems were used as analog elements which provided an exact model for magnetic hysteresis damping. During the design phase, analog simulation enabled APL to establish electromagnet dipole moment strengths and amplifier gains which would effect the most rapid despin and damping of oscillations as well as minimum steady state magnetic tracking errors. In addition, these simulations provided flight training whereby the operating modes of the control system could be changed as dynamic conditions dictated and thus effect more rapid damping or more accurate magnetic stabilization. Final simulations. which employed the flight hardware, confirmed the dynamic electrical performance of the control system as well as established the attitude performance which could be expected in orbit.

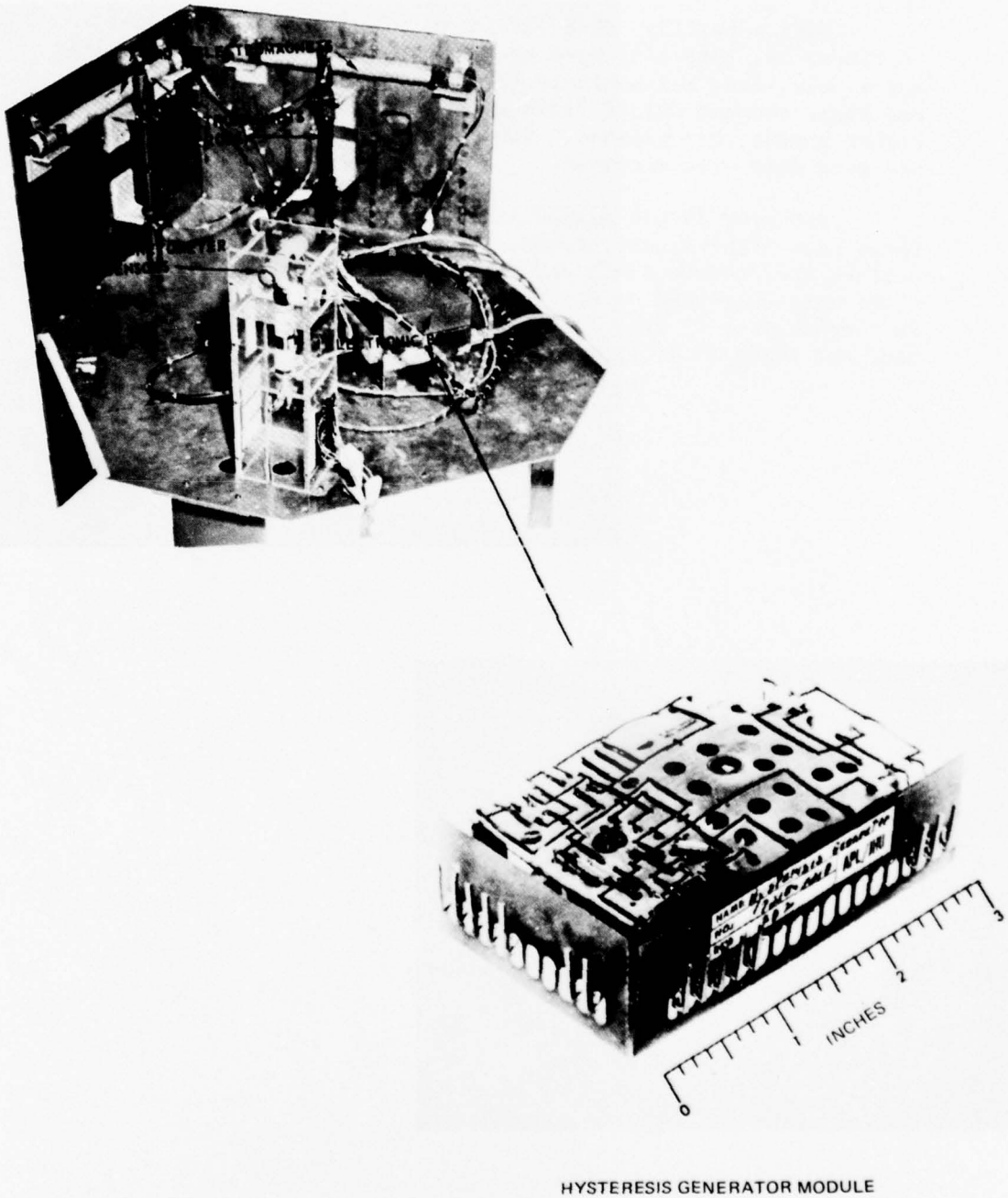

HYSTERESIS GENERATOR MODULE

Fig. III-4 RAE-1 Magnetic Attitude Control System Hardware

FLIGHT RESULTS

NASA satellites AE-B (Explorer 32, 1966 44A) and RAE-1 (Explorer 38, 1968 55A) were successfully launched on 25 May 1966 and 4 July 1968, respectively (lines 12 and 14, Table 1). A second stage command cutoff failure on Explorer 32 resulted in a much higher apogee than planned. However, the MACS functioned as planned and good data were received.

Explorer 38 was placed into a temporary elliptical orbit for three days after launch. Then, the apogee motor was ignited to achieve the desired orbit and inclination. Spacecraft despin operations were completed on 8 July, and the antennas were extended in increments from 22 July to 8 October 1968. The satellite was later declared to be fully operational.

IV

SOLAR PROTON MONITOR (IMP F AND G)

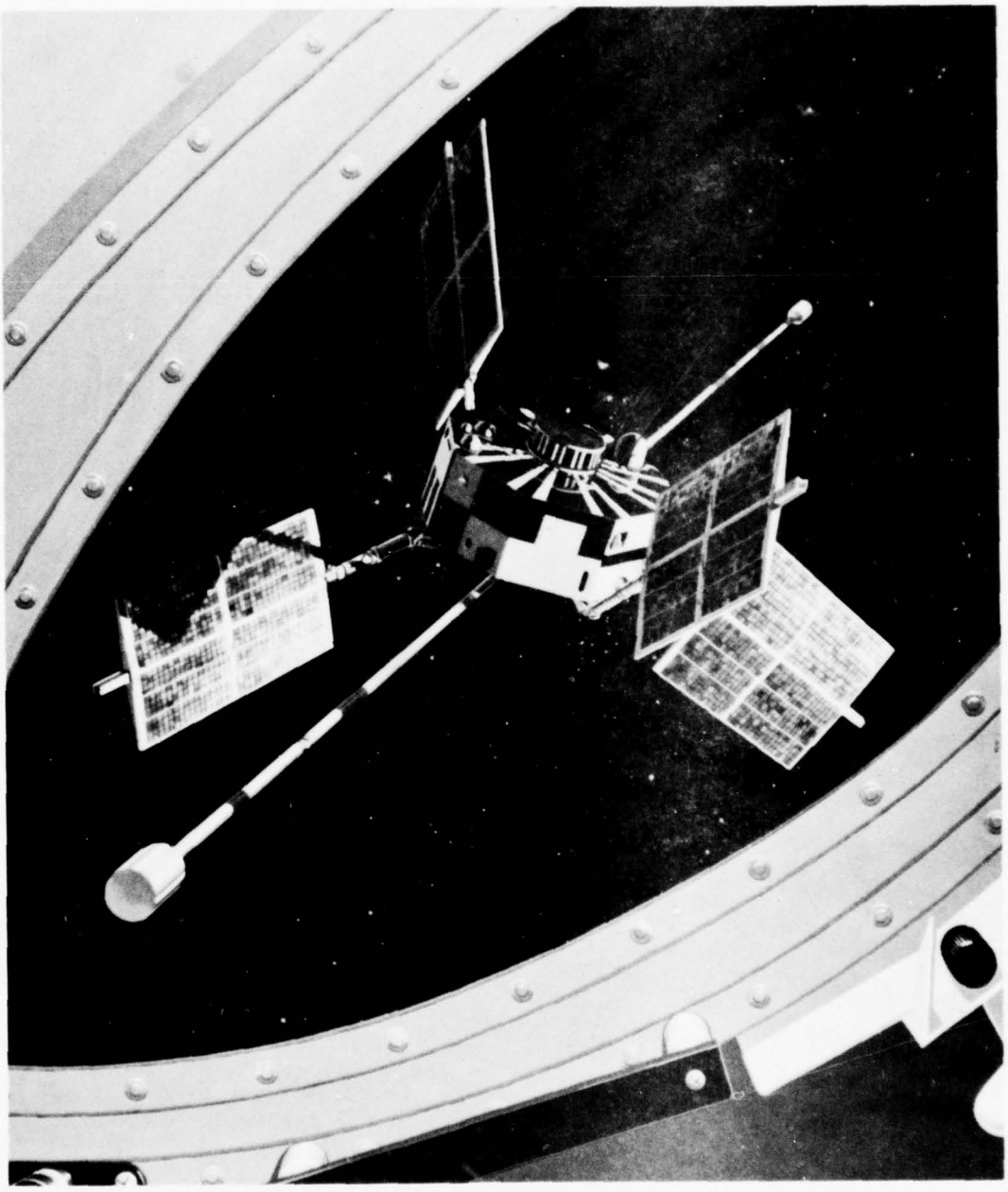

Fig. IV-1 IMP-F Spacecraft, Artist's Concept

IV

SOLAR PROTON MONITOR (IMP F AND G)

BACKGROUND

In June 1965, a joint proposal was issued by NASA/GSFC and APL outlining the requirements of a Solar Proton Monitor (SPM) that could be flown on the GSFC-designed IMP (Interplanetary Monitoring Platform) -F and -G spacecraft (Fig. IV-1). SPM features were similar to those of the Solar Proton Intensity and Composition Experiment (SPICE), which was designed about the same time to collect similar data during the ballistic trajectories of sounding rockets.

APPLICATION

During a seven year period (1956-1963) prior to the initial SPM proposal, there were at least 64 occasions when the sun accelerated nuclei to energies greater than a few MeV and these particles were subsequently detected in the vicinity of the earth. Such solar cosmic ray events are of fundamental importance for not only do they provide information on solar processes, but their propagation characteristics provide new clues to the magnetic field configurations in the vicinity of the sun and in interplanetary space. Furthermore, these solar particle outbursts pose important considerations for manned space travel in such programs as the (then) forthcoming Apollo Program.

The primary purpose of the SPMs flown aboard the IMP satellites was to provide systematic monitoring of solar cosmic rays over at least half a solar cycle. The basic requirements for such a monitoring program were:

1. To furnish simple, reliable flux and spectral measurements,

2. To operate over a wide flux range and, in particular, to provide coverage for very large events, and

3. To provide a simple and easily reproducible detector system to form the basis of an operational monitoring program.

EQUIPMENT DESCRIPTION

The IMP-F and -G Solar Proton Monitors were similar and consisted of an array of solid state detectors designed to measure

proton intensities in the following energy ranges: $1 \leq E_p \leq 10$ MeV, $E_p \geq 10$ MeV, $E_p \geq 30$ Mev, and $E_p \geq 60$ MeV. The overall design goal was to achieve a standard, rather simple detection scheme specifically intended for detecting solar protons. Separate detectors were used for each energy range, and combinations of discriminator levels and shielding thicknesses were employed to define the energy response of each channel. Such a method allowed for accurate, absolute flux determinations and for accurate unit to unit comparisons when using a series of payloads to monitor the solar flux over an extended time period (≥ 0.5 solar cycle). Since the specific goal of observing solar protons requires that useful data be obtained only at high magnetic latitudes or outside the magnetosphere, discrimination techniques for screening out a background flux of high energy (>100 keV) electrons were not included.

Table IV-1 lists the main characteristics of the various detectors including estimated count rates based on maximum observed solar proton flux values. Also shown are the cosmic ray background rates that must be considered when observing low level solar proton fluxes.

Channel 1 and Channel 2 Detectors

Each of these two higher energy channels consisted of three solid state detectors mounted on orthogonal axes and surrounded by a hemispherical shield (Fig. IV-2a). This arrangement provides an optimum method of obtaining a large area and a relatively smooth geometric factor when using disk shaped detectors. The shielding thickness is by far the most important factor in determining the energy threshold in this arrangement. As indicated, the thicknesses used were 5.6 mm Cu and 1.6 mm Cu.

The detectors used were surface barrier solid state detectors, fully depleted, 700 microns thick, having a usable surface area of 0.83 cm^3 and a noise level nominally <20 keV at the operating bias voltage. These units fully depleted at <150 volts and were operated at 200 volts. Radiation damage effects for channels 1 and 2 were negligible for several years due to the high bias levels, the shielding thickness, and mode of operation.

Channel 3

This detector consisted of a 3 mm cubic Li drifted solid state detector surrounded by a 170 mg/cm^2 (0.63 mm) Al shield (Fig. III-2b). The detector had a noise level of <50 keV at its operating bias of 200 volts. With a disciminator level of 300 keV, the energy threshold was raised ~25 keV. Radiation damage effects for this detector were thus negligible for the first year in orbit.

Table IV-1

Solar Proton Monitor Characteristics, IMP F and G

Channel	Energy Response	Geometric Factor(a)	Max. Observed Solar Proton Flux (MSPF)	Expected Count Rate from MSPF	Expected Count Rate from Cosmic Ray Background of ~ 2 cm^{-2} sec^{-1}	Approximate Weight of Detector Assembly and Shielding
1	$E_p \geq 60$ Mev	$\frac{2\pi}{4\pi} \times 3$ cm^2	$5(10)^3$ cm^{-2}sec^{-1} (c)	$7.5(10)^3$cps	3 cps	280 gms
2	$E_p \geq 30$ Mev	$\frac{2\pi}{4\pi} \times 3$ cm^2	$2(10)^4$ cm^{-2}sec^{-1} (b)	$3(10)^4$cps	3 cps	170 gms
3	$E_p \geq 10$ Mev	$\frac{2\pi}{4\pi} \times .146$ cm^2	$2(10)^5$ cm^{-2}sec^{-1} (c)	$1.5(10)^4$cps	.15 cps	40 gms
4	$1 \leq E_p \leq 10$ Mev	.425 cm^2 ster and 4.25 cm^2 ster	$3.3(10)^4$ cm^{-2}sec^{-1}ster^{-1}(d)	$1.4(10)^4$cps and $1.4(10)^5$cps	very small	125 gms

(a) Approximate values only. Used to give estimate of an expected count rate. Does not include detector position and orientation on payload, orbit geometry, and particle distribution (loss cone) considerations.

(b) From Solar Proton Manual (SPM), Edited by F. B. McDonald, NASA TR R-169.

(c) From SPM 30 Mev point and an E^{-3} differential energy spectrum.

(d) From "Solar Protons and Magnetic Storms in July 1961," G. F. Pieper, A. J. Zmuda, C. O. Bostrom, and B. J. O'Brien, J. Geophys. Res., 67, 4959-4981, 1961.

THE JOHNS HOPKINS UNIVERSITY
APPLIED PHYSICS LABORATORY
LAUREL MARYLAND

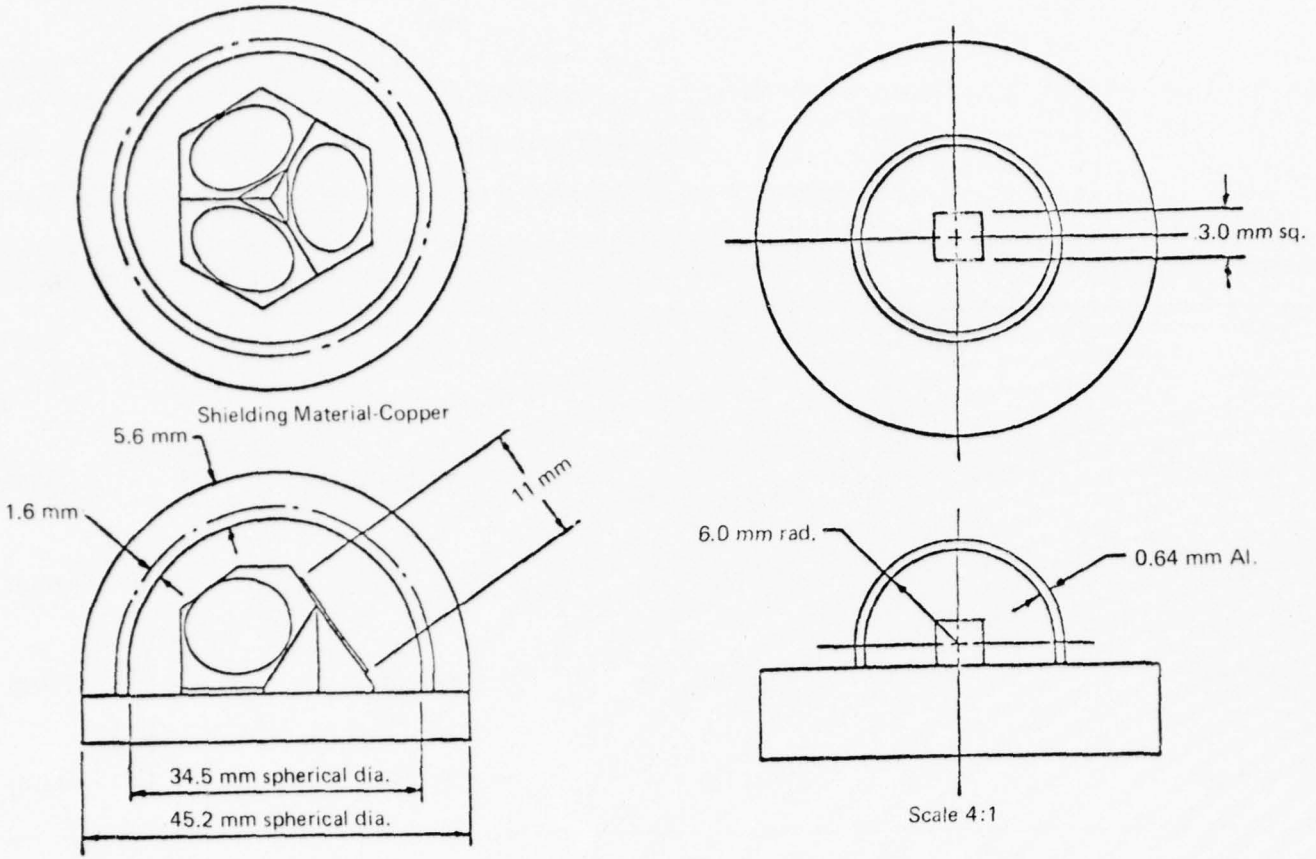

(a) Channels 1 and 2 detector

(b) Channel 3 detector

Fig. IV-2 SPM Detector Outline Drawings, IMP F and G

Channel 4

Protons in the energy interval 1-10 MeV were measured by an 86 microns thick silicon surface barrier solid-state detector of 2 cm^2 area. A collimator used with this detector restricted the viewing direction to 60° full angle normal to the spacecraft spin axis. The resultant geometrical factor was 1.7 cm^2 ster (±10%). The detector was shielded from light by a 0.25 mil aluminized Mylar film. Bilevel electronic discrimination provided two channels; in one channel protons between 1 and 10 MeV were measured, and in the other channel particles depositing more than 3.6 MeV were counted. Electron counting in the 1-10 MeV proton channel was insignificant due to the thinness of the detector. Counts were accumulated for 19.2 seconds in each of the two channels twice every 2.73 minutes.

FUNCTIONAL OPERATION

Refer to Fig. IV-3 for a block diagram that shows the various components of the IMP-F and -G SPM and their functional relationship. Proton detection in a known range of energies was accomplished with semiconductor reverse biased junctions as these are very sensitive devices with reasonable noise characteristics. The detector output, a charge proportional to the incident proton energy, was amplified by a charge sensitive preamplifier (transfer function is voltage output per charge input) of good noise characteristics. The preamplifier voltage output was then differentiated and amplified, differentiated again, and (with the level determined by a discriminator) further amplified. The combined threshold characteristics of the detector shielding and discriminator level allowed count outputs for particles of greater than a preset value.

Detectors

The four SPM detectors were of various cross sections and employed massive copper shielding to obtain the desired detection characteristics. As installed in the spacecraft, the three dome shields protruded above the payload top surface (thin aluminum domes were mounted on the payload surface to maintain an RF shield around the payload inner structure) and the fourth detector looked out the side. The channel 1, 2, and 3 detectors were designed to detect protons of energy levels above 60, 30, and 10 MeV, respectively. The channel 4 detector provided data of a more complex nature: being extremely thin (86 microns), the energy absorbed per incident particle is equal to the particle energy (considering protons) up to about 3 MeV and then decreases as the particle passes through the detector and the energy deposition per unit

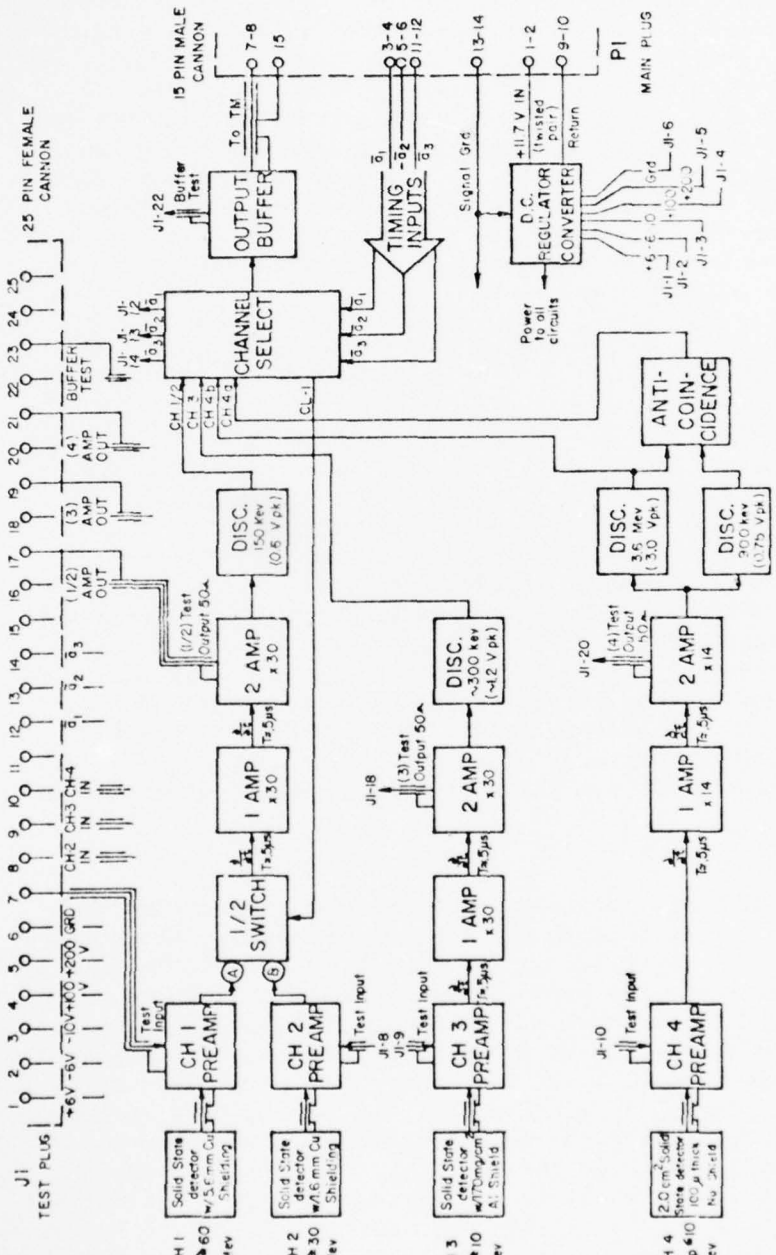

Fig. IV-3 SPM Block Diagram, IMP F and G

thickness of detector drops as particle energy increases. The detector alone thus provided a bandpass of detection energies to incident protons (restricted by shielding to not more than 30° from normal); for the IMP-F and -G SPM this bandpass was set (by the following lower level discriminator) to between 1 and 10 MeV.

Protons in excess of 30.1 MeV energy, however, can produce a detector output in excess of the 900 keV lower level discriminator level if their energy level and angle of incidence through the cylindrical copper shield used to restrict the look angle of the detector falls within certain bounds. The worst case is for protons penetrating the detector on a trajectory parallel with its surface, all with energies above 30.1 MeV would trigger the lower level discriminator. This problem was relieved considerably by the use of the upper level discriminator and anticoincidence circuitry. The upper level discriminator was set at the 3.6 MeV detection level to detect almost all protons between 30.1 and 160 MeV so that the anticoincidence circuit restricted detection to incident protons between 1 and 10 MeV and at extreme angles and energy levels above 160 MeV.

A fifth channel of information, designated as channel 4b, was also included to provide counts from the upper level discriminator of channel 4 so that background noise and deadtime estimates could be determined to improve the 1 to 10 MeV counts.

Signal Analysis

The SPM electronics were used to process the charge outputs from the detectors in such a manner to minimize additional system noise, allow counting up to the limit set by the spacecraft telemetry system, and commutate the detector channel outputs to spacecraft TM storage register in synchronism with the spacecraft timing inputs. A double differentiation scheme (about 0.5 μs) was used in each amplifier string to allow fast counting with minimum offset at high rates. The step output of the preamplifier in each channel was amplified and double differentiated, then detected by a discriminator which was adjustable (to allow exact preflight trim) and which produced a standard pulse. The discriminator output was connected to an output buffer circuit only when so selected.

Counting and storage of the number of counts in a given time from one of the five detection channels were accomplished in conjunction with the satellite telemetry system which included a digital data processor with several possible modes of operation. The SPM was used in conjunction with a "S-T" (Signal-(or)-Time) type accumulator. The accumulator functioned to accumulate (count) until it overflowed and then count clock pulses for the rest of the accumulation period. Thus, for low counting rates, the accumulator read

out the number of pulses counted and for high counting rates read the time after overflow.

Telemetry Interface

The SPM was assigned channels 14 and 15 of frame 0 of the spacecraft telemetry sequence. This provided 16 bits of data per sequence which were sufficient for only one of the five different measurements performed by the experiment. To provide for commutation of the measurements, three lines corresponding to the first three bits of the payload sequence counter, drove a SPM "Channel Selector" (internal to the SPM) allowing eight different time commutated readouts. Not all eight were unique as there were only five combinations of particle detectors and discriminator detection levels; therefore, SPM channels 3, 4a, and 4b repeated twice during the eight payload sequence interval. Positive synchronization was maintained since the drive signals were obtained from the least significant three bits which were read out in the payload sequence count (a 16-bit format). This sequence number was read out twice in each payload sequence, first as TM channels 14 and 15 of frame 7 and again as TM channels 14 and 15 of frame 15.

FLIGHT RESULTS

The Solar Proton Monitor was successfully launched aboard the NASA satellites Explorers 34 (IMP F, 1967 51A) and 41 (IMP G, 1969 53A) on 24 May 1967 and 21 June 1969, respectively (lines 13 and 15, Table 1). Figure IV-4 shows the IMP-G satellite installed on the Delta launch vehicle the day before launch.

Fig. IV-4 IMP-G Spacecraft on Thor-Delta Launch Vehicle

V

ITOS SOLAR PROTON MONITOR

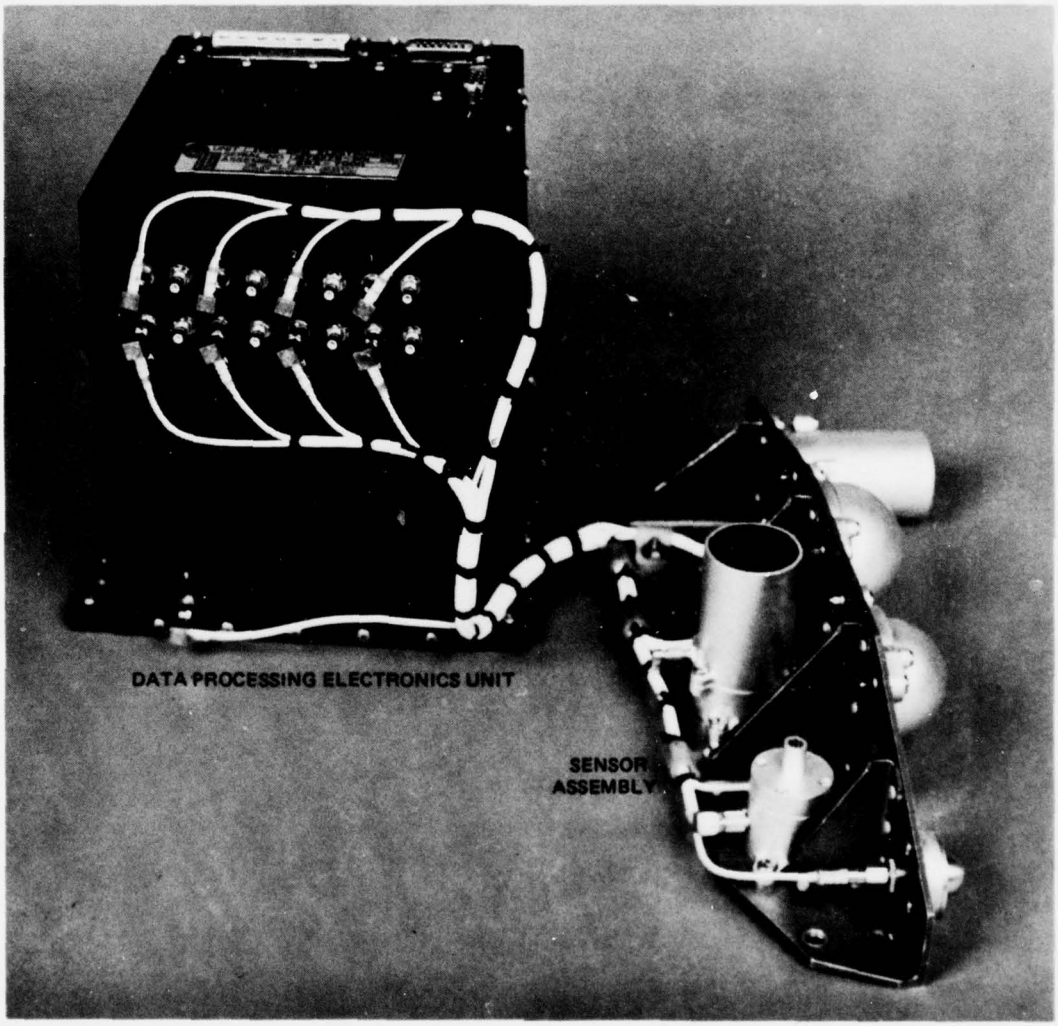

Fig. V-1 ITOS Solar Proton Monitor

V

ITOS SOLAR PROTON MONITOR

BACKGROUND

A number of Solar Proton Monitor (SPM) units were fabricated for flight aboard the ITOS (Improved TIROS Operational Satellite) series of satellites. Developed by APL for the Environmental Science Services Administration (now the National Oceanic and Atmospheric Administration), they were used to measure and continuously monitor the flux and energy spectrum of protons in the vicinity of the earth.

In recent years, information from many sources has been used to advance our understanding of the properties of solar proton fluxes. Such parameters as frequency of occurrence, distribution of intensity, directional properties, energy spectra, and relative fluxes of heavier nuclei accompanying the protons have been roughly estimated. With regard to advancing our understanding further, systematic monitoring is invaluable, both as a source of data in its own right and as a supplement to information provided by more specialized instrumentation.

APPLICATION

As part of the ITOS secondary sensors subsystem, the SPM was designed to measure the proton fluxes encountered in the satellite orbit, to convert these measurements to a floating-point binary code, and to store these data in the incremental tape recorder for subsequent playback and transmittal to ground stations. The SPM data could also be telemetered on a real-time basis.

The SPM was used in conjunction with other satellite-borne and ground based sensors to provide warnings of solar proton storms. These warnings may be used in several ways: for the protection of personnel aboard spacecraft and high altitude aircraft, to alert users of radio frequency links (VLF through HF) of possible ionospheric disturbances so that alternate radio paths or frequencies may be selected in advance, and to minimize the possibility that a nuclear detection method may be falsely triggered by a proton event.

EQUIPMENT DESCRIPTION

The ITOS SPM flight hardware (Fig. V-1) consisted of a sensor assembly, a data processing electronics unit, and an electrical harness.

Sensor Assembly

Six sensors (Table V-1) mounted on an L-shaped bracket comprised the sensor assembly. One surface of the sensor bracket contained four sensors (1, 2, 3, and 6) which were pointed away from the earth at all times during the normal satellite orbit. The other surface contained two additional sensors (4 and 5) which were oriented along the orbit normal.

Sensors 5 and 6 each contained two solid state detectors that were used to detect protons and alpha particles at several different energy levels. The other four sensors contained the equivalent of single element detectors, three sensors were proton sensors and one was an electron flux monitor. High energy electrons contained within the Van Allen belts could contaminate the proton sensor data, while the electron detector responded to electrons only. In the polar regions, however, there are few electrons in the response range of any detector, and essentially pure proton data could be obtained. The cutoff in counting rate of the electron detector was used to define the edges of the trapping regions.

Data Processing Electronics Unit

The data processing electronics unit, which weighed 2.48 kg and measured 15.82 cm wide by 15.24 cm deep, contained the circuitry required for processing the SPM sensor output data. This consisted of the amplifier-discriminator chains for each data channel, the data encoder to compress and format the SPM information, and a power supply to generate the detector bias voltage and the DC voltage required by the electronics.

Each SPM channel accumulated counts in a scaler designed to accommodate up to 20 bits of data. Actually, only 15 to 19 bits were used in each counter, depending on the maximum capacity required for a particular data channel. At the end of each accumulation, the data word was converted to a 9-bit floating point binary format by breaking the number into a characteristic (N) and a mantissa (M) so that the data word took the form $M2^N$. In this system, four bits were allotted to the characteristic and five bits to the mantissa, yielding a conversion accuracy of 1 part in 2^5 (approximately 3%).

The ITOS SPM data were simultaneously available in two forms with the primary data form being a nonreturn-to-zero (NRZ) code supplied to track 1 of the incremental tape recorder (ITR) via the data format converter (DFC). These data were recorded throughout the orbit and played back on command over a Command and Data Acquisition (CDA) station.

Table V-1

ITOS SPM Detector Characteristics

DETECTOR AND WORD DESIGNATION	ENERGY RANGE (MeV) (a) PROTONS	ALPHAS	ELECTRONS	ABSORBER	FIELD OF VIEW	LOOK DIRECTION	GEOMETRIC FACTOR (cm^2 ster)	ACCUMULATION TIME (sec)	DUTY CYCLE (percent)	WORD NUMBER (h)	LOGIC (i)	DISCRIMINATION LEVELS (MeV)
1	≥60	≥240	>8	4.98 g/cm^2 Cu (dome) (c)	2π ster	ZENITH	6.28	12	100	6	- - -	0.15
2	≥30	≥120	>2.15	1.42 g/cm^2 Cu (dome) (c)	2π ster	ZENITH	6.28	12	100	11	- - -	0.15
3	≥10	≥40	>60	0.17 g/cm^2 Al (dome) (c)	2π ster	ZENITH	0.791	12	100	16	- - -	0.30
41	2.09 2.37		≥0.140	16.7 mg/cm^2 Ni (d)	CONE 6.5 DEGREES HALF ANGLE 0.040 ster	PERPENDICULAR TO ORBIT PLANE	2.74×10^{-3}	3	50 (g)	2,12	$D_1\overline{D_2}$	D_1 = 0.10
42	>2.37		≥0.770 LOW EFF					3	50 (g)	7,17	D_2	D_2 = 0.75
51 (61)	0.27 0.56	0.36 0.70	>200 LOW EFF	0.222 mg/cm^2 Ni (e)	CONE 20 DEGREES HALF ANGLE 0.38 ster	DETECTOR 5, PERPENDICULAR TO ORBIT PLANE; DETECTOR 6, ZENITH	0.38	1.2 (1.2) (f)	10 (10)	3 (13)	$A_1\overline{A_2}\overline{B}$	A_1 = 0.20
52 (62)	0.56 1.05	0.70 1.2	- - -					1.2 (1.2)	10 (10)	4 (14)	$A_2\overline{A_3}\overline{B}$	A_2 = 0.50
53 (63)	1.05 3.2	1.2 4.1	- - -					1.2 (1.2)	10 (10)	5 (15)	$A_3\overline{A_4}\overline{B}$	A_3 = 1.0
54 (64)	3.2 60	>12.5	- - -					1.2 (1.2)	10 (10)	8 (18)	A_1B	A_4 = 4.0
55 (65)	- - -	12.5 30	- - -					1.2 (1.2)	10 (10)	9 (19)	A_4B	B = 0.30 (SAME FOR DETECTORS 5 AND 6)
56 (66)	60-86 +BKGD (b)	BKGD (b)	- - -					1.2 (1.2)	10 (10)	10 (20)	$\overline{A_1}B$	

NOTES:

(a) PRIMARY CONTRIBUTOR OVER POLAR CAPS DURING SOLAR PROTON EVENT IS UNDERLINED.
(b) BACKGROUND (BKGD) IS COUNT FROM PARTICLES PENETRATING SHIELDING (PRESENT TO SOME EXTENT IN ALL CHANNELS).
(c) SHIELDING (EXCEPT FOR DOME) IS ≥60 MeV PROTON EQUIVALENT OF Cu.
(d) SHIELDING (EXCEPT FOR APERTURE) IS ≥50 MeV PROTON EQUIVALENT OF Cu.
(e) SHIELDING (EXCEPT FOR APERTURE) IS ≥30 MeV PROTON EQUIVALENT OF Cu.
(f) 3 CHANNELS OF DETECTOR 5 ACCUMULATED SIMULTANEOUSLY DURING WORDS 1 AND 2, AND 3 CHANNELS DURING 6 AND 7.
3 CHANNELS OF DETECTOR 6 ACCUMULATED SIMULTANEOUSLY DURING WORDS 11 AND 12, AND 3 CHANNELS DURING 16 AND 17.
(g) 41 AND 42 EACH SAMPLED TWICE PER 12 SECOND FRAME.
(h) WORD ORDER IS FOR REAL TIME (AND RECORD) MODES; ON PLAYBACK, IT IS REVERSED. WORD 1 IS THE BARKER CODE.
(i) REFER TO RCA LOGIC DIAGRAM 1976102.

As an alternate means of transmitting the SPM data to the ground, the 3.9 kHz subcarrier oscillator of the 136.77 MHz beacon could transmit the return-to-bias (RB) code supplied by the SPM unless a higher priority function had been commanded. With this alternative, real-time SPM data were radiated by the beacon continuously except for brief interruptions for command verifications and (when commanded) housekeeping data. It was thus possible to use the Space Tracking and Data Acquisition Network (STADAN) and other receiving sites to acquire SPM data. This arrangement was valuable because on many orbits the data being stored on the ITR could not be played back until the satellite was in range of the next CDA site. The beacon transmission avoided a prolonged delay in data acquisition, and timely warnings of a solar proton storm could thus be assured.

FUNCTIONAL OPERATION

Refer to Fig. V-2 for a block diagram that shows the various components of the ITOS SPM and their functional relationship.

Sensor Assembly

Proton Sensors 1 and 2. Each of these two higher energy channels consisted of three 700-micron thick silicon surface barrier detectors mounted on orthogonal axes and surrounded by a hemispherical copper shield. The three outputs were wired in parallel to provide a fairly uniform cross section over a complete hemisphere. The only difference between the two units was the thickness of the shielding dome, its thickness being by far the most important factor in determining the energy threshold of the detectors.

Proton Sensor 3. This detector consisted of a lithium-drifted silicon detector in the shape of a 3 mm cube, surrounded by a thin aluminum shield. The dimensions of this detector were kept small due to the large proton flux in the energy range $E_p > 10$ MeV that is possible following solar-flare events. At lower latitudes, measurements of electron data represented the major contribution of this detector.

Electron Sensor. The electron sensor (sensor 4) consisted of a single detector wafer inside a shielding mount with an aperture that defined the sensor look angle. A thin light shield served to prevent extraneous signals should the detector look toward the sun. A thermistor was located in the base of the sensor to determine the temperature of the assembly. The difference in temperature between detectors was small. Operation of the

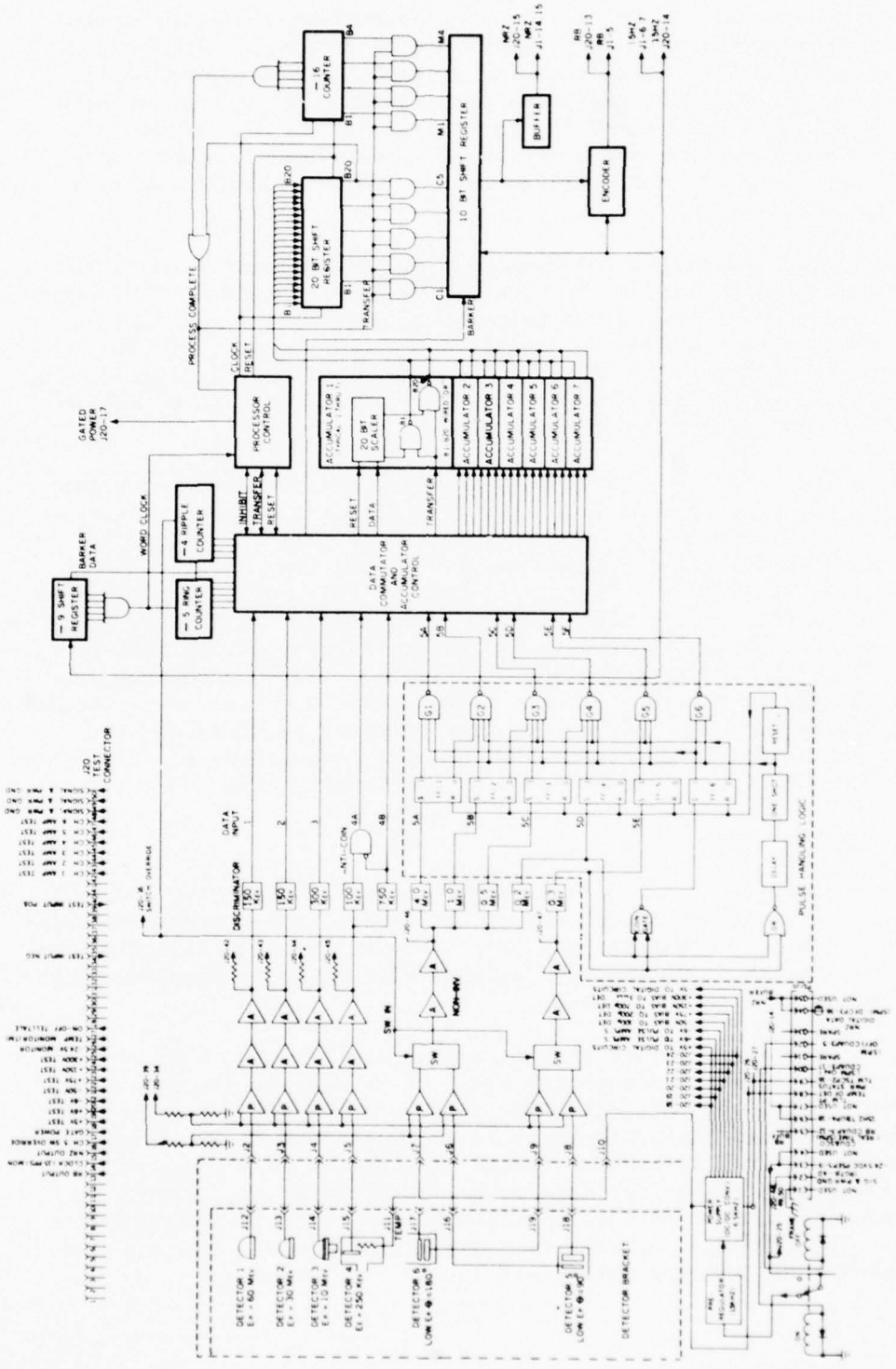

Fig. V-2 ITOS-1 Solar Proton Monitor Block Diagram

electron detector differed from the other sensors in that the last amplifier output had two pulse height discriminators (designated upper level and lower level) which fed an anticoincidence circuit. The function of the anticoincidence was to generate a pulse if only the lower level discriminator was triggered and not if both the upper and lower level discriminators fired. The anticoincidence circuit output and upper level discriminator outputs were subcommutated into one data accumulator which was read out four times each frame.

Dual-Channel Proton Sensors 5 and 6. Sensors 5 and 6 were identical except for orientation on the sensor bracket. This sensor design consisted of a telescopic arrangement of two surface barrier devices, a 100-micron thick detector backed by a 200-micron thick detector. These sensors provided data on lower energy proton fluxes beginning at 270 keV and extending up to 60 MeV as well as alpha particles from 12.5 to 32 MeV.

The data from these detectors were subcommutated into two amplifier channels, one for both front detector elements and the other for both rear detectors. The outputs from the five discriminator units for these chains were fed to the low energy channel pulse handling logic. The front and rear detector arrangement was used to determine the direction and energy level of incident particles; e.g., a particle detected in both the front and rear detectors by coincidence methods was defined as coming through the opening aperture with an energy level within a given range, whereas a particle detected only in the rear detector probably came in through the shielding due to the geometric properties of the sensor and the detectors and was used in determining background rates.

Data System

Data Format. The data system was a fixed program special purpose digital processor designed to control and process the data from the signal analysis circuits. The data system circuitry comprised a stack of multi-layer printed circuit boards mounted above the signal analysis section.

Data were applied to this system via 11 input lines: the channel 1, 2, and 3 discriminators, the channel 4 anticoincidence circuit and upper level discriminator, and the six outputs of the pulse-handling logic. These 11 input lines were commutated into a group of seven time shared binary scalers in which data were accumulated. The scaler data were time-division multiplexed and compressed into a frame of 20 nine-bit words for recording on the ITR. The 180-bit frame was read out at the normal clock rate of 15 bits/s (12 seconds per frame).

Each 180-bit data frame began with a nine-bit Barker word of the form 111000101, followed by 19 words of radiation flux data. The 11 output lines from the signal analysis section were applied to seven binary scalers. The 60 MeV, 30 MeV, and 10 MeV proton channels had scalers which were not time-shared. Discriminator data were applied to these three scalers for almost the full frame time, and interrupted only for scaler sampling and reset once per 12-second frame. The energetic electron channel data were provided via two input lines commutated into one scaler. Two interleaved 3-second (1/4 frame) accumulation intervals were provided per frame for each of the two data input lines. The directional low energy proton channels provided data on six lines commutated into three scalers. Each scaler provided two interleaved data samples of 1.2-seconds duration per frame.

The 19 data samples per frame were provided in the order shown in Table V-1. The duty cycle, direction angle, and accumulation time for each data sample are also given. Scaler data samples were taken and processed for the format given in the table. Processing consisted of logarithmic compression of 15 to 19 bits of scaler data into a nine-bit word, consisting of a four-bit characteristic followed by a five-bit mantissa, all most significant bits first.

Control Unit. The control unit provided the necessary control signals for the commutator, processor, and scaler units. At the beginning of each word interval in the data frame, the control unit energized the processor to perform a readout cycle on a scaler. Refer to the Word Number column of Table V-1 for the sequence of scaler readouts.

The control cycle was initiated by the setting of the control enable flip-flop at the start of each word. The setting of this flip-flop energized the power switch and 75 kHz astable multivibrator, and enabled the control counter. In state 00, the control counter cleared all processor flip-flops that receive gated power.

On the first clock pulse from the astable multivibrator, the control counter went to state 10 and the addressed scaler data were enabled to parallel transfer into the processor by a transfer pulse on that scaler's transfer line. The 01 state provided a reset to the addressed scaler and either state (10 or 01) inhibited data from being applied to the scaler input. The third clock pulse placed the control in state 11 where the control clock was interrupted and the processor clock enabled. The processor clock remained present until a process complete was received, at which

time the control flip-flop was reset and gated power removed. The processing time was between 50 and 400 μs and was dependent upon the scaler data.

Data Compression Processor. The data compression processor received selected scaler data in parallel and performed a logarithmic conversion of the data. The output was a serial word nine bits in length, in the form of a characteristic and a mantissa to base 2.

The processor consisted of a 20-bit parallel-input shift register, a four-bit synchronous binary counter, and a 10-bit output shift register. Processing was performed by parallel entry of the selected scaler data, followed by right-shifting (multiplication by 2) until either 15 shifts had occurred or a logic 1 appeared in the most-significant-bit position of the 20-bit shift register. When this occurred, the five most significant register bits and the four complemented shift pulse counter bits were parallel-transferred into the output data register, and the process-complete signal was generated. During the last word of each frame, the Barker word was serially entered into the output register. Since no data were parallel-transferred into the processor at word time W1, the operation of the processor did not interfere with the Barker word.

The data coming from the processor in NRZ form were supplied directly to the spacecraft incremental tape recorder. In addition, the data were encoded into an RB signal by the encoder prior to being sent to the telemetry subsystem. A sample of the SPM data format, showing both the NRZ and RB patterns, is shown in Fig. V-3.

Scalers. Each scaler consisted of from 15 to 19 flip-flops arranged into a binary weighted ripple counter with gated parallel transfer output. Inputs to each scaler were data, transfer, and reset signals. The scaler counted data pulses as long as they were supplied, and parallel-transferred via output gates on command. The transfer command was followed by a reset to all zeros.

Table V-2 lists the seven scalers with their corresponding data channels, maximum expected counts over the sampling period for these channels, and scaler capacity. The maximum count rates for the proton channels were based on data obtained from the Solar Proton Intensity and Composition Experiment (SPICE) rocket probe experiment flown into the solar proton event of 2 September 1966. Maximum electron rates were based on the electron-spectrometer data obtained from APL Satellite 5E-1 (1963 38C). The peak rates listed in Table V-2 are, in all cases, at least an order of magnitude greater than the maxima derived from these experiments.

*UPON ITR PLAYBACK THE ORDER OF THE DATA IS REVERSED
NOTE: BIT RATE IS 15 Hz

Fig. V-3 ITOS SPM Data Format

Table V-2

ITOS SPM Solar Capacity

Scaler No.	Channel No.	Max. Expected Count	No. Bits	Capacity
1	10	1.2×10^5	19	5.2×10^5
2	20	3.6×10^5	19	5.2×10^5
3	30	2.4×10^5	19	5.2×10^5
4	41	3.0×10^5	19	5.2×10^5
	42	1.5×10^4		
5	51,61	3.0×10^4	17	1.3×10^5
	54,64	7.2×10^4		
6	52,62	3.0×10^4	15	3.3×10^4
	55,65	4.8×10^3		
7	53,63	3.0×10^4	15	3.3×10^4
	56,66	3.6×10^3		

FLIGHT RESULTS

The ITOS Solar Proton Monitors were flown aboard the following satellites:

Satellite	Launch Date	Reference
ITOS-1 (TIROS-M)	23 Jan 1970	line 16, Table 1
NOAA-1 (ITOS-A)	11 Dec 1970	line 21, Table 1
NOAA-2 (ITOS-B)*	21 Dec 1971	line 26, Table 1
NOAA-2 (ITOS-D)	15 Oct 1972	line 28, Table 1
ITOS-E*	16 June 1973	line 33, Table 1
NOAA-3 (ITOS-F)	6 Nov 1973	line 35, Table 1
NOAA-4 (ITOS-G)	15 Dec 1974	line 40, Table 1
NOAA-5 (ITOS-H)	29 July 1976	line 48, Table 1

*Failed to orbit.

surface of the aluminum shell, and thermistors are installed in grooves cut in the shell wall. The thermistors form opposite legs of a Wheatstone bridge which provides the proportional control of the heater element current. The assembly is once again wrapped with alternate layers of aluminized Mylar and Fiberglas, and then placed in a cylinder that forms the outer shell of the oscillator.

At atmospheric pressure, the layers of Mylar and Fiberglas provide only about 5°C per watt insulation; however, at about 10^{-4} torr or less, this insulation becomes very effective as it must since heater power is limited to a maximum of one watt. The thermal stabilization process typically requires two to three days after the vacuum environment has been achieved, dependent mainly upon the particular crystal and oscillator assembly. The degree to which temperature stability is maintained is too small for direct measurement; therefore, oscillator frequency is an indirect measure of heater performance. The stabilization process is marked by the slowing of the frequency drift toward the specified crystal value; e.g., 5×10^{-10} parts per day after three days and 1×10^{-10} parts per day after 30 days.

Oscillator operation at atmospheric pressure will not result in equipment damage. Whereas the short term noise will be about normal, the drift rate will be high and the absolute frequency will be about 20 parts per million higher than normal. The first step in the acceptance tests of an oscillator is to determine its stabilization characteristics. This is usually accomplished at APL by first multiplying both the oscillator signal and a reference signal from a cesium standard to 100 MHz, mixing these two signals and measuring the frequency of the difference signal at various averaging times, for example, 1, 10, 100, and 1000 seconds. A significant number of samples at each averaging time, e.g., about 30, is then used to calculate the rms (standard deviation) value. A plot of typical results is shown in Fig. VI-4b. Once the frequency drift rate has been established, the sensitivity to temperature and voltage changes can be measured. This is performed by measuring the offset in the frequency curve being plotted when temperature or voltage are changed. This assumes that there is no change in drift rate that accompanies the temperature or voltage change, a good assumption at least to the first order. Results of such tests indicate typical temperature sensitivities, referenced to a -32 volt supply, on the order of 5×10^{-11} per degree centigrade and voltage sensitivities on the order of 5×10^{-12} per volt.

FLIGHT RESULTS

Doppler Beacons were flown aboard the following satellites:

Satellite	Launch Date	Reference
1970 16A	4 Mar 1970	line 17, Table 1
1970 40A	20 Apr 1970	line 18, Table 1
1970 98A	18 Nov 1970	line 20, Table 1
--*	17 Feb 1971	line 22, Table 1
1971 22A	24 Mar 1971	line 24, Table 1
1971 76A	10 Sep 1971	line 25, Table 1
1973 14A	9 Mar 1973	line 30, Table 1
1973 46A	13 Jun 1973	line 32, Table 1
1973 88A	10 Nov 1973	line 36, Table 1
1974 20A	10 Apr 1974	line 38, Table 1
1974 85A	29 Oct 1974	line 39, Table 1
1975 51A	8 Jun 1975	line 41, Table 1
1975 114A	4 Dec 1975	line 42, Table 1
1976 38C,D,&J**	30 Apr 1976	line 46, Table 1
1976 65A	8 Jul 1976	line 47, Table 1
1977 56A	27 Jun 1977	line 49, Table 1
1977 112A,B,&E**	8 Dec 1977	line 52, Table 1
1978 29A	16 Mar 1978	line 54, Table 1

*Failed to orbit.
**Multiple Satellite Dispenser Program.

All beacons that were orbited have operated satisfactorily, and tracking stations have submitted doppler data of generally excellent quality.

SPM data obtained during the ITOS missions are being correlated with data from other satellites (e.g., IMP, Vela, and Pioneer), sounding rockets, and with ground based optical/radio sightings. The long-term goal of this data gathering and correlation activity is to obtain a better understanding of the interaction between solar radiation and the earth's environment by providing a systematic monitoring of the proton fluxes over an extended period of time, especially during the prevailing solar cycle.

VI

DOPPLER BEACON

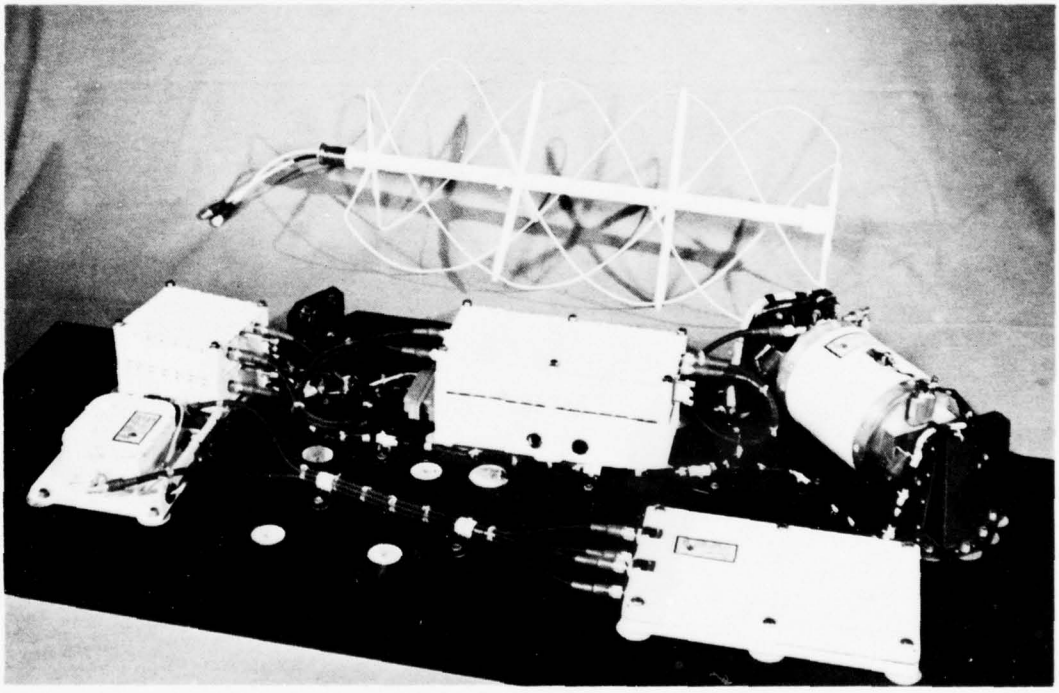

Fig. VI-1 Doppler Beacon

VI

DOPPLER BEACON

BACKGROUND

The doppler tracking systems supplied by APL in 1960 for the Discoverer launch vehicles (refer to Transit-on-Discoverer, Section I) were essentially breadboard beacons assembled mostly from satellite parts on hand. Development of the first in a series of dedicated Doppler Beacons was initiated at APL in early 1969. The first beacons (Fig. VI-1) were supplied for use on U.S. Air Force vehicles of opportunity. Several beacons (Fig. VI-2) were also supplied to the Naval Research Laboratory (NRL) for the Multiple Satellite Dispenser (MSD) 180 Program and, more recently, a number of beacons were fabricated for use with a Navigation Package (NAVPAC) Experiment.

APPLICATION

The Doppler Beacons are used in conjunction with stations of the TRANET (Tracking Network) system and portable Geoceiver stations to provide dense satellite orbit determination data in support of scientific space operations. In the MSD 180 Program application, a cluster of three similar satellites was launched by one vehicle into nearly identical orbits so that they were within a few miles of each other at all times. The beacon system on each satellite provided signals from which five ground stations (also developed by APL) could derive doppler data for use in determining the satellite positions. To identify the signals, each beacon oscillator radiated signals offset from the nominal frequencies of 162 and 324 MHz so that the received signals at the stations did not overlap. In addition, the beacon oscillator provided 5 and 20 MHz signals directly to the satellite telemetry system clocks.

EQUIPMENT DESCRIPTION

Table VI-1 lists the major Doppler Beacon components (less antenna), their weights and dimensions, and associated power requirements.

FUNCTIONAL OPERATION

Doppler Beacon operation is based on the radio doppler system of satellite navigation. First pioneered by APL in the late

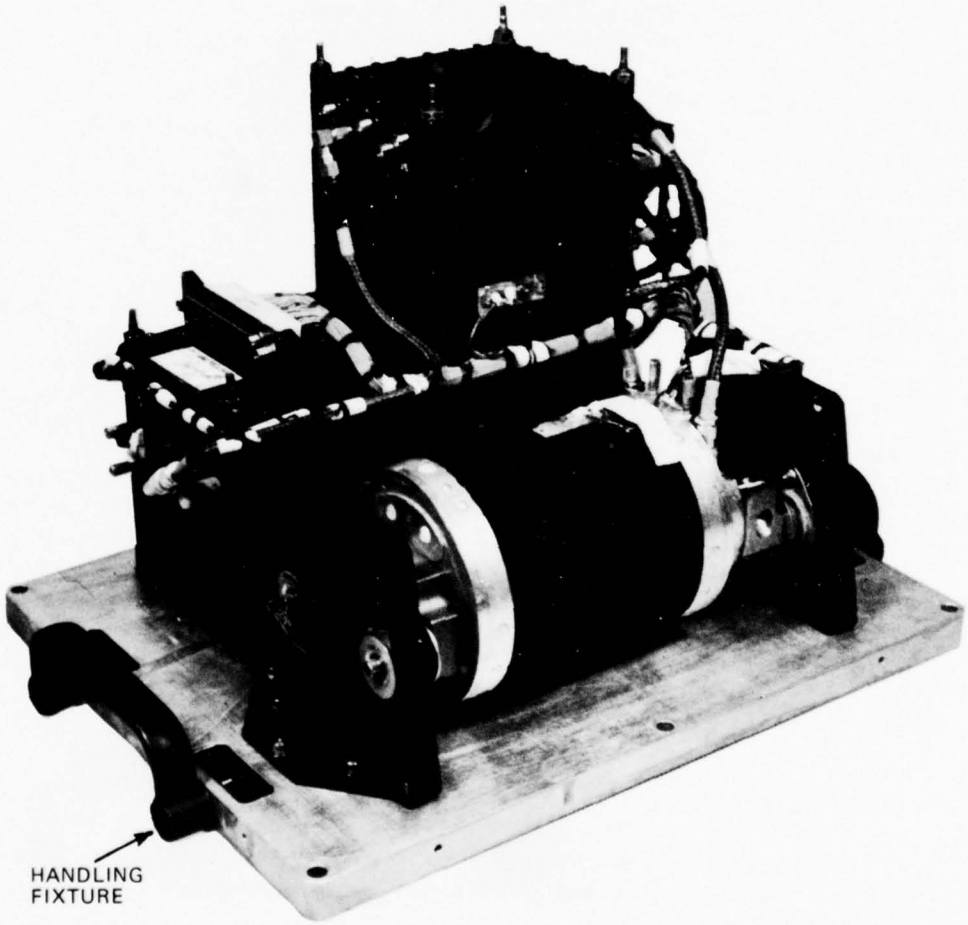

Fig. VI-2 Doppler Beacon, MSD 180 Program

Table VI-1

Doppler Beacon Characteristics

Unit	Weight (kg)	Dimensions (cm)	DC Power
Oscillator	1.44	8.89 Dia. x 16.5[a]	1.25 W[b]
Frequency Synthesizer	0.56	8.57 x 18.73 x 3.49	1.00 W
DC/DC Converter	0.72	8.57 x 18.73 x 3.81	1.25 W[c]
162 MHz Power Amplifier	0.32	8.57 x 9.84 x 3.49	1.00 W
324 MHz Power Amplifier	0.32	8.57 x 9.84 x 3.43	2.25 W
Totals	3.36		6.75 W

(a) Includes shock mounts.

(b) Includes 0.5 W oscillator and 0.75 heater power, corresponding to an ambient temperature of approximately 21.1°C. Maximum heater power is 1 W.

(c) Based on losses in -12 V regulator and converter when operating at approximately 80% efficiency.

1950s, this system utilizes precise measurements of the frequency shift, or doppler effect, of fixed frequency radio transmissions that are observed by ground stations as a function of time. The transmitters are controlled by an ultrastable oscillator such that the continuous wave signals are essentially drift free, and multiple frequencies are chosen so that refraction corrections can be made.

System

The Doppler Beacon consists essentially of a low frequency source, a frequency synthesizer, and 162 and 324 MHz power amplifiers (Fig. VI-3). The beacon employs an ultrastable crystal controlled oscillator that uses redundant fifth overtone 5 MHz crystals. Very accurate temperature control is provided by completely redundant proportional-controlled heaters. Any combination of oscillators or heaters is selectable by command. The 5 MHz signal is used to snythesize 54 MHz signals by first multiplying to 15 MHz, dividing by 5 to 3 MHz, and then multiplying by 18 to 54 MHz. Two buffered 54 MHz outputs are provided by the synthesizer for driving the two power amplifiers. The power amplifiers multiply the 54 MHz signal by the appropriate factor (3 or 6), and amplify the signals to sufficient levels for radiation. Typical output powers are 0.25 watt for the 162 MHz and 0.4 watt for the 324 MHz power amplifiers. A DC/DC converter is used to provide a -12 volt regulated power supply for the oscillator and a -32 volt supply for the remainder of the beacon circuitry.

Oscillator

The dual 5 MHz oscillator, which has been used in various APL spacecraft since 1961, employs 5 MHz fifth overtone (exact frequencies depend upon the individual crystal offset) natural quartz crystals that are used in a basically modified Pierce circuit. Two completely redundant oscillator circuits and associated crystals are packaged together in a single welded cordwood module. All crystals selected for use in APL satellites have upper temperature turning points of 70° ± 5°C, and crystals that will be used in the same oscillator are matched with turning points of within 0.1°C.

The cordwood module is encapsulated with polyethylene foam and fitted into a metal enclosure to provide thermal mass. After the metal enclosure has been wrapped with many alternate layers of insulating aluminized Mylar and Fiberglas, it is installed in a thin walled aluminum shell. Also installed in the shell is a welded cordwood module consisting of separate amplifiers, AGC detectors, second voltage regulators, and the heater control circuitry (Fig. VI-4a). The heater element is attached to the outer

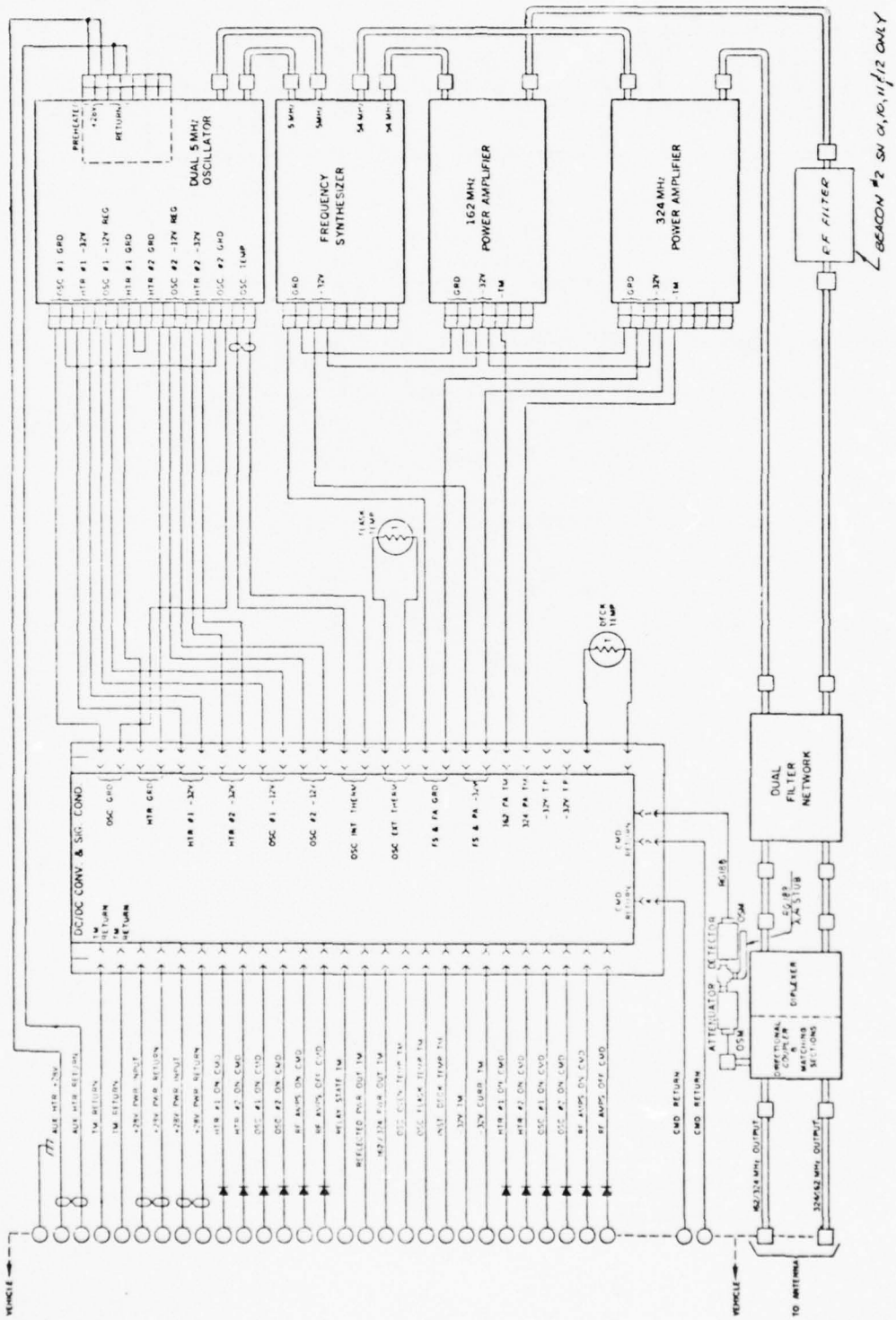

Fig. VI-3 Doppler Beacon System Block Diagram

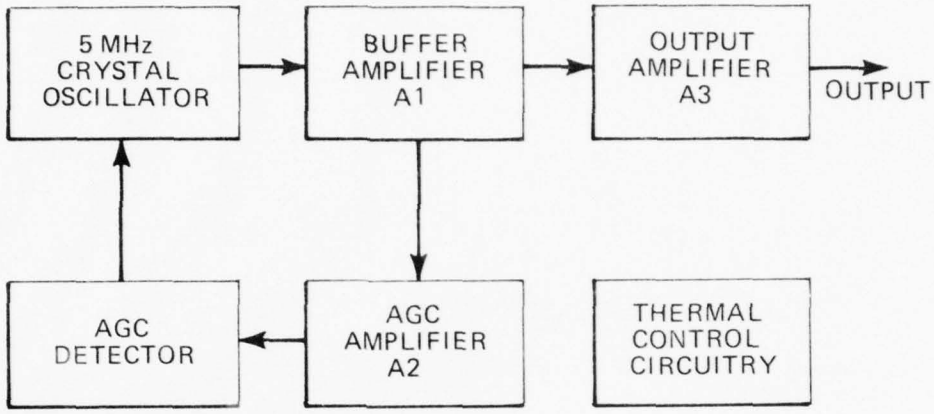

(a) SIMPLIFIED BLOCK DIAGRAM

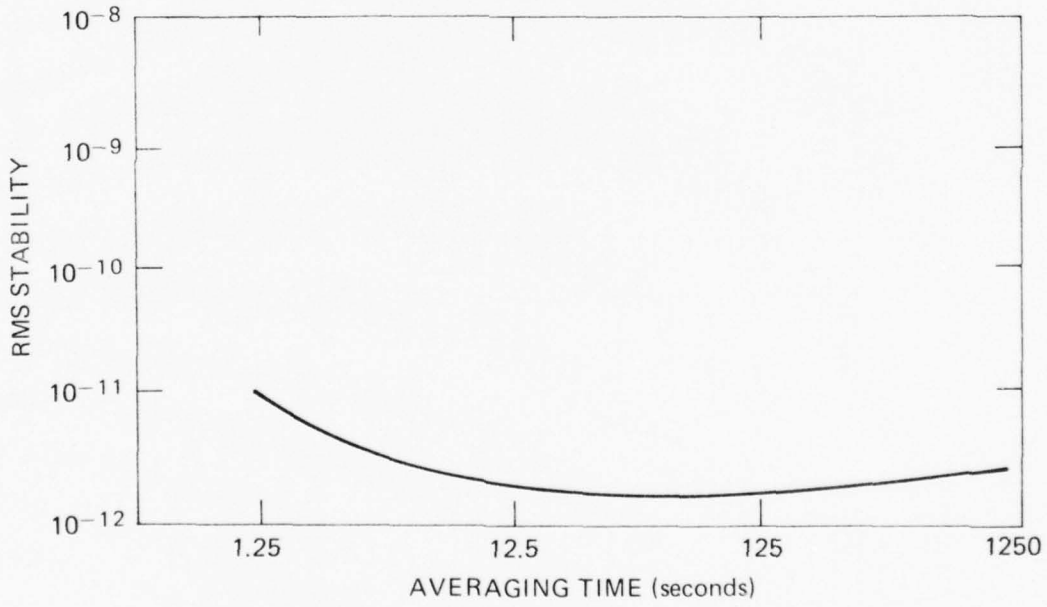

(b) RMS STABILITY VERSUS AVERAGING TIME

Fig. VI-4 Dual 5 MHz Oscillator Block Diagram and Typical RMS Stability Curve

surface of the aluminum shell, and thermistors are installed in grooves cut in the shell wall. The thermistors form opposite legs of a Wheatstone bridge which provides the proportional control of the heater element current. The assembly is once again wrapped with alternate layers of aluminized Mylar and Fiberglas, and then placed in a cylinder that forms the outer shell of the oscillator.

At atmospheric pressure, the layers of Mylar and Fiberglas provide only about 5°C per watt insulation; however, at about 10^{-4} torr or less, this insulation becomes very effective as it must since heater power is limited to a maximum of one watt. The thermal stabilization process typically requires two to three days after the vacuum environment has been achieved, dependent mainly upon the particular crystal and oscillator assembly. The degree to which temperature stability is maintained is too small for direct measurement; therefore, oscillator frequency is an indirect measure of heater performance. The stabilization process is marked by the slowing of the frequency drift toward the specified crystal value; e.g., 5×10^{-10} parts per day after three days and 1×10^{-10} parts per day after 30 days.

Oscillator operation at atmospheric pressure will not result in equipment damage. Whereas the short term noise will be about normal, the drift rate will be high and the absolute frequency will be about 20 parts per million higher than normal. The first step in the acceptance tests of an oscillator is to determine its stabilization characteristics. This is usually accomplished at APL by first multiplying both the oscillator signal and a reference signal from a cesium standard to 100 MHz, mixing these two signals and measuring the frequency of the difference signal at various averaging times, for example, 1, 10, 100, and 1000 seconds. A significant number of samples at each averaging time, e.g., about 30, is then used to calculate the rms (standard deviation) value. A plot of typical results is shown in Fig. VI-4b. Once the frequency drift rate has been established, the sensitivity to temperature and voltage changes can be measured. This is performed by measuring the offset in the frequency curve being plotted when temperature or voltage are changed. This assumes that there is no change in drift rate that accompanies the temperature or voltage change, a good assumption at least to the first order. Results of such tests indicate typical temperature sensitivities, referenced to a -32 volt supply, on the order of 5×10^{-11} per degree centigrade and voltage sensitivities on the order of 5×10^{-12} per volt.

FLIGHT RESULTS

Doppler Beacons were flown aboard the following satellites:

Satellite	Launch Date	Reference
1970 16A	4 Mar 1970	line 17, Table 1
1970 40A	20 Apr 1970	line 18, Table 1
1970 98A	18 Nov 1970	line 20, Table 1
--*	17 Feb 1971	line 22, Table 1
1971 22A	24 Mar 1971	line 24, Table 1
1971 76A	10 Sep 1971	line 25, Table 1
1973 14A	9 Mar 1973	line 30, Table 1
1973 46A	13 Jun 1973	line 32, Table 1
1973 88A	10 Nov 1973	line 36, Table 1
1974 20A	10 Apr 1974	line 38, Table 1
1974 85A	29 Oct 1974	line 39, Table 1
1975 51A	8 Jun 1975	line 41, Table 1
1975 114A	4 Dec 1975	line 42, Table 1
1976 38C,D,&J**	30 Apr 1976	line 46, Table 1
1976 65A	8 Jul 1976	line 47, Table 1
1977 56A	27 Jun 1977	line 48, Table 1

*Failed to orbit.
**Multiple Satellite Dispenser Program.

All beacons that were orbited have operated satisfactorily, and tracking stations have submitted doppler data of generally excellent quality to the Satellite Control and Communications Center at APL.

VII

ORBITING FROG OTOLITH EXPERIMENT

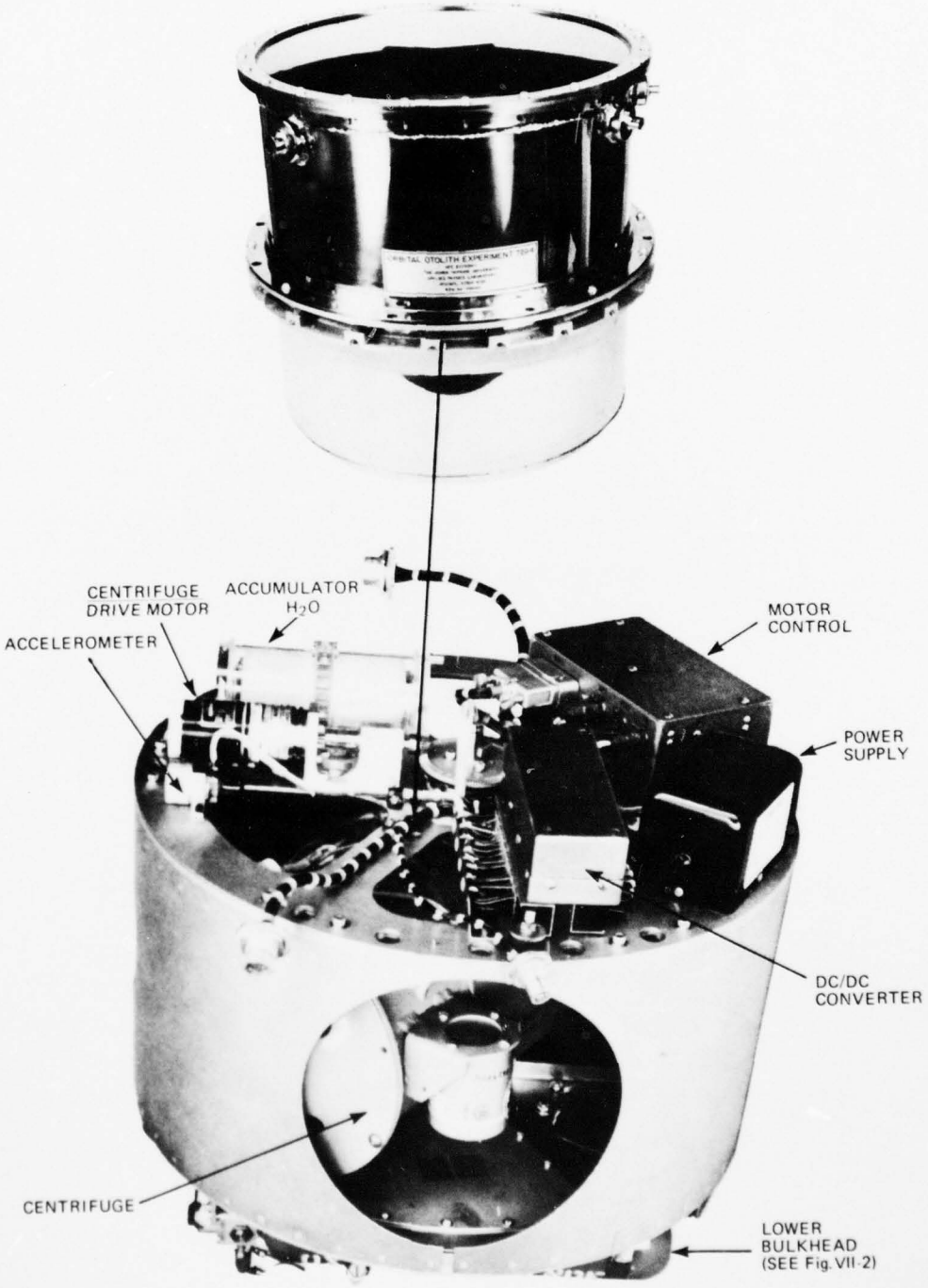

Fig. VII-1 Orbiting Frog Otolith Experiment

VII

ORBITING FROG OTOLITH EXPERIMENT

BACKGROUND

Sensory, motor, and vegetative disorder of vestibular origin have been observed to occur in men and animals during short periods of weightlessness caused by flying airplanes through Keplerian trajectories. There are several existent hypotheses which attempt to explain these disorders; common to most of them is the proposition that the disorders produced by weightlessness are related to the otolith system. The purpose of the Orbiting Frog Otolith Experiment (OFOE) was to obtain the first direct recording of the otolith responses in a weightless environment. A frog (Rana Catesdiana) was chosen as the subject because it is small enough to be practical for spaceflight, it is amphibious and therefore capable of surviving in an air environment while surgery was performed, and it has an otolith system similar to that in man.

The OFOE was developed by Dr. T. Gualtierotti of the University of Milan, Italy, while a Resident Research Associate under the auspices of the National Academy of Sciences working at the NASA/Ames Research Center. The Applied Physics Laboratory designed and fabricated the experiment payload (Fig. VII-1) for the Ames Research Center.

APPLICATION

The OFOE mission involved placing two bullfrogs whose vestibular nerves had been implanted with passive microelectrodes into a weightless environment for several days. During that time, they were subjected to repeated accelerations of up to 0.5 g, and the otolith system activity of each frog was monitored via the vestibular implants. The frogs were contained throughout the flight in a biopackage consisting of a self-contained life support system and a small water-filled centrifuge capable of developing a 0.5 g force at the otolith level. Electrical impulses were recorded and then telemetered to ground tracking stations.

During prelaunch and launch periods, real-time data were continuously telemetered to receiving stations, while in the orbital phase the data were recorded for transmission to ground stations. It was expected that data would be obtained for a period of three days, after which the experiment would be considered at an end (actually, the mission lasted six days). Since only data

obtained during the flight were required for evaluation, no attempt was made to recover the biopackage.

EQUIPMENT DESCRIPTION AND OPERATION

The OFOE capsule housing was a pressure-tight vessel 33.66 cm in diameter and about 46.35 cm long. Both the bottom closure and the removable lid were slightly domed to prevent "oil canning" should pressure reversals be encountered. About 15.24 cm from the bottom of the vessel was a support ring to which the inner assembly containing the life support and operating equipment was fastened. Two electrical receptacles were located near the top of the vessel; one accommodated power supply and data transmission lines and the other provided power to the experiment pyrotechnics.

The inner structure consisted essentially of upper and lower bulkheads (Fig. VII-2) joined by a cylinder which had cutouts to permit access to the centrifuge assembly. The centrifuge assembly (Fig. VII-3) housed the experimental frogs. The centrifuge drive motor was mounted on the upper bulkhead, and signal amplifiers and an accelerometer were mounted on the centrifuge. Other electronic equipment mounted on the upper bulkhead included an inverter, a set of slip rings, a converter, the centrifuge drive motor control unit, and a gas pressure transducer.

The life support system was mounted on the lower bulkhead and included a 0.48 liter oxygen bottle, a pressure reducer and regulator, an artificial lung, CO_2 absorber, and water supply. A water pressure transducer, also mounted on the lower bulkhead, allowed a constant check of the pressure in the water circulation system. A relief valve ensured that the gas pressure in the oxygen line never exceeded the ambient pressure in the canister by more than 12.7-15.2 cm of water. This valve was primarily used to prevent a build-up of oxygen pressure in the accumulator.

Centrifuge Assembly

The centrifuge consisted of a cylinder 15.24 cm in diameter by 34.3 cm long with end caps. Centrally located shafts, held in place by ball bearings mounted in the upper and lower bulkheads, were located at right angles to the cylinder in the vertical plane to form the rotational axis for the centrifuge. The centrifuge was locked in position and was not released until after the spacecraft was in orbit and fully stabilized.

Thin shallow-domed end caps were bolted to each end of the centrifuge with intervening rubber gaskets to prevent leakage. In

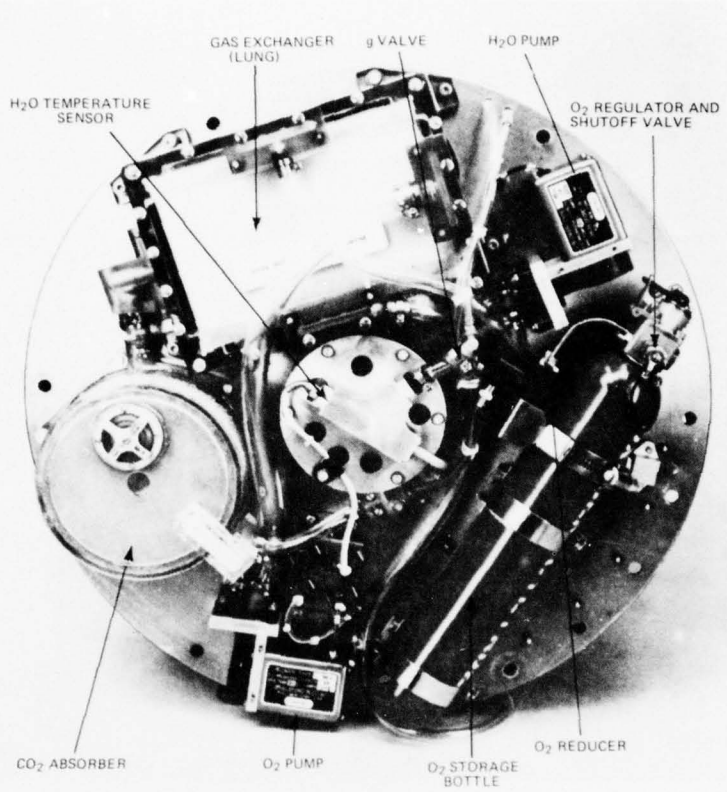

BOTTOM VIEW

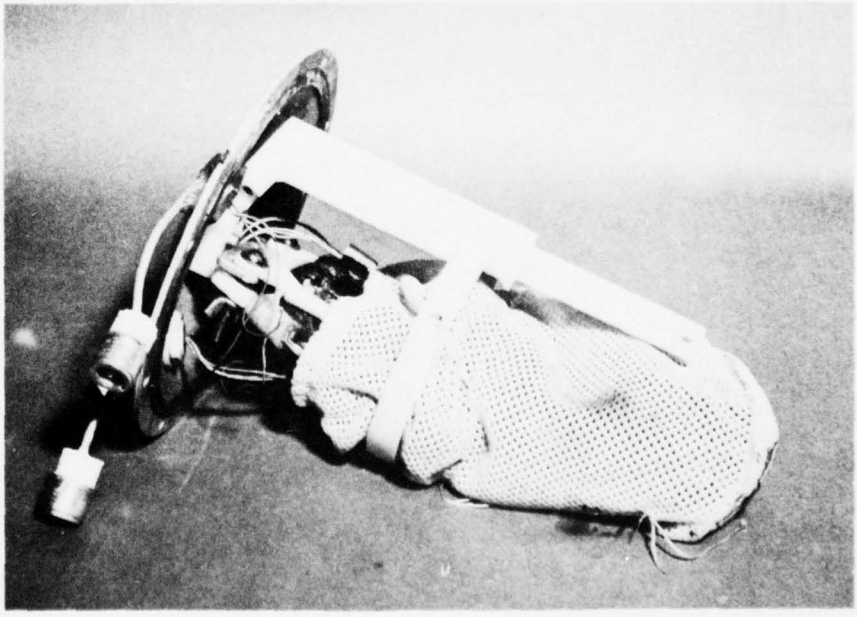

INSTRUMENTED FROG SPECIMENS

Fig. VII-2 OFOE Bottom View and Specimens

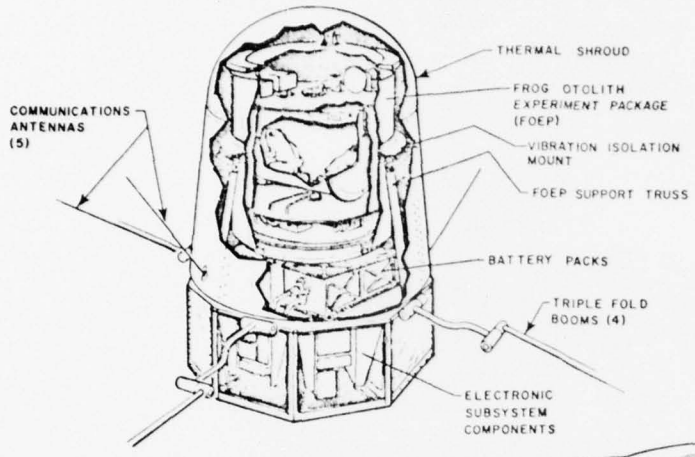

OFOE SPACECRAFT

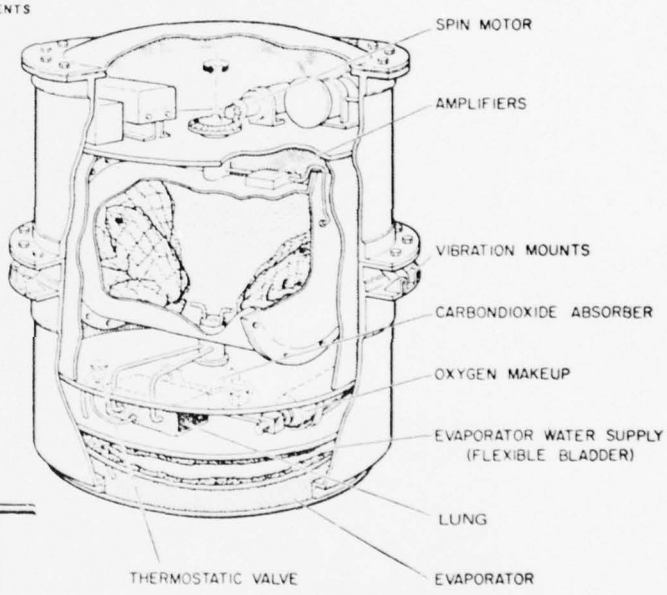

OFOE CUTAWAY VIEW

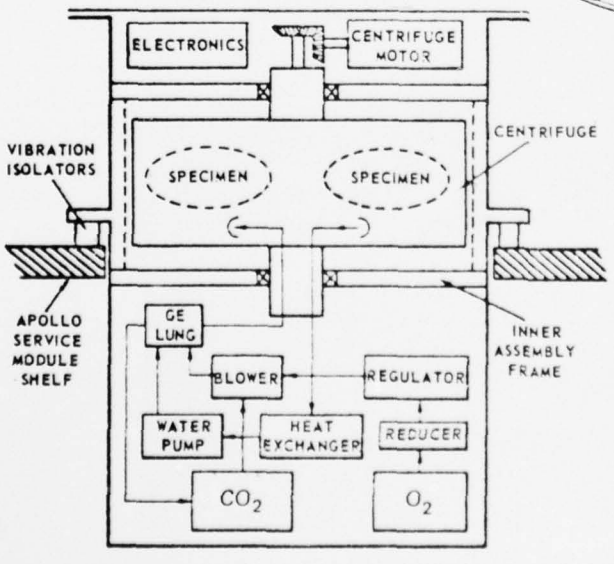

FUNCTIONAL OPERATION

Fig. VII-3 OFOE Cutaway View and Functional Operation

the center of each cap was a fitting which allowed the frog specimens to be fully instrumented and mounted directly to the end cap before insertion into the centrifuge. The electrical leads from the EKG and otolith probes passed through three waterproof glands in each end cap.

Life Support System

Since it was necessary to ensure survival and normal functioning of the frogs, the OFOE contained a life support system (LSS) to maintain a regulated environment for the frogs. The LSS was designed to meet the physiological requirements of two frogs weighing approximately 350 g each. The frogs were demotorized to prevent them from dislodging the implanted electrodes and to reduce their metabolic rates. In this condition, the frogs required no artificial respiration and would remain healthy, without being fed, for periods as long as a month. The demotorized frogs were completely submerged in water after insertion in the centrifuge. The water served as a cushion against the high accelerations and vibrations of launch and was the medium which carried oxygen to the frogs' skins and carried away heat and carbon dioxide.

The LSS consisted of two closed loops; one contained liquid and the other contained gas. The interface between loops was at a lung which consisted basically of a selectively permeable membrane of silicone rubber that separated the liquid and gas. The membrane passed oxygen from the gas to the liquid side and carbon dioxide from the liquid to the gas side. The frogs (in the centrifuge) were in the liquid loop which from the lung to the frogs contained water and dissolved oxygen and from the frogs back to the lungs contained water and free carbon dioxide. A small pump was used to circulate the water.

Since the frogs continually discarded pieces of skin and other matter, it was necessary to provide a large area of fine filtration material around them to prevent fouling of the water circulation system. The filter consisted of two fine polyurethane cylinders which also acted to diffuse the flow of water around the frogs.

The gas loop consisted of a circuit through which oxygen was circulated by a small pump. The pump supplied pure oxygen to the lung where some of it passed into the liquid loop and the rest of it became mixed with carbon dioxide coming from the liquid loop. From the lung, the oxygen-carbon dioxide mixture was passed through a bed of Baralyme which absorbed carbon dioxide, and from the Baralyme, the pure oxygen was returned to the pump and recirculated. As oxygen was used by the frogs, it was replenished from the small oxygen tank.

Limited control of the temperature of the frogs' environment was provided by the water evaporator which maintained the water temperature at about 16°C. The evaporator pan covered the dome in the lower bulkhead and was provided with a relief valve set at 0.0106 kg/cm. The evaporator water supply was contained in a rubber bladder supported by the ring in the vessel immediately above the lower dome. In operation, a thermostat located in the LSS water circuit closed when the water temperature exceeded 16°C thereby actuating a valve timing circuit so that a valve between the bladder and the evaporator opened periodically for a given length of time. As a result of the residual sea level ambient pressure inside the vessel, water was forced from the bladder through the valve and into the evaporator. Internal heat loads were transferred through a heat exchanger to the evaporator and dissipated in evaporating the water. When the temperature had been lowered enough to open the thermostat, the valve was closed and no more water was allowed to flow.

SPACECRAFT SUBSYSTEMS

The OFOE spacecraft (Fig. VII-3) weighed 132.5 kg and was 76.2 cm in diameter and 119.4 cm long. Its lower section housed the experiment electronics and was octagonal in shape while the upper section was a truncated cone with a spherical cap. A yo-yo despin assembly was located around the satellite, and four triple-folded booms were located at 90° intervals. After separation from the launch vehicle, the despin cables were deployed to despin the satellite essentially to 0 rpm. Then the four booms were extended to limit the total acceleration to 10^{-3} g, thus providing the weightless environment essential to the experiment.

A PCM/FM/FM telemetry system that used two 10 watt 400 MHz transmitters operated in two modes as shown in Fig. VII-4. The multiplexer mode select switch controlled which two channels of otolith data (frog A or frog B) would modulate a given transmitter. The playback real-time switch controlled whether playback or real-time data were transmitted. In the playback position, data recorded on an onboard magnetic tape recorder were played back at four times the recorded speed when the satellite passed over a ground tracking station.

The timing and programming system consisted of a solid state programmer used to initiate all standard time functions within the spacecraft such as despin initiation, boom deployment, and experiment initiation. It also provided for three different experiment program routines selectable from the ground. The spacecraft timing pulses were generated by an onboard time code generator which was housed within the telemetry system PCM encoder.

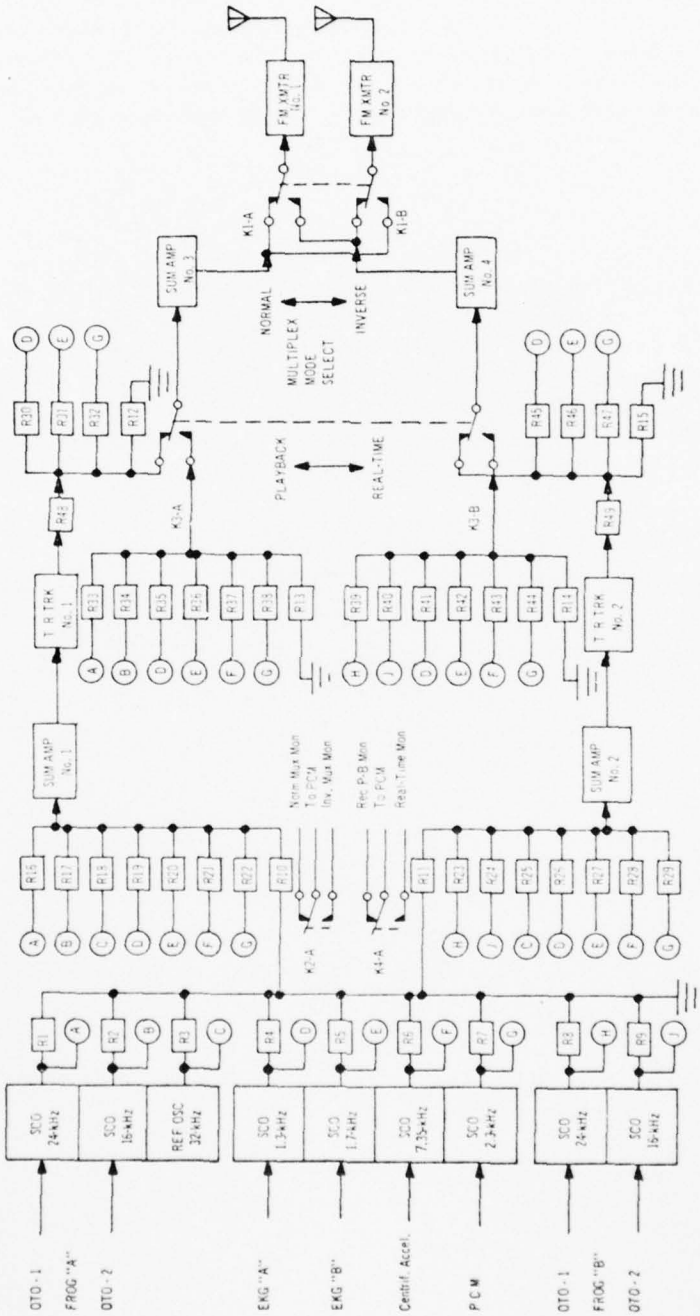

Fig. VII-4 OFOE Telemetry System Block Diagram

The command and control system consisted of a primary tone digital command subsystem and a backup subsystem utilizing straight tones. The backup subsystem used separate components (receiver and tone decoder) from that of the primary subsystem and was activated when no commands to turn on the telemetry transmitter were received for 128 minutes by the primary subsystem. The primary command subsystem had a 70-channel command capability; however, approximately one-half of these command channels were redundant for reliability reasons.

FLIGHT RESULTS

The OFOE was successfully launched into earth orbit on 9 November 1970 from Wallops Island, Virginia (line 19, Table 1). Six stations of the Goddard Flight Center STADAN (Space Tracking and Data Acquisition Network) obtained data for six days, which was the expected maximum period of proper functioning of the batteries that supplied power to the life support and monitoring systems. Scientific findings are presented in Ref. 1.

VIII

IMP-I SOLAR PROTON MONITOR

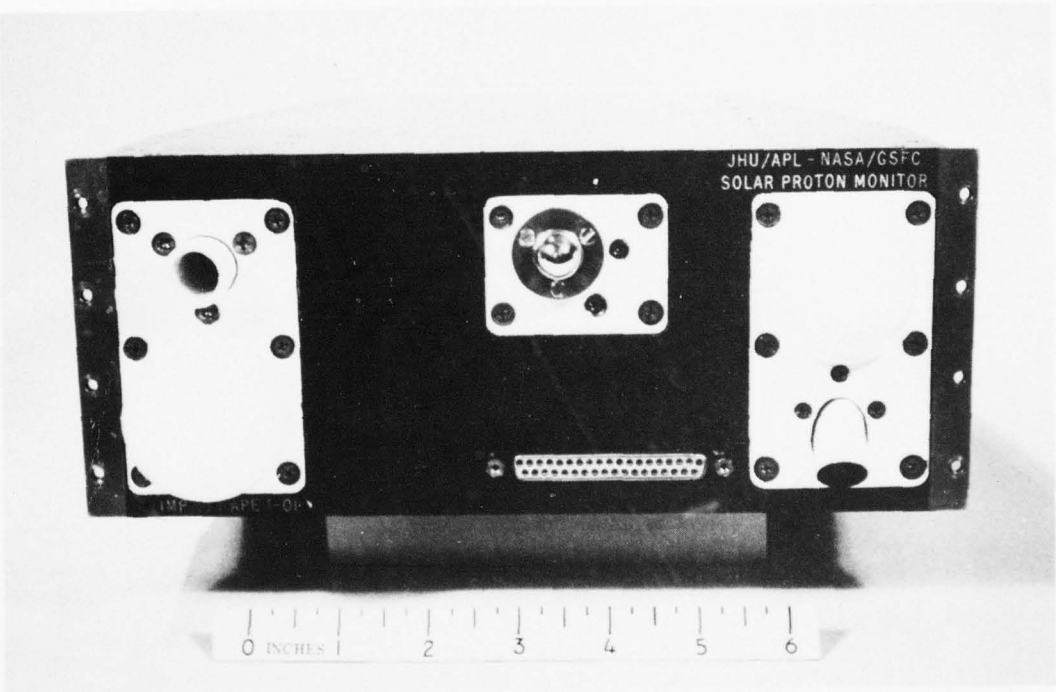

Fig. VIII-1 IMP-I Solar Proton Monitor

VIII

IMP-I SOLAR PROTON MONITOR

BACKGROUND

The need for monitoring solar energetic particles was recognized in the mid-1960s, and instrumentation for this purpose was designed jointly by NASA/GSFC and APL scientists. The first versions of the Solar Proton Monitor (SPM) were flown aboard a series of sounding rockets in the Solar Particle Intensity and Composition Experiment (SPICE) Program starting in 1966. Launched in May 1967, the IMP F (Interplanetary Monitoring Platform) was the first satellite to carry an SPM (refer to Section IV).

Within the last 15 years, the emission of energetic (1 to 1000 MeV) protons by the sun has been realized to be a fairly common occurrence, particularly near the peak of the solar activity cycle. From 1956 to 1963, such protons were detected in the vicinity of the earth on at least 64 occasions, either directly by satellite, rocket, or balloon techniques; or indirectly by ground based radio detection of their ionospheric effects.

APPLICATION

The SPM (Fig. VIII-1) was used to measure the energy spectrum, angular distribution, and intensity of charged particles in the interplanetary medium. The three basic monitoring channels employed omnidirectional detectors to measure protons with energy levels greater than 60, 30, and 10 MeV and were designed for simple, reliable, and reproducible operation.

Proton fluxes, in addition to being of great intrinsic scientific interest, can have important practical consequences since the more intense fluxes create a significant radiation hazard to manned spaceflight missions and give rise to intense, long duration blackouts in high frequency radio communications at high latitudes. In addition to the practical need for early warning of the occurrence of solar proton events, a basic scientific need exists for the routine monitoring of the properties of solar proton fluxes over an extended period of time (on the order of half a solar cycle). Solar protons are of fundamental scientific importance in providing information on particle acceleration processes at the sun. The data thus gathered are also used to determine the configuration of the magnetic fields in interplanetary space that influence the propagation of protons from the sun to the earth.

AD-A072 438 JOHNS HOPKINS UNIV LAUREL MD APPLIED PHYSICS LAB F/G 22/2
INSTRUMENTATION DEVELOPED BY THE JOHNS HOPKINS UNIVERSITY APPLI--ETC(U)
NOV 78 N00024-78-C-5384
UNCLASSIFIED APL/JHU/SDO-4100 NL

2 OF 3
AD
A072438

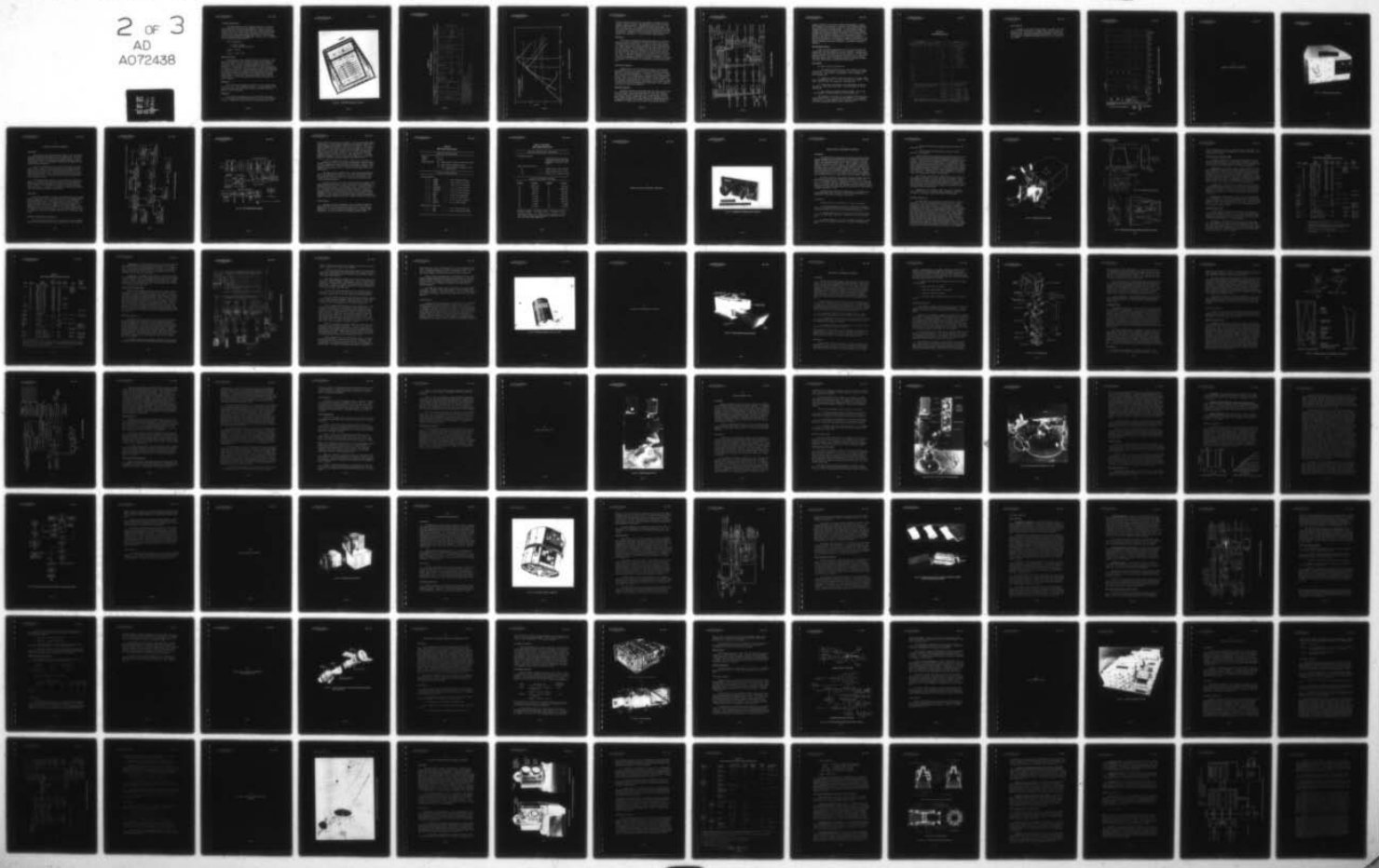

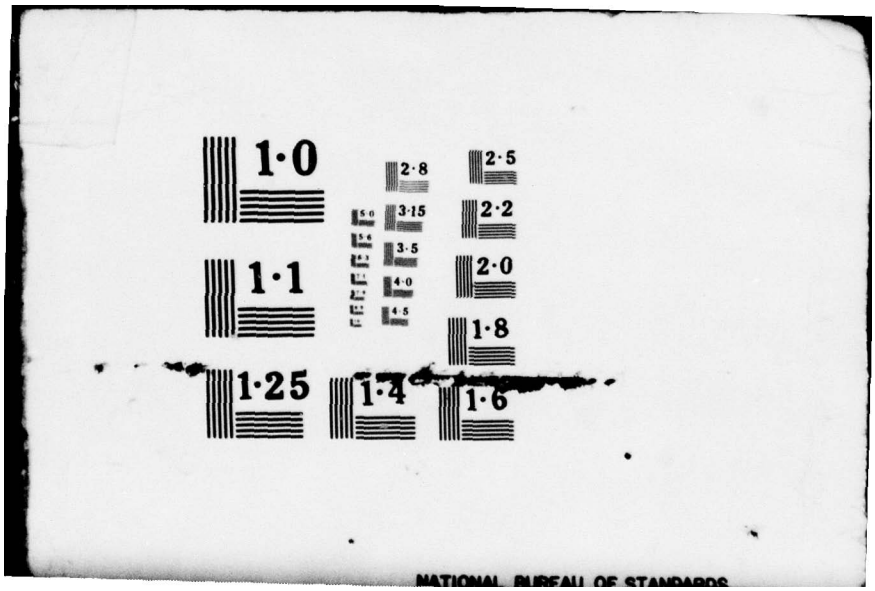
1·0
1·1
1·25
1·4
1·6
1·8
2·0
2·2
2·5
2·8
3·15
3·5
4·0
4·5
5·0
NATIONAL BUREAU OF STANDARDS

EQUIPMENT DESCRIPTION

The SPM consisted of five separate detectors, each using one or more solid state detector elements to cover the proton energy range from ~210 keV to ≥60 MeV and to measure low energy electrons and 8.2 to 20 MeV alpha particles. The detectors were secured to the front panel and the electronics were mounted in an RF shielded rectangular housing (Fig. VIII-2). The principal detector characteristics are summarized in Table VIII-1; following are the major SPM characteristics:

Power Consumption:

1.3 watts average
1.5 watts during calibration

Weight: 3.61 kg

Volume: 5,326.75 cm^3

Detectors 1 and 2

These detectors were identical except for shielding. Each detector consisted of a set of three surface barrier detectors, 0.85 cm^2 by 700 μm thick, connected in parallel and mounted on orthogonal axes to provide a uniform geometric factor over 2π steradians. System noise was about 40 keV, and the discriminator level was set at 150 keV. Since the detectors were fully depleted (overbiased by ≥25%) and a minimum ionizing particle deposited ≥250 keV, all particles with energies above the threshold set by the hemispherical shield were counted. This design allowed rather large changes in temperature, voltage, amplifier gain, detector resolution, etc. to be tolerated without a serious change in detector response.

Detector 3

This detector was similar to detectors 1 and 2 except that it was a 3 × 3 × 3 mm Li drifted detector. It was operated at 200 volts bias, which was sufficiently large to eliminate radiation damage at orbital altitude.

Detector 4

This detector consisted of two surface barrier devices, a 1 cm^2 × 50 μm detector (4A) backed up by a 1.5 cm^2 × 100 μm detector (4B). Figure VIII-3 shows curves of energy absorption (ΔE)

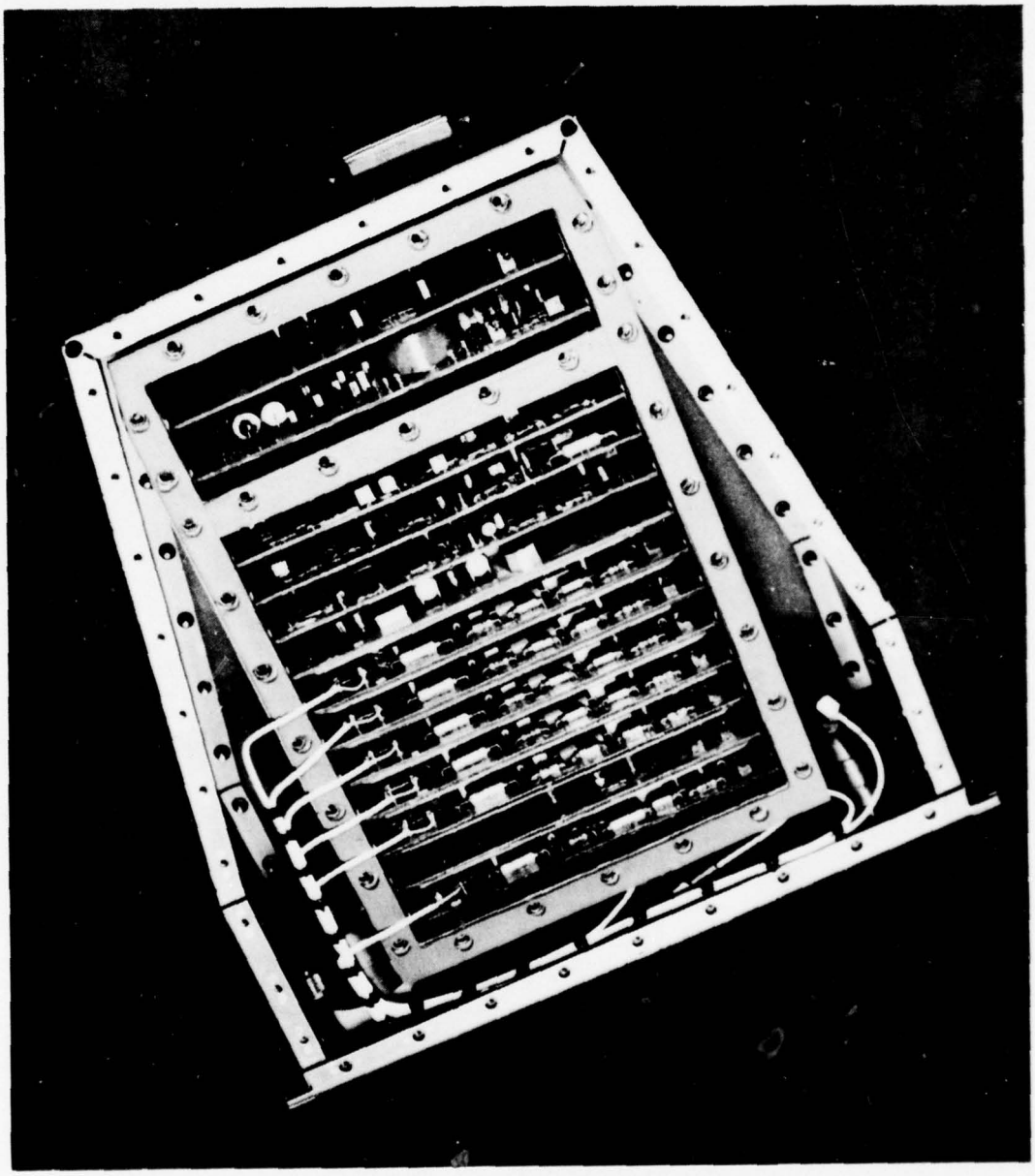

Fig. VIII-2 IMP-I SPM Electronics, Top View

THE JOHNS HOPKINS UNIVERSITY
APPLIED PHYSICS LABORATORY
LAUREL, MARYLAND

Table VIII-1

IMP-I SPM Detector Characteristics

Channel Designation	Energy Range (MeV) (a)			Absorber	Field of View	Look Direction	Geometric Factor (e) (cm^2 sr)	Accumulation Time (seconds)	Duty Cycle	Accumulator	Discriminator Levels (MeV)	Logic (i)
	Protons	Alpha Particles	Electrons									
1	≥60	≥240	≥8	4.98 g/cm^2 Cu (dome) (b)	2π sr	⊥ spin axis	6.28	5.12 (f)	50%	A	0.15	--
2	≥30	≥120	≥2.15	1.42 g/cm^2 Cu (dome) (b)	2π sr	⊥ spin axis	6.28	5.12 (f)	50%	B	0.15	--
3	≥10	≥40	≥0.60	0.17 g/cm^2 Al (dome) (b)	2π sr	⊥ spin axis	0.791	5.12 (f)	50%	C	0.30	--
41	0.21 - 0.53	0.4 - 0.72	(0.15, low eff.)	0.22 mg/cm^2 Ni (c)	Cone 10° half-angle, 0.096 sr	⊥ spin axis	0.096	5.12 (f) and (g)	50% and (h)	A and D	A_1 = 0.15 A_2 = 0.46 A_3 = 2.89 B = 0.20 (i)	$A_1\bar{A}_2\bar{B}$
42	0.53 - 2.2	0.72 - 3.2	----					5.12 (f) and (g)	50% and (h)	B and E		$A_2\bar{A}_3\bar{B}$
43	2.2 - 7.5	20 - 170	----					5.12 (f)	50%	C		$A_2\bar{A}_3B$
44	---	3.2 - 20	----					(g)	(h)	F		A_3B
5	≥0.18	≥0.7	≥0.01	None (d)	Cone, 10° half-angle, 0.096 sr	135° to spin axis	~0.0096	(g)	(h)	G	Above noise	--

(a) Primary contributor in interplanetary space is underlined.
(b) Shielding (except for dome) is ≥60 MeV proton equivalent of Cu.
(c) Shielding (except for aperture) is ≥30 MeV proton equivalent of Cu.
(d) Shielding (except for aperture) is ≥50 MeV proton equivalent of Cu.
(e) Not valid for galactic cosmic ray spectrum.
(f) High bit rate mode; at low bit rate, accumulation time = 20.48 seconds.
(g) 1.5 seconds/sector × 8 sectors/revolution × 5 revolutions = 60 seconds (per 81.92 seconds
(h) Total = 73% or 9.1% per sector.
(i) Channel 4 contains two detectors. A levels on front detector, B levels on rear detectors.

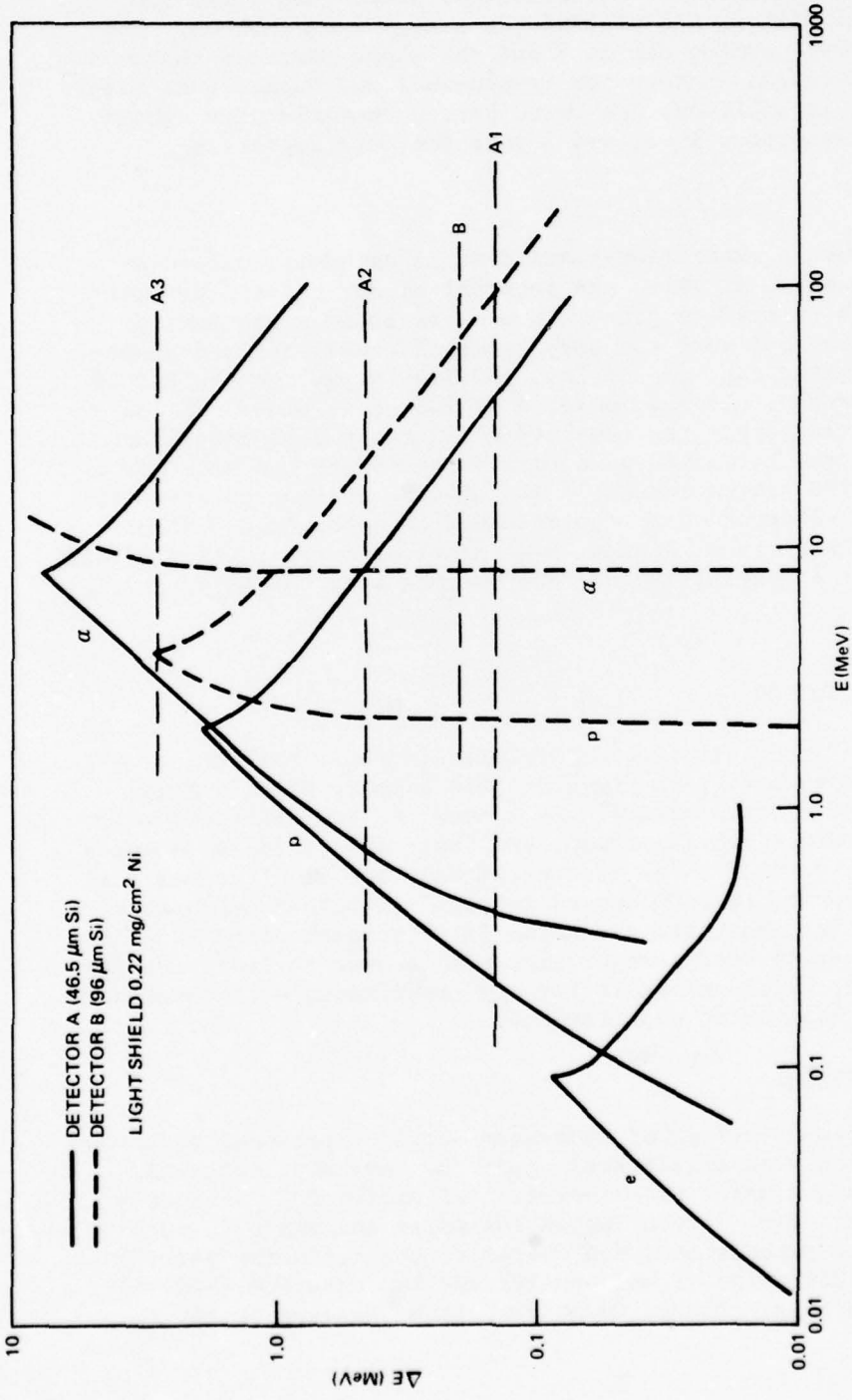

Fig. VIII-3 Channel 4 ΔE-E Characteristics

versus particle energy (E) for this channel, including absorber effects. Electron, proton, and alpha-particle curves are given, assuming normal incidence. Discriminator levels and logic are given in Table VIII-1, and yielded the energy ranges shown. The two lowest energy proton channels and the alpha-particle channels were sectored (eight sectors per revolution) and summed over five revolutions. In addition, the three proton channels were subcommutated with detectors 1, 2, and 3 into the data registers.

Detector 5

This was an experimental solid-state detector, called an avalanche detector, in which the internal electric field was sufficiently high to produce gain. It was the solid state anology of a Geiger tube but with the advantages of a well defined geometry, high counting rate capability, and low energy threshold (~10 keV for electrons). It was operated at 200 volts bias. The output was sectored (eight per revolution), but the look direction was 135° from the satellite spin axis to eliminate the need for a sun shield. The proton threshold was similar to that of detector 4 so that the electron contribution could be determined. Since this was an experimental device, a separate on command was provided to eliminate the possibility of interference with the main experiment.

FUNCTIONAL OPERATION

Figure VIII-4 shows the SPM block diagram. Each detector had associated with it a charge-sensitive preamplifier, voltage amplifiers, and discriminators. In channel 4, two detectors were used in a telescope configuration, and their discriminator outputs were combined to yield three proton channels and an alpha-particle channel. Note that the SPM had an integral in-flight calibrator and circuitry for measuring the noise level of each channel. These two features constituted a major improvement over earlier versions of the SPM and, while desirable for any experiment, were especially valuable in a monitoring experiment.

Avalanche Detector

Particles entering the avalanche detector produced electron-hole pairs which were accelerated under the very high internal electric fields, causing the liberation of additional, similarly accelerated carriers. Depending on the point and angle of incidence, depth of penetration, and energy of the impinging particle, a charge multiplication of between 10^2 and 10^3 occurred (Ref. 1). Consequently a single factor to convert from incident energy to

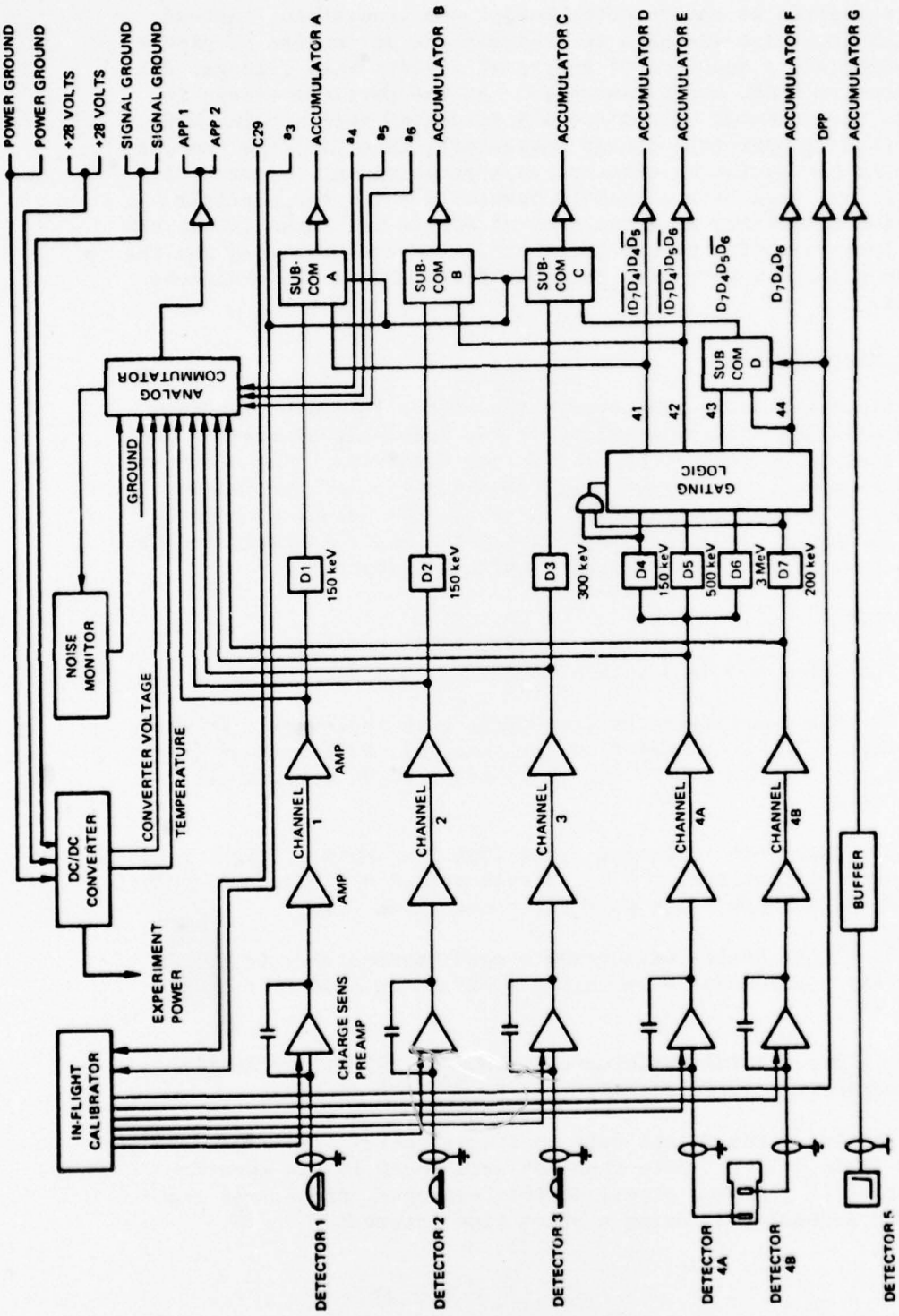

Fig. VIII-4 IMP-I SPM Block Diagram

charge collected at the detector output was impossible, instead an efficiency curve was used to indicate the percentage of particles counted as a function of energy at a given bias voltage, discriminator setting, and temperature. As the particle energy increased, the detector pulses quickly saturated (did not increase in magnitude as particle energy increased), thus limiting the usefulness of the avalanche detector as a proportional counter. Instead, it was used as a threshold device in which the particle collection efficiency as a function of energy was essential to the proper interpretation of the threshold. The circuits used for the junction detectors were also suitable for use with the avalanche detector.

Average Noise Monitor

Since the noise characteristics of the junction detectors changed with age and temperature, it was desirable to monitor the noise level as an indication of detector condition. The SPM noise monitor measured the average noise at the output of the last pulse amplifier in each channel except the avalanche detector channel. This high signal level, low-impedance point was relatively immune to pickup and provided a suitable monitoring point.

Data Format

The IMP-I SPM data consisted of:

1. Six counting rates from three rate registers. Accumulation time = 20.48 seconds (low bit rate, L); 5.12 seconds (high bit rate, H). Cycle time - two snapshots = 40.96 seconds (L); 10.24 seconds (H).

2. Thirty-two counting rates from four sets of eight registers. Accumulation time = 5 × 1/8 spin period ≈ 7.5 seconds. Cycle time = 81.92 seconds = one page (L) = one album (H).

3. Eight analog measurements read sequentially in APP 22 and APP 46. Cycle time = one album - 327.68 seconds (L); 81.92 seconds (H).

4. One digital performance parameter (DPP). Cycle time = two snapshots = 40.96 seconds (L); 10.24 seconds (H).

The locations of the data in the telemetry format are specified in Table VIII-2. Note that the data found in the specified locations (i.e., timing signal states, sequence, frame, and channel) were accumulated during a prior time interval.

Table VIII-2
IMP-I SPM Data Format

Item	Timing Signals				Position			SPME Data	
	a_3	a_4	a_5	a_6	Seq.	Frame	Ch.	ID	Detector
1	1	1	1	1	0	0	5, 6	1	>60 MeV p
2					0	4	6 → 15	41s	0.21-0.56 MeV p
3					0	8	5, 6	2	>30 MeV p
4					0	12	6 → 15	42s	0.56-2.2 MeV p
5					2	0	5, 6	3	>10 MeV p
6					3	8	5(DPP_{a_3})	CAL	Cal on-off
7	0	1	1	1	0	0	5, 6	41	0.21-0.56 MeV p
8					0	4	6 → 15	44s	8.2-20 MeV α
9					0	8	5, 6	42	0.56-2.2 MeV p
10					0	12	6 → 15	5s	>10 keV e^-
11					2	0	5, 6	43	2.2-7.5 MeV p
12					3	8	4(APP 22)	AN0	Analog Ch. 0 = 0 volts
13	1	0	1	1	0	0	5, 6	1	
14					0	8	5, 6	2	
15					2	0	5, 6	3	
16					3	8	5(DPP_{a_3})	CAL	
17	0	0	1	1	0	0	5, 6	41	
18					0	8	5, 6	42	
19					2	0	5, 6	43	
20					3	8	4(APP 46)	AN1	Analog Ch. 1 = power on
	(Items 1-11 and 13-19 repeat at page rate = a_4 rate → 8192 seconds (L); 20.48 seconds (H)). (Items 12 and 20 repeat in the format but change information, and identification is derived from timing signals as shown below.)								
21	0	1	0	1	3	8	4(APP 22)	AN2	Analog Ch. 2 = temp.
22	0	0	0	1	3	8	4(APP 46)	AN3	Analog Ch. 3 = noise 1
23	0	1	1	0	3	8	4(APP 22)	AN4	Analog Ch. 4 = noise 2
24	0	0	1	0	3	8	4(APP 46)	AN5	Analog Ch. 5 = noise 3
25	0	1	0	0	3	8	4(APP 22)	AN6	Analog Ch. 6 = noise 4A
26	0	0	0	0	3	8	4(APP 46)	AN7	Analog Ch. 7 = noise 4B
	(SPME channels AN0-AN7 repeat at album rate = a_6 rate → 327.68 seconds (L); 8192 seconds (H)). (Note: timing signal (a_3, a_4, a_5, a_6) state 0 means negative, 1 means positive.)								

FLIGHT RESULTS

Operation of the Solar Proton Monitor, launched into orbit aboard the IMP-I satellite on 13 March 1971 (line 23, Table 1), was excellent. Data from the satellite indicated that all subsystems of the instrument operated satisfactorily. Figure VIII-5 is a summary of subsystem performance for the first 11 months of the mission.

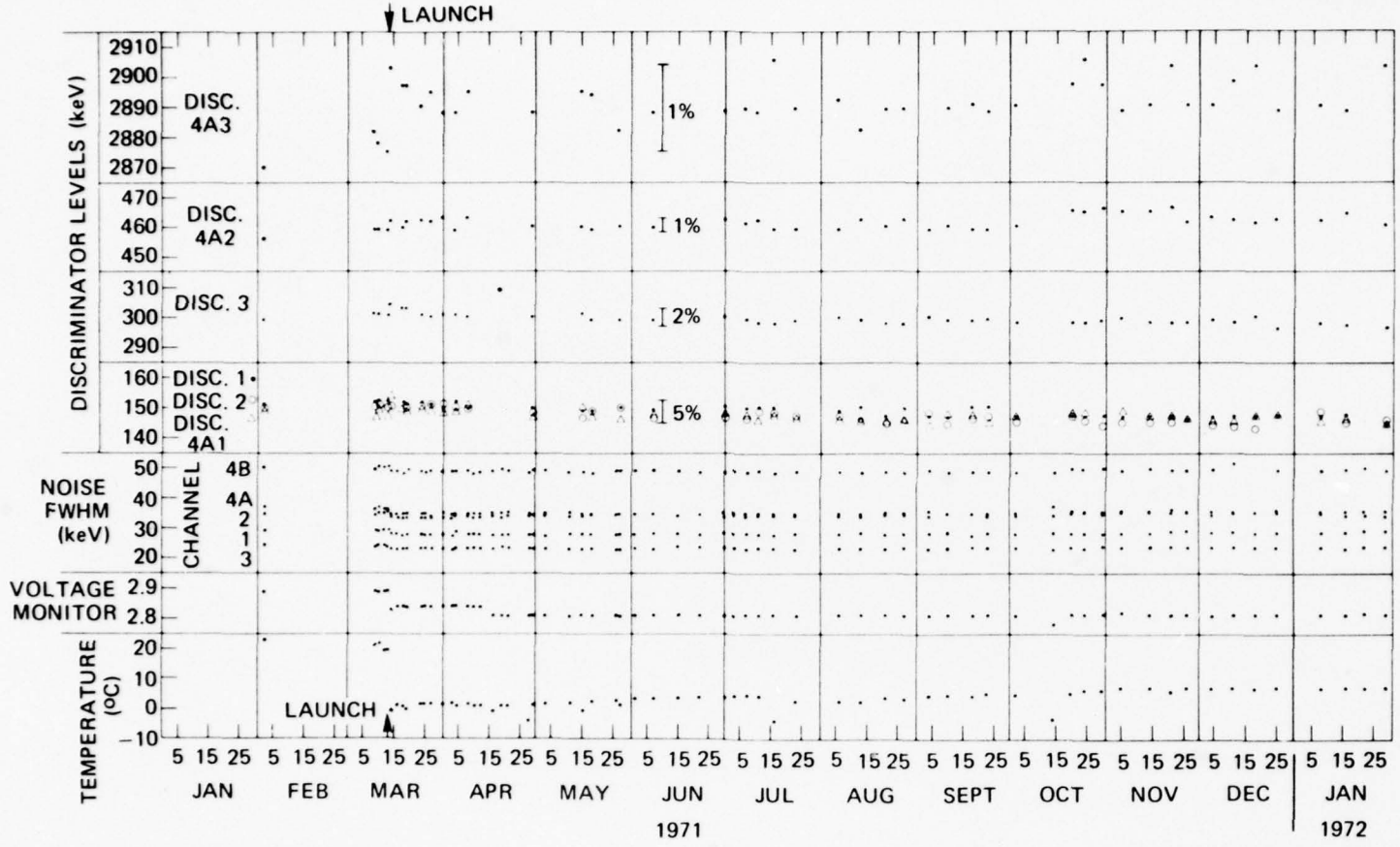

Fig. VIII-5 IMP-I SPM Performance Summary During First 11 Months of Mission

THE JOHNS HOPKINS UNIVERSITY
APPLIED PHYSICS LABORATORY
LAUREL, MARYLAND

IX

ENERGETIC PARTICLES EXPERIMENT

Fig. IX-1 Energetic Particles Experiment

IX

ENERGETIC PARTICLES EXPERIMENT

BACKGROUND

The Energetic Particles Experiment (EPE) for the Interplanetary Monitoring Platforms (IMP)-H and -J missions (Fig. IX-1) was designed to study the low energy particle populations. It was a joint research effort of the Space Environment Laboratory (SEL) of the National Oceanic and Atmospheric Administration (NOAA) and the Applied Physics Laboratory.

Most of the experiment electronics were designed and fabricated at APL. However, the main telescope (five surface barrier detectors with collimator and electron deflection magnet) was designed and fabricated by SEL. Two additional detectors, F and G, were provided by APL. Ground support equipment and payload qualification were primarily an APL effort while SEL directed the particle calibration work.

The equipment was delivered to Electro-Mechanical Research (EMR), Inc., College Park, Maryland, after initial qualification. EMR provided payload integration and performed all work required prior to launch. APL provided test support as needed during payload qualification. Figure IX-2, the EPE vital operations diagram, shows the program interagency relationships.

APPLICATION

The EPE was designed to measure low energy protons, electrons, and alpha particles in the interplanetary medium, the magnetosheath, and the geomagnetic tail, and in the vicinity of the boundaries separating these regions. The measurements were used to study the physics governing the origin, transport, and energy changes of charged particles within these regions and between regions. The IMP-H and -J orbits, nearly circular at 30 to 40 R_E, permitted regular sampling of the several regions and, when both spacecraft were in operation, permitted simultaneous observations in different locations.

EQUIPMENT DESCRIPTION AND OPERATION

The EPE instrument (Fig. IX-3) consisted of a main telescope assembly and two auxiliary detectors, and utilized silicon surface

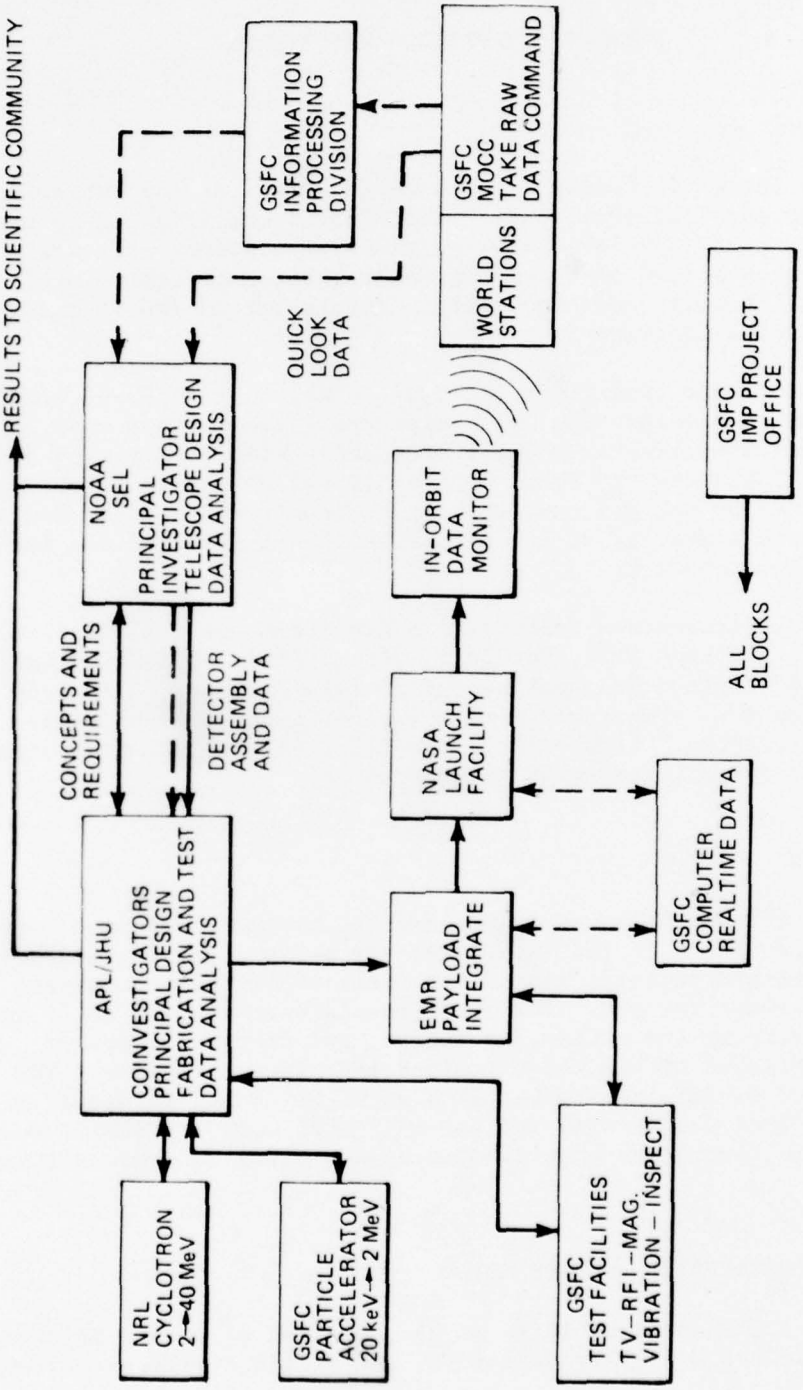

Fig. IX-2 EPE Vital Operations Diagram

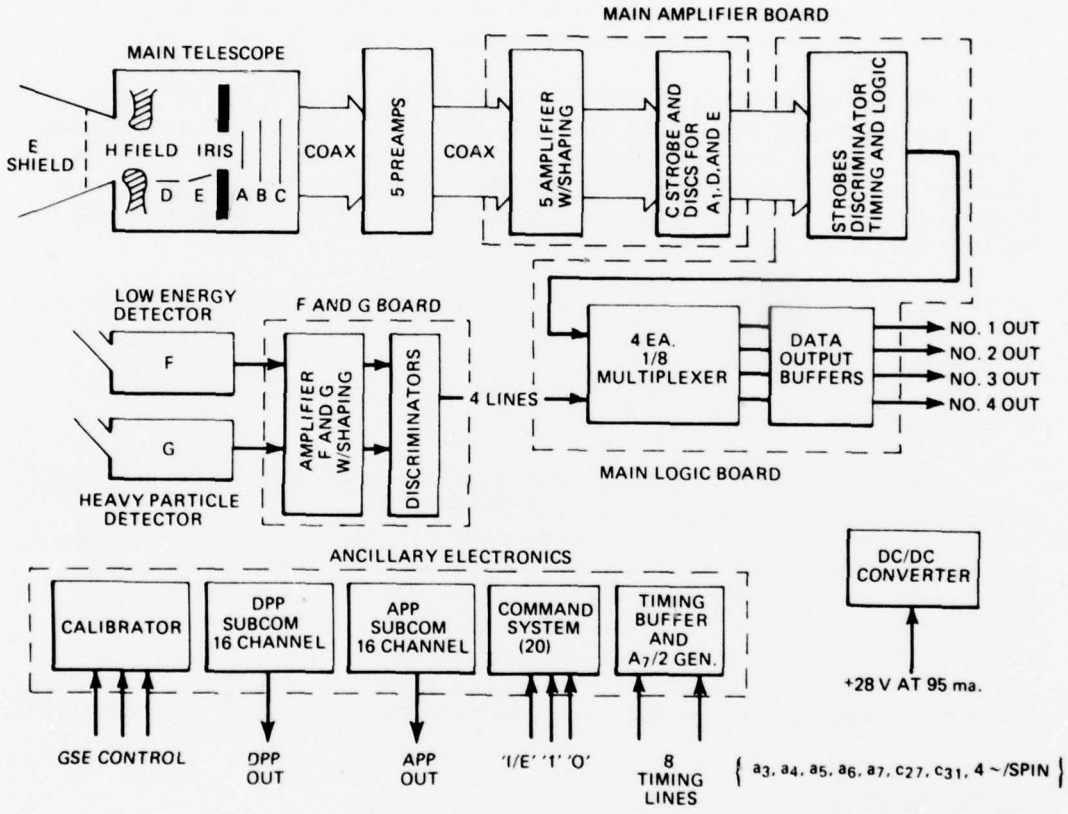

Fig. IX-3 EPE Simplified Block Diagram

barrier solid state detectors throughout. The main telescope assembly contained a three-element telescope which was swept clear of low energy electrons by a magnet placed in the collimator. The telescope consisted of detectors A (50μ thick × 25 mm^2), B, and C (each 500μ thick × 50 mm^2) whose outputs were used singly and in coincidence to cover the energy ranges 50 keV to 25 MeV for protons and 2 MeV to 35 MeV for alpha particles. Also in the main telescope assembly were two detectors, D and E (each 300μ thick × 3 × 6 mm), which were mounted to one side and used the magnet in an analyzing capacity to measure electrons between 30 keV and 200 keV.

Of the two separate detectors, F (100μ thick × 25 mm^2) was an ultra-low noise unit with a single discriminator level set around 20 keV to measure low energy electrons and protons. Detector G was ultra-thin (~5μ thick × 25 mm^2) and had discriminator levels set to measure alpha particles and $Z \geq 3$ particles with energy above ~150 keV/nucleon.

The main telescope assembly had a look direction perpendicular to the satellite spin axis, but the F and G detectors looked at 45° to the spin axis in order not to view the sun directly. All channels were sectored by 8 or 16 to obtain angular distributions of the particles measured.

The instrument also included complete analog and digital housekeeping systems to maintain current information on the experiment modes and the condition of the detectors. Some 21 commands were used to control power supplies, discriminator levels, logic selections, etc. A comprehensive electronic in-flight calibrator provided a thorough check on the experiment electronics from the preamplifiers through the output logic and permitted routine calculation of discriminator level settings for comparison with prelaunch calibrations. Summary equipment characteristics for the EME are listed in Table IX-1.

FLIGHT RESULTS

Energetic Particles Experiments were successfully launched aboard the IMP-H and IMP-J satellites (lines 27 and 34, Table 1), respectively); both are operating satisfactorily. Data are being obtained by the GSFC Multisatellite Operation Control Center and processed by the GSFC Information Processing Division (IPD).

Table IX-1

EME Technical Data Summary

Physical Characteristics		
Height:	12.7	cm
Weight:	3.18	kg
Power Required:	2.6	watts nominal @ 25°C & 28.0 Volts input
	2.8	watts during command sequence
	3.1	watts during calibrate sequence (1/60 duty cycle)

Particle Identification			
Main Telescope:			
L - 1	$A_1\bar{A}_2\bar{B}_1$	.....	30 to 200 keV protons
L - 2	$A_2\bar{A}_4\bar{B}_1$	.....	200 to 800 keV protons
L - 3	$A_4\bar{A}_5\bar{B}_1$	.....	0.80 to 2.1 MeV protons
L - 4	$A_4\bar{A}_5B_1\bar{B}_2\bar{C}$	.....	2.1 to 4.5 MeV protons
L - 5	$A_3\bar{A}_4B_2\bar{B}_3\bar{C}$	.....	4.5 to 8.5 MeV protons
L - 6	A_2B_1C	.....	8.5 to 25.0 MeV protons
L - 9	$\bar{A}_2B_1\bar{C}$	.....	Cosmic Ray Background
L - 10	$A_5\bar{B}_1$	.....	2.2 to 8.4 MeV alphas
L - 11	$A_6B_1\bar{C}$	.....	8.4 to 16.0 MeV alphas
L - 12	$A_5\bar{A}_6B_2\bar{C}$	.....	16 to 35 MeV alphas
Main Electron Detectors:			
L - 7	$D_1\bar{D}_2$	.....	30 to 100 keV electrons
L - 8	$E_1\bar{E}_2$	.....	100 to 200 keV electrons

Table IX-1 (Concluded)
EME Technical Data Summary

Particle Identification (Concluded)

Low Energy Detector:

F	.....	Electrons and protons above 15 keV (This level may vary dependent on detector noise level)

Heavy Particle Detector:

G_1	.....	Alphas greater than 500 keV
G_2	.....	Alphas greater than 1.6 MeV
G_3	.....	Particles of Z greater than 2

Nominal Discriminator Settings

Channel	Setting	Channel	Setting
A_1	30/50 keV[1]	C	100 keV[4]
A_2	200 keV[2]	D_1	30/50 keV[1]
A_3	500 keV	D_2	100 keV
A_4	800 keV	E_1	100 keV
A_5	2.5 MeV	E_2	200 keV
A_6	3.5 MeV	F	15/30 keV[1]
B_1	100 keV[3]	G_1	500 keV[5]
B_2	3.6 MeV	G_2	1.0 MeV[5]
B_3	9.0 MeV	G_3	2.6 MeV[5]

[1]Command variable, [2]A Channel strobe, [3]B Channel strobe, [4]C Channel strobe, [5]G_1 = 600, G_2 = 2.0, and G_3 = 11.0 for IMP J, which reflected new information revealed by late data from other IMP spacecraft.

X

CHARGED PARTICLE MEASUREMENT EXPERIMENT

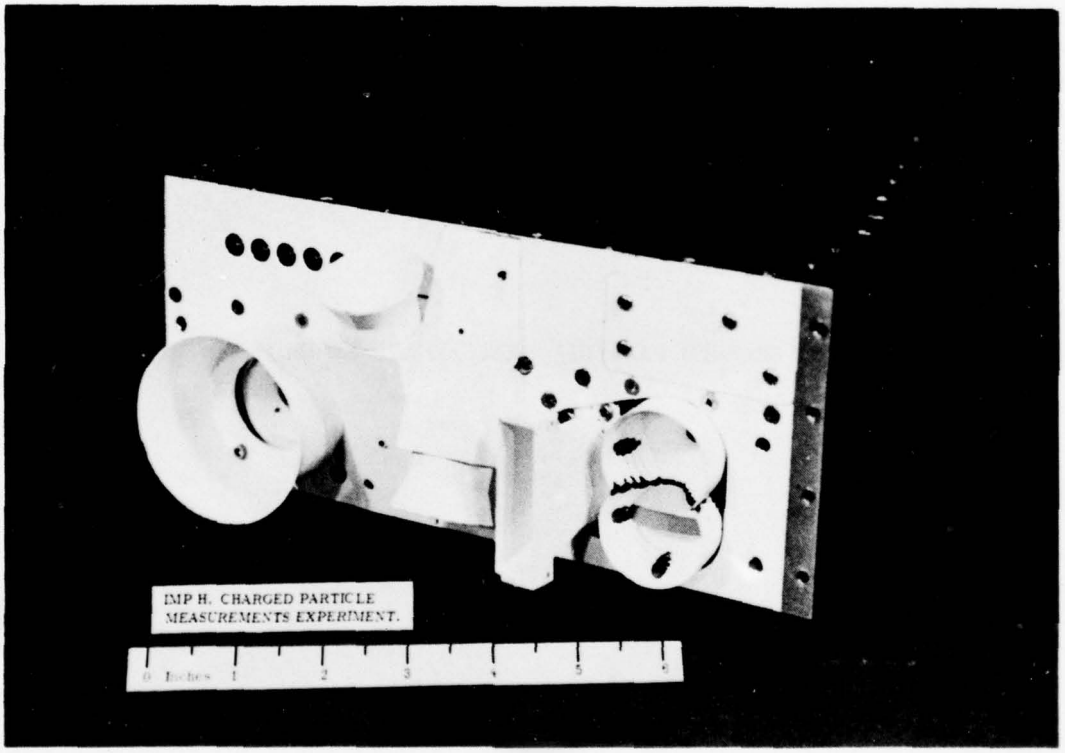

Fig. X-1 Charged Particle Measurements Experiment

X

CHARGED PARTICLE MEASUREMENT EXPERIMENT

BACKGROUND

The NASA-sponsored Interplanetary Monitoring Platform (IMP) Program represented the mainstream of the United States research effort in fields and particles from the early 1960s to the early 1970s. APL experiments were flown on IMPs F through J, and are presently operating on IMPs H and J. As discussed in Sections IV and VIII, the -F, -G, and -I experiments provided continuous monitoring of solar protons from 1967 through 1974, and the data were used extensively by the worldwide scientific community. These detectors provided data on proton intensities in the energy ranges 1 to 10, greater than 10, 30, and 60 MeV; the IMP-H and -J missions were to obtain data over a wider range and with greater sensitivity.

The Charged Particle Measurement Experiment (CPME) was first proposed for the IMP-H and -J missions in 1967 by the team of Dr. S. M. Krimigis, Principal Investigator, and Drs. T. P. Armstrong and J. A. Van Allen, when Dr. Krimigis was at the University of Iowa. When Dr. Krimigis joined The Johns Hopkins University Applied Physics Laboratory in 1968, the CPME program was transferred to the Space Development Department of APL.

A separate and complementary instrument, the Energetic Particles Experiment (EPE), was also flown aboard the IMP-H and -J satellites. The EPE is discussed in Section IX.

APPLICATION

The objectives of the CPME (Fig. X-1) were as follows:

1. Study the absolute intensities, propagation characteristics, local angular distribution, and energy spectra of energetic electrons, protons, and $Z \geq 2$ nuclei emitted from the sun,

2. Measure absolute flux, energy spectra, and solar modulation of the low-energy component of cosmic ray electrons and protons,

3. Measure absolute intensities, angular distribution, and energy spectra of charged particles in the earth's magnetospheric tail,

4. Observe intensities and energy spectra of solar X-ray emission, and

5. Provide long-term monitoring of the more intense galactic X-ray sources.

Areas in which these observations are being applied include studies of the anisotropic diffusive propagation of electrons, protons, and nuclei as a function of energy and helicentric radial distance. This may resolve ambiguities in the propagation model caused by anisotropies in the early part of a solar flare event, and the question of energy and/or velocity dependence of the propagation mechanism can be illustrated. It may also provide a means for studying macroscopic properties of the interplanetary magnetic field and for an evaluation of the radial dependence of the diffusion coefficient. The influence of solar modulation on galactic cosmic ray intensity may thus be ascertained.

Since primary electrons were measured down to 0.2 MeV, information on the origin of cosmic rays and the relevant portion of the nonthermal galactic radio spectrum may be provided. It may also further the understanding of contributions to primary electron flux from p-p collisions between cosmic-ray protons and interstellar hydrogen and thus provide a means for studying the interplanetary modulation mechanism.

Measurement of the primary cosmic ray proton components should answer questions concerning solar modulation, solar wind convection, and particle diffusion into the solar system.

EQUIPMENT DESCRIPTION

The CPME employed two different charged particle detection techniques. The first technique involved the use of a three-element solid-state detector array in a dE/dx and E telescopic arrangement placed within a plastic anticoincidence scintillator. An opening in the front of the scintillator defined its look angle. The Proton Electron Telescope (PET) measured electrons, protons, alpha particles, and nuclei with $Z \geq 3$ in several energy ranges. The second detection technique involved an array of Geiger-Mueller (GM) tubes sensitive to electrons and X-rays. Three GM tubes called the Geiger Telescope (GT), were placed inside an anticoincidence scintillator which again defined look angles. Two additional GM tubes, called the North-South Telescope (NST), were directed along the spacecraft spin axis and normal to the GT. Figure X-2 shows the detector look angles with respect to the experiment package and the spacecraft spin axis, while Fig. X-3 provides an

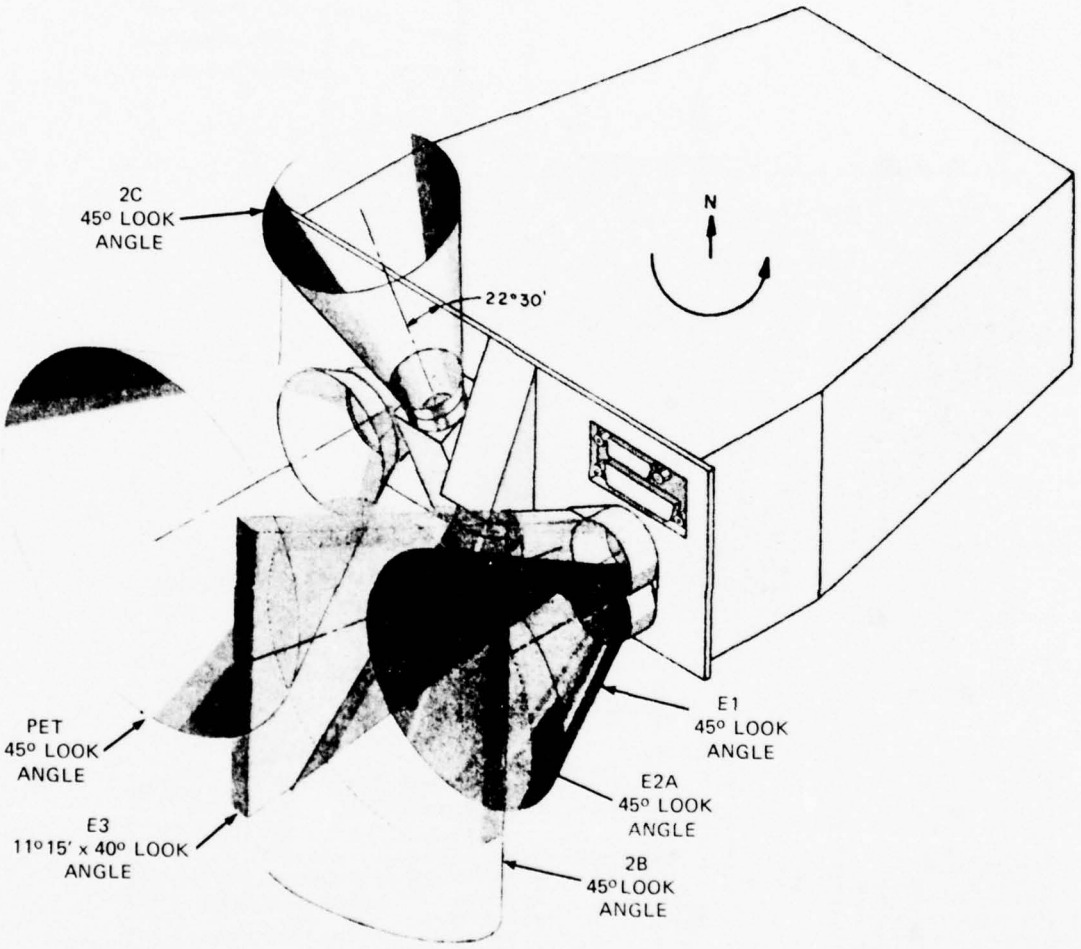

Fig. X-2 CPME Detector Look Angles

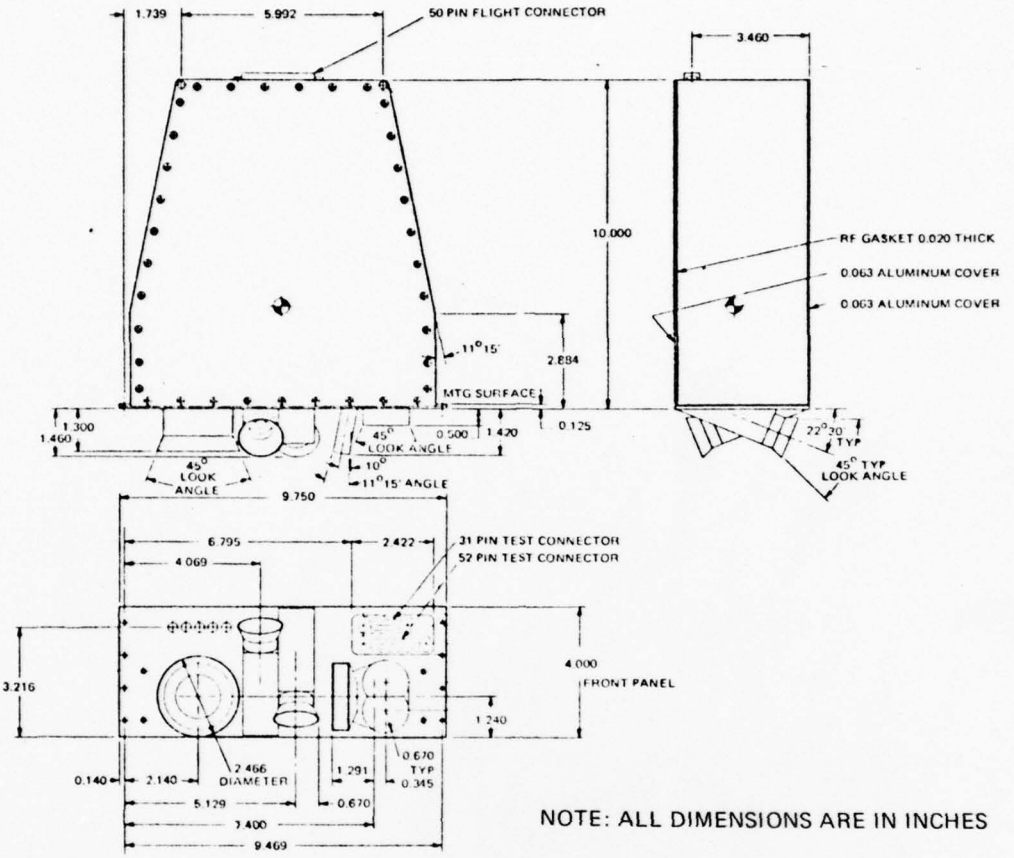

NOTE: ALL DIMENSIONS ARE IN INCHES

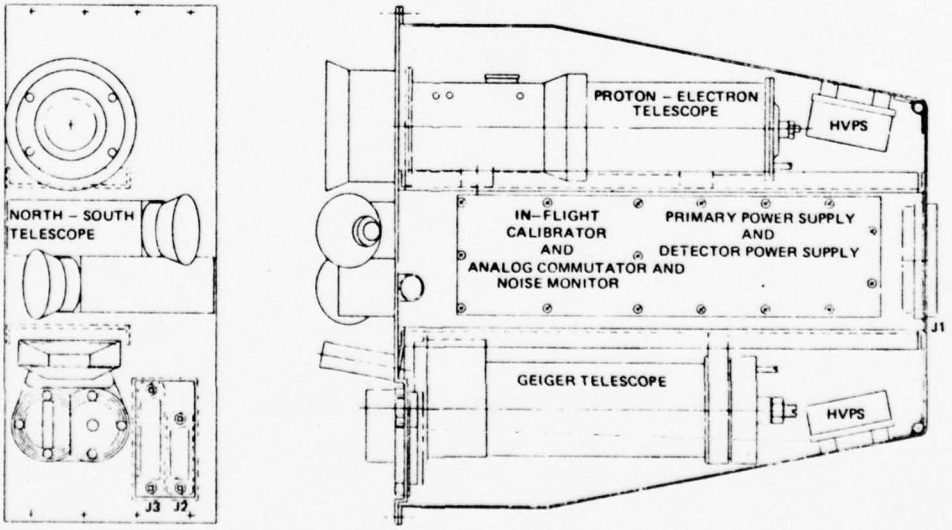

Fig. X-3 CPME Outline Drawing and Major Component Locations

outline drawing and shows the locations of major components. Detector characteristics are summarized in Table X-1 for IMP H, and in Table X-2 for IMP J.

Proton Electron Telescope (PET)

The PET consisted of an array of three solid-state detectors and supporting units. The detectors functioned to identify particle type and determine particle energy. The characteristics of the detectors are discussed in the following paragraphs.

Detector D1. This detector was a totally depleted silicon surface barrier detector with a nominal thickness of 40 μm and an active area of 2.0 cm^2 mounted in a shockproof transmission ring of boron nitride. Detector noise, measured at 23°C with a bias voltage of 20 volts, was about 20 keV fwhm. Resolution for 5.477 MeV alpha particles, measured at 23°C with operating bias voltage, was less than 50 keV fwhm. The aluminum and gold surface coatings were 40 $\mu gm/cm^2$ thick, which corresponds to an energy loss of about 15 keV in the aluminum for 5.477 MeV alpha particles.

Detector D2. This detector was a 900 μm totally depleted silicon surface barrier detector of 2.0 cm^2 active area mounted in a shockproof transmission ring of boron nitride. Detector noise, measured at 23°C with a bias voltage of 250 volts, was about 22 keV fwhm. Resolution of 5.477 MeV alpha particles was less than 35 keV fwhm.

Detector D3. This detector was a 2700 μm lithium drifted (total thickness, 3000 μm) silicon detector with an active area of 2.0 cm^2 mounted on an aluminum transmission ring. Detector noise, measured at 23°C with a bias voltage of 450 volts, was in the range of 13 to 23 keV fwhm. Resolution for 5.477 MeV alpha particles bias voltage, was 70 keV fwhm.

Geiger Telescope (GT)

The GT, which measured solar and cosmic X-ray fluxes in several energy ranges, consisted of a set of three Geiger-Mueller (GM) tubes and supporting units. The GM tubes acted as the basic radiation measuring devices in this telescope. The physical and operational characteristics are described below.

GM Tube E1. This LND-705 GM tube was a neon plus halogen quench gas filled tube with an effective diameter of 0.093 inch with very thin mica end windows (0.3 to 0.4 mgm/cm^2 mica). Internal gas pressures were between 30 to 40 cm Hg. The plateau lengths were >200 volts with a slope of approximately 0.03 to 0.15%/volt. Operating voltage was about 700 volts.

Table X-1

IMP-H CPME Detector Measurement Summary

Particle Type	Channel Designation	Energy Interval (MeV/Nucleon)	Minimum Time Resolution† (sec)	Geometric Factor (cm^2 sr)	Angular Data Sampling*	Detector Type	Field of View and Viewing Direction
		Proton-Electron Telescope					
Protons	P1	$0.29 \le E_p \le 0.50$	10.24	1.51	8 sectors	Solid-State Detectors and Anticoincidence Plastic Scintillator	45° full angle in ecliptic plane
	P2	$0.50 \le E_p \le 0.97$	10.24	1.51			
	P3	$0.97 \le E_p \le 1.85$	10.24	1.51			
	P4	$1.85 \le E_p \le 4.50$	10.24	1.51			
	P5	$4.50 \le E_p \le 7.90$	10.24	1.51			
	P6	$7.90 \le E_p \le 13.7$	10.24	1.51			
	P7	$13.7 \le E_p \le 25.2$	5.12	0.32	**		
	P8	$25.2 \le E_p \le 49.5$	10.24	0.32	8 sectors		
	P9	$49.5 \le E_p \le 95.0$	5.12	0.32			
	P10	$95.0 \le E_p \le 138.0$	10.24	0.32			
	P11	$190.0 \le E_p \le 500.0$	10.24	0.32			
Alphas	A1	$0.64 \le E_n \le 1.17$	20.48	1.51	8 sectors		
	A2	$1.17 \le E_n \le 1.74$	10.24	1.51			
	A3	$1.74 \le E_n \le 4.30$	10.24	1.51			
	A4	$4.30 \le E_n \le 11.5$	10.24	1.51			
	A5	$11.5 \le E_n \le 26.0$	5.12	0.32	**		
	A6	$26.0 \le E_n \le 52.0$	5.12	0.32	8 sectors**		
$Z \ge 3$	Z1	$\sim 0.77 \le E_n \le 3.2$	5.12	1.51	8 sectors		
$Z \ge 6$	Z2	$\sim 1.60 \le E_n \le 3.2$	10.24	1.51			
$Z \ge 20$	Z3	$\sim 3.35 \le E_n \le 7.6$	10.24	1.51			
Electrons	E4	$0.22 \le E_e \le 2.5$	10.24	1.51	8 sectors**		
	E5	$0.50 \le E_e \le 2.5$	10.24	1.51			
	E6	$0.80 \le E_e \le 2.5$	10.24	1.51			
Integral Protons	M	$E > 35$ MeV/Nucleon	5.12	28 cm^2			omnidirectional
		Geiger Telescope					
Electrons Protons X-Rays	E1	$E_e > 0.016$ $E_p > 0.220$ 4 to 16 Å, 0.32 X 10^{-4} ergs/cm^2-ct	5.12	0.015 0.015	8 sectors	705 GM Tube	45° full angle in ecliptic plane
Electrons Protons X-Rays	E2A	$E_e > 0.03$ $E_p > 0.57$ 1.5 to 12 Å, 0.11 X 10^{-6}	10.24	0.17 0.17 ergs/cm^2-ct	8 sectors	704 GM Tube	
Electrons Protons X-Rays	E3	$E_e > 0.085$ $E_p > 2.20$ 1.5 to 7.5 Å, 0.31 X 10^{-7}	40.96	0.110 0.110 ergs/cm^2-ct	32 sectors	7115A GM Tube	11° 15' X 40° fan-shaped collimator in ecliptic plane.
	S	$E > 50$ MeV/Nucleon	5.12	28 cm^2		Anticoincidence Scintillator	Omnidirectional
		North-South Telescope					
Electrons Protons	E2B	$E_e > 0.016$ Directional $E_p > 0.210$ Directional $E_p \ge 60$ MeV+ Omnidirectional	10.24	0.022 0.022		705 GM Tube (South)	45° full angle at 22° 30' from ecliptic south.
Electrons Protons	E2C	$E_e > 0.016$ Omnidirectional $E_p > 0.220$ Omnidirectional $E_p \ge 60$ MeV+ Omnidirectional	10.24	0.022 0.022		705 GM Tube (North)	45° full angle at 22° 30' from ecliptic north.

† The duty cycle of all channels is 100% with the following exceptions: E3, 76.43%; P1, E2A, E1, 38.21%; A1, 19.10%

* Those channels for which there is no entry are spin-averaged. Channels P1 and E4 share a single sector subcommutator; channels A1, A6, Z1, P8 share a single sector subcommutator. Also, channels E2A and E3 share a single subcommutator.

** Both spin-averaged and sector information is obtained.

\+ Vertical incidence on detector wall; average threshold for isotropic flux is closer to ~ 90 MeV.

Table X-2

IMP-J CPME Detector Measurement Summary

Particle Type	Channel Designation	Energy Interval (MeV/Nucleon)	Minimum Time Resolution† (sec)	Geometric Factor (cm^2 sr)	Angular Data Sampling*	Detector Type	Field of View and Viewing Direction
		Proton-Electron Telescope					
Protons	P1	$0.29 \le E_p \le 0.50$	10.24	1.51	8 sectors	Solid-State Detectors and Anticoincidence Plastic Scintillator	45° full angle in ecliptic plane
	P2	$0.50 \le E_p \le 0.96$	10.24	1.51			
	P3	$0.96 \le E_p \le 2.00$	10.24	1.51			
	P4	$2.00 \le E_p \le 4.60$	10.24	1.51			
	P5	$4.60 \le E_p \le 15.0$	10.24	1.51			
	P7	$15.0 \le E_p \le 25.0$	5.12	0.32			
	P8	$25.0 \le E_p \le 48.0$	10.24	0.32			
	P9	$48.0 \le E_p \le 96.0$	5.12	0.32			
	P10	$96.0 \le E_p \le 145.0$	10.24	0.32			
	P11	$190.0 \le E_p \le 440.0$	10.24	0.32			
Alphas	A1	$0.59 \le E_n \le 1.14$	20.48	1.51	8 sectors		
	A2	$1.14 \le E_n \le 1.80$	10.24	1.51			
	A3	$1.80 \le E_n \le 4.20$	10.24	1.51	8 sectors‡		
	A4	$4.20 \le E_n \le 12.0$	10.24	1.51			
	A5	$12.0 \le E_n \le 28.0$	5.12	0.32			
	A6	$28.0 \le E_n \le 52.0$	5.12	0.32			
$Z \ge 3$	Z1	$0.70 \le E_n \le 3.30$	5.12	1.51	8 sectors‡		
$Z \ge 6$	Z2	$1.45 \le E_n \le 3.30$	10.24	1.51	8 sectors‡		
$Z \ge 20$	Z3	$3.10 \le E_n \le 8.80$	10.24	1.51			
$Z \ge 3$	Z4	$6.0 \le E_n \le 105.0$	10.24	1.51			
Electrons	E4	$0.22 \le E_e \le 2.5$	10.24	1.51	8 sectors‡		
	E5	$0.50 \le E_e \le 2.5$	10.24	1.51			
	E6	$0.80 \le E_e \le 2.5$	10.24	1.51			omnidirectional
Integral Protons	M	$E > 35$ MeV/Nucleon	5.12	28 cm^2			
		Geiger Telescope					
Electrons Protons X-Rays	E1	$E_e \ge 0.013$ E_p 0.162 4 to 17 Å, 0.26×10^{-4}	5.12 ergs/cm^2-ct	0.015 0.015	8 sectors	705 GM Tube	45° full angle in ecliptic plane
Electrons Protons X-Rays	E2A	$E_e \ge 0.031$ $E_p \ge 0.593$ 1.5 to 12 Å, 0.11×10^{-6}	10.24	0.17 0.17 ergs/cm^2-ct	8 sectors	704 GM Tube	
Electrons Protons X-Rays	E3	$E_e > 0.085$ $E_p > 2.20$ 1.25 to 7.5 Å, 0.27×10^{-7}	40.96	0.220 0.220 ergs/cm^2-ct	16 sectors	7115A GM Tube	11°15′ × 40° fan-shaped collimator in ecliptic plane.
	S	$E > 50$ MeV/Nucleon	5.12	28 cm^2		Anticoincidence Scintillator	Omnidirectional
		North-South Telescope					
Electrons Protons	E2B	$E_e \ge 0.012$ Directional $E_p \ge 0.133$ Directional $E_p \ge 60$ MeV⊥ Omnidirectional	10.24	0.022 0.022		705 GM Tube (South)	45° full angle at 22°30′ from ecliptic south.
Electrons Protons	E2C	$E_e \ge 0.017$ Omnidirectional $E_p \ge 0.232$ Omnidirectional $E_p \ge 60$ MeV⊥ Omnidirectional	10.24	0.022 0.022		705 GM Tube (North)	45° full angle at 22°30′ from ecliptic north.

†The duty cycle of all channels is 100% with the following exceptions: E3, 51.56%; P1, E2A, E1, 25.78%; A1, 19.10%.

*Those channels for which there is no entry are spin-averaged. Channels P1 and E4 share a single sector subcommutator; channels A1, A3, Z1, Z2 share a single sector subcommutator. Also, channels E2A and E1 share a single subcommutator.

‡Both spin-averaged and sector information is obtained.

⊥Vertical incidence on detector wall; average threshold for isotropic flux is closer to ~ 90 MeV.

GM Tube E2A. This LND-704 GM tube was an argon plus halogen quench gas filled tube with an effective diameter of 0.25 inch. The mica end windows had thicknesses in the range 1.5 to 2 mgm/cm^2 mica. Internal gas pressures were about 57 cm Hg. The plateau lengths were >200 volts with a slope of approximately 0.11%/volt. Operating voltage was about 850 volts.

GM Tube E3. This LND-7115 GM tube was a custom-made krypton plus halogen quench gas filled pancake tube with an effective diameter of 0.40 inch. The mica end window had a thickness of 1.5 mgm/cm^2 mica. Internal gas pressures were 8 to 15 cmHg. The plateau lengths were 100 volts with a slope of 0.02 to 0.07%/volt. Operating voltage was about 900 volts.

North-South Telescope (NST)

The NST, which measured pargicle and proton fluxes from the directions of the north and south ecliptic poles (within 22.5°), consisted of a pair of GM tubes and supporting items. A collimator and holder comprised the housing assembly. The collimator was made of brass and allowed GM tubes E2B and E2C to have a conical look angle, for nonpenetrating particles, of 45° full angle. The holder was made of aluminum and held the collimators so that their axes were 22.5° from the vertical, or north-south polar axis. The purpose of this slight inclination from vertical was to prevent the satellite body from obstructing a portion of the view angle. The combination of brass collimator and aluminum holder provided shielding to a minimum of 60 MeV for protons in all directions except the look angle.

FUNCTIONAL OPERATION

Referring to Fig. X-4, each of the PET detectors, including the anticoincidence photomultiplier, had as associated charge-sensitive preamplifier followed by voltage amplifiers and pulse height discriminators. Outputs from the discriminators were routed to the channel logic section where coincidence and anticoincidence functions determined charge species and energy levels. Timing pulses were generated from the first voltage amplifier stage by a limiting amplifier and timing mark one-shot. This circuit produced a strobe pulse at the zero-crossing point of each input pulse. In this manner, timing accuracy was preserved over the full dynamic range of the channel.

Coincidence pulses were generated in AND gates where the timing signals were mixed with the PET photomultiplier anticoincidence

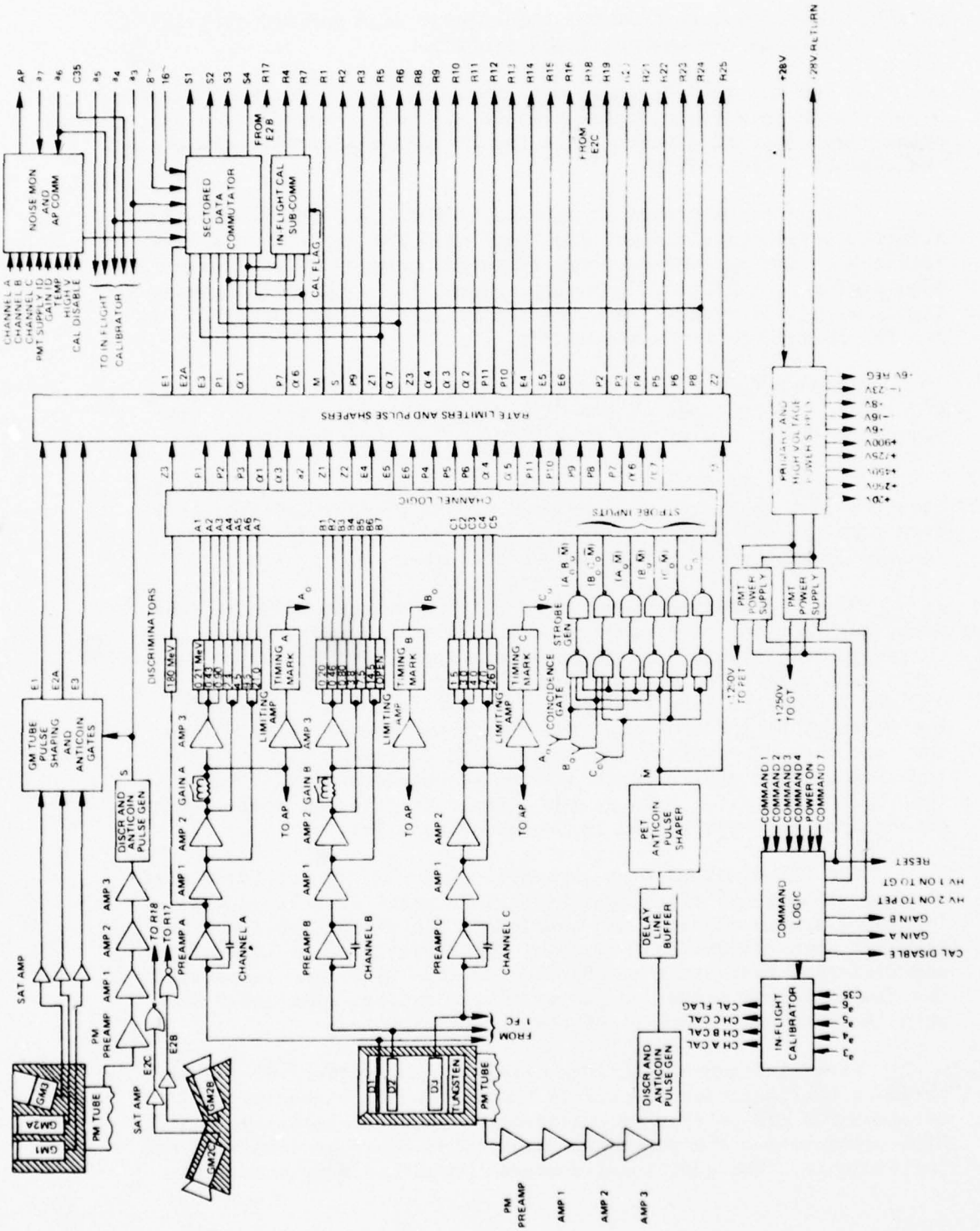

Fig. X-4 CPME System Block Diagram

pulses. Strobe pulses from the coincidence gage sampled discriminator outputs in the channel logic section.

A 180 MeV discriminator was coupled directly to preamplifier A to measure iron group nuclei signals ($Z \geq 20$). Named Z3, this signal was combined directly with the PMT anticoincidence signal in the channel logic section.

The anticoincidence signals in both the PET and GT were from scintillator-photomultiplier combinations. The two channels were identical. Timing, however, was different because GT used leading-edge timing to inhibit GM signals, whereas PET used trailing-edge timing with a delay line added to match zero-crossing detection in the PET pulse-height discriminators.

Each GM tube output was used to drive a saturating pulse amplifier. In the case of the GT tubes, the saturated pulse outputs were combined with the PM tube signal for anticoincidence.

The rate limiter and pulse shaper section contained one-shot circuits that generated standardized output pulses for data interface with the spacecraft encoder. Rise and fall times were controlled as well as a maximum set on the output pulse rate.

Several outputs were divided by sector accumulators. This sectoring, controlled by the spacecraft optical aspect system, channeled the outputs into eight equal sectors around the spacecraft spin axis. To keep the total number of accumulators to a minimum and at the same time sector as many outputs as possible, the sectored data commutator time-sequenced several signals into the sectored data registers. In the case of signal E3, the sectored data commutator further divided the sectors into 32 subsectors under control of spin divide signals from the OA system. The data outputs are summarized in Tables X-1 and X-2.

The PET discriminator thresholds and the channel logic were checked with the in-flight calibrator. A train of test signals following a ramp envelope was applied to the PET preamplifier in parallel with the detector signals. Different preamplifier pairs and different test-pulse height combinations were used to optimize the discriminator tests. Calibration occurred automatically once each 46 hours under control of the spacecraft clock.

Several command functions permitted the control of the experiment configuration. Power to the in-flight calibrator could be commanded off in case of calibrator failure. Similarly, the high voltages for the photomultiplier tubes could be commanded off individually. Two additional commands permitted a reduction in

amplifier gains on the A and B detectors in case of detector failures. The total number of commands required was minimized by having the individual commands latch in one direction only. They were reset together by reapplication of the power on command.

Several analog parameters and the command status were telemetered through one analog performance (AP) parameter. The noise monitor measured equivalent rms amplifier noise from the PET detectors, and the AP commutator multiplexed the independent readings into one output along with temperature and power-supply voltage readings.

The CPME power supply system consisted of a primary supply containing a frequency stabilized chopper, a DC-to-DC converter, and voltage regulators. The primary supply also developed a square-wave drive to a detector high-voltage supply and to two PMT power supplies.

FLIGHT RESULTS

Charged Particle Measurements Experiments were successfully launched aboard the IMP-H and IMP-J satellites (Fig. X-5) on 23 September 1972 and 20 October 1973, respectively (lines 27 and 34, Table 1), and are operating satisfactorily. The sensitivities of the CPME instruments are such that studies are carried out from quiet-time galactic intensities to intense solar flare events, to the detection of electrons originating in the magnetosphere of Jupiter. The data represent a large reservoir of physical measurements which are presently being analyzed by scientists at APL, the University of Kansas, and the NOAA/Space Environment Laboratory.

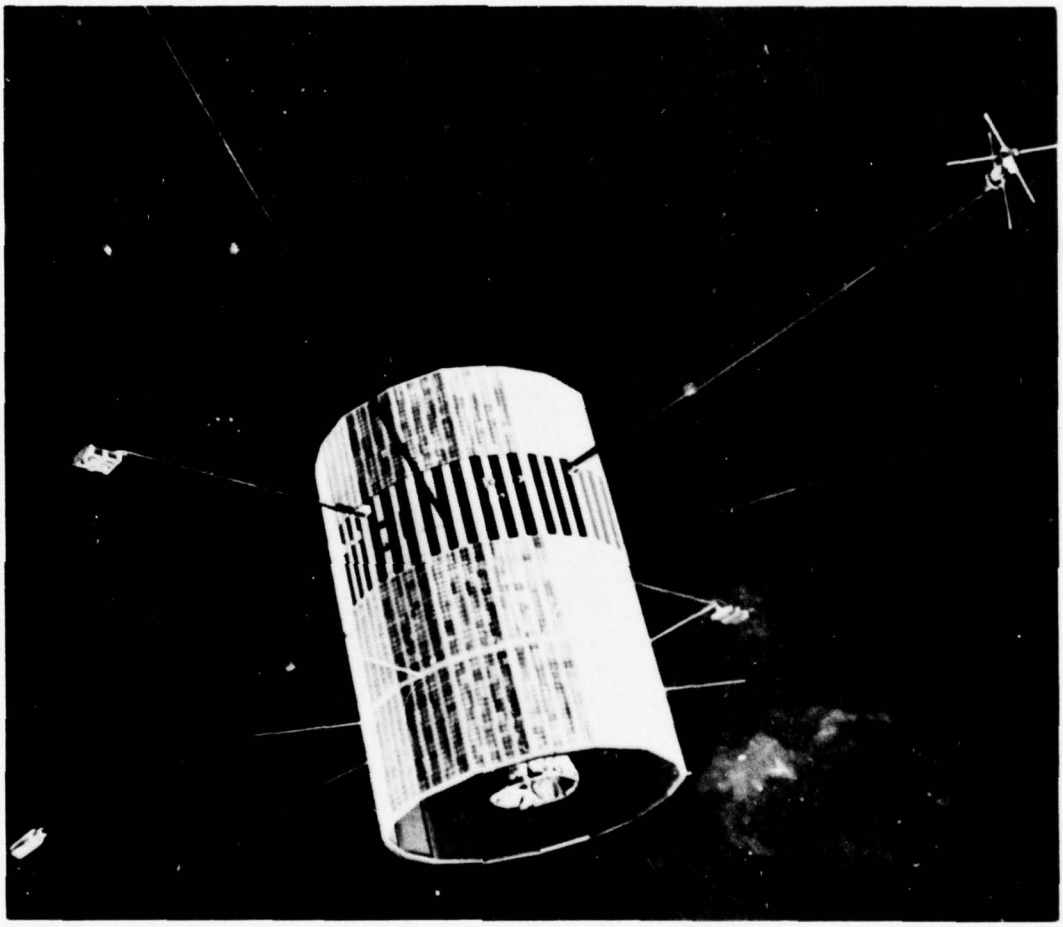

Fig. X-5 IMP-H and-J Satellite, Artist's Concept

XI

ULTRAVIOLET SPECTROMETER EXPERIMENT

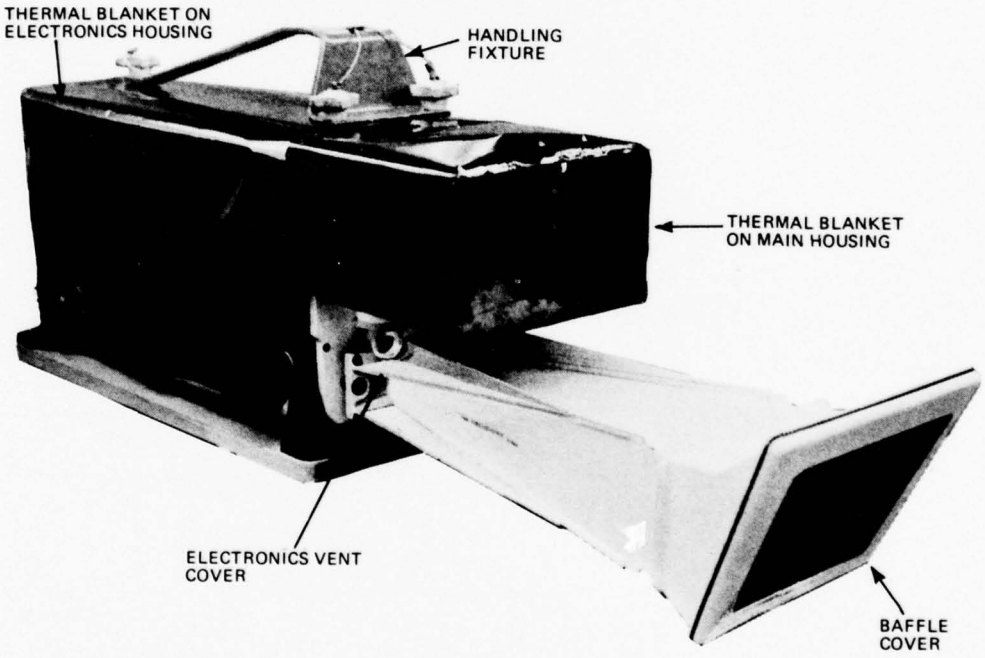

Fig. XI-1 Ultraviolet Spectrometer Experiment

XI

ULTRAVIOLET SPECTROMETER EXPERIMENT

BACKGROUND

The Ultraviolet Spectrometer (UVS) Experiment Program S169, under contract from the NASA Manned Spacecraft Center, was implemented to perform measurements in the far ultraviolet spectrum as part of the Apollo 17 lunar mission. Dr. W. G. Fastie of the Department of Physics/JHU was Principal Investigator; APL responsibilities included the design and fabrication of two Fastie-Ebert spectrometers for flight use, a mockup for astronaut training, a prototype unit, a qualification unit, and UVS test equipment. Also, a thermal test model and units for engineering evaluation and cross calibration were provided from parts and assemblies on hand.

The UVS design was derived from the extensive experience of the Principal Investigator and co-experimenters in the development of a variety of Ebert scanning monochrometers for experiment aboard sounding rockets, satellites, and interplanetary vehicles. However, the following features represented advances in design and performance with respect to the earlier flight spectrometers:

1. A multiple angled external entrance baffle to reduce scattered light impingement on the photomultiplier tube (PMT).

2. Photomultiplier electronics and data system that provided wide dynamic range and a limit of detection dictated by dark current noise pulses emitted by the FMT.

3. An image tripling mirror system at the exit slit to increase the sensitivity of the spectrometer.

The net result of these features was to provide an instrument with a sensitivity of at least one order of magnitude improved over Ebert systems previously used in space experiments, and which also exhibited greatly improved scattered light characteristics.

APPLICATION

The UVS (Fig. XI-1) was developed to perform quantitative measurements of the composition of the atmosphere of the moon during various degrees of solar illumination as part of the continuing analysis of the interaction of the solar wind with the lunar

surface. Determination of the lunar atmosphere composition was by detection of the resonance reradiation of energy in the ultraviolet region (1180 Å to 1680 Å). Specifically, the primary experimental objective was to determine the atomic composition, density, and scale height for each constituent of the lunar atmosphere. Secondary objectives were as follows:

1. Measure the temporary atmosphere created by the lunar module engines.

2. Measure the lunar UV albedo.

3. Study the lunar darkside fluorescence.

4. Measure UV galactic emission.

5. Study the atomic hydrogen distribution in the earth's geotail.

EQUIPMENT DESCRIPTION

The mechanical design of the UVS was modular to provide for simplified assembly and subcomponent interchangeability. These modules, shown in Fig. XI-2, are described in the following paragraphs.

The baffle, or sunshade, contained rectangular baffle plates that formed a rectangular, pyramid shaped field-of-view to minimize the effects of scattered radiation. It was about 48.3 cm long, and the inside surfaces were painted black to reduce light reflection. The entrance baffle was thermally and electrically connected to the front plate by through bolts. The external surface was coated with a special white paint having an α/ε of 0.21/0.85. Since the remainder of the UVS was insulated from its environment, the baffle was the primary radiator and absorber of heat energy.

The electronics module contained an intergrated PMT, a pulse amplifier and discriminator, a high voltage supply for the PMT, a low voltage DC/DC converter, pulse counting circuitry, and telemetry preconditioning circuitry. This module also contained the spacecraft and GSE electrical interface connectors.

The front plate served as a mounting base for the baffle, electronics housing, the entrance and exit slits, inner baffle, image tripling mirrors, and diffraction grating with associated motor driven scan mechanism. The entrance and exit slits were slots machined about 0.198 cm wide by 5.69 cm long and 0.198 cm

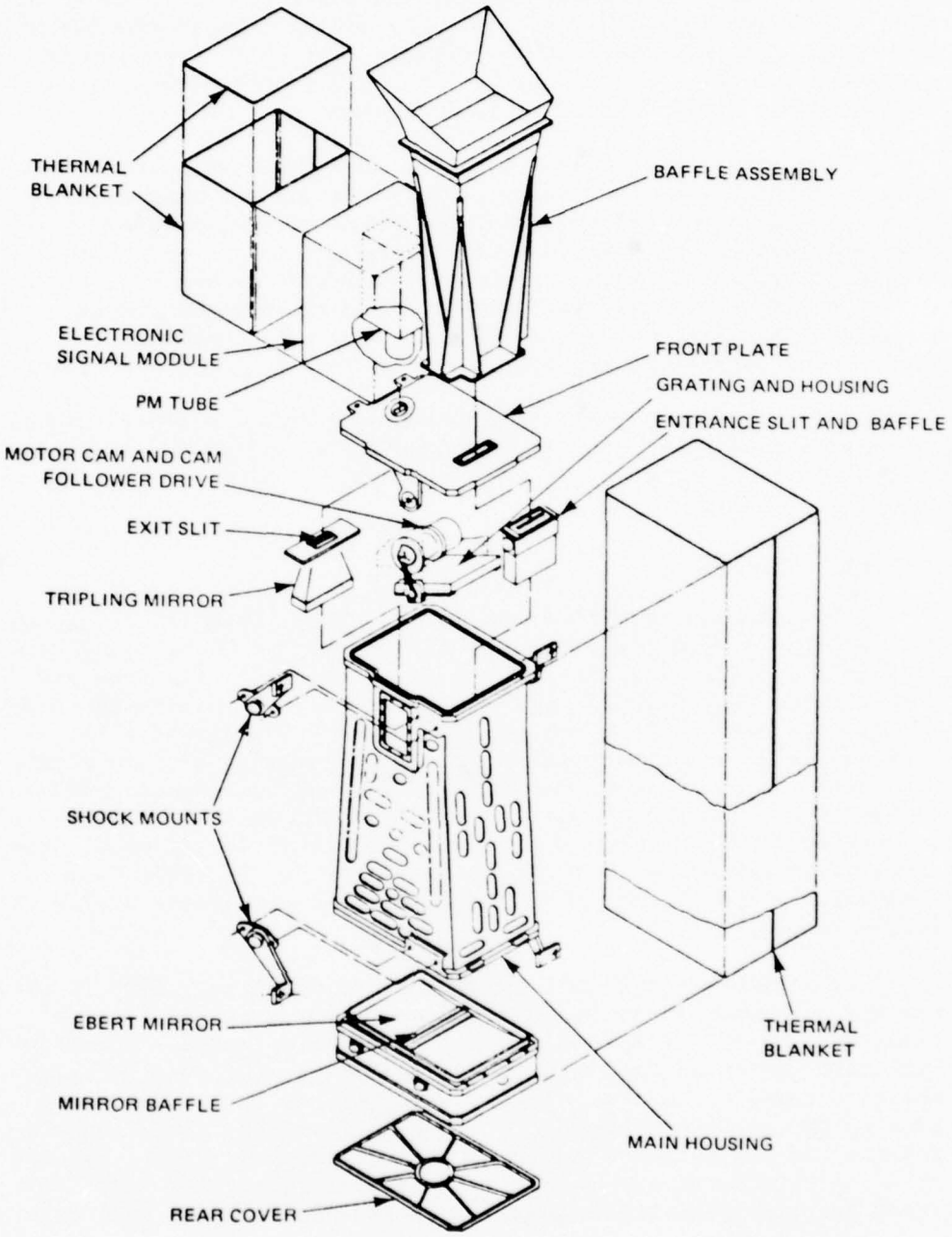

Fig. XI-2 UVS, Exploded View

wide by 0.228 cm long, respectively. A 0.127 cm thick rectangular aluminum tube (the inner baffle) had small fin sections to reduce scattered light and admit only the direct rays in the field-of-view to the input half of the mirror. The exit mirrors were about 0.51 cm thick and 11.481 cm long, and trapezoidal in shape. The ends were about 3.18 cm by 1.27 cm wide.

The main housing was a machined aluminum casting that served as a light-tight box for the optical system and the supporting structure for other UVS modules. The Ebert mirror, mounted in a separate machined housing that was bolted to the aft end of the main housing, was divided into input and output halves by a light baffle strip. The input half acted as a collimator to provide parallel light incident on the grating, and the output half focused the diffracted light from the grating onto the exit slit.

As an integral unit, the UVS was completely enclosed within super-insulation blankets of aluminized Mylar and Kapton sheets except for the baffle, front plate, interface connectors, and mounting pads.

Grating Mechanism

The grating mechanism was used to cycle the grating through the 1180-1680Å wavelength range. It consisted of a motor and gear reducer drive, cam and follower, grating housing, reflective diffraction grating, and fiducial mark detector. A synchronous motor and gear reducer unit, which required about 2.5 watts at a frequency of 100 Hz, drove the cam in one direction at a uniform rate to repeat the wavelength scan cycle once every 12 seconds. The radius of the cam groove, as a function of the angle of rotation, controlled the wavelength scan profile as a function of time. The groove also served to retain and prevent the cam follower from damaging the cam because of vibration-induced chattering during the Apollo launch.

The fiducial mark detector consisted of a small slit in the cam through which infrared light, emitted by a gallium arsenide light source, could pass to a phototransistor detector. The fiducial mark indicated the end of scan, and its output synchronized the word format. The cam follower was fastened to a shaft which rotated the grating through a 5° angle. The angular relationship between the cam follower and the normal to the grating was adjustable. A theodolite was used to set the grating angular position to match the precise relative position of the cam follower to 1215.65 Å.

Ebert Mirror

The Ebert mirror was made of Cervit and coated on its polished surface with aluminum and magnesium fluoride. Overall,

dimensions were about 23.5 cm long by 16.0 cm wide by 4.6 cm thick, with a spherical radius of 100 cm. A baffle strip about 2.3 cm wide separated the mirror surface into two halves.

The optical design of the UVS was that of an Ebert spectrometer whose optical components consisted of an external baffle, entrance slit, Ebert mirror, scanning diffraction grating, exit slit and mirror, and photoelectric sensor. The external baffle may be described as a multiple angled horn designed so that light originating outside the specified field of view is greatly attenuated because of multiple reflection before passing through the entrance slit. Figure XI-3 diagrams the optical system and external baffle, and shows the look angle from the Scientific Instrument Module (SIM) of the Command System Module (CSM).

The mirror collimated the radiation admitted by the entrance slit, redirected the radiation onto the diffraction grating, and refocused the diffracted radiation onto the exit slit. Optical vignetting was reduced to virtually zero by use of the exit slit mirrors.

FUNCTIONAL OPERATION

Figure XI-4 shows the UVS block diagram together with those functions directly associated with the scientific data gathering system such as the PMT, pulse amplifier and discriminator, counting and timing circuits, and the output register.

Digital Counting System

A digital counting system followed the PMT. Outputs from the photomultiplier, which consisted of approximately 10 ns pulses of 10^5 to 10^7 electrons, were processed by the pulse amplifier and discriminator (PAD). The PAD integrated and amplified each pulse, and provided threshold discrimination. Pulses with energies above the selected threshold generated a standardized pulse for further counting. Pulses below the predetermined threshold of ≈ 3 mV were rejected. A threshold discriminator drove a one-shot multivibrator that generated the standard pulse to drive the counter. The one-shot had a pulse width of about 0.8 μs, and a dead time of about 0.8 μs. Thus, for every 10 ns input pulse greater than the selected threshold, a standardized 0.8 μs (approx.) pulse was generated, except for the situation where input pulses would arrive closer than 1.6 μs, at which time the system became overloaded. Thus, the maximum periodic rate at which the system counted was approximately 625,000 pulses/second.

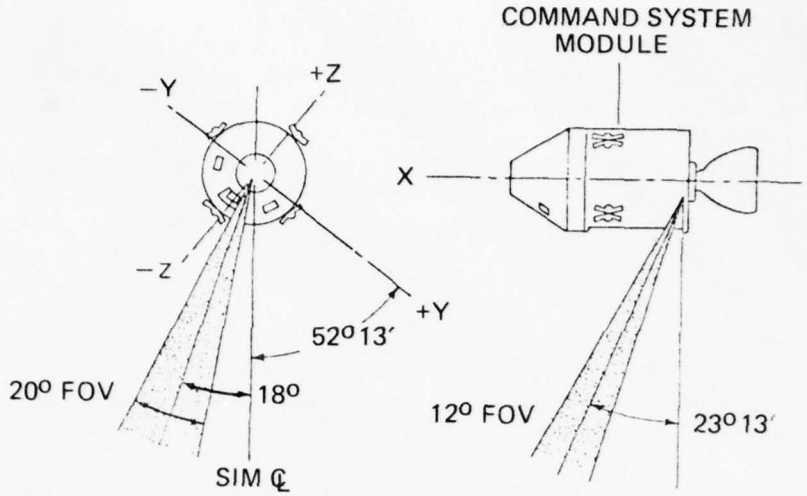

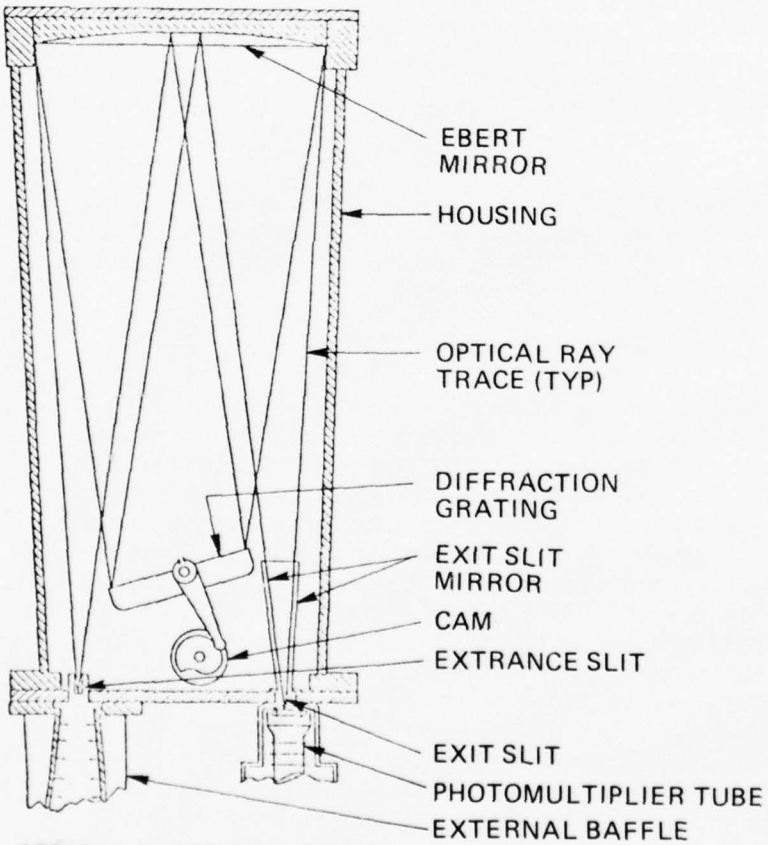

OPTICAL SYSTEM DIAGRAM

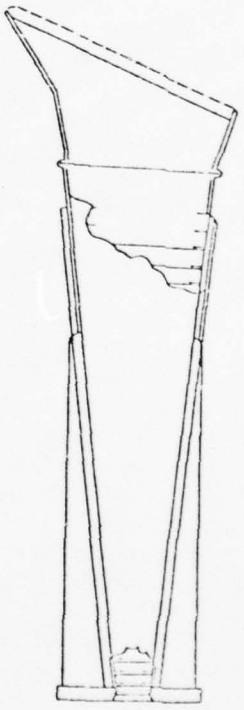

EXTERNAL BAFFLE

Fig. XI-3 UVS Optical System, External Baffle, and Orientation

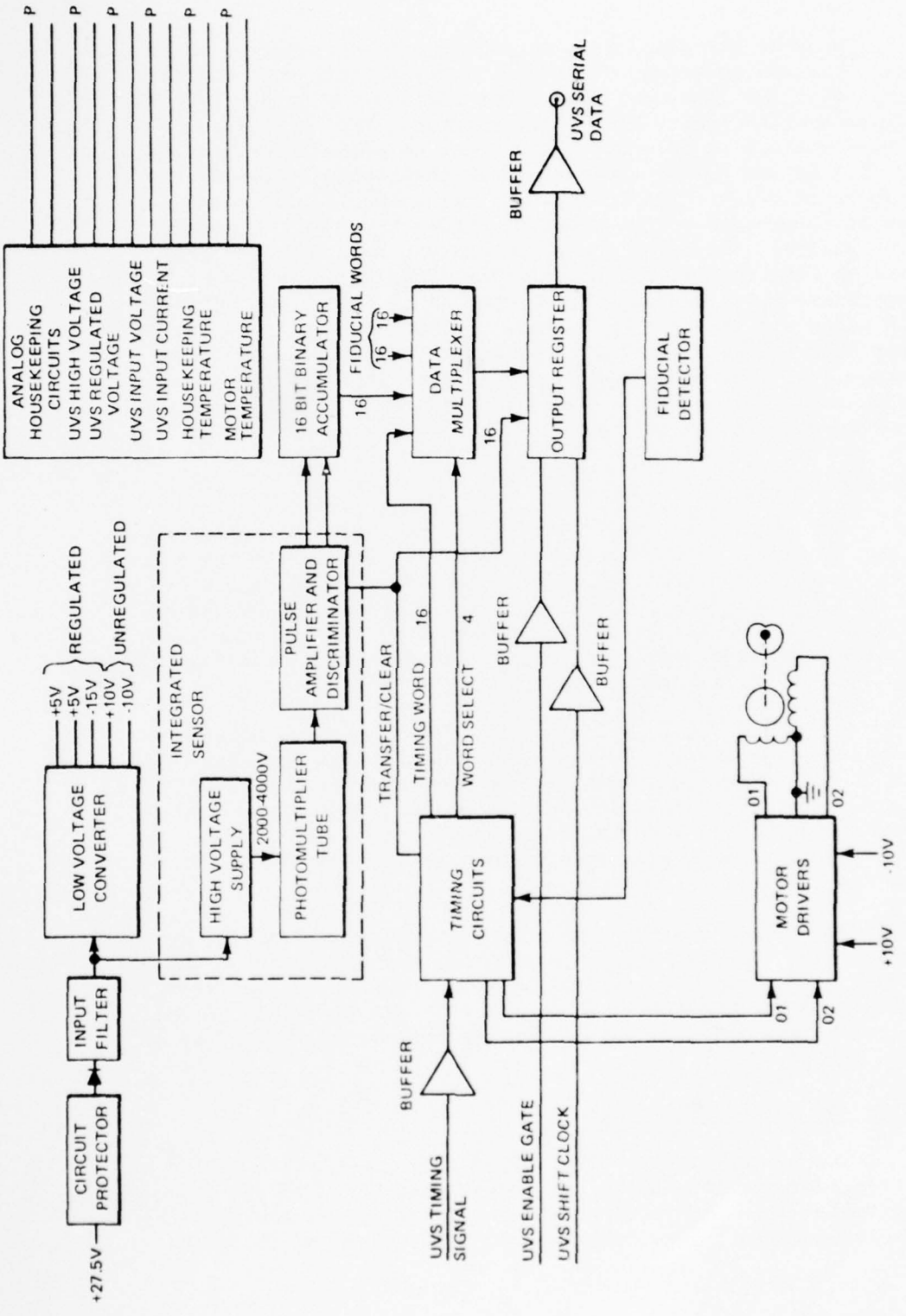

Fig. XI-4 UVS Block Diagram

Because the generation of photoelectrons occurred at random times, the system became nonlinear; however, this nonlinearity affected only the result at high count rates. The output from the PAD was counted by the 16-bit accumulator. The accumulator counted the 0.8 μs pulses for a 0.1 second period. At the end of each 0.1 second period (as defined by the timing circuits) the accumulator transferred its data to the output register and was cleared to prepare it for counting during the next 0.1 second count period. The clear operation and the data transfer took place in less than 30 μs, therefore causing negligible loss in the accumulator count period. Data transfer to the output register took place via the data multiplexer. The use of a 16-bit accumulator allowed the digital electronics to accumulate 65 536 pulses every 0.1 second, while the PAD could generate only approximately 62,500 pulses/0.1 second. Thus, the system could not overflow to cause ambiguities in the data.

Data Multiplexer

The data multiplexer normally transmitted scientific data in the accumulator to the output register. During the cam flyback time, however, the multiplexer inserted special fiducial words into the output register. The cam flyback time was about 0.5 second, i.e., five 16-bit words could be transmitted in that time. All five special words were initiated by the detection of a fiducial mark located on the cam at the end of scan position.

Words 1 and 2 formed a special fixed pattern, selected because such a pattern could not occur naturally in the data pattern. Word 3, called the scan period word, recorded the number of 2.5 ms intervals occurring between fiducial marks. This was nominally 12 seconds; hence, the word would nominally record 4800 counts. Words 4 and 5 were also special sync words. Words 4 and 5 were identical to words 2 and 1, respectively.

The output register was a 16-bit parallel-to-serial register. Data were entered in parallel via the data multiplexer at the end of each 0.1 second accumulation period. Upon arrival of the UVS enable gate and the UVS shift clock, the data were then serially shifted to the UVS data output line via the buffer amplifier as shown in Fig. XI-4.

Timing and Counting Circuits

The timing circuits controlled the accumulation period and the transfer of all data to the output register. Proper data word synchronism with the wavelength scan system was accomplished by the fiducial mark detector. Generation of two-phase square wave,

required for the motor drive electronics, was also accomplished by the timing circuits. All counting of photoelectrons was synchronized with the grating position to establish the wavelength reference. Thus, the fiducial mark detector signal was used to synchronize a divide-by-40 counter once during each 12 second scan. The divide-by-40 counter was driven from the 400 Hz UVS timing signal, and generated the 0.1 second intervals for the accumulator. Thus, the accumulator counting circuits were maintained in synchronism with the grating drive system.

The snyc word code (words 1, 2, 4, and 5) was also generated by the timing circuits, upon arrival of the fiducial pulse. The code was generated and injected into the data stream via the data multiplexer. The special timing word (word 3) was also injected into the data stream by the timing circuits. This word was generated by a 16-bit counter that recorded the number of 400 Hz pulses between fiducial marks. This number gave information on any possible variations of motor speed. Since the hysteresis synchronous motor required a two-phase 100 Hz square wave drive, the timing circuits used the 400 Hz timing reference to generate the motor drives. Flip-flop circuits, appropriately gated, accepted the 400 Hz signal and divided it into two 100 Hz square waves having a phase relationship of 90°.

The fiducial mark detector consisted of a solid-state light-emitting diode and a photo transistor, followed by a comparator and one-shot multivibrator. The diode emitted light to the photo transistor via a 0.0254 cm slot in the cam. Output from the photo transistor was amplified and used for triggering a one-shot multivibrator. The fiducial mark detector synchronized the divide-by-40 counter in the timing system. Thus the electronic data system was synchronized with the wavelength scan. The fiducial mark was positioned so that it could be generated at the beginning of the flyback period.

The housekeeping electronics generated six analog telemetry functions. The circuits consisted of integrated operational amplifiers to serve as buffers between the Scientific Data System (SDS) analog system and the primary sensors. For the bus voltage function, resistor scaling circuits were used to drive the output operational amplifiers. The bus input current was measured by differentially sensing the voltage across a resistor inserted in series with the 28 volt DC return. Two temperature measurements were made by sensing the voltage across a thermistor-resistor bridge network driven by a precision voltage reference. All telemetry function outputs were 0 to 5.0 volts full scale.

A current sensing device was provided to limit the 28 volt bus current delivered to the UVS should an electrical failure

occur in the UVS. A solid-state switch would open the 28 volt bus in approximately 5 ms should the current exceed the 1.5 ampere limit. The circuit breaker would reset automatically should bus power be removed and reapplied.

FLIGHT RESULTS

The Apollo 17 launch countdown began on 1 December 1972 and continued until liftoff on 7 December (line 29, Table 1). During this period, the UVS performed properly and data were monitored continually via the spacecraft SDS. After liftoff, the spacecraft operated nominally and achieved earth orbit after 11 minutes and 47 seconds of powered flight. Translunar injection occurred at 3:12:36.

Mission Operations

Data were obtained while the CSM was in lunar orbit and during transearth coast under the conditions identified in the following modes:

Mode I - Data were collected when the CSM +X axis was aligned to the velocity vector and the SIM bay centerline aligned to the nadir. Data were collected during one lunar orbit and during crew rest periods, with emphasis on a 15 minute period spanning CSM sunset terminator crossing.

Mode II - Data were collected when the CSM +X axis was aligned to the velocity vector and the SIM bay centerline to the nadir. Data were collected during crew rest periods, with emphasis on a 15 minute period spanning CSM sunrise terminator crossing.

Modes I and II permitted observation of the lunar atmosphere during predawn and postsunset periods, whereby the lunar atmosphere is illuminated and the lunar surface is not; a condition allowing resonantly scattered radiation to be observed. The remaining operating time in these modes provided a measure of the lunar albedo and, possibly, lunar phosphorescence.

Mode III - Data were collected during two lunar orbits with the spectrometer optical axis pointing at grazing incidence to the lunar surface. This mode provided a look through a long atmospheric path against a galactic background which maximized the instrument's signal strength.

Mode IV - Considering the moon an occulting disk, the UVS viewed zodiacal light both parallel and perpendicular to the ecliptic plane, and scanned several predetermined bands on the celestial sphere.

Mode V - Data were collected during transearth coast with the spectrometer axis aligned to different celestial coordinate positions.

Mode VI - The spectrometer was operated during transearth coast while the CSM was in passive thermal control. Modes V and VI permitted the investigation of the presence and distribution of atomic hydrogen between the earth and the moon, and determination of ultraviolet emission of galactic and extragalactic sources. Controls were furnished in the CSM for the crew to activate and deactivate the instrument and to open and close the Reaction Control System plume protective door that covered the baffle entrance.

Apollo 17 entered lunar orbit on the fourth day of mission operations. Also on the fourth day, the SIM bay door was jettisoned, and shortly thereafter the UVS was activated. After lunar orbit injection, lunar orbital scientific exploration was initiated and completed with the transearth injection maneuver which occurred during the eleventh day of operations. Splashdown occurred on the fourteenth day.

Performance Evaluation

The UVS obtained numerous useful data throughout the entire mission. All experiment objectives were achieved. Spectrometer operation was normal although the instrument experienced a photomultiplier tube dark current of 25 counts per second, which was considerably higher than 0.7 counts per second measured during preflight tests. The high dark count was attributed to cosmic radiation, and was about an order of magnitude higher than expected. Although the UVS dark count remained higher than normal throughout the mission, it did not impair the ability to measure the lunar albedo on the sunlit side or the Lyman-alpha at 1216Å on the dark side, nor did it impair the ability to measure the hydrogen density in the lunar atmosphere.

XII

SKYLAB EXPERIMENT M131

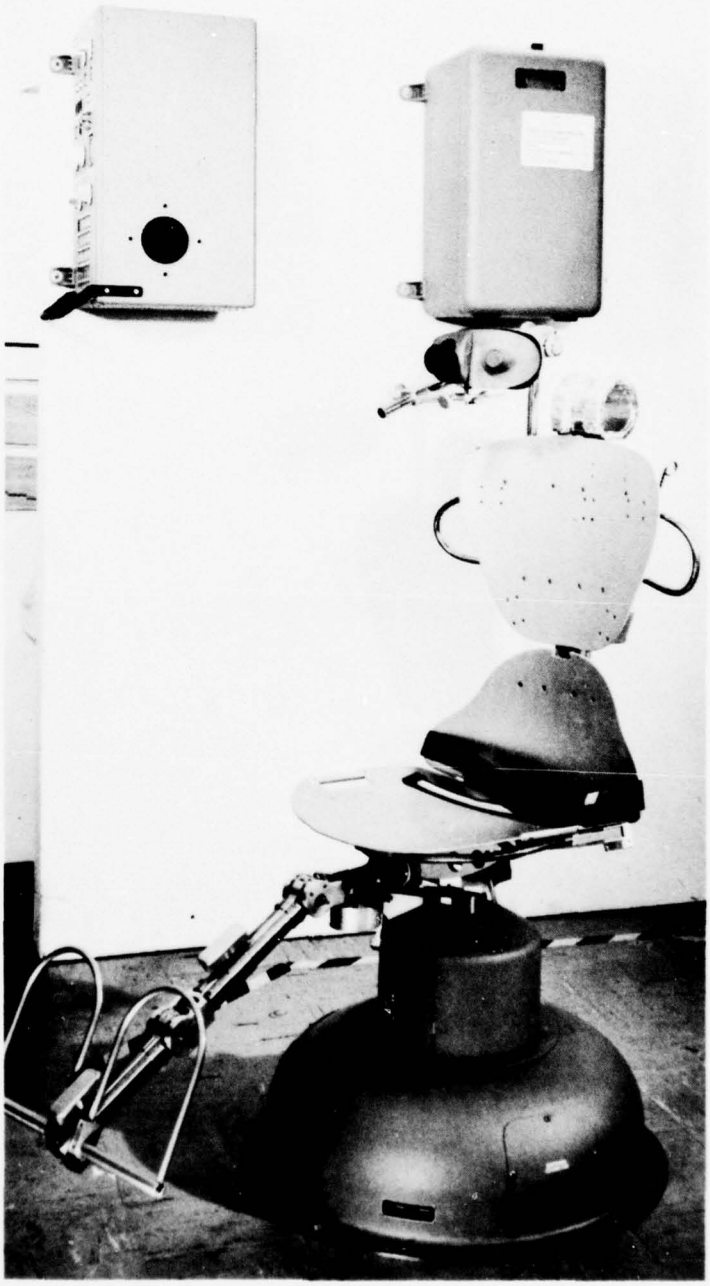

Fig. XII-1 Skylab Experiment M131

XII

SKYLAB EXPERIMENT M131

BACKGROUND

Skylab, originally called the Apollo Applications Program, was the successor to the Gemini and Apollo programs. It consisted of three manned missions of 28, 59, and 84 days duration, respectively, in a large earth-orbiting space station. Each mission included a series of in-flight medical and physiological experiments designed to provide an in-depth study of individual body systems and a comprehensive understanding of man's reaction to long term weightless flight. Biomedical experiment data were obtained in the areas of neurophysiology, musculoskeletal physiology, biochemistry, hematology, cytology, and cardiovascular and respiratory metabolic functions.

The Skylab Experiment M131 (Fig. XII-1), developed by APL for the Naval Aerospace Medical Research Laboratory and the NASA/Lyndon B. Johnson Space Center, was to test the human vestibular function.

APPLICATION

Physiological considerations suggest that the response of the vestibular system can be substantially modified during weightlessness, and that such modifications affect susceptibility to motion sickness and judgment of spatial localization. The evaluation of such effects requires the measurement of responses to precisely controlled accelerations before, during, and after exposure to prolonged zero-gravity conditions. For this purpose, a precisely controlled rotating chair was designed, fabricated, tested, and installed in the Skylab orbital workshop (OWS). This chair was used in three test modes to evaluate the astronauts' vestibular systems.

To evaluate the subject's detection of small angular accelerations, the chair was rotated through any of 24 acceleration profiles, which ranged between 0.020° and 6.0°/s^2. To evaluate the changes in the subject's perception of motion, the chair was rotated at any of 10 constant velocities while the seated subject executed certain prescribed head and upper-body movements. The test was to establish the degree to which a subject's motion sensitivity changed as a result of zero-gravity exposure. To evaluate the ability of a blindfolded subject to retain spatial

orientation in the absence of tactile cues, the chair was extended into a litter, or reclining, position and then tilted into a combined pitch-roll attitude.

The major feature of the chair was its ability to impart very smooth, tightly controlled, rotational accelerations and velocities to the vestibular organs of a seated test subject. The chair and its servo control system were capable of performing at levels below the sensitivity threshold of the normal vestibular organs.

The specific experimental objectives were as follows:

1. To acquire pertinent data to establish the validity of measurements of specific behavioral/physiological responses influenced by vestibular activity under one- and zero-g conditions.

2. To determine man's adaptability to atypical vestibular conditions and to predict habitability of future spacecraft when subject to conditions involving subgravity and Coriolis forces.

3. To measure the accuracy and variability in the judgment of spatial coordinates based upon atypical gravity receptor cues and inadequate visual cues.

EQUIPMENT DESCRIPTION

The major Skylab Experiment M131 equipment (Fig. XII-2) consisted of the rotating litter chair, the control console, and the equipment stowage. The equipment stowage included the storage cabinet and items normally stowed: the OTG (otolith test goggles), blindfold, biteboards, readout device, and the reference sphere.

Rotating Litter Chair (RLC)

The RLC was a precision electric motor driven rotating chair which could also be tilted as a chair or as a litter in a combined pitch-roll plane while in the static mode. Its folding construction of tubular frame and metallic seat and back permitted the conversion from the stowed configuration (Fig. XII-3) to the upright and litter modes. Proximity sensors were installed about the chair for detecting and signaling the proper tilt of the head in the four cardinal directions.

The chair drive, or motor base assembly, consisted essentially or a 66.04 cm diameter hemispherical fairing which covered the motor housing, power amplifier, and nitrogen system. The chair

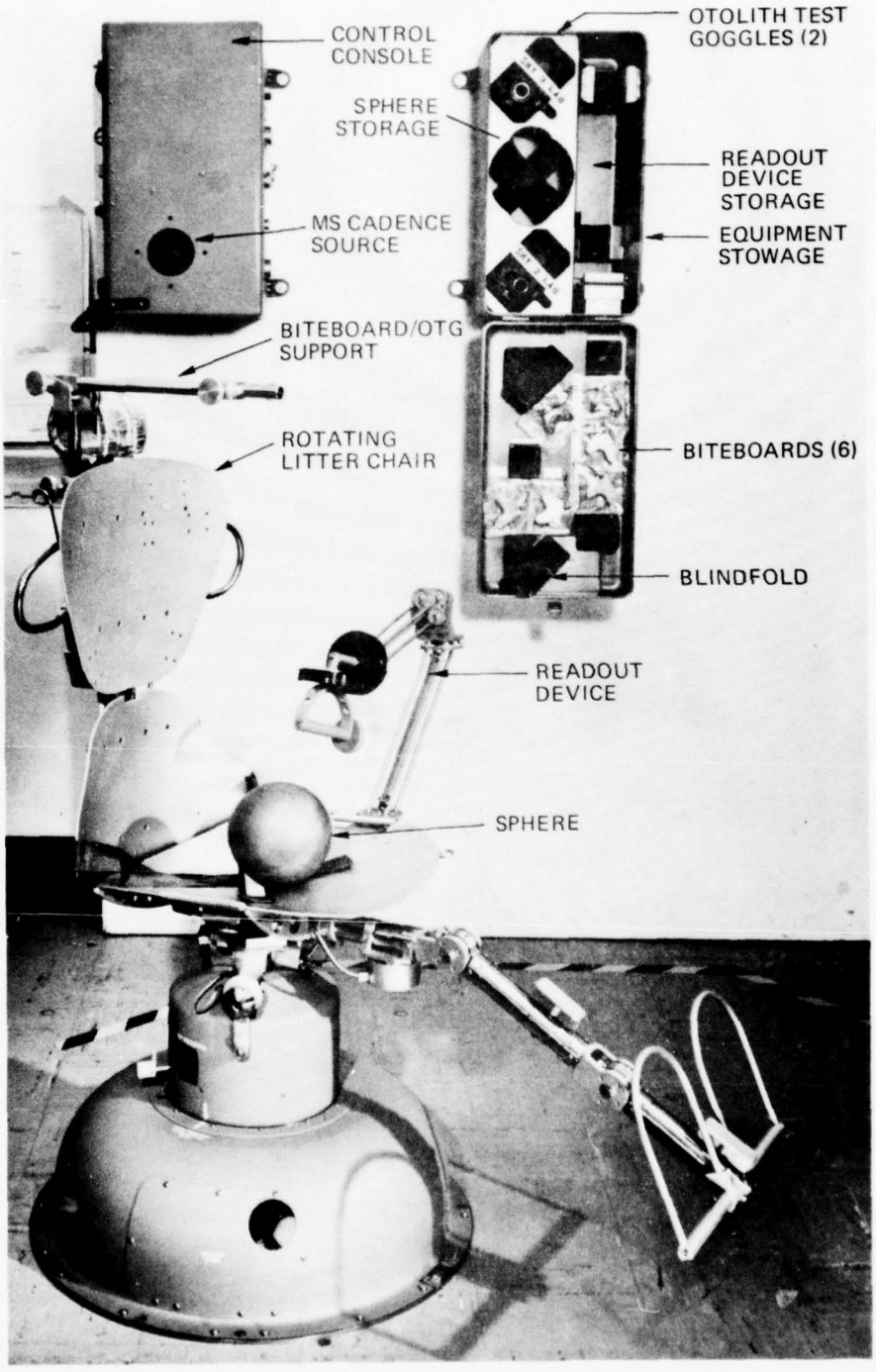

Fig. XII-2 Skylab Experiment M131 Major Equipment

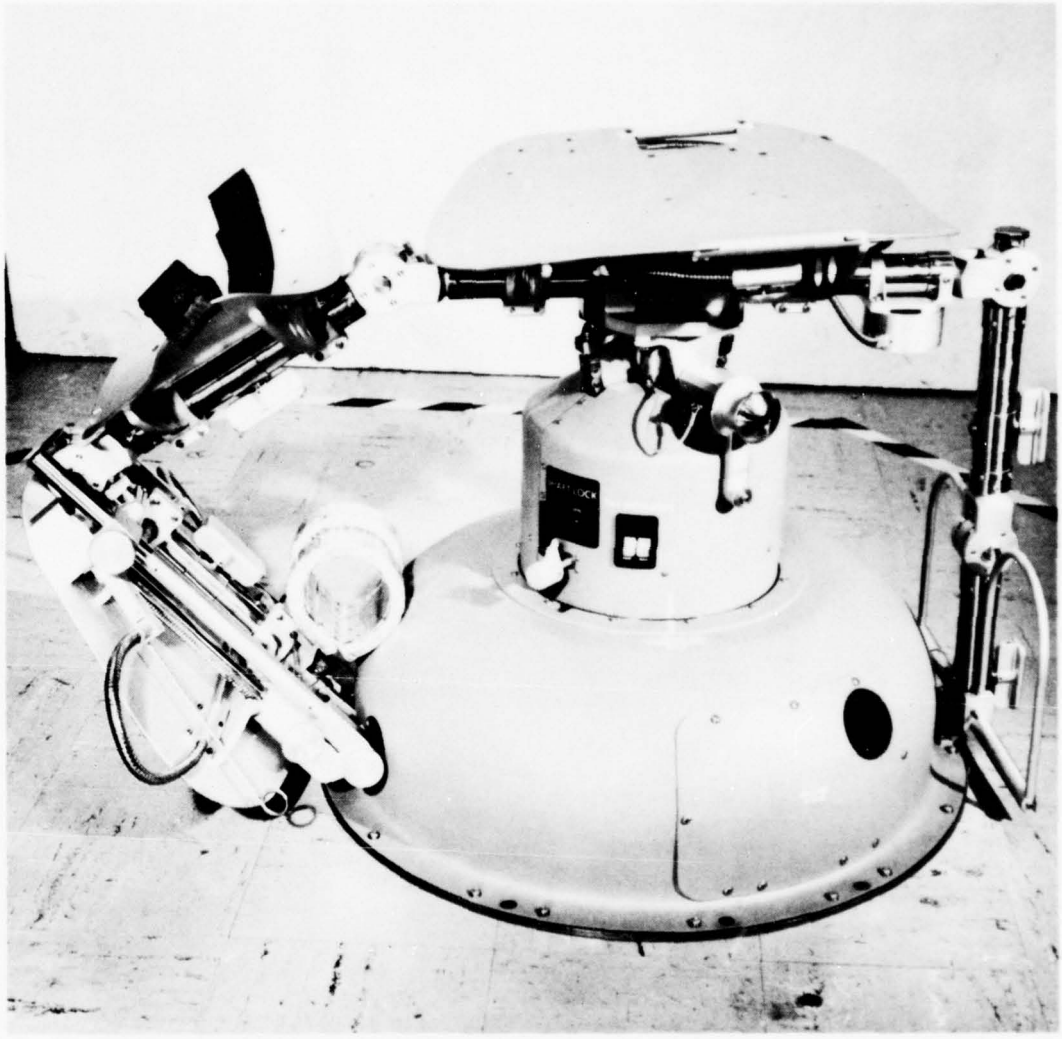

Fig. XII-3 Experiment M131 Configured for Launch

drive shaft extended through the top of the fairing to a maximum of 44.72 cm above the floor. The motor housing consisted primarily of a sealed aluminum cylinder containing the motor, tachometer, drive shaft, and bearings. The motor and tachometer, mounted in tandem along the lower end of the drive shaft and contained within a pressurized housing, consisted of a wound armature which was attached directly to the drive shaft, a permanent magnet field attached to the stationary motor housing, and a brush ring also attached to the housing. The shaft was supported at the upper end of the housing by a class 7 radial ball bearing, and at the lower end by a pair of class 7 angular contact ball bearings which accommodated both radial and thrust loads on the shaft. The thrust bearings and associated lubricant were tested under a 90.7 kg axial load for a total of 240,000 revolutions over a period of 280 hours, with no visible degradation in either the bearings or the lubricants.

To prevent oxygen or corrosive contaminants from entering the motor housing and affecting the brushes or bearings, an atmosphere of dry nitrogen was maintained within the motor housing at approximately 5-13 cm of water above the ambient pressure.

The motor was servo controlled and had the capability of rotating the seated subject within the limits of 1-30 rpm with an accuracy of ±1%. To eliminate uncontrolled stimulation and allow sensitive functional measurements of the vestibular organs, rotation was accomplished by direct motor coupling with no slack and little vibration.

Control Console

The control console contained all controls necessary to conduct the various experiments. The control functions were placed in three groupings: those associated with the MS tests, those associated with the OGI tests, and those which were common to both OGI and MS operations.

Controls common to both tests included the main power switch, a tachometer, a master test button, the OGI/MS mode and direction rotary switches, the system reset pushbutton and indicator, and a fault indicator that lit if the chair was accelerated to over 35 rpm, or if adequate nitrogen pressure was not detected in the motor housing, or if the power amplifier overload detector had activated, or if the chair acceleration exceeded approximately $60°/s^2$.

Equipment Stowage Items

Otolith Test Goggle (OTG). The OTG was used to measure the visual space orientation in two dimensions and provided the visual target for the oculogyral illusion.

Biteboards. The biteboards were of stainless steel superimposed with cast materials of each subject's dental impressions to hold the OTG precisely and comfortably in position over the observer's eyes.

Reference Sphere, Magnetic Pointer, and Readout Device. These items were used for measuring spatial localization using nonvisual clues. The magnetic pointer was held against the reference sphere and moved by the observer while the subject's judgments were measured by a three dimensional readout device that allowed free translational movement.

Support Equipment. Additional support equipment included an instruction and questionnarie sheet for use in the evaluation of motion sickness sensitivity, and a recorder to record the observer's voice comments.

FUNCTIONAL OPERATION

In order to impart closely controlled angular accelerations and velocities to a seated subject, a direct-drive brush-type DC torque motor was used as the prime mover. The angular velocity of the chair was sensed by a precision-grade, brush-type DC tachometer that formed the feedback element in a closed-loop, angular-velocity servo. This combination, and associated electronics, controlled the oculogyral illusion acceleration rates to within 1% (plus 0.0015°/s^2) of the selected value (a, below). This same system maintained the chair to within 1% (plus 0.05 rpm) of the selected constant velocity rates (b, below) while it underwent variations in torque loading as the test subject changed his body position during the motion sensitivity test.

OGI STEP	ANGULAR ACCELERATION (deg/s^2)	OGI STEP	ANGULAR ACCELERATION (deg/s^2)
1	0.020	13	0.300
2	0.024	14	0.380
3	0.030	15	0.475
4	0.038	16	0.600
5	0.048	17	0.760
6	0.060	18	0.950
7	0.076	19	1.200
8	0.095	20	1.510
9	0.120	21	1.900
10	0.150	22	2.400
11	0.190	23	3.000
12	0.238	24	6.000

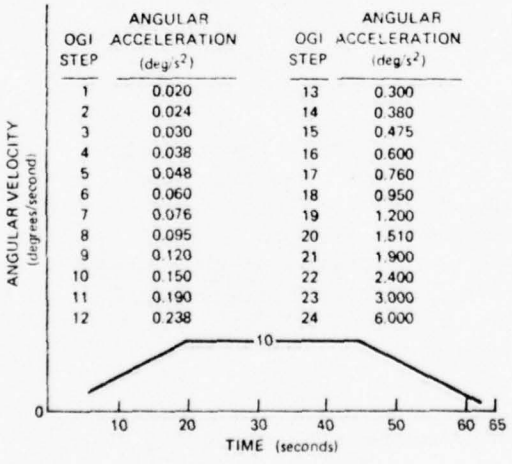

(a) Oculogyral angular-acceleration/time test profile.

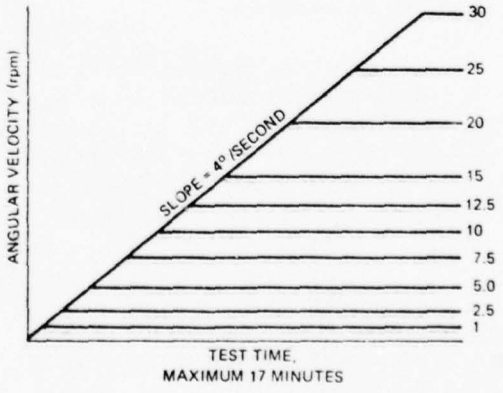

(b) Motion sensitivity angular-velocity/time test profile.

During the OGI threshold test, the subject was seated in the rotating chair and wore the OTG which contained a fixed visual target. The chair was then accelerated and decelerated at specific rates. The subject verbally reported the direction of apparent (hence the term illusion) lateral motion, if any, of the fixed visual target in the OTG. This illusion was the result of stimulation of the fluid in the semicircular canal of the inner ear caused by acceleration and deceleration of the chair.

The electrical control system consisted of an angular velocity profile generator and a servo loop. The profile generator provided a desired command angular velocity-time profile. Positive and negative reference voltages (Fig. XII-4) from zener diode power supplies and precision resistive dividers provided DC voltages that were proportional to a desired MS or OGI velocity-time profile. The appropriate voltages for a particular program were selected by the MS or OGI program select switches on the control console. When a profile was to be generated for a test, these voltages were switched by the control switches to the input of the command integrator, a chopper stabilized DC operational amplifier. The control switches were actuated by the control programmer by various electrical timing circuits. When a constant DC voltage was fed into the integrator, its output was the integral of the constant input voltage and therefore a linear ramp function. Since a velocity ramp represents a constant acceleration or deceleration, it follows that a particular constant input voltage to the integrator represents a particular constant acceleration or deceleration. When a constant voltage was applied to the integrator input and then removed (or the input was set to zero), the integrator output would be the expected ramp function until the input was set to zero. The integrator "held" the last value on the ramp function until the input was again changed from the zero value. The analog voltage being "held" represented a constant angular velocity. When deceleration from this constant velocity was desired, a constant voltage of opposite polarity was fed to the integrator. The output of the integrator then approached zero voltage, and the chair decelerated under the control of the program linearly to zero velocity. When this occurred the chair remained at zero velocity until another test was started.

The output of the profile generator was the command input to the servo loop. The integration in the servo loop, which makes this a type I servo system, guaranteed zero angular acceleration and deceleration errors in the chair shaft motion in the steady state. The output of the servo integrator was fed to a solid-state linear power amplifier. The output of the amplifier was connected to the direct-drive DC torque chair motor. A precision DC tachometer mounted on the shaft of the chair measured the chair

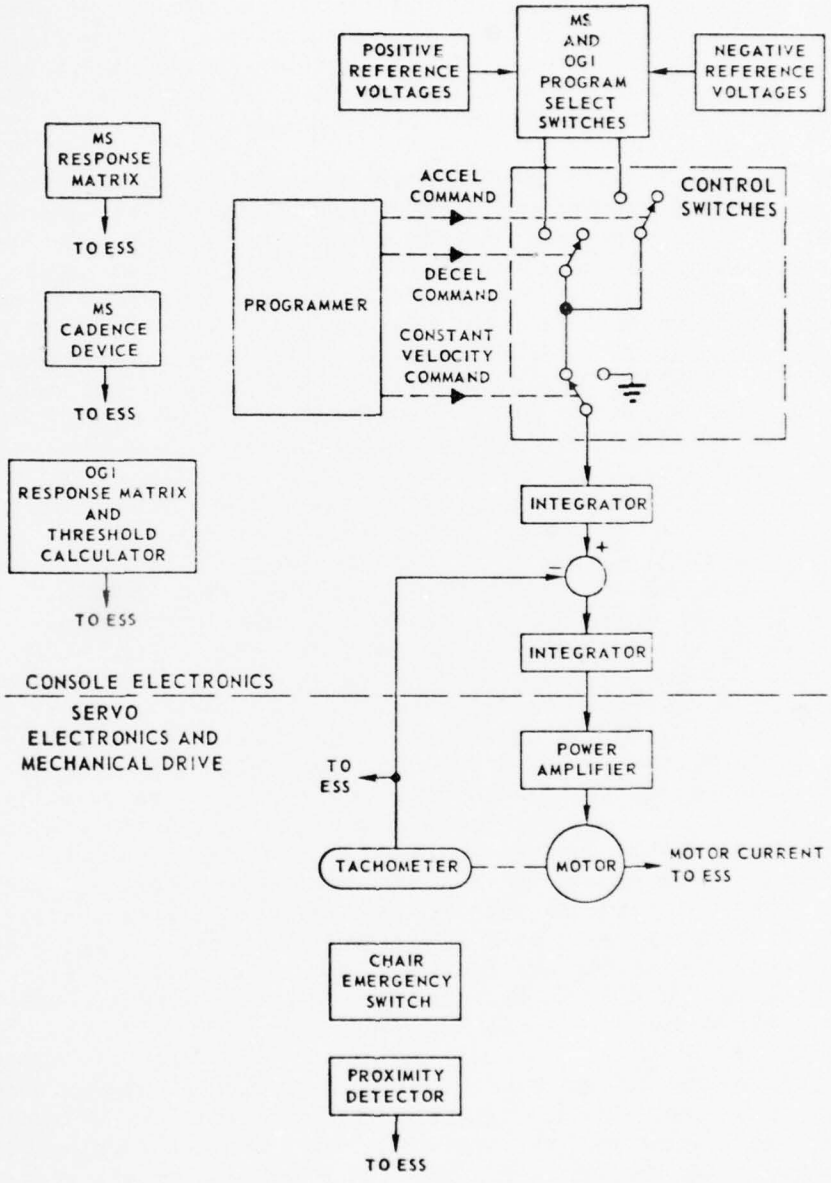

Fig. XII-4 Skylab Experiment M131 Simplified Functional Block Diagram

angular velocity in terms of a voltage analog. The actual chair angular velocity was then compared to the commanded angular velocity, in terms of analog voltages, at the input of the servo integrator.

Several devices such as an OGI threshold computer, an OGI and MS keyboard for recording the subject's responses to these tests, and an audio cadence signal were included to assist the operator and subject in performing the experiments.

During the nonrotational portion of the tests, the chair shaft was locked and the electrical system disabled. The chair could then be extended into a litter position, and the subject blindfolded and strapped to the chair. The observer then slowly tilted the chair from the horizontal to a ±20° position with an accuracy of 0.5°. When a preselected position was reached, the blindfolded test subject aligned a hand-held pitch and roll scale with an unseen reference axis within the space laboratory. His ability to identify his position accurately was an indication of the degree to which the subject depended upon tactile clues for spatial orientation.

FLIGHT RESULTS

The Experiment M131 equipment was operated without failure during the three manned Skylab missions. Good data were obtained throughout each mission by both the crewmen and by telemetry to ground stations. Scientific findings are presented in Ref. 1.

XIII

PHOTOELECTRON SPECTROMETER

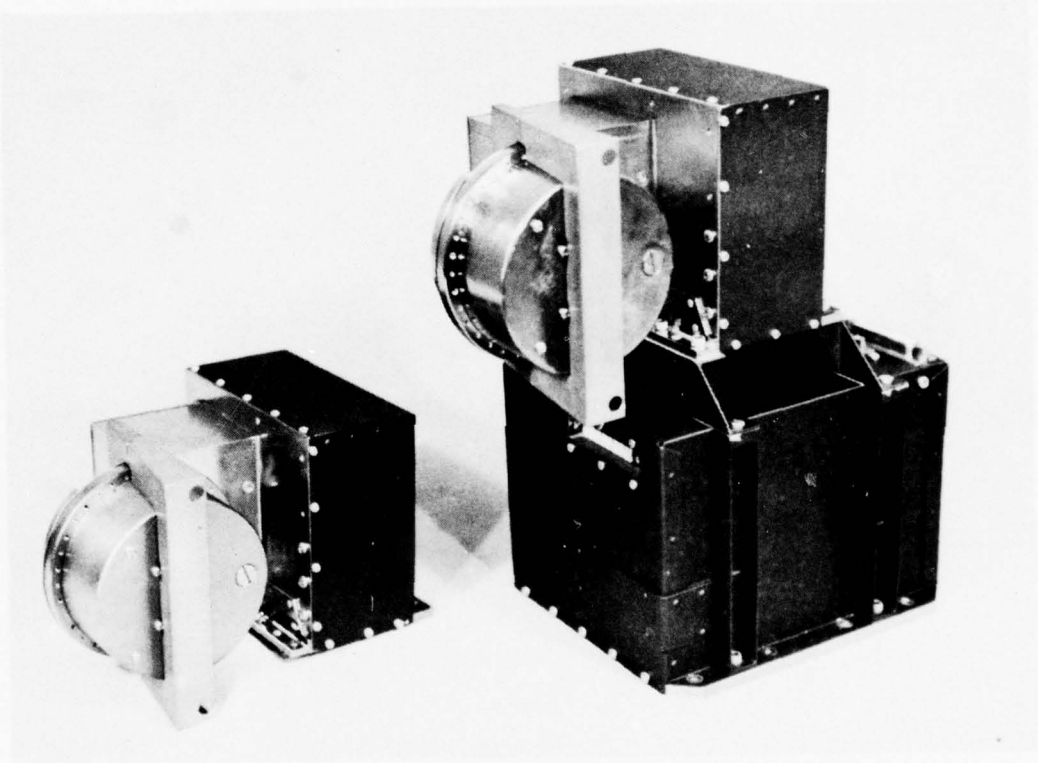

Fig. XIII-1 Photoelectron Spectrometer

XIII

PHOTOELECTRON SPECTROMETER

BACKGROUND

The Photoelectron Spectrometer (PES; Fig. XIII-1) designed and developed by APL was part of the complement of scientific instruments aboard three NASA Atmospheric Explorer (AE) satellites that were designed and flown to obtain data on the physics of the earth's upper atmosphere. The goal of the AE-C, -D, and -E spacecraft series was to carry out a coordinated investigation of the chemical and energy processes that control the structure of the thermosphere and produce its spatial and temporal variations. The first satellite, AE-C (Fig. XIII-2), was launched into a 68° inclined orbit in the previously unexplored altitude range between 130 and 300 km to elucidate the nature of the processes that control the structure of the upper atmosphere. Similarly, AE-D was launched into a polar orbit and AE-E was launched into an equatorial orbit.

The principal investigator was Dr. J. P. Doering of The Johns Hopkins University Department of Chemistry, and two coinvestigators were from APL. The experiment was similar to those used by Doering et al. (Refs. 1 and 2) on sounding rocket experiments, but modifications were incorporated to make the instrument suitable for satellite use.

APPLICATION

The PES was designed to measure the intensity, angular distribution, and energy spectrum of low-energy electrons in the earth's thermosphere. The instrument measured electrons with energies from 1 to 500 eV. Two high-resolution modes allowed detailed observation of electrons with energies between 1 and 100 eV and between 1 and 25 eV. This capability was particularly valuable, since no data existed on electron distribution below 10 eV.

EQUIPMENT DESCRIPTION

The PES contained two identical electron detectors (sensor assemblies) and one control and data-handling package (main electronics assembly). Sensor No. 1 was mounted on the satellite upper baseplate about 20° off the +X axis and sensor No. 2 was

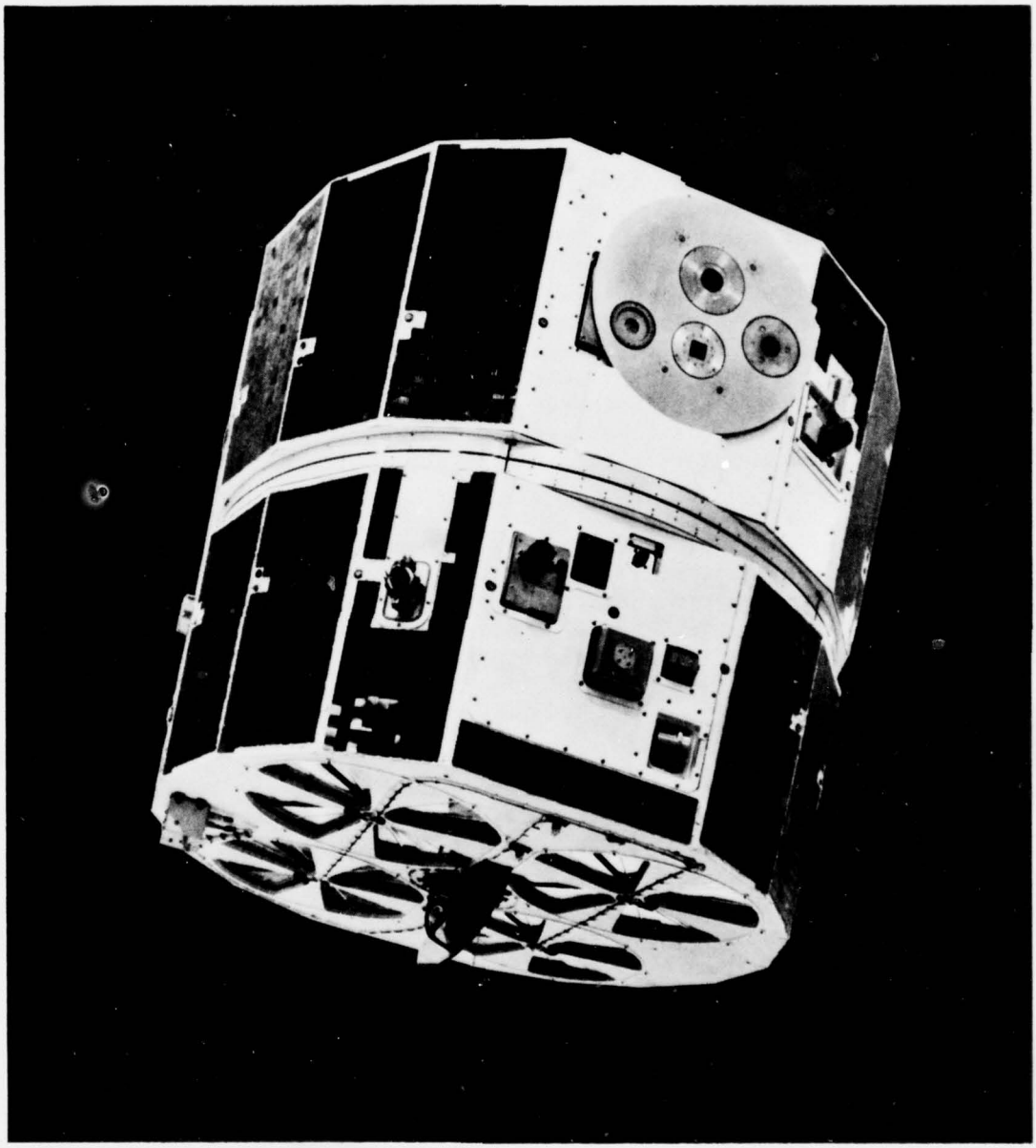

Fig. XIII-2 Atmosphere Explorer-C Spacecraft

mounted on the main electronics assembly and secured to the upper baseplate about 20° off the -X axis. The sensors protruded through the spacecraft thermal blanket and solar panel, and were rotated so that the sensor field of view was not obstructed by the spacecraft surface. In this configuration, the sensors were capable of monitoring simultaneous electron activity in both directions along the geomagnetic field lines.

To avoid shadowing of electrons by the spacecraft (Ref. 3), the sensors were elevated from the upper baseplate by 139.7 cm, resulting in a vantage point 15.24 cm below the spacecraft upper surface.

Sensor Assembly

Each sensor (Fig. XIII-3) contained a concentric hemisphere electrostatic analyzer, an electron multiplier and its associated high-voltage bias supply, and analog electronics which included a preamplifier, amplifier, discriminator, and rate limiter. The dual hemisphere electrostatic analyzer consisted of two metal hemispheres mounted concentrically and insulated electrically from each other as well as from ground. A molybdenum annulus restricted particle access to the analyzer except through a 1.3 mm opening at the analyzer entrance. Molybdenum was used because of its dimensional and surface stability; such stability was essential to prevent charge accumulation (and therefore field distortion) at the analyzer apertures.

The entrance and exit apertures were baffled to reduce data contamination from ultraviolet light. The baffles consisted of holes in the outer hemisphere large enough to include the solid angle determined by the entrance and exit collimators, yet small enough to leave the electric field between the hemispheres virtually undisturbed. Ultraviolet light passing through the entrance baffle caused secondary electron emission upon striking the rear cover. A copper plate biased at +50 volts was installed behind the entrance baffle to collect these secondary electrons.

A Ni-63 radioactive source was installed in the magnetic shield directly above the exit aperture baffle hole so that β emission from the source passed through the baffle to strike the electron multiplier, producing a background count for calibration of the sensor electronics.

The electron multiplier bias supply (Ref. 4) produced voltages up to 4500 volts, and special packaging techniques were employed to avoid damage from corona discharge. Since materials outgas to some degree in a high vacuum, it was likely that the

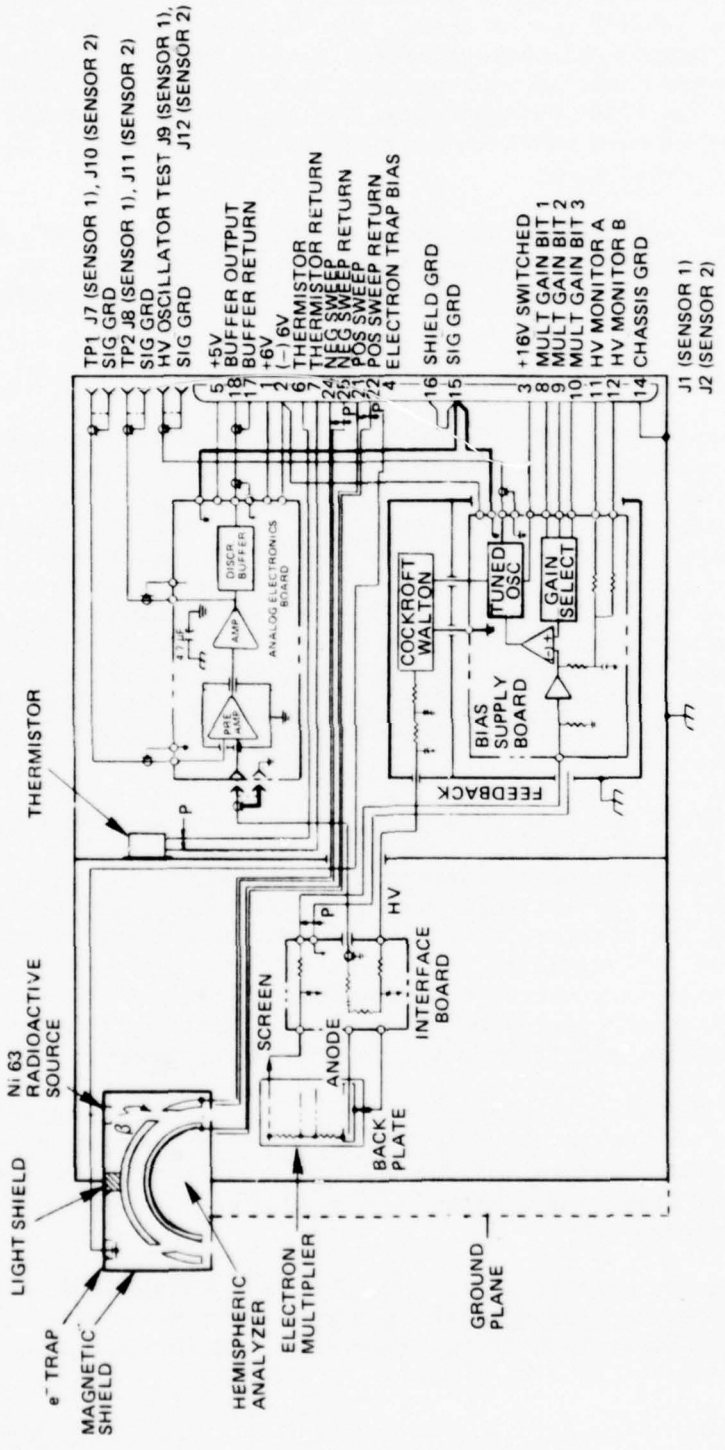

Fig. XIII-3 PES Sensor Block Diagram

high-voltage supply would experience occasional arcing because of increased local pressure caused by outgassing either in a vacuum chamber or in orbit.

Increasing the spacing between components in critical areas reduces but does not eliminate the likelihood of arcing. A compromise PES fabrication technique used an inorganic material to house and isolate each individual component in the Cockcroft-Walton type multiplier. The components were laid out with minimum spacing, and cavities were machined into an inorganic material as shown in Fig. XIII-4. Corona paths existed only in the seams between cavities. If arcing did occur, no permanent low impedance paths were formed. The low-voltage components of the bias supply were mounted on a printed circuit board but separated from the high-voltage section by an electrostatic shield.

The analog electronics (Ref. 5) consisted of a charge sensitive preamplifier, dual amplifiers, a voltage discriminator, and an output buffer. The preamplifier collected the charge appearing at the electron multiplier anode and produced an output voltage proportional to its magnitude. The output signal of the preamplifier was then processed by a cascaded pair of pulse amplifiers before being applied to the pulse height discriminator.

Main Electronics Assembly

The main electronics assembly housed the circuits that produced the required sensor signals including power, hemisphere sweep voltages, and high-voltage commands. The main electronics circuits also adjusted the experiment operating mode, calibrated the hemisphere deflection sweep supply, accumulated the sensor output pulses, monitored housekeeping items, and handled data going to and from the spacecraft subsystems. All PES/spacecraft electrical interfaces were made through a 50-pin connector mounted in the main electronics assembly.

The main power supply was mounted in an electrostatically shielded enclosure to minimize radiated RFI. The digital data system contained PMOS data registers. Since there were more susceptible to radiation damage than TTL registers, the digital data system was placed in a location that took maximum advantage of incidental shielding. In addition, two 0.46 cm aluminum plates were rivited to the side of the main electronics cover to increase shielding against radiation that impinged perpendicularly to the solar panels.

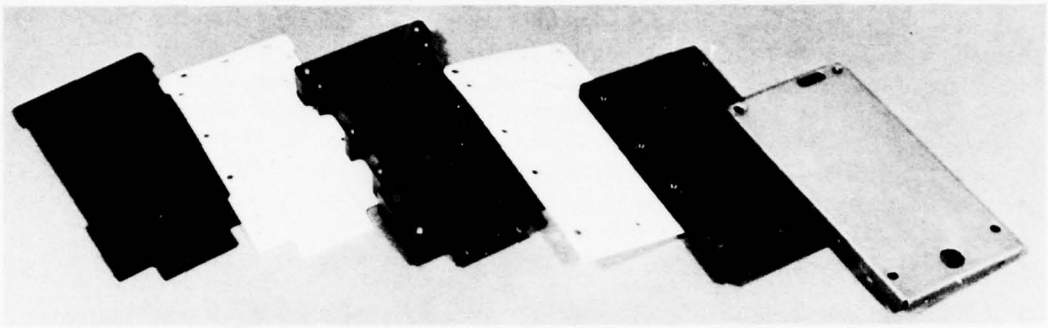

a

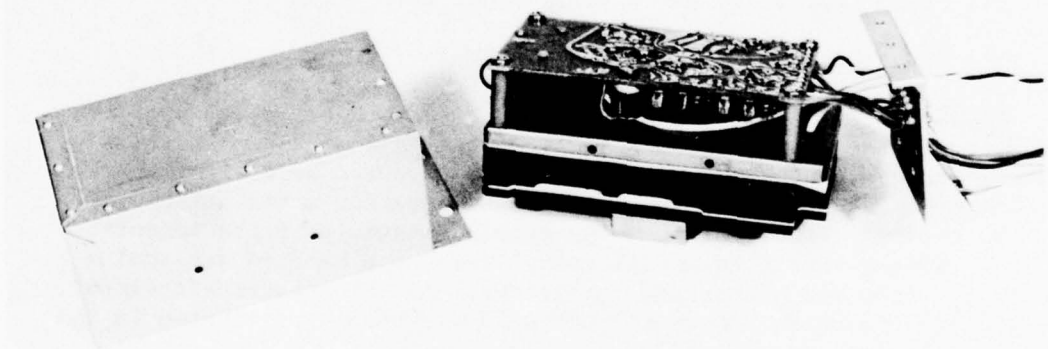

b

Fig. XIII-4 Bias Supply Construction and Cockcroft-Walton Component Isolation to Reduce Corona Effects

FUNCTIONAL OPERATION

Sensor Assembly

Electrostatic Analyzer. Electrons entered the electrostatic analyzer via a 9° by 20° collimator. When the voltage difference between the hemispheres was ΔV, electrons with energy of approximately $2\Delta V$ were bent in a semicircle between the hemispheres to strike the electron multiplier. Electrons with energy of less than $2\Delta V$ collected on the inner hemisphere, and electrons with energy of more than $2\Delta V$ collected on the outer hemisphere.

A ground plane was provided near the collimator entrance to reduce the effect of spacecraft electric fields on the electrons' trajectories prior to their entering the analyzer. After entering the analyzer, the electrons remained subject to path distortion because of magnetic fields, including those generated by the spacecraft and the earth; therefore, the hemispheres were enclosed with magnetic shielding material. The highly permeable shields were composed of 80% Ni, 15% Fe, and 5% Mo and were a minimum of 0.0762 cm. A Helmholtz coil used to test the effectiveness of the shield indicated that a field strength of 7 gauss could be applied along the most susceptible axis before particle data were seriously compromised. Since the shield of the electron gun (used as the particle source) may become ineffective at the higher field intensities, 7 gauss was the minimum upper useful limit of the flight magnetic shield.

Distortion of the magnetic field in the vicinity of the instrument impeded a clear interpretation of the apparent measured electron energy and angular distribution. A field of several hundred gamma may in fact distort the distribution of low energy electrons entering the instrument field of view. Consequently, a great deal of attention was given to the problem of assuring magnetically clean spacecraft.

Any ultraviolet light that passed through the analyzer into the electron multiplier would cause counts that were indistinguishable from electron counts. To reduce this possibility, holes were cut in the outer hemisphere to baffle the light. Secondary electron emission was collected on an electron trap which consisted of a copper plate biased at +50 volts.

The baffle hole in the exit portion of the electrostatic analyzer was a convenient opening for β particles from the Ni-63 radioactive source. These β particles provided a known background count to calibrate the electron multiplier gain. The nominal calibration count rate was 2 to 3 per second, which exceeded the estimated cosmic ray background count of less than 1 per second.

Electron Multiplier. After an electron emerged from the electrostatic analyzer, it struck the first dynode of a 20-stage Johnston Laboratories focused mesh electron multiplier (MM-1-5NG). The screen of the multiplier was biased at 9% of the total multiplier voltage and was used to accelerate the electron to an energy sufficient to produce secondary emission upon contact with the first dynode of the multiplier. Each subsequent dynode liberated additional electrons, resulting in a nominal gain of 10^6 for a multiplier bias voltage of 3000 volts (screen voltage of 270 volts). Increasing the bias to 4500 volts raised the gain to about 10^9. It should be noted, however, that these were average gain values, and the multiplier actually displayed a rather broad pulse height distribution that must be considered during calibration.

The electron multiplier was housed in a compartment separated from the other electronic circuits and kept free of material that could degrade the exposed multiplier. Only the necessary bias and filter components were mounted with the multiplier.

Electron Multiplier Bias Supply. As the electron multiplier operated, degradation occurred in the final dynode stages because these stages emitted the greatest number of electrons per pulse. The resulting loss in multiplier gain was offset by the use of a commandable bias supply. Initially, the multiplier was baised near the minimum bias supply output of 3000 volts. The bias was increased upon command as required in seven equal increments to a maximum output of 4500 volts.

Analog Electronics. The charge output of the electron multiplier was collected at the input of a charge-sensitive preamplifier. Two pulse shaping and amplifying stages, a discriminator, and a rate limiter followed the preamplifier.

Experimental results indicated that a discriminator setting of 10^5 electrons was adequate to produce a counting efficiency of approximately 80% at a bias supply setting of 3200 volts when the multiplier was new.

Bipolar pulse shaping was used with a zero crossing time of about 0.5 μs in the unsaturated mode, resulting in amplifier rate limiting of about 2 million pps (particles per second). The buffer circuit was rate-limited so that the maximum electron count rate from the sensor was nominally 250,000 pps.

Main Electronics Assembly (Fig. XIII-5)

The PES electrostatic analyzer selected electrons with energy of $2\Delta V$ when ΔV volts were applied across the hemispheres. However, the electron entered the analyzer on a zero-potential

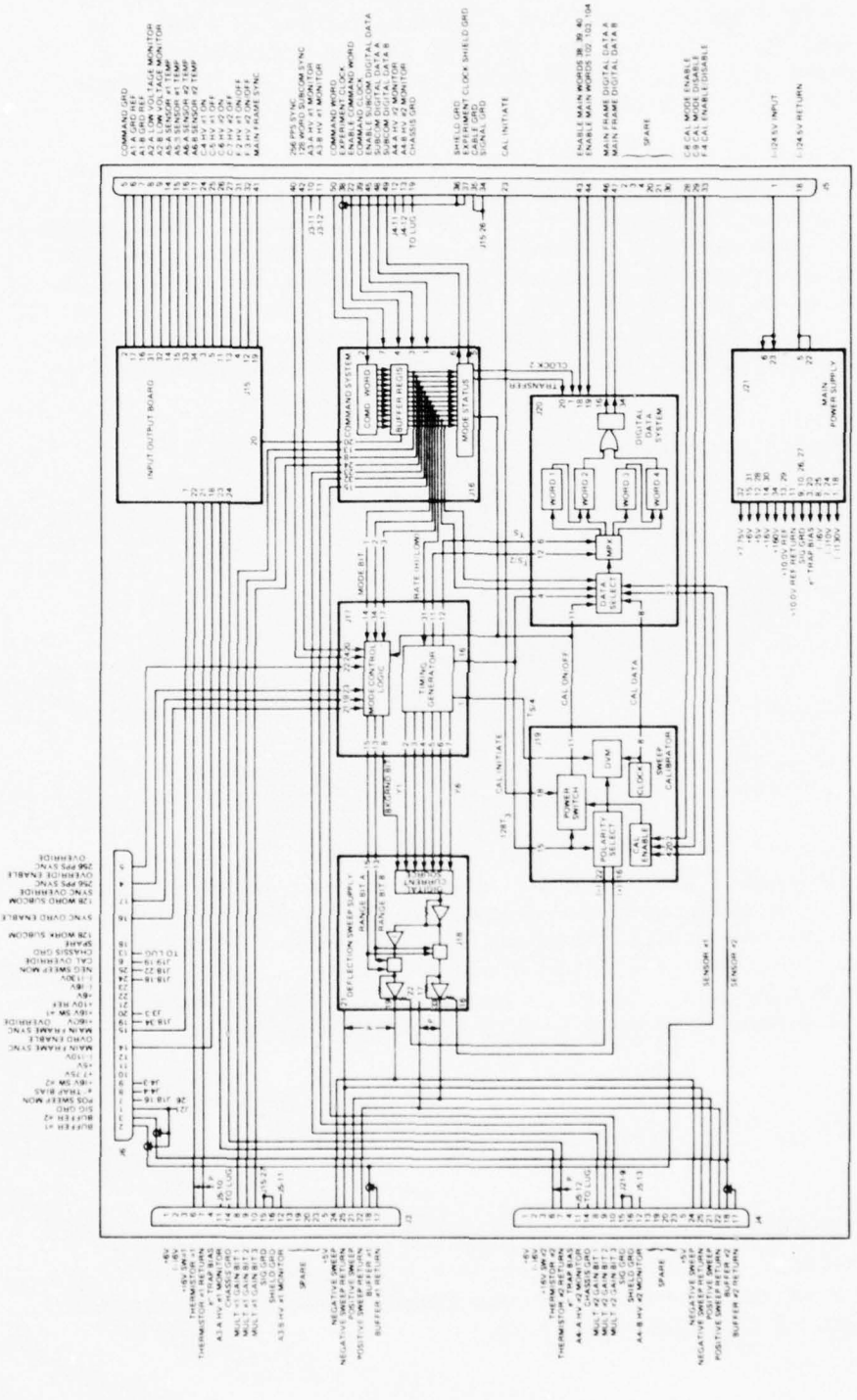

Fig. XIII-5 PES Main Electronics Unit Block Diagram

electric field line with respect to the spacecraft chassis. Therefore, the ratio of hemisphere potentials was carefully selected to maintain the electron path at zero potential so that the electron would travel in a smooth semicircle between the hemispheres. It was determined (Ref. 6) that for the PES analyzer dimensions, a 500 eV electron required +140.35 volts applied to the inner hemisphere and -109.65 volts applied to the outer hemisphere.

The deflection sweep supply was a digital/analog (D/A) converter that produced synchronized positive and negative linear ramps with maximum voltages of +140.4 and -109.6 volts. The ramps contained 64 steps and had commandable gain networks that provided for a selection of one of three sweeps with maximum sweep energies of 500, 100, or 25 eV (35 eV on AE-D and -E*). Consequently, the theoretical analyzer resolution was 25 eV/63 $\approx$ 0.4 eV. Local electric and magnetic fields, however, limited the practical resolution to about 2 eV.

Experiment Operating Modes

The three deflection sweeps were used in combinations that produced five energy range operating modes:

1. In Mode I, all three ramps were used, with the 25 eV ramp being used 50% of the time and the remaining time being equally shared by the 100 to 500 eV ramps.

2. In Mode II, the 25 and 500 eV ramps were alternated.

3. Modes III, IV, and V used single ramps with peaks of 25, 100 and 500 eV, respectively.

In addition to the five energy range modes, there were fast and slow modes. When the satellite spin rate was less than approximately 4 rpm, the deflection sweep operated in the slow mode in which there were 64 voltage steps and 64 data words per ramp. At higher spin rates, the deflection sweep operated in the fast mode in which there were still 64 steps per ramp but only 16 data words per ramp; i.e., each data word contained data from four steps on the ramp.

*Data from AE-C revealed important structure in the 25-30 eV region. Therefore, the low energy sweep was changed to 0-35 eV for the AE-D and -E instruments to obtain improved energy resolution for this part of the spectrum.

The PES was allotted four main frame telemetry words for sensor (particle) data. These words were used to transmit any of the following information:

1. Sensor No. 1, particle data only,

2. Sensor No. 2, particle data only,

3. "Sensor Alternate," in which particle data were taken alternately from each sensor at 4-second intervals, and

4. Deflection sweep calibration data, and 8-second sequence, initiated by command, which measured and transmitted the deflection sweep voltage at each step of the deflection sweep ramp.

Weight and Power Requirements

The following PES weights include the thermal shields and the test connector cover but not the external cables:

Experiment Designation	Sensor No. 1	Sensor No. 2 plus Main Electronics
Protoflight instrument	1338 g	2827 g
First flight instrument	1274 g	2771 g
Second flight instrument	1266 g	2761 g

PES power requirements were as follows:

	Experiment Configuration			Current Drain from -24.5 Volt Bus (mA)		
	High-Voltage Monitor 1	High-Voltage Monitor 2	Calibrator	SN121	SN342	SN563
	Off	Off	Off	80	80	81
	Off	Off	On	105	105	106
Normal Operating Condition	3.86 kV	3.86 kV	Off	103	103	105
	4.5 kV	4.5 kV	Off	108	108	110

FLIGHT RESULTS

Photoelectron Spectrometers were launched into orbit aboard the AE-C, AE-D, and AE-E satellites on 13 December 1973, 6 October 1975, and 20 November 1975, respectively (lines 35, 41, and 43, respectively, Table 1). Data obtained from the PES onboard SE-C were used in the first general classification of low-energy (1-500 eV)

electron fluxes in the high latitude ionospheric regions with high resolution energy spectra measurements. In addition to the energy spectra already associated with the normal day airglow, four major classes of low-energy electrons were identified (Ref. 7).

Launched into a polar orbit, the PES aboard AE-D provided energy-time spectrograms of low energy (0-500 eV) electrons over the north polar region at altitudes between 300 and 1200 km (Ref. 8) when the satellite orbital plane was aligned within a few hours of the noon-midnight local time meridian. While good PES data were received, a major satellite system failure caused the failure of all onboard experiments and subsequent satellite reentry.

The daytime photoelectron energy spectrum was measured at altitudes above 154 km with the PES onboard AE-E. Much higher energy resolution spectra than previous AE-C results were obtained (Ref. 9).

XIV

APOLLO-SOYUZ ULTRAVIOLET ABSORPTION EXPERIMENT MA-059

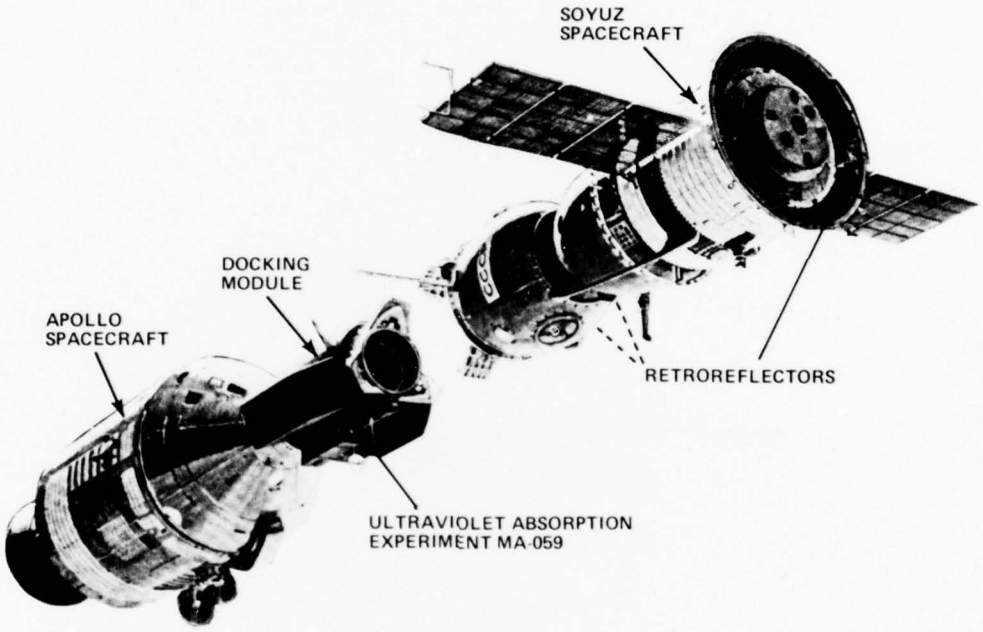

Fig. XIV-1 Ultraviolet Absorption Experiment MA-059 Aboard Apollo Soyuz Test Project

XIV

APOLLO-SOYUZ ULTRAVIOLET ABSORPTION EXPERIMENT MA-059

BACKGROUND

The principal objective of the Apollo-Soyuz Test Project (ASTP) was the docking of a United States Apollo and a Soviet Union Soyuz spacecraft in earth orbit to test compatible rendevous and docking equipment and procedures. An additional objective of major importance was the program of scientific investigations conducted during the mission. The ASTP experiments package comprised 28 separate experiments of which five, including the Ultraviolet Absorption (UVA) Experiment MA-059 (Fig. XIV-1), involved the participation of both spacecraft. The successful ASTP mission started with the Soyuz launch from the Baykonur, Kazakhstan launch complex on 15 July 1975. Seven and one-half hours after the Soyuz launch, the Apollo spacecraft was launched from the NASA John F. Kennedy Space Center to eventually, about 45 hours later, dock with the Soyuz. Joint operations were conducted at the near-earth altitude of about 220 km for two days, after which Soyuz landed in the USSR on 21 July and the Apollo landed near Hawaii on 24 July.

Principal Investigators for the APL-supplied UVA Experiment were from the NASA Lyndon B. Johnson Space Center and the University of Michigan. Co-investigators were from the University of Pittsburgh and Harvard University.

APPLICATION

The objective of the UVA Experiment was to measure the concentration of atomic oxygen and atomic nitrogen in the atmosphere by UV absorption and resonance scattering spectroscopy. Secondary objectives were as follows:

1. To measure the abundance of atomic oxygen and nitrogen within the ambient cloud around the Soyuz spacecraft.

2. To determine the atmospheric gas temperature.

3. To measure the atomic oxygen variation within the orbital path.

4. To determine the atmosphere natural wind velocity.

One of the uses of these data was to permit the evaluation of the effects of the supersonic transport (SST) and other producers of high altitude contaminants on the upper atmosphere.

EQUIPMENT DESCRIPTION

The UVA Experiment (Fig. XIV-2) employed a modified version of the spectrometer provided by APL for the Apollo 17 lunar mission (refer to Section XI). The unit was modified by removal of the entrance baffle, which was replaced with collecting optics and an ultraviolet lamp housing. In addition, new power supplies and an electronics system were developed to adapt the unit for the ASTP mission. A star-tracking type sensor, used in conjunction with the retroreflector on Soyuz, was added to enable the Apollo astronauts to point the experiment accurately at the Soyuz spacecraft. A new grating drive cam was also designed for the spectrometer, and a new electronics system was designed to interface the experiment with the Apollo telemetry system.

Spectrometer Assembly

The spectrometer assembly consisted of two resonance lamps, an incandescent lamp, a startracker and telescope, and a UV spectrometer. The nitrogen and oxygen lamps were mounted in a cluster around the entrance aperture to the spectrometer. The angular spread of the lamps was 3°, and had the following characteristics:

Lamp	Wavelength (Å)	Intensity (Photons/s)
Oxygen	Triplet: 1302.17, 1304.87, & 1306.04	10^{13}
	Doublet: 1355.60 & 1358.52	
Nitrogen	Triplet: 1199.55, 1200.23, & 1200.71	2×10^{12}
	Doublet: 1492.62 & 1494.67	

The visible lamp contained two redundant incandescent bulbs which illuminated the retroreflector to activate the startracker electronics and determine experimnent pointing.

The spectrometer was a 0.5 m focal length Ebert-Fastie scanning, grating spectrophotometer that used two 52 × 2 mm slits; the entrance slit was collimated on the grating and the grating was imaged on the exit slit. The incoming light signal photons

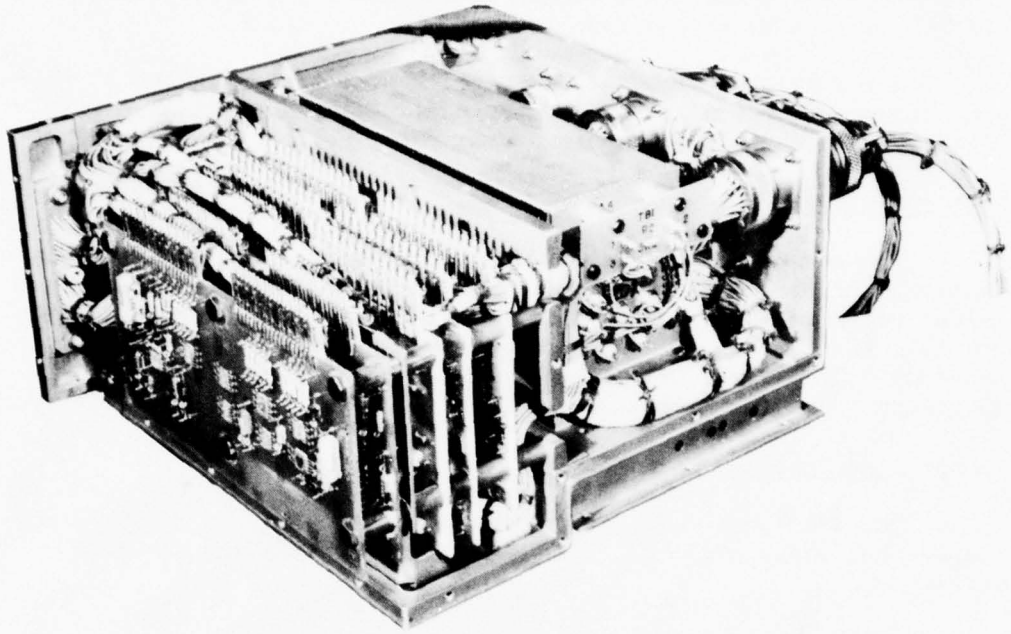

Experimental Interface and Control Electronics

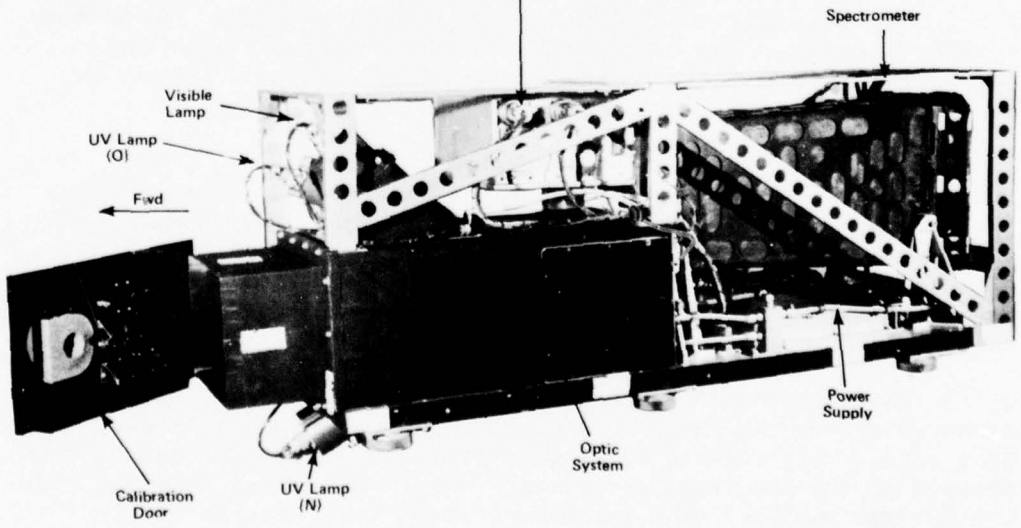

Fig. XIV-2 UVA Experiment

were counted by a photomultiplier tube and digital counting electronics. The grating drive mechanism scanned 1200, 1304, 1356, and 1495 Å in a 12 second scan program.

A startracker with a field of view of 6° in pitch and 3° in yaw, aligned to the spectrometer optical axis, was provided to calibrate and monitor the spectrometer pointing.

Retroreflector

The retroreflector array (RRA) that was mounted on the Soyuz consisted of three individual arrays, each with seven individual corner reflectors, having a reflector flatness of $\tau/10$ measured at τ = 6328 Å. The total reflectivity of the RRA was 50% between 1200 and 1500 Å, and the return beam deviation for the total array was no greater than 4 arc seconds.

Physical Parameters

The UVA experiment measured 384.0 mm × 1054.1 mm × 498.88 mm, and weighed about 40.7 kg. Total power consumption was about 85 watts.

FUNCTIONAL OPERATION

Figure XIV-3 is a simplified functional block diagram of the UVA experiment. Light from the UV lamp was reflected off the transmitting mirror to the Soyuz retroreflector. At the same time, visible light was also transmitted to the Soyuz spacecraft. The return beams were used by the startracking sensor to provide pointing information to the astronauts and by the UV spectrometer to measure UV absorption.

The electronics system generated a 400 Hz timing signal for the spectrometer which was synchronized with the PCM telemetry data system in the ASTP Apollo Command Service Module. The output data from the spectrometer consisted of photon counts taken over 0.1 second intervals and which were supplied to the telemetry system as 120 16-bit words every 12 seconds. After 12 seconds, the spectrometer grating drive cam repeated its frequency scan.

The electronics system also generated signals for the two UV lamps to switch the lamps on and off so that only one lamp was on at a time. This reduced background noise and eliminated lamp interference at the spectrometer entrance slit. The output from the startracker was analyzed by a special-purpose analog circuit in the

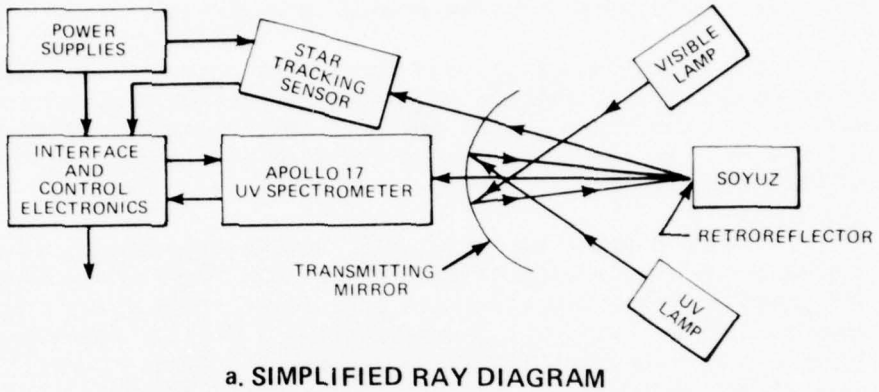

a. SIMPLIFIED RAY DIAGRAM

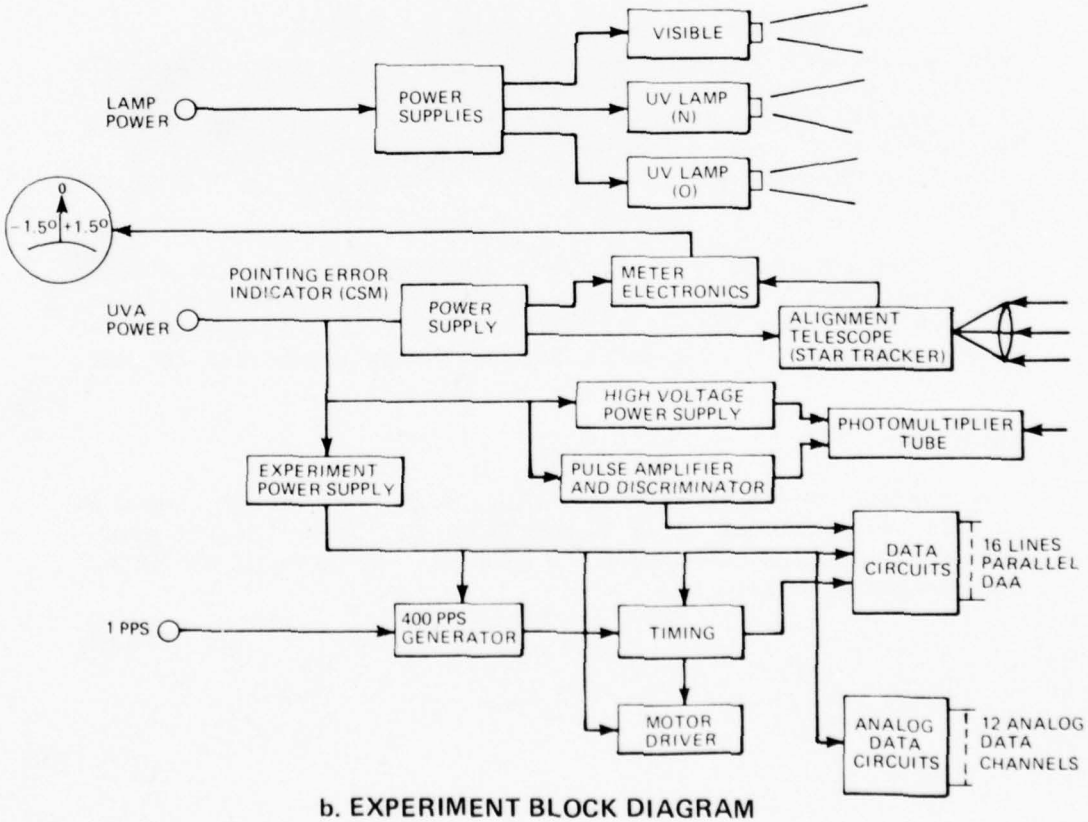

b. EXPERIMENT BLOCK DIAGRAM

Fig. XIV-3 UVA Experiment Simplified Ray and Block Diagrams

electronics system. This circuit drove a pointing error meter which the Apollo astronauts used to aim the UVA experiment at the Soyuz retroreflectors.

The electronics system also included analog circuitry to monitor 12 housekeeping functions in the experiment. These functions were telemetered to the ground in real time.

The electronic parts and integrated circuits were packaged on three multilayer printed circuit boards which were mounted parallel to the three boards designed for the Apollo 17 spectrometer system. In addition, one of the Apollo 17 boards was modified to work with the new system.

Ground support equipment for the UVA experiment, which included bench test equipment (BTE), was also supplied by APL. The BTE provided power and simulated spacecraft signals for comprehensive preflight testing of the hardware. A digital panel meter allowed all housekeeping functions and the 15 DC power supply voltages to be monitored. A digital printer provided hard copy of these functions plus the spectrometer outputs and time of day.

Provision was made for supplying to the UVA a simulated pulse count from the BTE. This pulse count was inserted into the UVA PAD (pulse amplifier and discriminator), located electrically following the photomultiplier tube, to enable testing of the UVA PAD and all follow-on electronics. This pulse count could be varied from zero to the maximum count processed by the UVA Experiment.

The UVA cam motor could be stopped by enabling the motor position control. This allowed the cam to stop at any position (or wavelength) during a rotation and remain at this location for fixed wavelength testing until the motor stop signal was removed.

FLIGHT RESULTS

First in-flight data were taken with the UVA Experiment on 16 July 1975, one day after launch (line 42, Table 1), and good data were obtained throughout the mission. Scientific findings are presented in Ref. 1.

XV

NAVPAC
(NAVIGATIONAL PACKAGE)

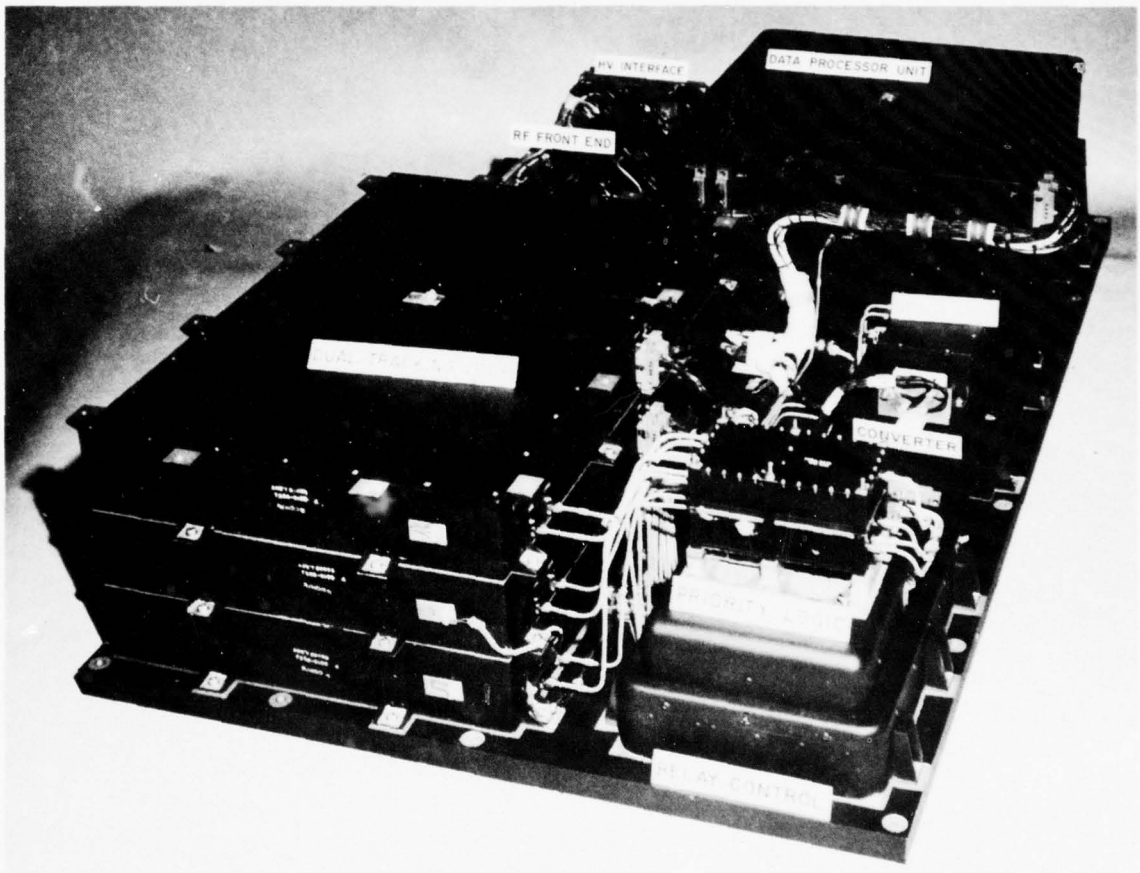

Fig. XV-1 NAVPAC (Navigational Package)

XV

NAVPAC (Navigational Package)

BACKGROUND

The accurate determination of the orbit of a low-altitude satellite is subject to uncertainties due to such factors as atmospheric drag effects and gravity field model errors. Consequently, for precise position determinations, a large network of ground stations is required to obtain doppler tracking data from such satellites. Installation and operation of these stations can be expensive, especially if they are remotely located. Also, geographical or political constraints may make station establishment impossible or impracticable.

In 1975, a program was initiated that had as its objective and requirement the determination of a satellite orbit using satellite-to-satellite doppler tracking. The NAVPAC (Navigational Package) experiment (Fig. XV-1) was designed and developed by APL to meet the program goals, and a flight system was delivered and launched by June 1977.

APPLICATION

The NAVPAC experiment is used primarily to provide very accurate satellite positioning through denser measurements than would be possible from a limited number of TRANET stations and Geoceivers. Other uses of NAVPAC data include atmospheric density studies and improvement of the gravity field model.

EQUIPMENT DESCRIPTION

NAVPAC instrumentation includes a multisatellite receiver used to automatically acquire and track signals from as many as three simultaneously-in-view Navy Navigation Satellites. A three-axis miniature electrostatic accelerometer (MESA), developed by Bell Aerospace Corp., is used to sense all non-gravitational accelerations of the satellite host vehicle (HV). The antenna system consists of a 400 MHz dipole and a left-hand circular polarized quadrafilar helix for 150 MHz reception, both mounted on a deployable boom. The 400 MHz dipole allows reception of left and right-hand circular polarized signals as transmitted by different types of NAVSATS. Size and weight were not primarily limiting factors in the initial NAVPAC

design, and the system was packaged in the most expedient configuration. Power, volume, and weight requirements (less MESA) follow:

Power: 16 W at 28 V DC

Volume: (a) Instrument Envelope - 25.4 cm × 71.12 cm × 116.84 cm
(b) Antenna Envelope - 162.56 cm × 21.59 cm OD

Weight: (a) Instrument Panel - 60.78 kg
(b) Antenna - 2.04 kg.

FUNCTIONAL OPERATION

The multisatellite receiver (Fig. XV-2) consists of a frequency synthesizer, three dual channel (two frequency) tracking loops (DTLs) with associated control logic, and two RF sections. Each RF section contains a narrowband preselect filter, preamplifier, and IF amplifier. Receiver system requirements include:

1. Automatic acquisition and tracking of NAVSAT signals without pass alert information (i.e., predictions of when a NAVSAT will be in view), and automatic reacquisition of the signal after a signal fade (e.g., due to an antenna null).

2. Rejection of signals not containing NAVSAT type modulation.

3. Acquisition and tracking of signals whose doppler characteristics (i.e., rate of change and total rise-to-set excursion) are about twice that observed by a fixed ground station.

4. Circuitry to prevent any two DTLs from tracking the same NAVSAT. An optional mode of operation allows the three DTLs to acquire and track a single satellite.

The data processing unit (DPU) controls all data collection and movement in NAVPAC. The central processing unit (CPU) accepts digitized data from various DPU subsystems, and creates several data files in a temporary buffer. When the buffer is full, the contents are automatically transferred to a tape recorder for later transmission to a ground station. A tape recorder bypass mode allows data transfer directly from the buffer to the ground station should the recorder fail. The CPU accepts data from the time code generator (TCG), the MESA, the doppler and refraction counters for the three DTLs, the NAVSAT two-minute time mark (TMTM) and identification (ID) recovery electronics, HV time mark electronics, and the engineering and diagnostic telemetry electronics. The TCG

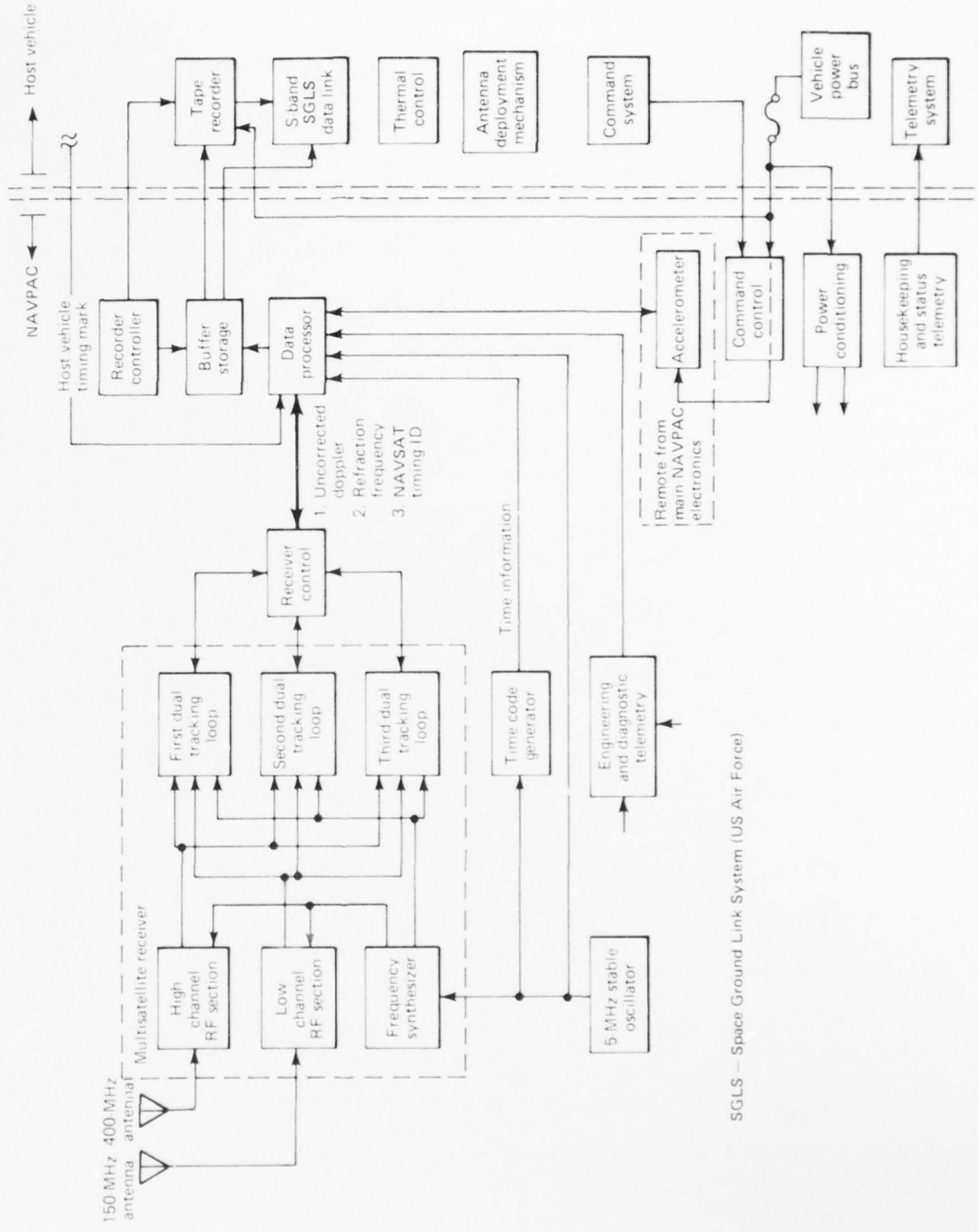

SGLS – Space Ground Link System (US Air Force)

functions as a counter driven by the ultrastable 5 MHz oscillator to create a precision time annotation mechanism.

The DC/DC converter converts the HV unregulated power into the various voltages needed by the receiver and data systems.

NAVPAC can be commanded into several configurations from oscillator and counter-only on to all-systems on. In addition, the buffer storage allocated to the various data types can be modified by command. This allows maximum flexibility if power constraints are imposed during the mission or should the equipment malfunction.

The following data are supplied by NAVPAC:

1. Uncorrected doppler referenced to 400 MHz.

2. Ionospheric refraction information, scaled by approximately ten, referenced to 400 MHz (a difference frequency derived from the 400 MHz and 150 MHz signals).

3. Demodulated NAVSAT signals from which the satellite TMTMs and ID are obtained. The NAVSAT time marks allow calibration of the data system TCG and are also required for navigation computations.

4. Accelerometer data, obtained from the MESA, and host vehicle timing marks.

FLIGHT RESULTS

The first NAVPAC was successfully launched on 27 June 1977 (line 49, Table 1). Prior to launch, NAVSAT tracking tests were performed at APL with the following results:

- Clock calibration error, <40 us, 1 sigma

- Average filtered noise, 10 to 15 cm.

In-orbit results have compared well with these measurements.

NAVPAC data are used by the Naval Surface Weapons Center (NSWC) to accurately reconstruct the host vehicle orbit and refine the gravity field model of the earth. The Air Force Geophysical Laboratory uses the MESA data for atmospheric density studies.

A second NAVPAC was successfully launched on 16 March 1978 (line 54, Table 1); additional NAVPAC systems are in various stages of fabrication and test.

XVI

LOW ENERGY CHARGED PARTICLE EXPERIMENT (VOYAGER)

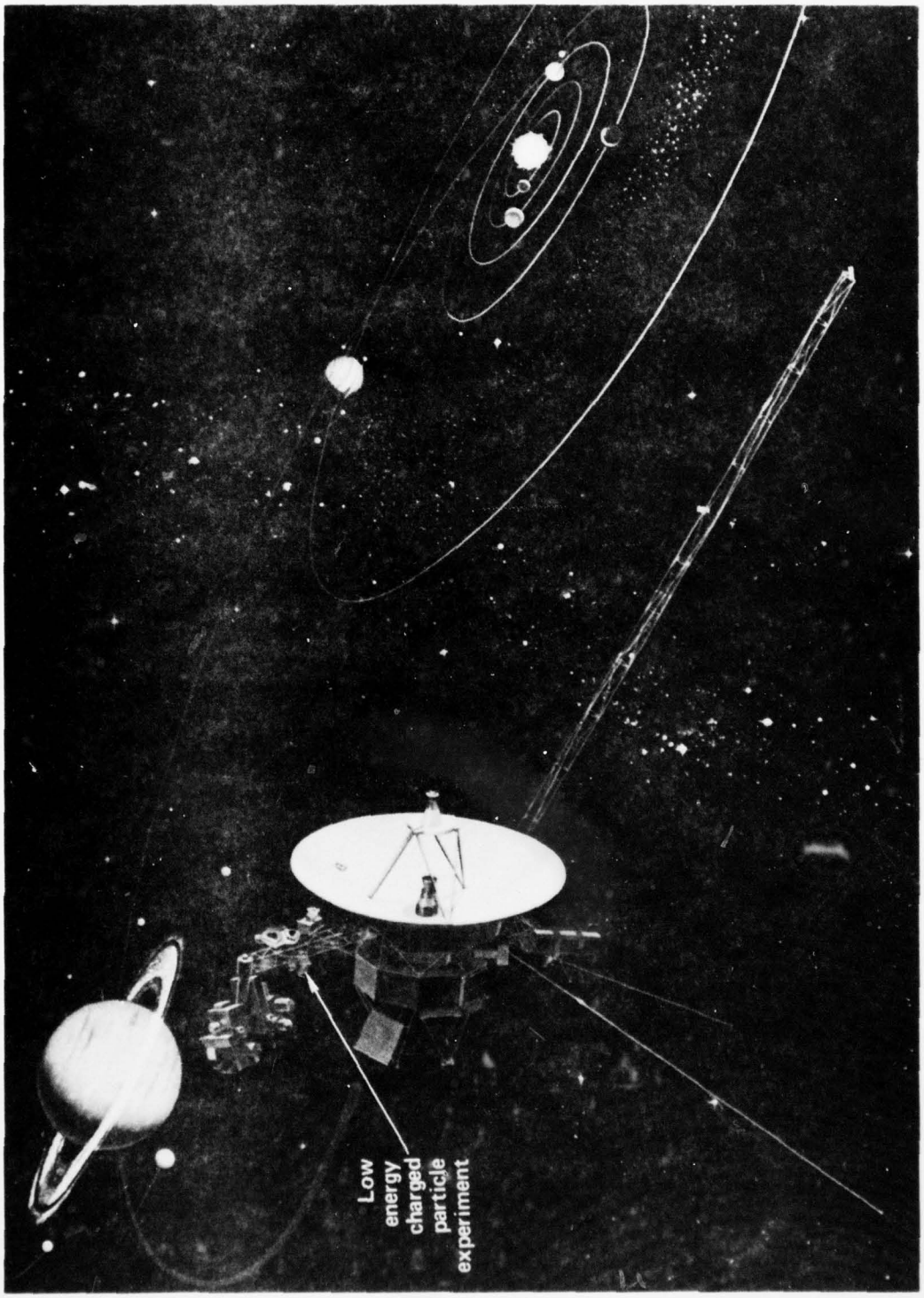

Fig. XVI-1 LECP Experiment Aboard Voyager, Artist's Concept

XVI

LOW ENERGY CHARGED PARTICLE EXPERIMENT (VOYAGER)

BACKGROUND

The NASA Voyager (formerly called Mariner Jupiter/Saturn) Program was implemented to obtain scientific data on the surface characteristics, atmospheric compositions, ionospheres, masses, sizes, and surrounding fields of Jupiter, Saturn, and many of their satellites. The rare alignment of the outer planets and the reduced outer planet flyby distances in the last half of the 1970s afforded an ideal opportunity for such a mission. Voyager spacecraft (Fig. XVI-1) instrumentation included a Low Energy Charged Particle (LECP) Experiment designed and fabricated by APL. The Principal Investigator for the experiment is Dr. S. M. Krimigis of APL, and co-investigators are Dr. C. M. Bostrom of APL/JHU, Dr. L. J. Lanzerotti of Bell Laboratories, Dr. W. I. Axford of the Max Planck Institute for Aeronomy, and Drs. C. Y. Fan, T. P. Armstrong, and G. Gloeckler of the Universities of Arizona, Kansas, and Maryland, respectively.

The LECP Experiment (Fig. XVI-2), the first APL instrument flown on a planetary probe, will provide comprehensive measurements on the time and spatial distribution and intensity of low energy nuclear particles in the interplanetary medium as well as in the vicinity of Jupiter, Saturn, Uranus, and perhaps Neptune. The experiment was developed under the sponsorship of the Office of Lunar and Planetary Programs at NASA Headquarters.

APPLICATION

The Voyager missions represent a unique opportunity to perform exploratory measurements at Saturn and probably Uranus, in the outer extremes of the interplanetary medium and (possibly) in the interstellar medium, and to conduct further studies of the Jovian environment. Studies that will be conducted using LECP experiment data include the following:

1. Investigate the existence, spatial extent, and dynamical morphology of Saturnian and Uranian magnetospheres and measure the spectral and angular distributions, composition, and plasma flows of particles in the radiation belts, bow shock, transition region, and magnetotail; determine the planetary and satellite magnetic moments and the nature of non-thermal radio emission.

2. Investigate the quasi-steady energetic particle flux in interplanetary space for studying solar modulation mechanisms, the

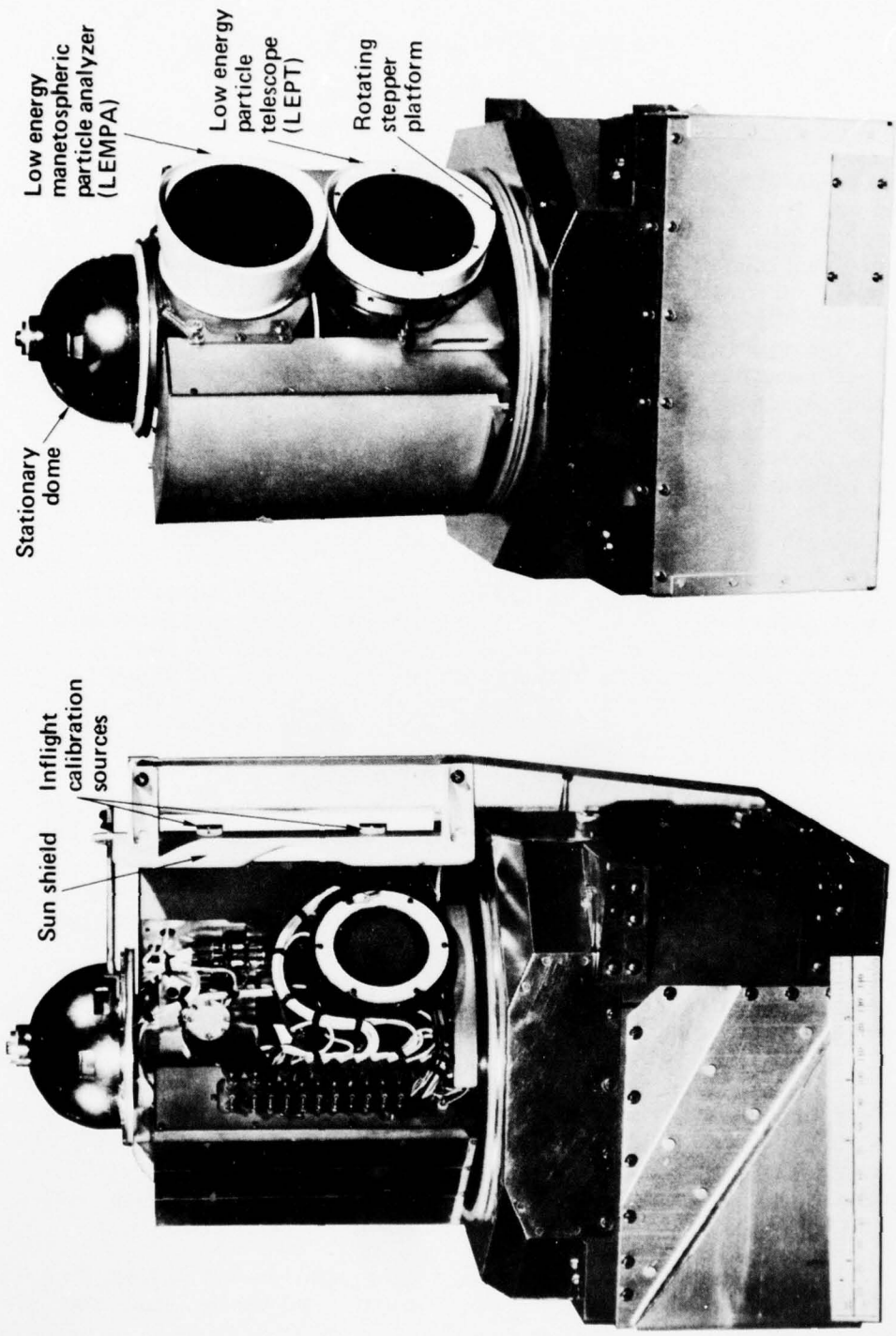

Fig. XVI-2 Low Energy Charged Particle (LECP) Experiment

radial gradient and radial scale of modulation, short term modulation effects, the solar, galactic, and planetary components, and particle acceleration mechanisms in the interplanetary medium, and (possibly) the terminus of the heliosphere.

3. Perform "second generation" studies (i.e., supplemental to those of Pioneer 10 and 11) of the composition, energy spectrum, and azimuthal and pitch angle distribution of Jovian magnetospheric charged particles bearing on questions of origin, transport, loss, and of sources of decameter and decimeter radio emission, including important satellite sweeping and source effects.

4. Study the energetic particle environments of natural planetary satellites and deduce satellite magnetic moments, conductivities, and the electrodynamics of the interaction with the planetary magnetospheres.

5. Make inferences concerning the origin and interstellar propagation of galactic cosmic rays, and their confinement times and path length distributions, by measuring the elemental and isotopic composition and anisotropy of galactic particles after the Saturnian (Uranian) encounter.

In addition, the propagation in the distant interplanetary medium of particles emitted at the sun will be studied by investigating their intensity-time profiles, energy spectra, gradients, and anisotropies and the charge and isotope composition. Also, an investigation will be conducted of large and small scale magnetic structures in the interplanetary medium and near planets using charged particle angular distributions in order to augment magnetometer measurements.

EQUIPMENT DESCRIPTION

The LECP Experiment uses 23 solid-state detectors configured in two distinct detector subsystems — the low energy magnetospheric pargicle analyzer (LEMPA), and the low energy particle telescope (LEPT). Design of the first subsystem (Ref. 1) is optimized for specific particle species, energies, and intensities expected near the planets; the second subsystem is optimized for interplanetary and interstellar measurements. Angular distributions in the ecliptic plane and pitch angle distributions are obtained using an eight-sector scanning motor. Detector characteristics are summarized in Table XVI-1; experiment weight and power requirements follow:

Table XVI-1

LECP Experiment, Summary of Detector Characteristics

DETECTOR DESIGNATION		DETECTOR DESCRIPTION	ENERGY RESPONSE NUCLEONS (MeV/nuc) OR ELECTRONS (e^-, MeV)	NUCLEAR[g] CHARGE RANGE	NUMBER OF PARAMETERS MEASURED	GEOMETRIC FACTOR $cm^2 sr$	DYNAMIC RANGE[a] $(cm^2 sec\ sr)^{-1}$
LEMPA Low Energy Magnetospheric Particle Analyzer		Det α Low Energy Protons & Ions	0.015 - 4, p 1-4, α	$Z \geq 1$ $Z \geq 2$	2[b]	0.12	$0.3 - 10^7$ (to $\sim 10^{12}$ in C.M.)
		Det β Low Energy Electrons	0.010 - 0.2, e^-	-----	2	~ 0.002	$50 - 10^8$ (to $\sim 10^{13}$ in C.M.)
		Det γ Medium Energy Electrons	0.2 - 1, e^-	-----	2	0.002	$10 - 10^8$
		Det δ, δ' High Intensity Composition	~ 0.26 - 7, p ~ 0.375 - > 4, α ~ 0.375 - > 12, $Z \geq 3$	$Z = 1$ $Z = 2$ $Z \geq 3$	1[d]	0.002	$\sim 0 - 10^{12}$
		Det AB High Energy-High Intensity Protons and Electrons	15 - 150, p > 2, e^- > 11, e^-	$Z \geq 1$ -----	1 1	0.03	$\sim 0 - 5 \times 10^{11}$
		Det β' Low Energy Electrons ⊥ to Ecliptic	0.010 - 0.2, e^-	-----	2[c]	0.002	$5 - 10^8$
LEPT Low Energy Particle Telescope	Low Energy Particle Aperture	Ultra Low Energy Total E (2μ)	0.093 - 0.18 0.047 - 0.14	$Z \geq 2$ $Z \geq 4$	1	~ 0.1	$\sim 0 - 10^5$
		Ultra Thin dE/dx vs E	0.48 - 1.4 0.15 - 3.0[f] ~ 0.13 - 10[f] ~ 0.07 - 13	$Z = 1$ $Z = 2$ $Z = 3$-10 $Z = 11$-28	2	~ 0.5	$\sim 0 - 10^5$
	High Energy Particle Aperture	Multi dE/dx vs E	3 - 31 6.3 - 60 7.4 - 115 > 0.5, e^-	$Z = 1, 2$ $Z = 3$-10 $Z = 11$-28 ---------	2,3 2	~ 4.0	$\sim 0 - 10^5$
		Four Parameter dE/dx	31 - 220 60 - 270 115 - ∞	$Z = 1, 2$ $Z = 3$-10 $Z = 11$-28	4 4 4	~ 2.3 ~ 2.3 ~ 2.3	$\sim 0 - 10^5$
		D3D4 High Sensitivity Penetrating	≥ 200 > 4, e^-	$Z = 1$ -----	2 2	~ 20 ~ 20	$\sim 10^6$ c/day[e]
		Anticoincidence	≥ 20	$Z \geq 1$	1	~ 200	$\sim 10^7$ c/day[e]

(a) Dynamic ranges are approximate. In current mode (C.M.), charge and energy resolution comments do not apply. Lower limit depends on RTG background which is $< 10^{-7}$ counts/second for certain LEPT channels.

(b) Magnetic deflection separates electrons and ions for LEMPA detectors α through δ; Z measurement is single parameter.

(c) Electrons are identified via scattering from a gold foil.

(d) Detector δ' scans perpendicular to ecliptic plane and uses no magnetic deflection.

(e) Cosmic ray background counting rate; range extends to $\sim 10^4$ times background.

(f) All tabular data for $Z \geq 3$ are "Nominal".

(g) Approximate energy ranges for Isotope Resolution:

Z = 1, 2	0.2 - 30 MeV/nucl.	(approx.)	($\Delta M = 1$)
Z = 3- 8	1.0 - 60 MeV/nucl.	(approx.)	($\Delta M = 1$)
Z = 9-16	3.0 - 90 MeV/nucl.	(approx.)	($\Delta M = 2$)

Power Consumption:

4.29	W	± 2% from 2.4 kHz at far encounter
4.15	W	± 2% from 2.5 kHz at near encounter
4.29	W	± 2% from 2.4 kHz at cruise
4.9	mW_{av}	± 2% from 30 VDC at cruise
102.0	mW_{av}	± 2% from 30 VDC at encounter.

Weight: 7460 grams.

Experiment complexity can be inferred from the following: Over 30,000 solder joints bond almost 6000 components within each instrument, the circuitry being based on the use of 261 custom-designed hybrids of 14 different types for amplification, discrimination, timing, pulse height analyzer, and data functions. Since the experiments are required to operate for at least six years and possibly 8-10 years as the spacecraft pass out of the solar system, many of the circuits are redundant and capabilities of the detector channels overlap.

Low Energy Magnetospheric Particle Analyzer (LEMPA)

LEMPA detectors (Fig. XVI-3) were designed for low energy thresholds (10-15 keV), clean separation of ions from electrons, good sensitivity, and large ($\sim 10^{11}$) dynamic range.

Detector α (protons, ions). This is the primary detector for measuring protons-ions at low energies ($\gtrsim$15 keV) with high sensitivity ($G \sim 0.12$ cm^2 sr) and good energy resolution. It consists of a 25 mm^2, 100 μm surface barrier totally-depleted detector, with the aluminum side facing the incoming particle flux (to minimize radiation damage). A rare-earth alloy magnet is used to deflect electrons with energies $\lesssim$400 keV away from the detector. These electrons are subsequently counted by detectors β and γ, and the α detector output is fed into window-type discriminators which provide continuous information in 10 proton-ion differential channels.

Detectors β and γ (electrons). These are the primary detectors for measurement of low energy ($\gtrsim$15 keV) electrons. Detector β is 5 mm^2, 100 μm thick, while detector γ is 5 mm^2, 100 μm thick; they are designed to measure the low and intermediate energy portions of the spectrum, respectively.

Detector β′ (electrons). This detector measures electrons over the same energy intervals as detector β but with a field of view centered 90° from that of β and perpendicular to the ecliptic plane. It mainly provides detailed angular distribution measurements not only in planetary magnetospheres, but also in the interplanetary medium. Essentially, complete electron pitch angle

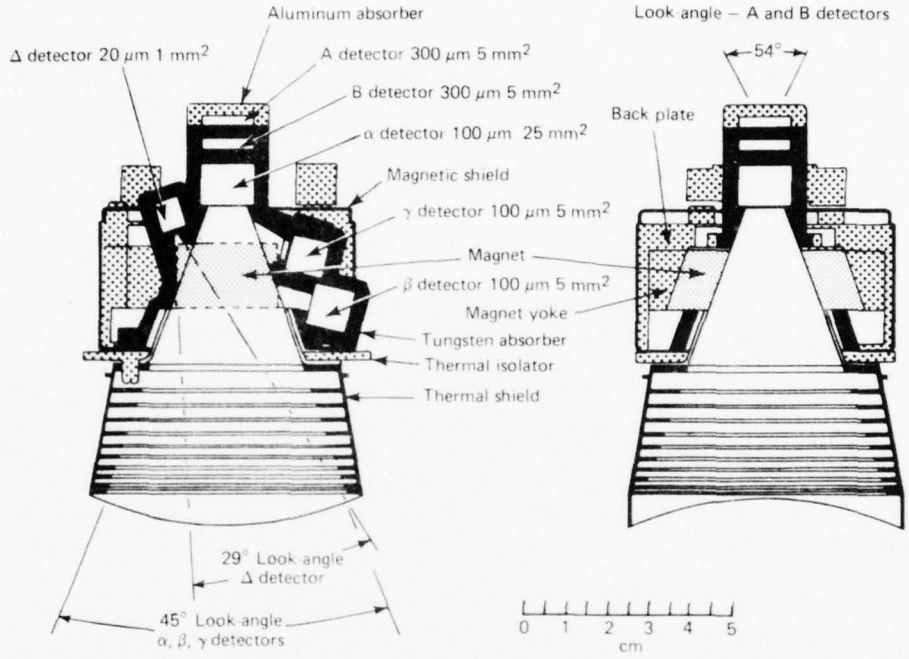

(a) Low energy magnetospheric particle analyzer

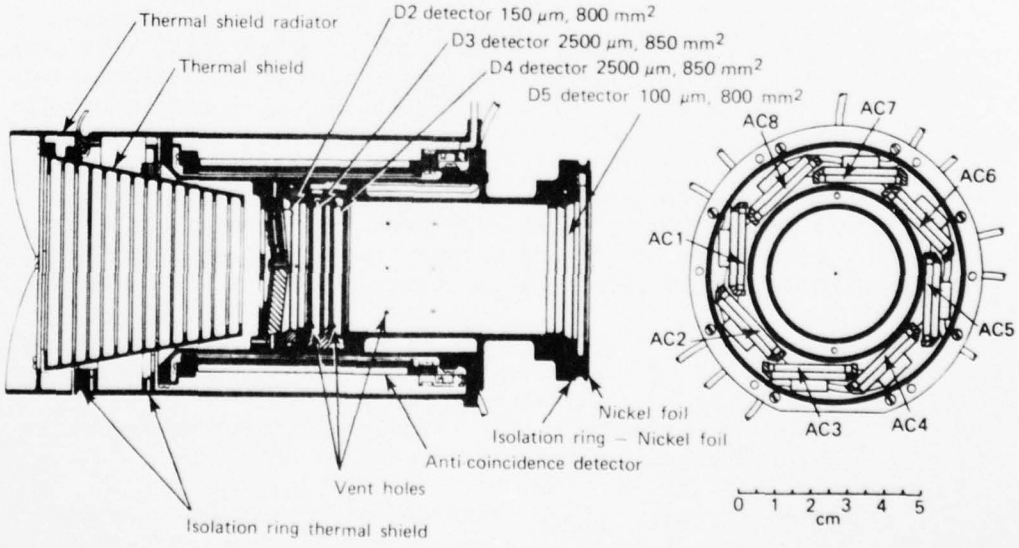

(b) Low energy particle telescope

Fig. XVI-3 LEMPA and LEPT Detector Subsystems

distributions are obtained during magnetospheric encounters by the use of an umbrella-like passive shield with narrow rectangular look angles. Detector β' is a 5 mm^2, 100 μm thick sensor and uses scattering from a gold surface to separate electrons and ions.

Detector δ (High Intensity Protons, α s and $Z \geq 3$ Nuclei). This will obtain high intensity proton, alpha particle and $Z \geq 3$ composition, energy spectra, and three-dimensional angular distributions in the Saturnian, Uranian, and Jovian radiation belts. The design is optimized for a radius of closest approach of ~5 R_J, and for the proton environment measured by the Pioneers 10 and 11 spacecraft. The sensor consists of a ~20 μm, 1 mm^2 totally-depleted surface barrier detector.

Detector δ′ (Protons, ions). This detector measures protons and ions at the same energy intervals as detector δ but with a field of view up to 90° from that of δ by sharing the umbrella passive shield with detector β'. Together, detectors δ and δ′ provide essentially complete three-dimensional proton and ion pitch angle distributions during magnetospheric encounters. Detector δ′ is 1 mm^2, 20 μm thick and utilizes the same electronics as detector δ.

Detectors AB (High Intensity — High Energy). Detectors AB are included to increase the dynamic range of the system in both energy and intensity to values well above those measured by detectors α, β, and γ. Both devices are 5 mm^2, ~300 μm thick surface barrier detectors spaced ~5 mm apart inside shielding material. In the forward direction, detector B is shielded by 2.6 gm/cm^2 brass and detector A by 0.35 gm/cm^2 magnesium.

Low Energy Particle Telescope (LEPT)

The LEPT (Fig. XVI-3) is based on a bidirectional telescope consisting of seven silicon surface barrier detectors comprising two multi-$dE/dx \times E$ detector systems (D1-D5) placed back-to-back and utilizing a common eight-element cylindrical lithium-drifted silicon detector shield (AC1-AC8).

Detector D1. The first detector of the dE/dx vs. E system consists of a set of two ~5 μm thick, 50 mm^2 and one ~2 μm thick, 25 mm^2 surface barrier detectors. Each detector is arranged at an appropriate angle to the axis of the telescope so that variation of the ΔE signal over the angular field of view of the telescope is minimized.

Detector D2. This large area (8 cm^2), ~150 μm thick detector serves as the total E detector for particles penetrating the D1 detectors. It is operated in anticoincidence with detectors A1 to A8, and in coincidence with detector D1. Pulses from this detector are log-amplified and fed into threshold discriminators for rate data and into a 256 channel pulse-height analyzer.

Detectors A1-A8. These detectors define an anticoincidence cylinder and have typical dimensions of 2.5 cm × 6 cm × 1 mm. Each pair of detectors has a separate preamplifier-amplifier chain and can be commanded off separately. By connecting two pairs of detector outputs together, two separate measurements of the omnidirectional penetrating particle rate are obtained.

Detectors D3 and D4. These detectors are used in a dE/dx vs. E combination to extend the energy range of the telescope from ~4 to ~40 MeV/nucleon. Both detectors are 2450 μm thick, 8.5 cm^2 lithium drifted devices which serve as total E sensors.

Detector D5. This detector is ~90 μm thick, 8 cm^2 and is used as a ΔE detector in the medium energy end of the LEPT. In combination with detectors D3 and D4, the output of detector D5 is fed to the particle identifier system to provide species rate data and priority information for the detailed pulse height analyses.

FUNCTIONAL OPERATION

Figure XVI-4 shows the LECP experiment system block diagram. The LEPT, or interplanetary/interstellar measurement subsystem, employs two basic particle identification and energy measurement techniques (Ref. 2). The first method is the conventional range-energy technique. The second method of identification (Ref. 3) relies on forming the product:

$$P = a\ \Delta E_1\ \Delta E_2^{\,b}\ ,$$

where ΔE_1 and ΔE_2 are the energies deposited in detectors 1 and 2 and a and b are constants. The product P is unique for each particle type and has a relatively constant slope on a log-log scale over a large range of particle energy. Appropriate "P" discriminator levels (which plot as P = constant) in conjunction with ΔE discriminators are used to distinguish particle types.

The pulse shaping and amplifier elements for each of the LEPT detectors are contained in electronics box No. 1 of Fig. XVI-4. The FET charge-sensitive preamplifiers for the LEPT detectors are basically of the same design. The circuit bias voltages, currents, and feedback networks are set with components external to the hybrid allowing one design to meet the diverse LEPT dynamic range and detector capacitance requirements.

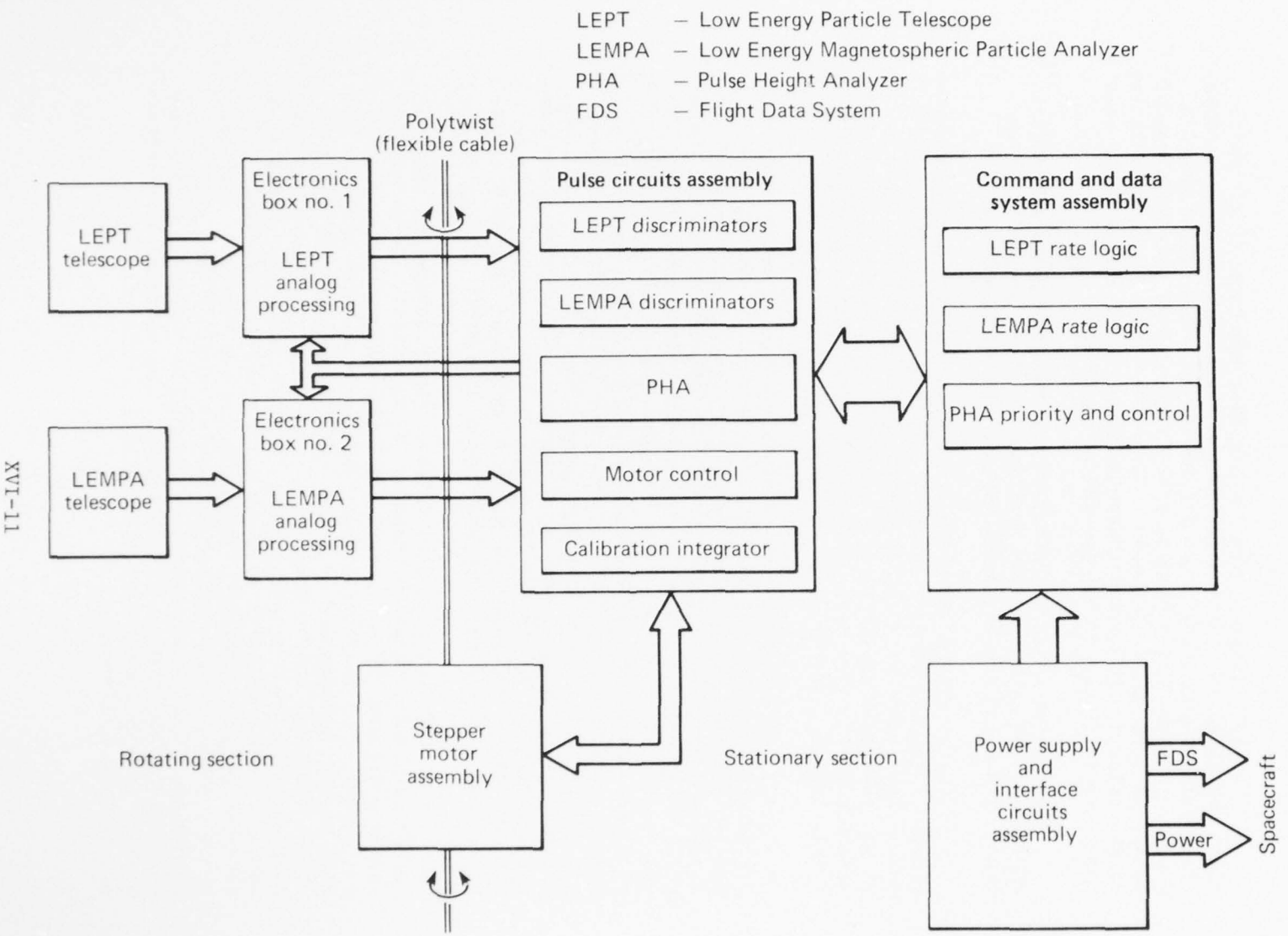

Fig. XVI-4 LECP Experiment, Simplified System Block Diagram

THE JOHNS HOPKINS UNIVERSITY
APPLIED PHYSICS LABORATORY
LAUREL MARYLAND

SDO 4100

The LEPT linear amplifiers are also one type of microcircuit, and external bias and filter components are added to produce the desired pulse shaping and dynamic range. Double-integration, double-differentiation bipolar pulse shaping with pole-zero cancellation is used in all channels. The pulse width from the beginning of the pulse to its zero-crossing is about 3 μs, and particle counting rates in excess of 10^5 pps can be handled.

The large range of particles and energies measured require the use of logarithmic pulse amplifiers. These amplifiers, combined with pulse summing amplifiers, perform the product "P".

Four two-input coincidence circuits register particle coincidence detection between adjacent detectors. Each circuit employs a low-power Schottky gate and operates with pulses as narrow as 25 ns, permitting a theoretical coincidence window of 50 ns. The actual coincidence window, determined by S/N ratio and timing walk considerations, is +800 ns.

The discriminators employ CMOS logic to conserve power and are packaged two-each in hybrid microcircuits. One-shots used to produce discriminator timing signals also employ CMOS dice and use a similar dual-circuit hybrid package. Logical combinations of 41 pulse height discriminators, together with coincidence timing, are used to form 47 different data channels. Particle events from the 47 rate channels are counted in 24-bit accumulation registers. The data are transferred and stored in 24-bit parallel-in serial-out registers until a "read" command is received. The data are then shifted into a 24- to 10-bit log compression circuit, and the compressed data are relayed to the spacecraft data system. The 24-bit accumulator and shift register are made from five CMOS large-scale integration dice which are housed in a hybrid microcircuit.

The LEMPA, or near-planet measurements subsystem, employs two primary identification methods. In the first, low and medium energy electrons are deflected into total energy detectors (beta and gamma) via a sintered cobalt-samarium rare earth magnet. The more massive protons and ions pass through the magnetic field to strike the total energy detector alpha. The low-noise alpha and beta channels allow measurement of electron and proton energies as low as 12 keV. As particle intensities increase and simple pulse counting becomes difficult, the alpha and beta detector currents are monitored, thus extending the useful range of intensity measurements. The second identification method employs a combination of shielding and energy loss to restrict the response of detectors A and B to high energy particles. The A-B detector system is arranged as a telescope.

AD-A072 438 JOHNS HOPKINS UNIV LAUREL MD APPLIED PHYSICS LAB F/G 22/2
INSTRUMENTATION DEVELOPED BY THE JOHNS HOPKINS UNIVERSITY APPLI--ETC(U)
NOV 78 N00024-78-C-5384

UNCLASSIFIED APL/JHU/SDO-4100 NL

3 OF 3
AD
A072438

END
DATE FILMED
9-79
DDC

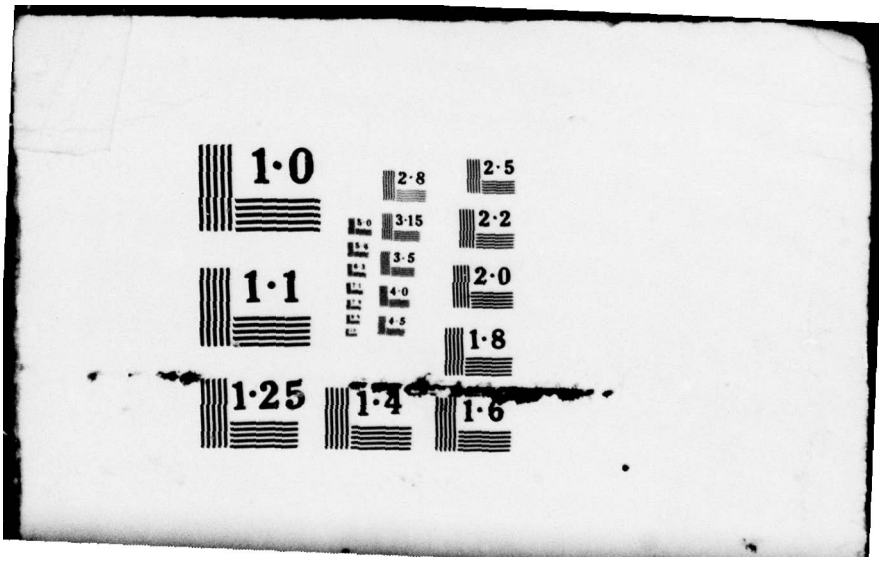
1·0
1·1
1·25
1·4
1·6
1·8
2·0
2·2
2·5
2·8
3·15
3·5
4·0
4·5

Since high energy electrons will be abundant near the planets, about 0.45 kg of tungsten is used as shielding to prevent high-energy electron contamination of the low-energy detectors. The high intensities of radiation trapped in the Jovian and (probably) the Saturnian magnetic fields require the use of extremely fast-pulse circuitry in several channels to prevent pulse pileup effects and saturation; this necessitated the development of special hybrid amplifiers and discriminators to handle counting rates in excess of 25×10^6.

Pitch Angle Distribution

With the Voyager spacecraft attitude very nearly fixed in inertial space, except during occasional maneuvers, a rotating platform (Fig. XVI-5) is used to obtain particle angular distribution measurements. The platform is driven by a stepper motor through eight 45° sectors. The sector rate is once every 24 seconds during planetary encounter, once every six seconds during Io encounter, and once every six minutes in the interplanetary medium. Pitch angle distributions are obtained by two additional detectors placed in a cone/dome combination in which the cone sets the azimuth view angle and holes in the dome set the elevation view angles. Thus, a single mechanism is used to obtain pitch angle distributions in two planes.

Other Experiment Systems

The large number of LECP discriminators and logic windows led to the development of a new calibration system (Ref. 4) for amplifier gains and discriminator settings, as well as detector

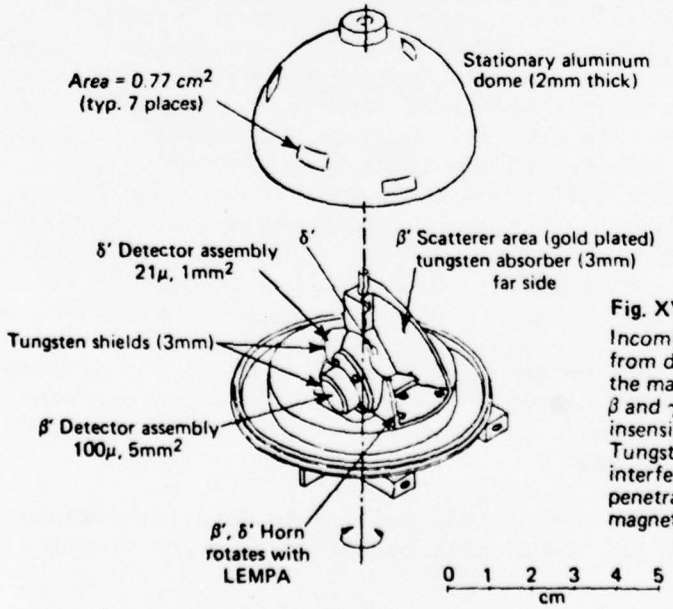

Fig. XVI-5 Dome Detector Assembly. Incoming electrons are swept away from detector α (a, Fig. XVI-3) by the magnet and counted in detectors β and γ. Detectors δ, δ' are insensitive to electrons of any energy. Tungsten shielding is to eliminate interference from high energy penetrating electrons in the Jovian magnetosphere.

noise and PHA linearity. The calibrator pulse drives the preamplifiers with a continuous pulse train. Discriminator pulses are selectively fed back to set the pulse amplitude such that the discriminator triggers at 12% and 88% rates. Both the detector noise and discriminator setting may then be deduced. In addition, radioactive sources provide a background count rate for calibration.

Detector voltages range from less than one volt for the thin D1 detectors to 450 volts for the thickest detectors. The power supply for the detectors is a sinewave oscillator Cockroft-Walton multiplier combination which is capable of producing bias voltages of many kilovolts (Ref. 5).

The experiment command receiver accepts 32-bit serial command words from the spacecraft and utilizes 12 of these bits in the form of four 10-bit command words and two address bits. Thus, 40 bits are available as commands to place the experiment into various operating modes. They are used primarily for switching power via hybrid power switches. For example, each of the detector amplifier channels can be individually disabled in case of failure. Also, the detector bias may be decreased by 25% upon command. In addition, there are motor speed, sector-select, and high-power motor drive commands. The last is employed if the motor develops a bearing wear problem.

FLIGHT RESULTS

Low Energy Charged Particle Experiments were successfully launched aboard Voyagers 2 and 1 on 20 August and 5 September 1977, respectively (lines 50 and 51, Table 1). Each was turned on about 22 minutes after injection into the Jupiter trajectory, and operation of both is satisfactory with good data being returned. The LECP Experiment scientific team will analyze and evaluate the nuclear particle data obtained in the interplanetary medium until Jupiter encounter which will occur in March 1979 (Voyager 1) and July 1979 (Voyager 2). At that time, details of the planetary environment will be observed. Encounter of Saturn will occur about two years later. An extended mission will allow Voyager to visit Uranus and perhaps Neptune, and eventually escape the solar system.

Three operational modes will be employed to obtain optimum coverage in the two environments encountered (i.e., the magnetospheres — distant and near — of Jupiter, Saturn, and Uranus, and the interplanetary medium):

1. Cruise Mode. During this mode, both detector systems (except AB, δ, and δ' of LEMPA) will collect data. The stepping

rate is one rev./48 min. This mode is appropriate for the interplanetary medium where particle fluxes are not large. The bit rate allocation is 2/3 for PHA data and 1/3 for rate data.

2. For Encounter Mode-Jupiter, Saturn, and Uranus. Sixty days prior to closest approach to the planet, the stepping platform rate is increased to one rev./min. The experiment bit rate increases to 600 bps. At this time, the bit allocation is 1/3 to PHA data and 2/3 to rate data.

3. Near Encounter Mode-Jupiter. At ~25 to 15 R_J all LEPT detectors are commanded off and all remaining LEMPA detectors (i.e., AB, δ, δ') are commanded on.

To ensure that LEPT and LEMPA data continuity is maintained, each of the two subsystems will be sampled equally between the far and near encounter modes. This is particularly desirable in the Saturn and Uranus encounters where long communication times and a totally unknown environment could compromise measurements in any one mode.

THE JOHNS HOPKINS UNIVERSITY
APPLIED PHYSICS LABORATORY
LAUREL, MARYLAND

SDO 4100
December 1978

XVII

PARTICLE FLUX MONITOR
(INTERNATIONAL ULTRAVIOLET EXPLORER)

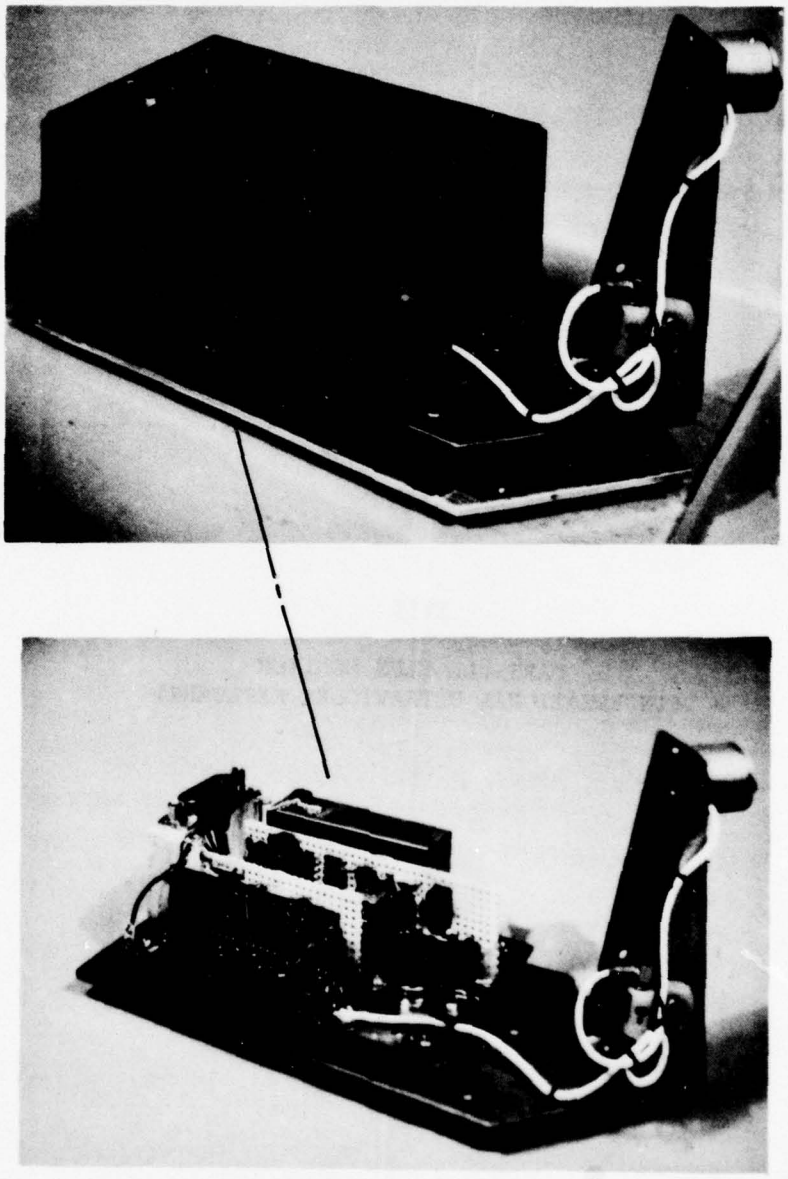

Fig. XVII-1 Particle Flux Monitor (International Ultraviolet Explorer)

XVII

PARTICLE FLUX MONITOR
(INTERNATIONAL ULTRAVIOLET EXPLORER)

BACKGROUND

In a telecon of 28 December 1977, APL was first queried on the possibility of providing a radiation detector for the International Ultraviolet Explorer (IUE) spacecraft then awaiting a 26 January 1978 launch at Cape Canaveral, Florida. The IUE camera system was sensitive to particle radiation and, since the planned orbit included several of the most intense regions of the outer Van Allen Belt, it was desired that a suitable device be employed to continuously measure the prevailing radiation levels. An appropriate instrument not being readily available, APL quickly assembled a device using spare parts and circuit designs from previous satellite programs. Subsequent tests on the hastily assembled breadboard indicated that the project was indeed feasible. With NASA/GSFC concurrence, APL then proceeded with the design and development of the Particle Flux Monitor (PFM) for the IUE (Fig. XVII-1). In the short period of 7 days, interface specifications were developed, hardware was fabricated and assembled, and functional and environmental tests were performed. A fully flight-qualified instrument was delivered to the launch site and integrated with the spacecraft just 16 days before launch (Fig. XVII-2).

APPLICATION

The 671 kg IUE, developed by NASA in cooperation with the European Space Agency and the British Science Research Council (BSRC) was launched to examine the ultraviolet spectral region 1150 Å - 3200 Å, a region which is inaccessible from the ground. It was recommended during the IUE Flight Readiness Review in mid-December 1977 that, to protect the camera system, a particle detector be installed on the spacecraft to monitor the energetic electron environment.

Apprised of the mission requirement and upon short notice, APL provided a Particle Flux Monitor that is now in routine use by IUE ground control center personnel to determine when camera operations should be suspended due to high radiation.

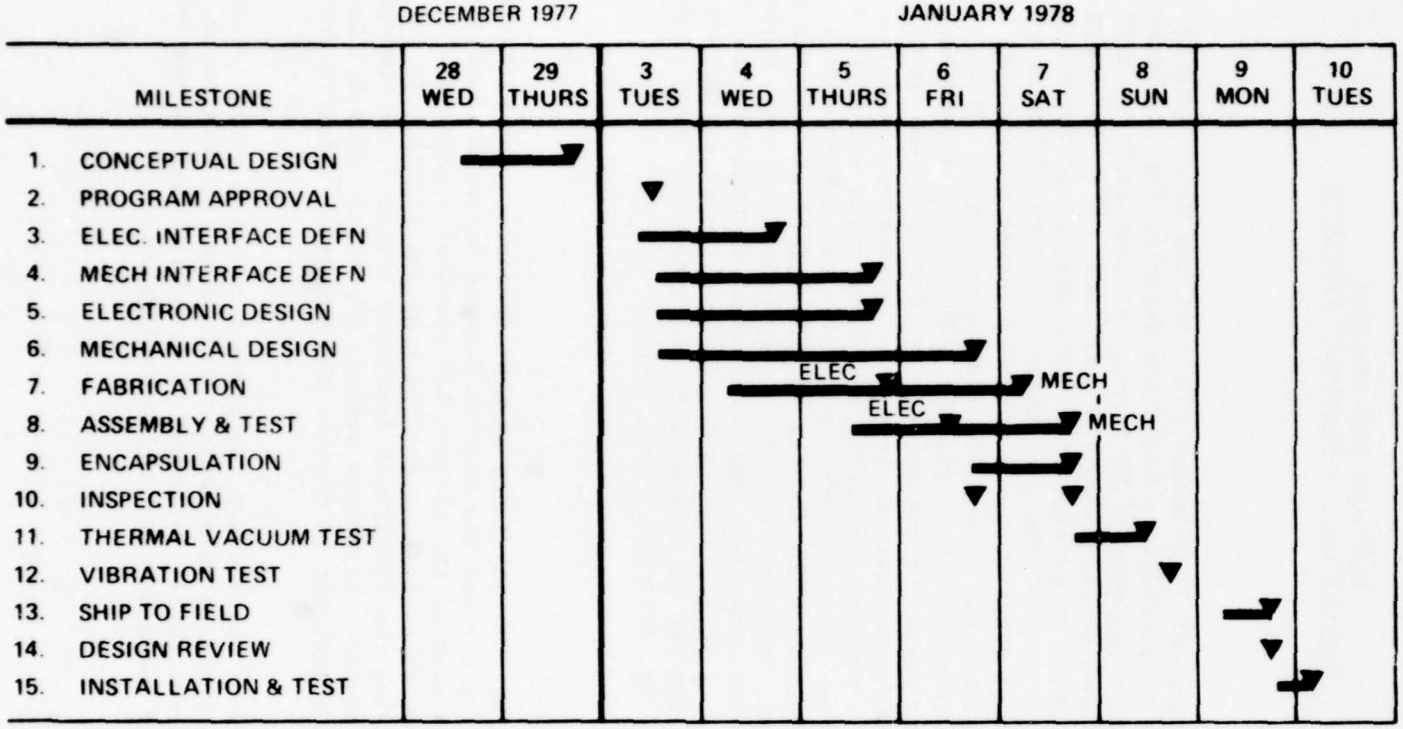

Fig. XVII-2 PFM (IUE) Accelerated Development Schedule

THE JOHNS HOPKINS UNIVERSITY
APPLIED PHYSICS LABORATORY
LAUREL, MARYLAND

EQUIPMENT DESCRIPTION AND OPERATION

An outline drawing and simplified block diagram of the PFM are shown in Fig. XVII-3. The detector is similar to that used in the gamma channel of the Low Energy Magnetospheric Particle Analyzer (LEMPA) on the Voyager spacecraft Low Energy Charged Particle Experiment. Refer to the preceding article (XVI) for a functional description of the LEMPA telescope. General PFM detector characteristics are as follows:

Type:	Li-Drift Silicon
Thickness:	963 μm
Area:	5.40 mm^2
Bias:	+100 V
Reverse Current:	0.050 μA @ +24°C
Noise:	4.10 keV @ +24°C
Capacity:	2.0 pf
Depletion:	25 V.

Following are the PFM unit electrical and weight requirements:

Power:	38 ma @ 28.0 V
Range:	10 cts/sec to 200K cts/sec
Output Level:	0 to 5 V DC
Output Impedance:	10K Ω in parallel with .01 μf
Weight:	565 g.

FLIGHT RESULTS

The Particle Flux Monitor was successfully launched aboard the International Ultraviolet Explorer on 26 January 1978 (line 53, Table 1). The PFM was turned on about one hour after launch and operation appeared normal. This was later confirmed when data from the first few orbits were examined and compared with prelaunch prediction of the radiation environment. GSFC and personnel from BSRC, developers of the UV television camera system, initially turned the UV camera on in a calibration and test mode and the PFM data were used to determine permissible operating times. Subsequent operations involved measuring UV camera background as a function of PFM output to determine safe levels of operation and to maximize observing times.

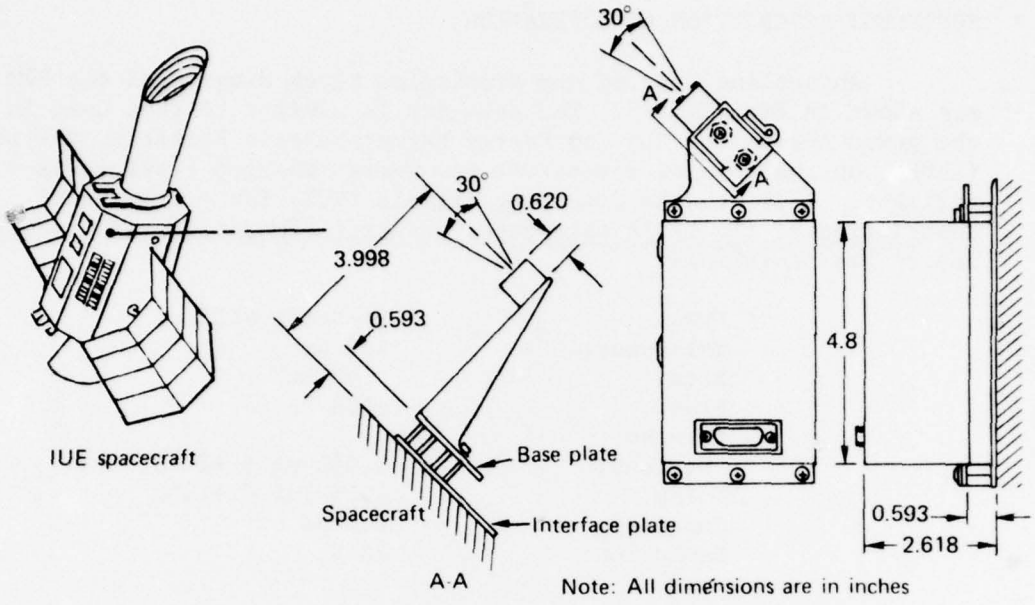

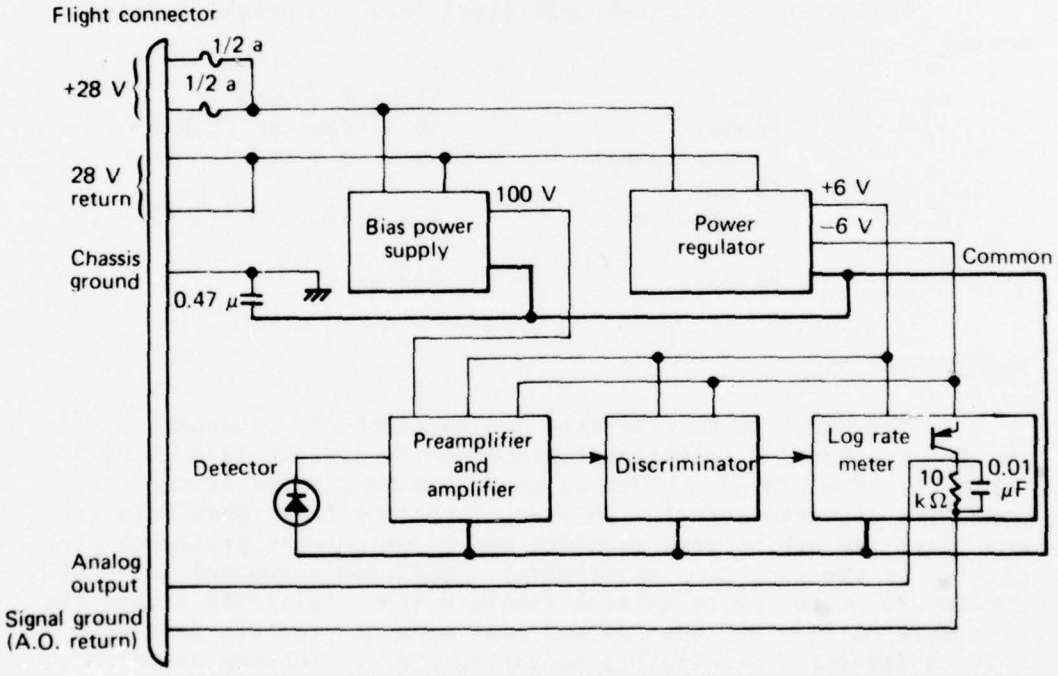

Fig. XVII-3 PFM (IUE) Outline Drawing and Simplified Block Diagram

THE JOHNS HOPKINS UNIVERSITY
APPLIED PHYSICS LABORATORY
LAUREL, MARYLAND

SDO 4100
November 1978

XVIII

SEASAT-A INSTRUMENTATION
(RADAR ALTIMETER, SAR DATA LINK, DOPPLER BEACON, LASER RETROREFLECTOR ARRAY)

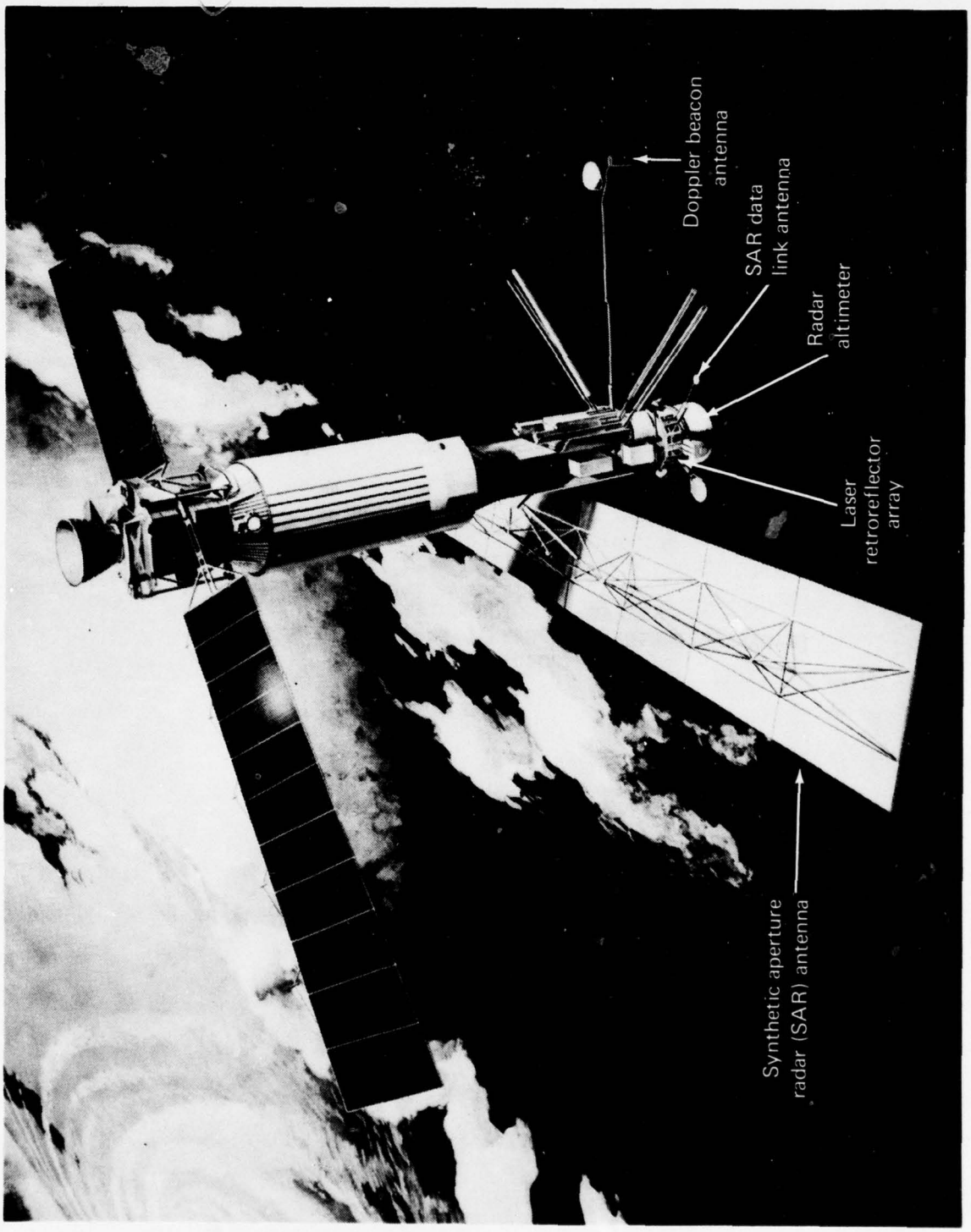

Fig. XVIII-1 SEASAT-A, Artist's Concept

XVIII

SEASAT-A INSTRUMENTATION (RADAR ALTIMETER, SAR DATA LINK, DOPPLER BEACON, LASER RETROREFLECTOR ARRA

BACKGROUND

The NASA SEASAT-A spacecraft (Fig. XVIII-1), the f satellite designed specifically for oceanographic observat launched in a proof-of-concept mission to evaluate techniq the global monitoring of oceanological and related meteoro phenomena from space, and to prove the feasibility of empl operational, multisatellite SEASAT network to monitor the on a continuous near-real-time basis. Major SEASAT-A inst tion included three types of radar and two different radio provide data on wave height and direction, surface wind sp direction, ocean surface topography and temperature, and t ice distribution and land areas.

APPLICATION

Several experiments were conducted with SEASAT-A; APL provided instrumentation for the Altimeter/Precision O termination (POD) Experiment and the Imaging Radar Experim APL radar altimeter provided very precise height measureme the satellite above the ocean surface, and of the signific height at the subsatellite point. The altitude measuremen combined with the precision ephemeris to determine sea-sur raphy. The POD Experiment data were obtained from several sources, including the doppler beacon and a laser retroref array (LRA) provided by APL.

The first satellite laser ranging experiment took 1964 using the LRA on the Beacon Explorer-B satellite (196 and this APL-fabricated satellite continues to serve as an laser ranging target (Ref. 1). The SEASAT LRA (Fig. XVIII passive POD device consisting of 96 quartz retroreflectors on a circular substrate surrounding the radar altimeter, r back to a receiving telescope pulsed beams of light direct satellite by a ground laser transmitter. The transit tim light pulses, coupled with angular data, provided a preci mination of satellite orbit.

The Imaging Radar Experiment employed a Synthetic Radar (SAR), developed by the Jet Propulsion Laboratory o fornia Institute of Technology, that provided all-weather of land and sea surfaces with a resolution of 25 m. As o

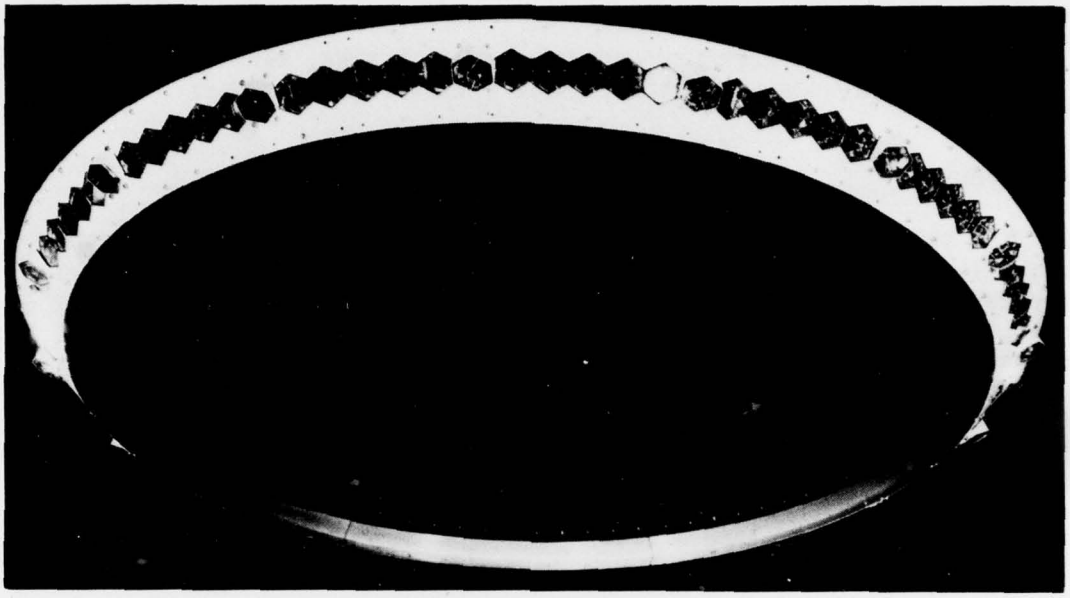

Assembled array

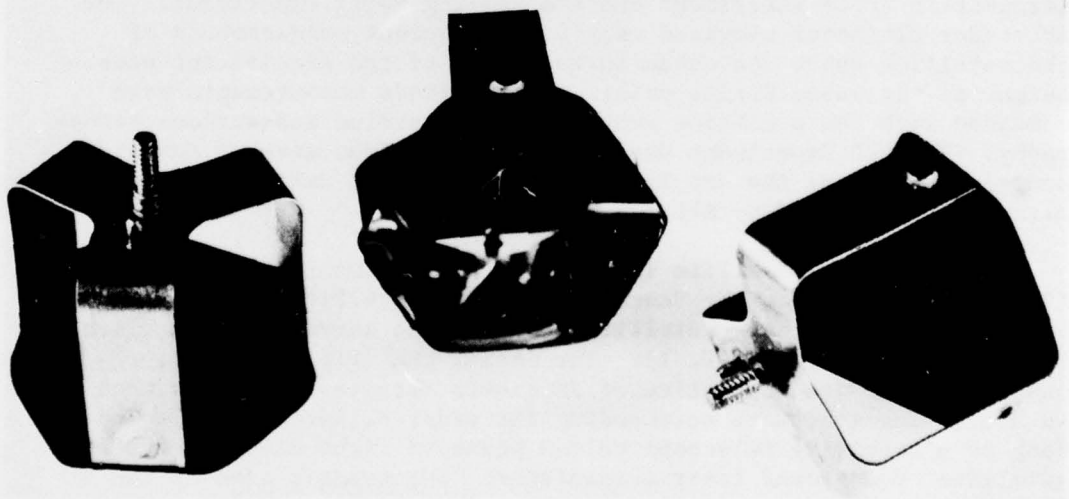

Retroreflectors

Fig. XVIII-2 Laser Retroreflector Array.

conceived, the wideband radar return signal was to be digitized at the spacecraft and the data telemetered on S-band. However, an APL study indicated that, for full resolution imagery, the onboard digitizing approach consumed more transmission bandwidth than was readily available. As an alternative, APL proposed an analog data link that used simple frequency translation of the L-band echo to S-band, thereby minimizing the RF allocation problem.

EQUIPMENT DESCRIPTION

Essentials of the doppler beacon provided by APL are discussed in Section VI of this publication, and laser retroreflector arrays and laser ranging have been described elsewhere (Refs. 1, 2). This section will deal mainly with the radar altimeter and the SAR wideband analog data link.

Radar Altimeter

NASA has supported the development of progressively more accurate satellite radar altimeters as part of the Earth and Ocean Physics Application Program (EOPAP). The SEASAT-A altimeter represented a third generation design that built on experience gained from the Skylab and GEOS-C programs. The altimeter consisted of a 1 m/1.5° beamwidth, nadir-looking, parabolic antenna, an attached RF section, and a remotely located signal processing section (Fig. XVIII-3). The altimeter generated a linear-FM waveform and transmitted it at a 2.4 kW peak power level, 13.5 GHz center frequency, and a 1000 Hz pulse repetition frequency (PRF). The high resolution permitted a 10 cm altitude precision and a 10 percent (or 0.5 m) wave height precision for wave heights between 1 and 20 m. The high pulse rate reduced the sampling variability of the altitude and wave height measurements.

Table XVIII-1 provides a comparison of Skylab, GEOS-C, and SEASAT-A altimeters. All three altimeters employed a similar traveling wave tube (TWT). The variation in return signal strength with altitude and footprint area required the use of pulse compression for GEOS-C and SEASAT-A, whereas Skylab, which operated at a lower altitude, could use a 100 ns uncompressed pulse. The 3.125 ns resolution of SEASAT-A (Ref. 3) defined a 1.7 km footprint diameter and required a longer pulse and a higher antenna gain to give a S/N ratio per pulse equal to or better than GEOS-C.

SAR Data Link

The SAR was designed to image swaths approximately 100 km wide with a 25 m resolution, and thus provide all-weather coverage

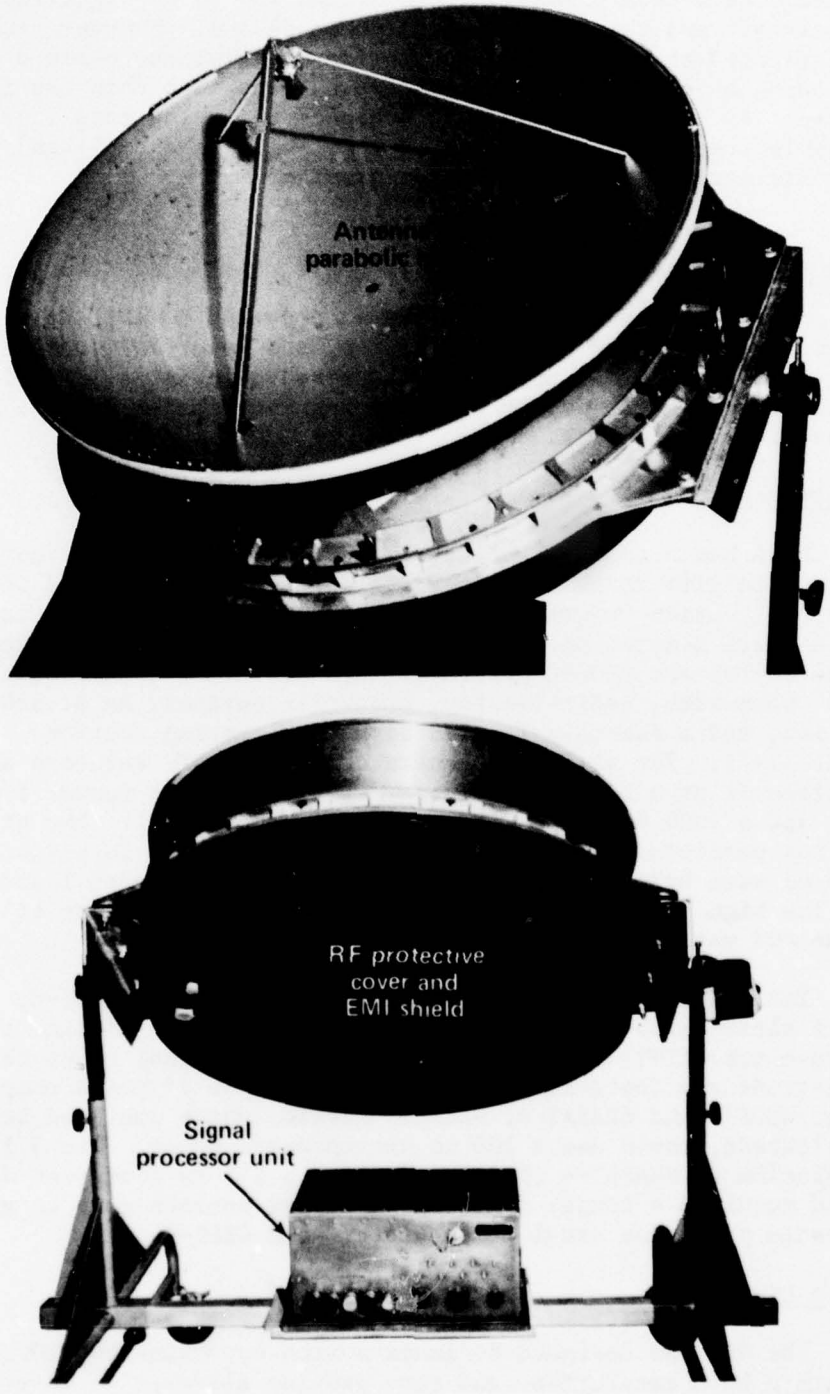

Fig. XVIII-3 Radar Altimeter.

at any time of day or night. The wideband analog data link developed by APL was used to transmit, receive, and demodulate the oscillator, timing generator, and receiver outputs from the SAR, making them available to ground based recording equipment. An analog data link design was preferred over more conventional digital schemes primarily to conserve RF bandwidth and also allow use of existing receiving station equipment.

Table XVIII-1

SEASAT-A Radar Altimeter Parameters Compared

Parameter	Skylab	GEOS-C	SEASAT-A
Mean Altitude (km)	435	840	800
Antenna Beamwidth (deg.)	1.5	2.6	1.6
Frequency (GHz)	13.9	13.9	13.5
Peak RF Power (kW)	2	2	2
Average RF Power (W)	0.05	0.24	6.5
Pulsewidth (Uncompressed)	100 ns	1 μs	3.2 μs
Pulsewidth (ns) (Compressed)	--	12.5	3.125
Repetition Frequency (Hz)	250	100	1020
Footprint Diameter (km)	8	3.6	1.7
Altitude Precision (rms)	< 1 m	< 50 cm	< 10 cm

The SAR data link (Fig. XVIII-4) consists of a spaceborne modulator/transmitter assembly, ground-based receiver/demodulator equipment, and the time-varying space-to-ground transmission link. The main RF input to the data link is the SAR return signal as obtained at the output of the SAR receiver at the L-band frequency. As shown in Fig. XVIII-5, the actual target echo occupies less than half of the interpulse period (IPP), but its position within the period is a variable that depends on orbit altitude and the rate of the pulse repetition frequency (PRF). The narrow RF pulses occur at the PRF and result from leakage of the main transmission through the receiver isolation circuitry. The remainder of the IPP is filled with white receiver noise at a level determined by the gain setting of the SAR receiver. Additional data-link inputs consist of the radar PRF timing pulses and the STALO signal.

The output signals from the data link are obtained from the demodulator and consist of the SAR return signal translated to a

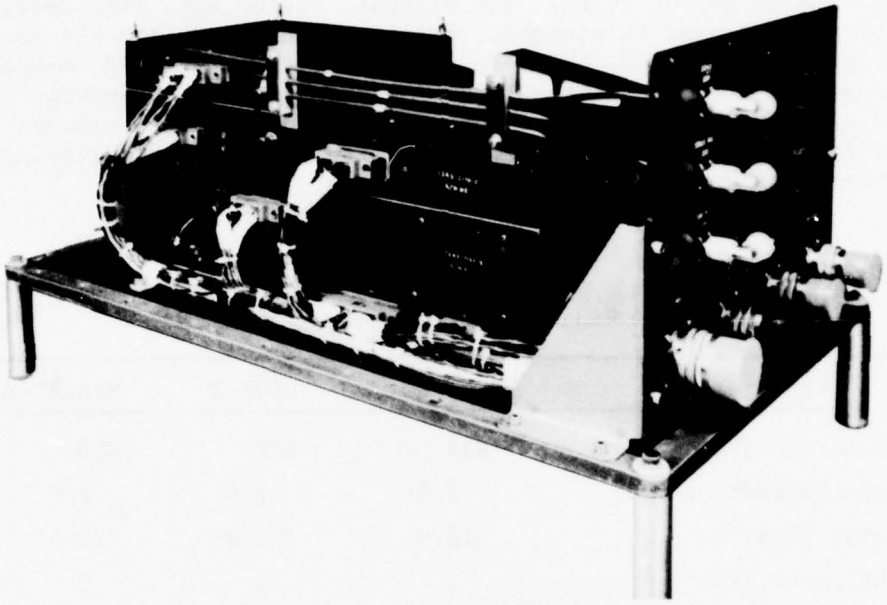

Modulator/transmitter

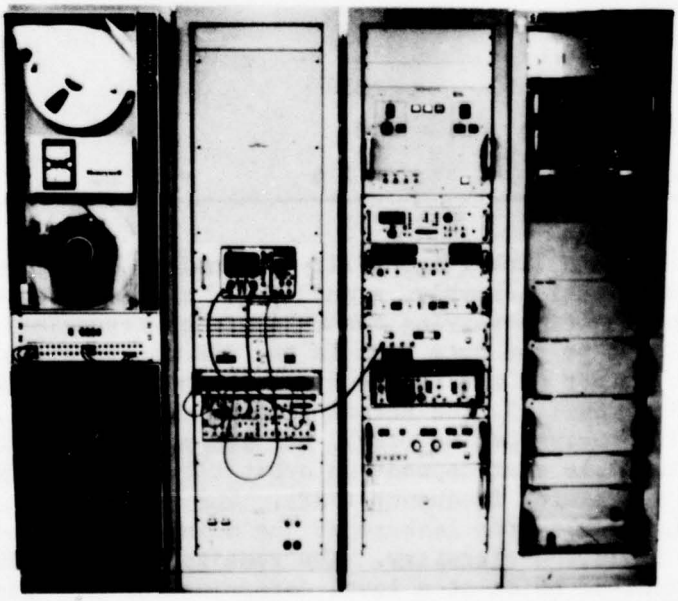

Receiver/demodulator/signal simulation/recording equipment

Fig. XVIII-4 SAR Data Link and Support Equipment.

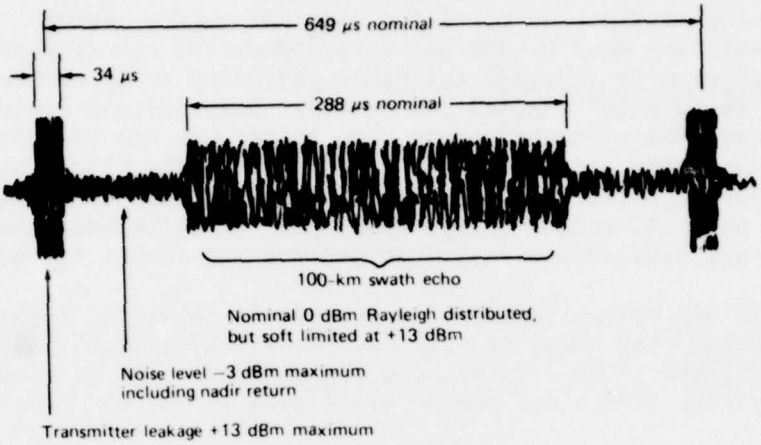

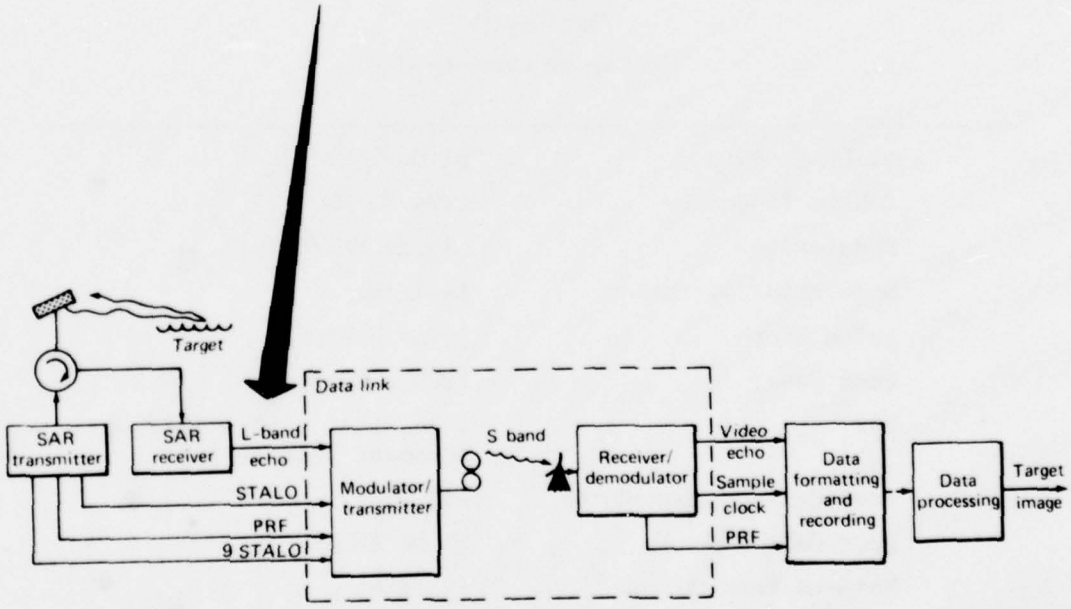

Fig. XVIII-5 SEASAT-A Synthetic Aperture Radar System Overview

to a video center frequency of 11.4 MHz, a sample clock at one-half the received STALO frequency (45.53 MHz), and a PRF pulse stream that is delayed to align in time (using prepass information) with the beginning of the echo portion of the SAR return signal. These three signals are used by the SAR data formatting and recording (SDFR) subsystem to digitize the echo, providing 5-bit samples at a rate of 45.53×10^6 samples per second. Digitization occurs only over the interval when the target echo is present and is initiated by the delayed PRF pulse from the demodulator. The final output from the SDFR consists of high-density digital tapes containing the video samples, status information, and Greenwich mean time (GMT). The tapes are processed off-line to produce the target images.

The SAR system (Ref. 4) is completely coherent; i.e., all RF, modulation, and sampling signals are derived from the stable local oscillator (STALO) within the transmitter. The pertinent characteristics of the SAR sensor are listed in Table XVIII-2.

Table XVIII-2
SAR Sensor Characteristics

STALO Frequency	91.059 MHz (f_s)
Center Frequency	1274.83 MHz (14 f_s)
Modulation	Linear FM (Chirp)
Modulation Deviation	±9.5 MHz
Pulse Width	34 μs Nominal
Peak Power	1200 W Nominal
PRF	1464, 1540, 1561, 1647 pps (Command selectable)
Rcvr Noise Temperature	650 K
Rcvr Gain Control	77 to 98 dB
Maximum Rcvr Output	+13 dBm

FUNCTIONAL OPERATION

Radar Altimeter

Major functional elements and a signal flow diagram of the radar altimeter are shown in Fig. XVIII-6. Key interface signals

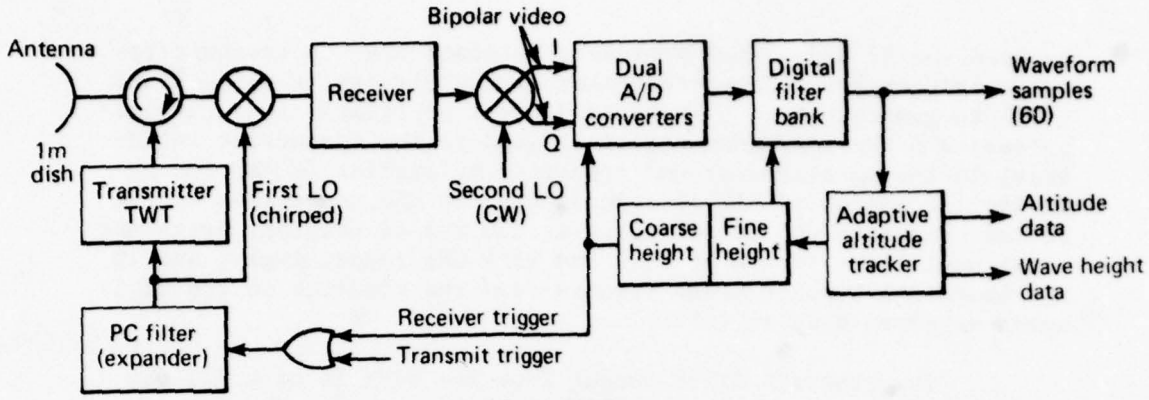

(a) Signal flow

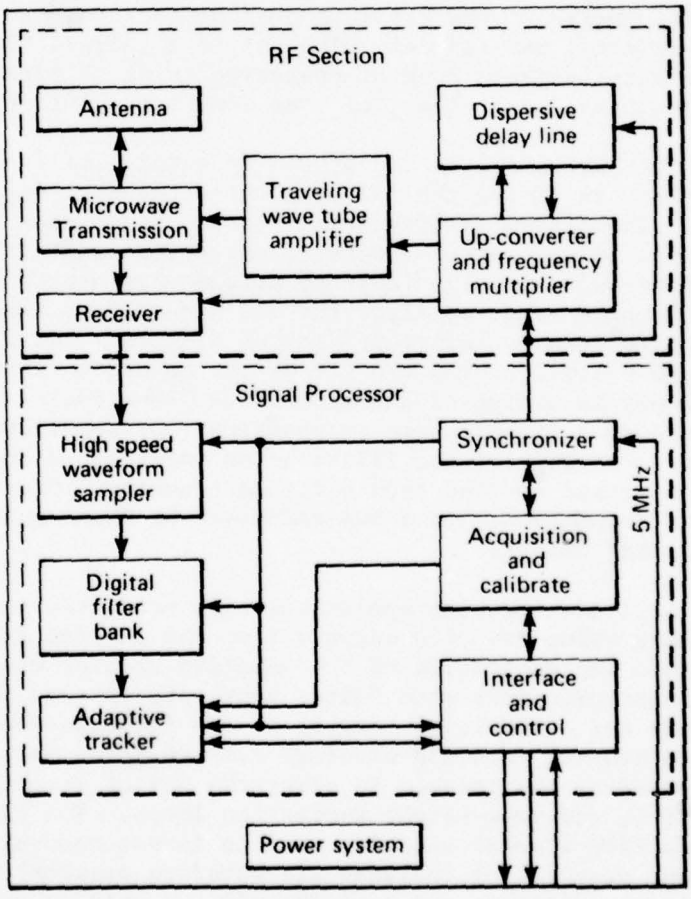

(b) System block diagram

Fig. XVIII-6 SEASAT-A Radar Altimeter Simplified Block and Signal Flow Diagrams

between the RF and signal processor sections are: a transmit/receive trigger from the synchronizer to the dispersive delay line (DDL) to generate both transmit and local oscillator (LO) chirped pulses; a 5 MHz reference signal (locked to the spacecraft reference) to the up-converter and frequency multiplier (UCFM) for coherent generation of all RF signals used in the conversion of the 80 MHz bandwidth DDL output pulse at 250 MHz to transmit drive and local oscillator pulses at 13.5 and 13.0 GHz respectively; and 10 MHz bandwidth bipolar video signals from the receiver to the high-speed waveform sampler (HSWS).

The transmit drive output from the UCFM is at a +20 dBm level; the driver TWT used on GEOS-C is eliminated. The TWT amplifier (TWTA) used a similar 2 kW TWT as on Skylab and GEOS-C; however, the 6.5 W average radiated RF power of SEASAT-A was a substantial increase over previous designs so that the TWTA represented a critical new element. The use of a chirped LO pulse resulted in a full-deramp mode of operation in which frequency domain filtering achieved the effect of time domain resolution.

The HSWS converts and stores 64 samples of I and Q video at a 20-MHz rate during the 3.2 μs receive interval defined by the LO pulse. The digital filter bank then accesses these samples sequentially in the interval between receptions and, in conjunction with a sine/cosine look-up table in a read-only memory (ROM), implements a phase rotation algorithm and accumulates sums over the 64 samples to form a contiguous bank of filters. The filter bank spacing and overall tuning are set by the manner in which the sine/cosine memory is addressed during each read-out cycle. Addressing corresponds to a linear phase progression representative of both the center frequency of the filter being implemented as well as a fine range offset derived from altitude tracking. Square-law detection is accomplished in a ROM addressed by the magnitude of the digital filter output.

Altitude tracking operations were conducted in the adaptive tracker using detected outputs from the digital filter bank. The hardware implementation of the adaptive tracker was built around a microprocessor with filter bank outputs read out as serial 9-bit words and accumulated (averaged) for 50 pulse-repetition intervals to provide smoothed waveform samples. The samples were then accessed by the tracker to close the height tracking, receiver gain control, and wave-height estimation loops. The flexibility of the adaptive tracker was also used to format and output basic measurement data (which included all waveform samples) to the TM system via an interface and control unit, as well as to interpret altimeter commands and control the sequencing of the altimeter through acquisition, track, and calibration states.

SAR Data Link

The satellite-borne modulation/transmitter functioned to encode the PRF pulse stream so that the SAR timing epochs, corresponding to RF transmission, could be recovered on the ground to better than 1 ns precision. The encoded PRF, STALO, and SAR return signals were multiplexed into a single 20 MHz S-band telemetry channel in such a way that the signals could be separated in the ground equipment. Finally, the composite RF signal was transmitted at a power level sufficient to ensure that the noise of the ground receiver did not significantly degrade recovery of the signals.

The PRF timing information (a, below) is transferred through the data link in the form of a PRN code. The PRF transmission epochs are used to reset a PRN code generator that produces a synchronized code output containing 4096 binary bits every PRF period. The code-generator clock signal is obtained by fixed division of the STALO frequency; the division factor is slaved to the PRF rate (selected by command to the SAR sensor) so that the code divides each IPP into exactly 4096 subintervals regardless of PRF. This high-resolution time code is used to biphase modulate an L-band pilot carrier obtained by frequency multiplication of the STALO. The modulator output is RF-summed with the pilot and echo signals to produce a composite L-band spectrum that is up-converted to S-band by mixing it with a coherent local-oscillator signal before amplification.

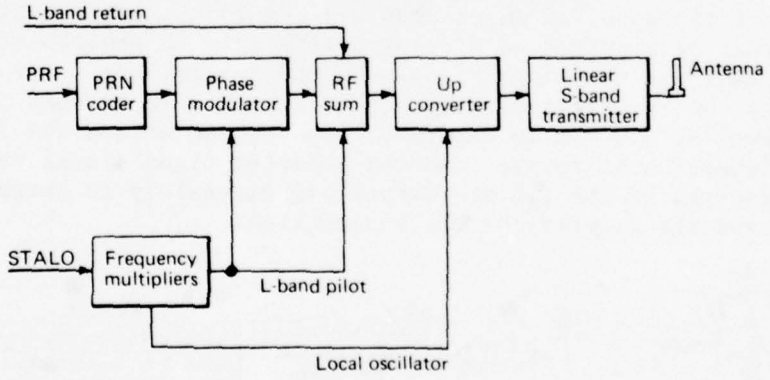

(a) Data-link spacecraft implementation

The transmitter composite RF output consists of pilot carrier and PRN spread-spectrum signals, which are constant at +14 dBm, the the variable SAR echo return. The RF gain of the data-link components is set so that, at a relatively high input echo level of 0 dBm, the transmitter output is 5 watts. Since the 1-dB gain compression of the transmitter occurs at 9 watts, it will operate

in its linear range most of the time. The data-link antenna is a quadrifilar helix with right-hand circular polarization and gain greater than 2.5 dB at a 20° ground-station elevation angle.

The major part of the transmitter power, under normal target situations, is taken up by the SAR echo. Since the echo is essentially wideband random noise, its density adds directly to the receiver noise density and become the dominant noise term in the recovery of the PRF and pilot signals. These signals also represent interference to the echo signal recovery, but their effect at the output of the image processor is small compared to that of the receiver noise.

The S-band signal is received by the 9-m dish antenna and amplified 20 dB by the parametric amplifier (b, below). The noise temperature of the receiving system is set by the dish/amplifier combination to about 90 K at a 20° elevation angle. The down-converter reduces the center frequency of the composite signal to 465.1 MHz by mixing with a stable 1800 MHz LO signal obtained by multiplication of the 5 MHz station frequency standard. The signal is then provided to the multifunction receiver (MFR), which phase-locks to the data-link pilot component and further reduces the center frequency to 110 MHz. In doing this the coherency of the signals is destroyed because the doppler shift has been removed from the center frequency but remains on the modulation. As the MFR phase-tracks, its LO signal at 132.4 MHz follows the phase changes of the received pilot that are due to satellite motion. This signal is provided as a doppler reference to reestablish coherency of the data-link signals in the demodulator. The MFR also uses the received pilot to adjust its RF gain so that the pilot level at 110 MHz is constant. By the AGC action the down-link attenuation is removed and the relative signal-level variations observed at the 110 MHz output are due solely to target cross section and the geometry of the target link.

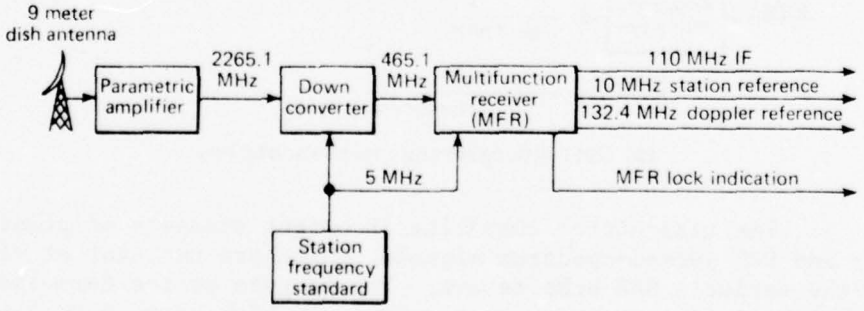

(b) STDN portion of data-link ground system

The MFR provides four signals to the demodulator, i.e., the 110 MHz IF, the 132.4 MHz doppler reference, a 10 MHz station reference, and a DC signal indicating the lock status of the MFR. The SAR-unique demodulator performs the remaining signal-recovery functions, which include decoding the PRN code to produce output PRF pulses, recovery of the STALO, final video down-conversion and amplification of the SAR return signal, and coherency correction using the doppler reference from the MFR.

FLIGHT RESULTS

SEASAT-A was successfully launched into orbit on 27 June 1978 (line 55, Table 1). First radar altimeter data taken of sea conditions on the Atlantic Ocean off the Delaware Bay indicated wave heights averaging 2 m. The observations were verified by measurements of surface conditions collected by aircraft and the GEOS-C satellite. On 10 October 1978, a malfunction in the spacecraft electrical system resulted in the termination of all onboard instrumentation. Prior to this, however, some 69 days of data were collected and are presently being processed.

High resolution images of the ocean surface showing waves, icebergs, coastal conditions, and ice leads were returned by the onboard SAR. The APL-provided microwave data link and ground station equipment for processing the signals into digital data functioned as expected. Figure XVIII-7 shows a SAR image of the Beaufort Sea area.

Excellent data were also obtained with the radar altimeter. Figure XVIII-8, which covers a short segment in the Atlantic Ocean, plots the difference between the altimeter height reading and a height derived from the Goddard Earth Model (GEM) 10B. The residual height data points that result reflect small scale departures from the geoid model as well as surface features caused by ocean dynamic processes including currents and tides. The trace is based on 1 second (10-sample) averages of height data points and demonstrates the low noise level of the SEASAT-A altimeter. The smallest division is 20 cm. The striking anomaly associated with the Puerto Rican Trench and the surface perturbation resulting from the Gulf Stream can be seen. Under the influence of the Coriolis force, a surface gradient proportional to the rate of flow and normal to the direction of flow is generated that forms the basis for mapping oceanic currents by altimetry.

The laser retroreflector array was used for accurate satellite positioning, and the doppler beacon operated satisfactorily to allow precise orbit determination.

SAR image, obtained by SEASAT-A on 11 July 1978, shows a portion of the Beaufort Sea ice pack west of Banks Island, Canada (right) and covers an area about 29 by 120 km. The region (northeast of Alaska and some 805 km inside the Arctic Circle) contains numerous ice, water, and land features. Stream channels, alluvial fans, and beaches are seen on Banks Island. The dark zone adjacent to the island is an area of shore fast ice composed primarily of first-year sea ice, 0.9 to 1.8 m thick. Linear pressure ridges are seen within the shore fast zone, and west of this zone is an area of open water (shore lead). At the western edge of the lead is a marginal ice zone composed of a mixture of open water and large and small rounded multi-year floes, typically 3 to 4.6 m thick, and some first-year ice. Further west is the main polar pack, made up of large floes up to 19.3 km in diameter, surrounded by new leads. A random pattern of pressure ridges is visible within the floes. The very bright areas within the floes indicate intensive surface roughness (rubble fields). Jet Propulsion Laboratory/NASA photo.

Fig. XVIII-7 SEASAT-A Synthetic Aperture Radar Imagery

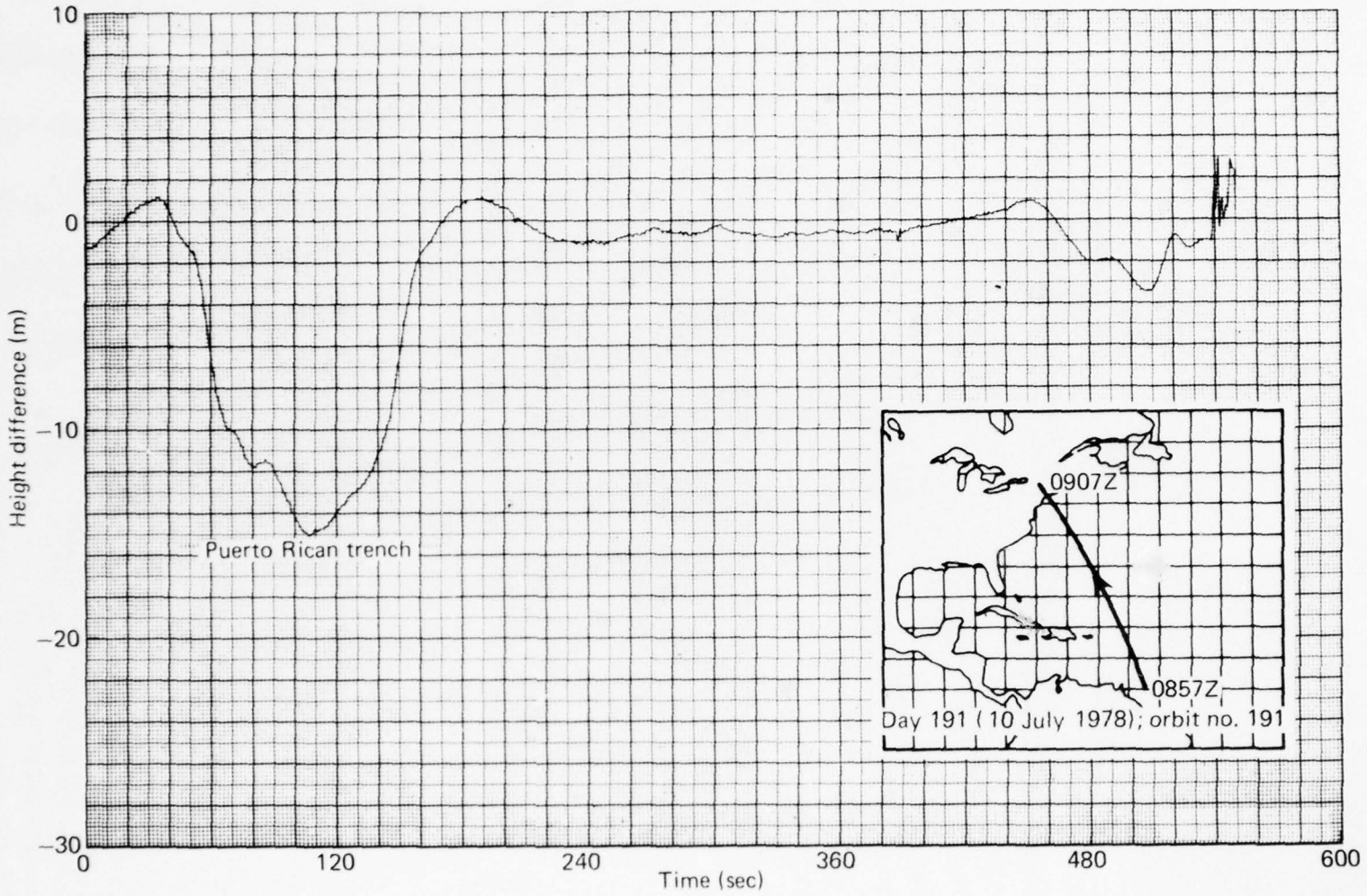

Fig. XVIII-8 Sea Surface Height Difference as Measured by GSFC Earth Model (GEM) 10B and SEASAT-A Radar Altimeter.

THE JOHNS HOPKINS UNIVERSITY
APPLIED PHYSICS LABORATORY
LAUREL MARYLAND

APPENDIXES

Appendix A

ABBREVIATIONS AND DEFINITIONS

AE	Atmosphere Explorer (satellite)
AP	Analog Performance
ASTP	Apollo-Soyuz Test Project
BE-B	Beacon Explorer-B (satellite)
BPS	Bits per Second
BSRC	British Science Research Council
CDA	Command and Data Acquisition
CDU	Command Distribution Unit
CPU	Control Processing Unit
CSM	Command System Module
D/A	Digital Analog
DB	Doppler Beacon
DDL	Dispersive Delay Line
DFC	Data Format Converter
DMA	Defense Mapping Agency
DPU	Data Processing Unit
DTL	Dual Tracking Loop
DODGE	Department of Defense Gravity Experiment (satellite)
DPP	Digital Performance Parameter
EMR	Electro-Mechanical Research, Inc.
EODAP	Earth and Ocean Physics Application Program
EPE	Energetic Particles Experiment
ESA	European Space Agency
ESS	Experiment Support System
ESSA	Environmental Sciences Services Administration (now NOAA)
FDS	Flight Data System
FET	Field Effect Transistor
FPB	Floating Point Binary

FWHM	Full-Width Half-Maximum
Geoceiver	Geodetic Receiver
GEOS	Geodetic Earth Orbiting Satellite
GEOS	Geodynamics Experimental Ocean Satellite
GM	Geiger-Mueller
GMT	Greenwich Mean Time
GREB	Galactic Radiation Energy Balance (satellite)
GSE	Ground Support Equipment
GSFC	Goddard Space Flight Center
GT	Geiger Telescope
HSWS	High-Speed Waveform Sampler
HV	Host Vehicle
ID	Identification
IMP	Interplanetary Monitoring Platform
IUE	International Ultraviolet Explorer
IPD	Information Processing Division (GSFC)
IPP	Interpulse Period
ITOS	Improved TIROS Operational Satellite
ITR	Incremental Tape Recorder
keV	Kiloelectron Volts
LECP	Low Energy Charged Particle
LEMPA	Low Energy Magnetospheric Particle Analyzer
LEPT	Low Energy Particle Telescope
LMSC	Lockheed Missiles and Space Co.
LO	Local Oscillator
LRA	Laser Retroreflector Array
LSS	Life Support System
MACS	Magnetic Attitude Control System
MESA	Miniature Electrostatic Accelerometer
MeV	Million Electron Volts
MFR	Multifunction Receiver
MS	Motion Sensitivity
MSD	Multiple Satellite Dispenser

MSOCC	Multisatellite Operation Control Center (GSFC)
NASA	National Aeronautics and Space Administration
NAVPAC	Navigational Package
NNSS	Navy Navigation Satellite System
NOAA	National Oceanic and Atmospheric Administration (formerly ESSA)
NRL	Naval Research Laboratory
NRZ	Nonreturn to Zero
NST	North-South Telescope
OFOE	Orbiting Frog Otolith Experiment
OGI	Oculogyral Illusion
OTG	Otolith Test Goggles
OWS	Orbital Workshop
PAD	Pulse Amplifier and Discriminator
PCA	Polar Cap Absorption
PES	Photoelectron Spectrometer
PET	Proton Electron Telescope
PD	Proton Detector
PFM	Particle Flux Monitor
PHA	Pulse Height Analyzer
PMOS	Positive Metal Oxide Semiconductor
PMT	Photomultiplier Tube
POD	Precision Orbit Determination
PPS	Pulses per Second
PRF	Pulse Repetition Frequency
RAE	Radio Astronomy Explorer (satellite)
RB	Return to Bias
R_E	Earth Radii
RFI	Radio Frequency Interference
RLC	Rotating Litter Chair
ROM	Read-Only Memory
RRA	Retroreflector Array
SAO	Smithsonian Astrophysical Observatory

SAR	Synthetic Aperture Radar
SCO	Subcarrier Oscillator
SDFR	SAR Data Formatting and Recording
SDS	Scientific Data System
SEL	Space Environment Laboratory (NOAA)
SGLS	Space Ground Link System (Air Force)
SIM	Scientific Instrument Module
SPICE	Solar Particle Intensity and Composition Experiment (Program)
SPM	Solar Proton Monitor
SPME	Solar Proton Monitor Experiment
SST	Supersonic Transport
STADAN	Space Tracking and Data Acquisition Network
STALO	Stable Local Oscillator
SUI	State University of Iowa
TCG	Time Code Generator
TIROS	Television Infrared Observation Satellite
TMTM	Two-Minute Time Mark
TOD	Transit-on-Discoverer
TRAAC	Transit Research and Attitude Control
TRANET	Tracking Network
TRIAD	Three bodied (satellite)
TTL	Transistor-Transistor Logic
TWT	Traveling Wave Tube
TWTA	Traveling Wave Tube Amplifier
UCFM	Up-Converter Frequency Multiplier
UVA	Ultraviolet Absorption
UVS	Utralviolet Spectrometer
VERLORT	Very Long Range Tracking
VLF	Very Low Frequency

Appendix B

REFERENCES AND BIBLIOGRAPHY

Section I

(1) "Transit-on-Discoverer Program," APL/JHU SGS/SGS-2, 10 January 1960.

(2) "Test Plan, APL Doppler Evaluation on Discoverer X," LMSD/352871, Lockheed Aircraft Corp., Missiles and Space Division, Sunnyvale, California, 29 January 1960.

(3) F. T. Heuring, "Discoverer XVII Optical Data Comparison to APL Ephemeris," APL/JHU SRA-73-61, 16 May 1961.

Section II

(1) G. F. Pieper, "INJUN, A Radiation Research Satellite," APL Technical Digest, Vol. 1, No. 1, September-October 1961, pp. 3-7.

(2) A. J. Zmuda, "Solar-Terrestrial Disturbances and Solar Protons in July 1961," APL Technical Digest, Vol. 1, No. 3, January-February 1962, pp. 16-20.

(3) G. F. Pieper, "The Artificial Radiation Belt," APL Technical Digest, Vol. 2, No. 2, November-December 1962, pp. 3-7.

(4) G. F. Pieper, A. J. Zmuda, C. O. Bostrom, and B. J. O'Brien, Solar Protons and Magnetic Storms in July 1961, APL/JHU TG 442, July 1962.

Section III

(1) F. F. Mobley, "Attitude Control System for the Atmosphere Explorer-B Satellite," AIAA Paper No. 65-432, AIAA 2nd Annual Meeting, July 1965.

(2) B. F. Tossman, "Magnetic Attitude Control System for the Radio Astronomy Explorer-B Satellite," AIAA Paper No. 68-855, AIAA Guidance, Control, and Flight Dynamics Conference, August 1968.

(3) F. F. Mobley and R. E. Fischell, "Magnetic Stabilization System," Applied Physics Laboratory Report U-SQR/66-3, July-September 1966.

(4) R. E. Fischell, "Passive Magnetic Attitude Control for Earth Satellites," Advances in the Astronautical Sciences, Vol. II, Western Periodical Company, No. Hollywood, California, 1963.

(5) F. F. Mobley et al., "Performance of the Spin Control System of the DME-A Satellite," AIAA/JACC Guidance and Control Conference Proceedings, p. 463, August 1966.

(6) R. E. Fischell, "Magnetic and Gravity Attitude Stabilization of Earth Satellites," Proceedings of the 2nd International Space Science Symposium, Florence, Space Research II, North-Holland Publishing Company, Amsterdam, 1961.

(7) B. E. Tossman, "Performance of Enhanced Magnetic Hysteresis System in Removing Spin and Tumble from DODGE," Applied Physics Laboratory Report U-SQR/67-3, July-September 1967.

Section IV

(1) A. F. Hogrefe, "A Solar Proton Monitor for IMP," APL/JHU S1P-162-66, 8 September 1962.

(2) N. F. Ness, "Magnetic Field Restraints for IMPs F and G," NASA/GSFC X-672-64-197, July 1964.

(3) C. O. Bostrom, "Entry of Low Energy Solar Protons into the Magnetosphere, Intercorrelated Satellite Observations Related to Solar Events 229-238, 1970. Proceedings of the Third Eslab/Esrin Symposium, Noordwijk, Netherlands, 16-19 September 1969. D. Reidel Publishing Co., Dordrecht, Netherlands.

(4) J. W. Kohl, "Solar Proton Monitoring," APL Technical Digest, Vol. 8, No. 1, September-October 1968, pp. 2-9.

(5) D. J. Williams and C. O. Bostrom, "Proton Entry into the Magnetosphere on May 26, 1967," J. Geophys. Res., 74, 3019-3036, June 1969.

(6) D. J. Williams, "Solar Proton Observations 1-10 MeV," Proceedings of the Seminar of the Study of Interplanetary Space Physics Using Cosmic Rays, 67-115, 1969. (Proceedings held at the Physical Technical Institute, USSR Academy of Sciences, Leningrad, USSR, 4-7 June 1969. Ed. A. I. Ioffe.) (Also published as NASA/GSFC Report X-612-69-258, June 1969.)

Section V

(1) S. A. Gary and R. E. Cashion, Solar Proton Monitor for TIROS-M and ITOS Spacecraft, APL/JHU CP 010, December 1971.

Section VI

(1) J. B. Oakes, W. J. Billerbeck, K. F. Read, "Design of an Ultrastable Oscillator for Satellites," APL Technical Digest, Vol. 2, No. 1, September-October 1968, pp. 10-14.

Section VII

(1) F. Bracchi, T. Gualtierotti, A. Morabito, and E. Rocca, "Multiday Recordings from the Primary Neurons of the Stratoreceptors of the Bullfrog," Acta Oto-Laryngologica, Supplement XXX, Distributed by the Almquist & Wiksell Periodical Co., Stockholm, Sweden.

(2) F. A. Oyhus and C. M. Blackburn, "Orbital Otolith Experiment Package Description," APL/JHU S4M-0-72, 16 October 1967.

Section VIII

(1) R. J. Locker and G. C. Huth, "A New Ionizing Radiation Detection Concept which Employs Semiconductor Avalanche Amplification and the Tunnel Diode Element," Appl. Phys. Letters, Vol. 9, No. 6, 15 September 1966, pp. 227-230.

(2) C. O. Bostrom and D. P. Peletier, "The IMP-6 Solar Proton Monitoring Experiment," APL/JHU CP 013, May 1972.

(3) D. P. Peletier, "In-Flight Calibration Systems for Particle Detector Experiments," IEEE Trans. Nuclear Sci., Vol. NS-17, No. 1, February 1970.

(4) R. E. Cashion, "IMP-I SPME Power Supply," APL/JHU S1P-412-69, 8 January 1969.

(5) D. P. Peletier, "Interpreting the IMP-I SPME In-Flight Calibration Data," APL/JHU S1P-584-70, 21 August 1970.

(6) S. A. Gary, Effect of Filtering on Noise and Timing in Nuclear Particle Detection, APL/JHU TG 1136, October 1970.

(7) C. O. Bostrom, "IMP-I SPME Ground-Test Computer Output Format," APL/JHU S1P-522-70, 23 January 1970.

(8) R. L. McCutcheon, "IMP-6 SPME Data Processing System," APL/JHU CP 021, December 1972.

Section IX

(1) A. F. Hogrefe, IMP H, J Energetic Particles Experiment (GWP), APL/JHU Experiment Requirements Document, November 1972.

(2) Mission Operations Plan 2-73, Interplanetary Monitoring Platform, IMP-J, NASA/GSFC Technical Memorandum X-513-73-255, August 1973.

Section X

(1) R. E. Cashion, J. W. Kohl, S. A. Gary, and D. P. Peletier, Charged Particle Measurements Experiment for Interplanetary Monitoring Platform Missions H and J, APL/JHU CP-025, July 1973.

(2) A. F. Hogrefe, "A Solar Proton Monitor for IMP," APL/JHU S1P-162-66, 8 September 1966.

(3) D. F. Hewett, "Program to Evaluate Electron Counting Efficiencies," APL/JHU S1P-955-73, 16 October 1972.

Section XI

(1) Final Report for Task II of the Ultraviolet Spectrometer Experiment, Space Development Department, APL/JHU SDO/CMO-455, February 1973.

(2) W. G. Fastie, "The Apollo 17 Far Ultraviolet Spectrometer Experiment, The Johns Hopkins University.

(3) UVS Experiment S169, BTE EMI Evaluation Test Report, MSC/TCSD EMC-R-EM8-005, September 1972.

Section XII

(1) A. Graybiel, E. F. Miler, and J. L. Homick, "Experiment M131 - Human Vestibular Function," pp. 169-220, The Proceedings of the Skylab Life Sciences Symposium, 27-29 August 1974, NASA Technical Memorandum TM X-58154, Vol. 1, November 1974.

Section XIII

(1) J. P. Doering, W. G. Fastie, and P. D. Feldman, "Photoelectron Excitation of N_2 in the Day Airglow," J. Geophys. Res., Vol. 75, No. 25, September 1970, pp. 4787-4802.

(2) P. D. Feldman, J. P. Doering, and J. H. Moore, "Rocket Measurements of the Secondary Electron Spectrum in an Aurora," J. Geophys. Res., Vol. 76, No. 7, March 1971, pp. 1738-1745.

(3) J. C. Armstrong, Spacecraft Interference with Low Energy Electron Measurements, APL/JHU CP 014, April 1972.

(4) D. P. Peletier, "A High Performance 4500 Volt Electron Multiplier Bias Supply for Satellite Use," IEEE Trans. Nuclear Sci., NS-20, No. 1, February 1973, pp. 107-112.

(5) S. A. Gary, "Analog Electronics for AE Photoelectron Spectrometer," APL/JHU S1P-910-72, April 1972.

(6) C. O. Bostrom, "AE-PES Deflection Plate Potentials," APL/JHU S1P-841-71, 1971.

(7) J. P. Doering, T. A. Potemra, W. K. Peterson, and C. O. Bostrom, "Characteristic Energy Spectra of 1-500 eV Electrons Observed in the High Latitude Ionosphere from Atmosphere Explorer-C," submitted to J. Geophys. Res., 1975.

(8) J. P. Doering, T. A. Potemra, and C. O. Bostrom, "Observations of Low Energy (0-500 eV) Electrons in the Polar Region from AE-D," Transactions, American Geophysical Union, Vol. 57, No. 4, SM 86, April 1976.

(9) J. P. Doering, W. K. Peterson, C. O. Bostrom, and T. A. Potemra, "High Resolution Daytime Photoelectron Energy Spectra from AE-E," Geophysical Research Letters, Vol. 3, No. 1, March 1976, pp. 129-131.

(10) D. P. Peletier, "Instrumentation for the Atmosphere Explorer Photoelectron Spectrometer," APL/JHU CP 030, November 1973.

Section XIV

(1) T. M. Donahue, R. D. Hudson, J. Anderson, F. Kaufman, and M. B. McElroy, "Ultraviolet Absorption Experiment MA-059," pp. 8-1 — 8-22, Apollo-Soyuz Test Project Preliminary Science Report, NASA Technical Memorandum TM X-58173, February 1976.

Section XV

(1) D. L. Zitterkopf, "The NAVPAC Dual Tracking Loop," APL/JHU S2T-0-160, 14 July 1976

(2) D. L. Zitterkopf, "NAVPAC Priority/Coherency Logic," APL/JHU S2T-0-150, 9 April 1976.

(3) J. C. Loessi, "NAVPAC Data Formatter and Tape Recorder Controller," APL/JHU S2T-0-175, 21 September 1976.

Section XVI

(1) S. M. Krimigis, T. P. Armstrong, W. I. Axford, C. O. Bostrom, C. Y. Fan, G. Gloeckler, and L. J. Lanzerotti, "The Low Energy Charged Particle (LECP) Experiment on the Voyager Spacecraft," APL/JHU Preprint 77-01, January 1977 (Space Science Reviews, in press, 1977).

(2) D. P. Peletier, S. A. Gary, and A. F. Hogrefe, "Mariner-Jupiter-Saturn Low Energy Charged Particle Experiment," IEEE Trans. Nucl. Sci., NS-24, 795, 1977.

(3) J. B. A. England, "A Fast Analogue Particle Identification System," Nucl. Instr. Methods, 106 (1973), 45-59.

(4) D. P. Peletier, "A Closed Loop Threshold Calibrator for Pulse Height Discriminators," IEEE Trans. on Nucl. Sci., Vol. NS-22, No. 1, February 1975, pp. 592-594.

(5) D. P. Peletier, "A High Performance 4500 Volt Electron Multiplier Bias Supply for Satellite Use," IEEE Trans. on Nucl. Sci., Vol. NS-20, No. 1, February 1973, pp. 107-112.

Section XVII

(1) J. T. Mueller, "Vibration Testing of the Particle Flux Monitor (PFM), International Ultraviolet Explorer (IUE)," APL/JHU S1P-569-78, 16 January 1978.

(2) C. O. Bostrom, "The Particle Flux Monitor for International Ultraviolet Explorer - A Short Story," APL/JHU SDO 4977, 17 January 1978.

Section XVIII

(1) M. W. Fitzmaurice, NASA Ground-Based and Space-Based Laser Ranging Systems, NASA Technical Paper 1149, January 1978.

(2) P. O. Minott, M. W. Fitzmaurice, J. B. Abshire, and H. E. Rowe, Prelaunch Testing of the GEOS-3 Laser Reflector Array, NASA Technical Paper 1138, January 1978.

(3) J. L. MacArthur, "Design of the SEASAT-A Radar Altimeter," Oceans' 76, 76CH1118-9 OEC, Proceedings of the Second Annual Combined Conference Sponsored by the Marine Technology Scoiety and the Institute of Electrical and Electronics Engineers, 13-15 September 1976, pp. 10B-1-10B-8.

(4) E. F. Prozeller and R. J. Heins, "A Wideband Analog Data Link for the SEASAT-A Synthetic Aperture Radar," EASCON '78 Record, 78CH1254-4, Proceedings of IEEE Aerospace and Electronic Systems Society, 25-27 September 1978, pp. 111-119.

(5) E. F. Prozeller, R. J. Heins, W. C. Trimble, and J. A. Trennepohl, A Coherent Demodulator for the Data Link of the SEASAT-A Synthetic Aperture Radar, APL/JHU CP-063, March 1978.